

RIGA TECHNICAL UNIVERSITY

Faculty of Materials Science and Applied Chemistry

Institute of Polymer Chemistry and Technology

Miķelis Kirpluks

Doctoral Student of the Study Programme “Chemical Engineering”

**DEVELOPMENT OF RENEWABLE
FEEDSTOCK BASED RIGID POLYURETHANE
FOAM AND NANOCCLAY COMPOSITES**

Doctoral Thesis

Scientific supervisors:

Dr. sc. ing.

UĢIS CĀBULIS

Dr. sc. ing. Associate Professor

SERGEJS GAIDUKOVS

RTU Press

Riga 2020

Never attribute to malice that which is adequately explained by stupidity.
/Robert J. Hanlon/

Kirpluks, M. Development of Renewable Feedstock Based Rigid Polyurethane Foam and Nanoclay Composites. Doctoral Thesis. Riga: RTU Press, 2020. 161 p.

Published in accordance with the decision of Promotion Council “RTU P-01” of May 5-6, 2020, Minutes No. 04030-9.1/3.

The Ph. D. Thesis has been carried out in the frame of the following research projects funded by European Community:

- FP 7 project EVOLUTION, 11/2012 – 11/2016; The Electric Vehicle revOLUTION enabled by advanced materials highly hybridized into lightweight components for easy integration and dismantling providing a reduced life-cycle cost logic;



- IMATECH – Latvian national Research program project: Innovative and multifunctional composite materials for sustainable buildings;



- COST action MP 1105 Flaretex, FLARETEX, 05/2012-06/2016; Sustainable flame retardancy for textiles and related materials based on nanoparticles substituting conventional chemicals;



- Project “Rigid Polyurethane/Polyisocyanurate Foam Thermal Insulation Material Reinforced With Nano/Micro Size Cellulose” Funded by ERDF, contract No 1.1.1.1/16/A/031, 01/2017-02/2019.



MINISTRY OF FINANCE
REPUBLIC OF LATVIA

NATIONAL
DEVELOPMENT
PLAN 2020



EUROPEAN UNION
European Regional
Development Fund

INVESTING IN YOUR FUTURE

DOCTORAL THESIS PROPOSED TO RIGA TECHNICAL UNIVERSITY FOR THE PROMOTION TO THE SCIENTIFIC DEGREE OF DOCTOR OF SCIENCE

To be granted the scientific degree of Doctor of Science (Ph. D.), the present Doctoral Thesis has been submitted for the defence at the open meeting of RTU Promotion Council on September 3, 2020 at 14:00 at the Faculty of Materials Science and Applied Chemistry of Riga Technical University, 3/7 Paula Valdena Street , Room 272

OFFICIAL REVIEWERS

Professor Dr. sc. ing. Jurijs Ozoliņš
Riga Technical University, Latvia

Professor Dr. chem. Andris Actiņš
University of Latvia, Latvia

Professor Dr. Arantxa Eceiza
Universidad del Pais Vasco, Leioa, Spain

DECLARATION OF ACADEMIC INTEGRITY

I hereby declare that the Doctoral Thesis submitted for the review to Riga Technical University for the promotion to the scientific degree of Doctor of Science (Ph. D.) is my own. I confirm that this Doctoral Thesis had not been submitted to any other university for the promotion to a scientific degree.

Miķelis Kirplūks (signature)

Date:

The Doctoral Thesis has been written in English. It consists of an Introduction; 3 Chapters; Conclusion; 123 figures; 27 tables; the total number of pages is 161. The Bibliography contains 12 titles.

ANNOTATION

Keywords: rigid polyurethane foam, bio-based polyols, intumescent flame retardant, thermal insulation, epoxidation

Rigid PU foams are versatile material commonly applied as a thermal insulation material. It can be applied as an impact absorption material in the automotive industry if material with sufficient mechanical properties has been developed. Further increase in mechanical properties can be achieved by developing nano-reinforced rigid PU foams.

Majority of commercially used rigid PU foams are produced from non-renewable petrochemical-based raw materials. Although, renewable feedstock, as well as recycled materials, can be used to obtain rigid PU foams with equal properties. In this work, several bio-based, as well as APP polyols, have been used to develop rigid PU foams.

Rigid PU foam thermal insulation material has to fulfil demanding flammability requirements. This is achieved by the introduction of different flame retardants into the material structure from which most common are halogenated flame retardants. Halogenated flame retardants are associated with different health hazards, thus their phase-out from the market can be expected. A good alternative to halogenated flame retardants are intumescent flame retardant solutions.

The results and discussion of this thesis are divided into three parts:

Part 1 describes the development of high-density rigid PU foam material for application as impact absorption material in the automotive industry. Sustainable origin polyols have been used to develop rigid PU foams and their influence on mechanical, thermal and morphological properties of the material has been studied. To further increase mechanical properties of the rigid PU foams a nano-composite with montmorillonite nano-clay was developed. Lastly, most optimal rigid PU foam formulations were upscaled to produce real scale automotive part, which was tested according to the European Union's crash test requirements.

Part 2 describes the development of rigid PU foam thermal insulation from bio-based polyols. Halogenated flame retardants were replaced using non-halogenated alternatives. Intumescent flame retardants, such as expandable graphite was used to significantly reduce the flammability of the rigid PU foam.

Part 3; during high-density rigid PU foam development it was discovered that used bio-based polyols have too low OH group functionality. Thus, the functionality of the polyols was increased by developing different bio-polyol synthesis method. Rapeseed oil, as well as tall oil, were used as feedstock for high functionality bio-based polyol synthesis. The first step was an epoxidation of the unsaturated moieties of the bio-based oils. Afterwards, oxirane ring opening with different polyfunctional alcohols and simultaneous transesterification/esterification reactions were used to obtain desired polyol structures.

The Doctoral Theses has been written in English, it consists of 161 pages, 123 figures, 27 tables and 259 reference sources.

ANOTĀCIJA

Atslēgas vārdi: cietais poliuretāna putuplasts, no atjaunojamām izejvielām iegūti polioli, “intumescenti” antipirēni, siltumizolācija, epoksidācija

Cietais poliuretāna putuplasts tiek plaši pielietots kā siltumizolācijas materiāls celtniecības industrijā, kā arī saldētavu un ledusskapju ražošanā. Mainot cietā poliuretāna putuplasta ražošanas tehnoloģiju, ir iespējams palielināt tā mehāniskās īpašības, lai to varētu pielietot kā trieciena absorbcijas materiālu autobūves industrijā. Izstrādājot cietā poliuretāna putuplasta nano-kompozītus ir iespējams vēl vairāk uzlabot tā mehāniskās īpašības.

Kaut arī ir iespējams iegūt cieto poliuretāna putuplastu no atjaunojamām izejvielām, vairums no rūpnieciski ražotā cietā poliuretāna putuplasta tiek iegūts, izmantojot naftas pārstrādes produktus. Dotajā promocijas darbā augstas efektivitātes cietais poliuretāna putuplasta materiāls tika iegūts no atjaunojamām izejvielām, kā arī no pārstrādāta PET polimēra.

Lai cieto poliuretāna putuplastu varētu izmantot kā celtniecības materiālu, tam ir jāatbilst noteiktai uguns reakcijas klasei. Lai varētu izturēt attiecīgos materiāla uguns reakcijas testus, materiāla sastāvā tiek iekļautas liesmu slāpējošas vielas – antipirēni. Vairums izmantoto antipirēnu ir halogēnu grupu saturošas vielas, kuru izmantošana ir saistīta ar negatīvu ietekmi uz cilvēka veselību. Promocijas darbā tika pētīta halogenēto antipirēnu aizstāšana ar “intumescentiem” antipirēniem no atjaunojamām izejvielām iegūtā cietā poliuretāna putuplastā.

Promocijas darbā iegūtie rezultāti ir sadalīti trīs darba daļās:

Pirmajā daļā tika izstrādāts cietais poliuretāna putuplasts ar paaugstinātām mehāniskajām īpašībām, kā arī tika iegūti cietā poliuretāna putuplasta un nano-mālu kompozīts. Potenciālais izstrādātā materiāla pielietojums ir triecien absorbcijas materiāls autobūves industrijā. Tika izstrādātas reāla izmēra automašīnas detaļas, kas tika testētas atbilstoši autobūves trieciena testiem.

Otrajā darba daļā tika izstrādāts cietā poliuretāna putuplasta siltumizolācijas materiāls, izmantojot no atjaunojamām izejvielām, iegūts polioli. Iegūtajā siltumizolācijas materiālā halogenētie antipirēni tika aizstāti ar mazāk kaitīgajiem “intumescentiem” antipirēniem.

Trešajā darba daļā tika sintezēti un raksturoti augstas funkcionalitātes polioli. Kā atjaunojamās polioliu sintēzes izejvielas, tika izmantotas rapšu un tallu eļļas. Polioliu sintēze tika veikta divās fāzēs, kur sākumā taukskābju nepiesātinātās dubultsaites tika epoksidētas dažādos apstākļos. Pēc epoksīda grupu ievadīšanas, tās tika atvērtas ar dažādiem polifunkcionāliem spirtiem, kā arī vienlaikus tika veiktas transesterifikācijas/esterifikācijas reakcijas.

Dotais promocijas darbs ir rakstīts angļu valodā, un tas satur 161 lapaspuses, 123 attēli, 27 tabulas un 259 citēti literatūras avoti.

Table of Contents

INTRODUCTION.....	12
1. LITERATURE REVIEW.....	16
1.1. Polyurethane Foams in Brief	16
<i>Polyurethane Material Chemistry</i>	16
<i>Polyols</i>	17
<i>Polyisocyanate</i>	18
Structure and Reactivity Polyisocyanates	20
Reactivity of Isocyanates	20
Production of Isocyanates Applied for Rigid PU Foam Production	21
1.2. Sustainable Polyol Development.....	21
<i>Epoxidation and Epoxy Ring Opening of Natural Oils</i>	22
<i>Transesterification of Natural Oils</i>	24
<i>Wood Biomass Derived Polyols</i>	25
Lignin Application in PU Materials.....	26
Tall Oil as PU Material Feedstock.....	27
<i>Bio-polyols Produced on an Industrial Scale</i>	28
<i>PET Glycolysis</i>	29
1.3. Rigid PU Foam Flammability	29
<i>Flame Retardants – Expandable Graphite</i>	30
2. MATERIALS AND METHODS	33
2.1. High-density Rigid PU Foam Development from Sustainable Raw Materials	33
<i>Polyols from Sustainable Raw Materials Used for Rigid PU Foam Development</i>	33
<i>Rigid PU Foam Sample Production</i>	35
Rigid PU Foam Sample Preparation in Open-top Mould	35
Rigid PU Foam sample Production in a Stainless Closed Type Steel Mould.....	36
2.2. Rigid PU Foam Nanocomposite Development	36
<i>Nanoclay Additives Used for Rigid PU Foam Reinforcement</i>	36
<i>X-ray Diffraction Analysis of Nanoparticle Dispersions in Polyols</i>	38
2.3. Development of Low Flammability Rigid PU Foam Thermal Insulation Composite	38
2.4. High Functionality Bio-based Polyol Synthesis from RO.....	39
2.5. TOFA Epoxidation.....	41
2.6. Polyol Analysis Methods	43
2.7. Rigid PU Foam Characterization Methods.....	44
<i>Rigid PU Foam Cell Size and Cell Density Determination from SEM Images</i>	45
<i>Rigid PU Foam Degree of Phase Separation Analysis Using FTIR</i>	45
3. RESULTS AND DISCUSSION	47
3.1. High-density Rigid PU Foam Development from Sustainable Raw Materials	47
<i>Sustainable Polyols Used for High-density Rigid PU Foam Development</i>	47
<i>High-density Rigid PU Foam Formulations</i>	48
<i>Different Sustainable Polyol Influence on High-density Rigid PU Foam Cell Morphology</i>	51
<i>Mechanical Properties of High-Density Rigid PU Foams</i>	53
The Compression Strength of PU Foams from Sustainable Polyols.....	53
Tensile Strength of PU Foams from Sustainable Polyols	54
<i>Thermal Properties of PU Foams from Sustainable Polyols</i>	55
Thermal Stability of PU Foams from Sustainable Polyols	55
The Glass Transition Temperature of PU Foams from Sustainable Polyols.....	56

<i>Characteristics of the PU Polymer Matrix of Developed Rigid Polyurethane Foams</i>	59
<i>Chemical Structure of Rigid PU Foams from Sustainable Polyols</i>	62
<i>Isocyanate Index Influence on Mechanical Properties of Rigid PU Foams</i>	64
<i>Density Influence on Mechanical Properties of Rigid PU Foams</i>	66
<i>High Strain Rate Deformation Testing of Rigid PU Foams</i>	68
<i>Split Hopkinson Pressure Bar Test of Rigid PU Foams</i>	68
<i>Rigid PU Foam High Strain Rate Compression Test</i>	69
<i>Predicting Compression Stress-Strain Behaviour of Developed Rigid PU Foams</i>	70
<i>Development of Impact Absorption Demonstrator for The Automotive Industry</i>	74
Introduction to EU FP7 Project Evolution	74
Development of the Nido EV Front Bumper – Crossbeam	75
The Manufacturing Process	76
Summary of the Project Evolution	77
<i>Conclusions of High-Density Rigid PU Foam Development</i>	77
3.2. Rigid PU Foam Nanocomposite Development	79
<i>APP Polyol and Nanoclay Dispersion</i>	79
<i>X-Ray Diffraction Analysis of Nanoparticle Dispersions in Polyols</i>	81
<i>Exfoliation of Cloisite 30B Nanoclay in Isocyanate</i>	84
<i>Morphological Properties of PU Foams Modified With Nanoclay</i>	85
<i>Mechanical Properties of Rigid PU Foams Modified with Nanoclay</i>	86
The Compression Strength of Rigid PU Foams Filled with Nanoclay	86
Tensile Strength of Rigid PU Foams Filled With Nanoclay	91
Thermal Properties of PU Foams Modified With Nanoclay	91
<i>Conclusions of Rigid PU Foam Nanoclay Composite Development</i>	92
3.3. Low Flammability Rigid PU Foam Thermal Insulation Composite	94
<i>TO Polyol Based Rigid PU Foams with Low Flammability</i>	94
<i>Thermal Conductivity of the Developed Rigid PU/PIR Foams</i>	95
<i>Mechanical and Morphological Properties of the Developed Rigid PU/PIR Foams</i>	96
<i>Flammability of Developed Rigid PU/PIR Foams</i>	99
<i>Reaction to Fire of Developed Rigid PU/PIR Foam</i>	103
<i>Summary of Low Flammability Rigid PU/PIR Foam Development</i>	106
<i>Conclusions of Low Flammability Rigid PU Foam Development</i>	107
3.4. High Functionality Bio-Based Polyol Synthesis from RO	108
<i>RO Epoxidation and Temperature Influence on the Epoxidation Process</i>	108
<i>Characteristics of High Functionality Polyols from Epoxidized RO</i>	110
<i>FTIR Analysis of High Functionality Polyols from Epoxidized RO</i>	111
<i>MALDI TOF Mass Spectrometry of RO Based High Functionality Polyols</i>	112
<i>Rigid PU Foam Development from RO Based High Functionality Polyols</i>	115
<i>Conclusions of High Functionality Polyol Synthesis from RO</i>	117
3.5. High Functionality Bio-Based Polyol Synthesis from TOFA	118
<i>TOFA Epoxidation with Acidic Catalysts</i>	118
TOFA Epoxidation with a Sulphuric Acid Catalyst	119
TOFA Epoxidation with Amberlite IR-120 H Ion Exchange Resin Catalyst	122
<i>Tall Oil Fatty Acid Epoxidation Kinetics</i>	125
Temperature Influence on TOFA Epoxidation Kinetics	125
TOFA Epoxidation Surface Reaction Kinetic Model	129
<i>Regeneration of TOFA Epoxidation Catalyst</i>	136
<i>Chemo-Enzymatic TOFA Epoxidation</i>	137
Double Bond and Hydrogen Peroxide Molar Ratio Influence on the TOFA Epoxidation	138
Effect of the Novozym® 435 Content on the TOFA Epoxidation Process	139

Effect of the Hydrogen Peroxide Concentration on the TOFA Epoxidation Process	140
FTIR Analysis During TOFA Epoxidation Process	141
<i>Overview of Chemo-Enzymatic TOFA Epoxidation</i>	143
<i>Conclusions of TOFA Epoxidation</i>	144
REFERENCES	146

ABBREVIATIONS

[AA]	Acetic acid content, mol per 100g oil
[AAs]	Adsorbed acetic acid content, mol per 100g oil
[EU]	Ethylenic unsaturation content, mol per 100g oil
[H ₂ O]	Water content, mol per 100g oil
[H ₂ O ₂]	Hydrogen peroxide content, mol per 100g oil
[OO]	Oxirane oxygen content, mol/L
[PA]	Peracetic acid content, mol per 100g oil
[PAs]	Adsorbed peracetic acid content, mol per 100g oil
[vs]	Vacant active site content, mol per g cat.
AA	Acetic acid
AAs	Adsorbed acetic acid
APP	Aromatic polyester polyol
C _t	Content of the total active sites of ion exchange resin catalyst, mol per g cat.
DEG	Diethyleneglycol
DEOA	Diethanolamine
DMA	Dynamic mechanical analysis
DMPP	Dimethyl-propyl-phosphate
DSC	Differential Scanning Calorimetry
EG	Expandable graphite
EPS	Expanded polystyrene
EU	Ethylenic unsaturation
EU _{ex}	Remaining degree of ethylenic unsaturation during synthesis, gI ₂ / per 100g
EU _i	Initial ethylenic unsaturation, gI ₂ per 100g
FOT	Flame out time, s
FP7	7 th Framework Programm
FR	Flame retardant
HRR	Heat release rate, kW/m ²
IF	Intumescent unwoven fabric
IT	Ignition time, s
k ₃	Epoxidation reaction rate constant, 100g oil per s·mol
k ₄	Reaction rate constant of the oxirane opening with acetic acid, 100g oil per s·mol
k ₅	Reaction rate constant of the oxirane ring opening with water, 100g oil per s·mol
k _a	Acetic acid non-dissociated adsorption rate constant, g cat. per s·mol
K _{AA}	Acetic acid adsorption equilibrium constant, L/mol
k _d	Peracetic acid desorption rate constant
K _{PA}	Peracetic acid adsorption equilibrium constant
K _S	Surface reaction equilibrium constant, L/mol
k _{sr}	Adsorbed acetic acid and hydrogen peroxide surface reaction rate constant, g cat. per s·mol
LOI	Limiting oxygen index
LS IWC	Latvian State Institute of Wood Chemistry
MARHE	Maximum average rate of heat emission, kW/m ²
M _c	Molecular weight between cross-links, g/mol
MT	Million tones
OO _{ex}	Experimentally determined content of oxirane oxygen, %
OO _{th}	Theoretical maximum oxirane content in 100 g of oil, %

PA	Peracetic acid
PAs	Adsorbed peracetic acid
pbw	Parts by weight
PET	Polyethylene terephthalate
pHRR	Peak of heat release rate, kW/m ²
PIR	Polyisocyanurate
Project EVolution	The Electric Vehicle revOLUTION enabled by advanced materials highly hybridized into lightweight components for easy integration and dismantling providing a reduced life cycle cost logic
PU	Polyurethane
r _a	Reaction rate of acetic acid non-dissociated adsorption, mol per s·g cat.
RCO	Relative conversion to oxirane, %
r _d	Reaction rate of peracetic acid desorption, mol per s·g cat.
REU	Relative ethylenic unsaturation, %
RIM	Reaction injection moulding
RO	Rapeseed oil
RO_DEOA	Rapeseed oil polyol from transamidation reaction with diethanolamine
RO_TEOA	Rapeseed oil polyol from transesterification reaction with triethanolamine
r _{sr}	Rate of irreversible surface reaction of adsorbed acetic acid and hydrogen peroxide, mol per s·g cat.
S	Selectivity of synthesis
SEM	Scanning electron microscope
TCPP	Tris(1-chloro-2-propyl)phosphate
TEOA	Triethanolamine
TGA	Thermogravimetric analysis
THR	Total heat released, MJ
TMA	Thermo Mechanical Analysis
TO	Tall oil
TO_DEOA	Tall oil polyol from amidation reaction with diethanolamine
TO_TEOA	Tall oil polyol from esterification reaction with triethanolamine
TOFA	Tall oil fatty acids
TSR	Total smoke released, m ² /m ²
TTI	Time to ignition, s
TTP	Time to peak of heat release rate, s
UBC	Unsaturated bond conversion, %
v _e	Crosslink density of the polymer mol/cm ³
VOC	Volatile organic compound
XPS	Extruded polystyrene
XRD	X-ray diffraction
λ	Thermal conductivity, mW/(m·K)

INTRODUCTION

The world is facing a rising variety of challenges due to increasing public concern about global sustainability, therefore, the development of advanced new materials and technologies for sustainable bio-based products is critical. Widespread R&D activities have been conducted to develop polymeric materials from sustainable feedstock and replace their petrochemical counterparts. Rigid polyurethane (PU) foams are an inseparable part of the global polymer market as they are utilized in a wide range of applications, such as thermal insulation in civil engineering and appliance industry, structural material and impact absorption material in the automotive industry, structural and buoyancy material in the marine industry, etc. In this work polymer material sustainability challenge is answered by the development of high-quality rigid PU from various bio-based and recycled feedstocks. The properties of the developed materials are up to industry quality standards and ready for the next stage of technology upscale.

Presented Doctoral Thesis demonstrates the development of rigid PU foam materials from sustainable feedstock with several large scale applications. PU materials are obtained in the reaction between a polyisocyanate moiety containing isocyanate groups ($-NCO$) and a polyol component containing hydroxyl groups ($-OH$). Sustainable origin polyols are the most promising way of introducing “green” chemistry into PU materials. Previously studied bio-based polyols from tall oil (TO) and rapeseed oil (RO) have been utilized to develop high-density structural strength rigid PU foams applicable in the automotive industry. Furthermore, sustainable polyols derived from recycled polyethylene terephthalate (PET) side-stream were also investigated for the same application. The mechanical properties of the developed high-density rigid PU foam were further increased by the addition of montmorillonite nanoclay reinforcement filler. Materials with the most optimal properties were chosen for real scale automotive part development and testing.

In the frame of this Doctoral Thesis rigid PU foam, thermal insulation material from TO based polyol with the goal to reduce material’s flammability was also developed. It was concluded that it is possible to replace conventional potentially harmful halogenated flame retardants with intumescent expandable graphite flame retardant.

Lastly, during high-density rigid PU foam development it was discovered that bio-based polyols lack the functionality to obtain mechanically strong material, thus a new approach of high functionality bio-based polyol synthesis was investigated. The roadmap of presented Doctoral Thesis is depicted in Fig. 1 in which the work is split into three parts where the first part describes studies related to the automotive industry, the second part is related to the development of low flammability thermal insulation material, and the third part depicts improvement of rapeseed oil and tall oil polyol synthesis methods.

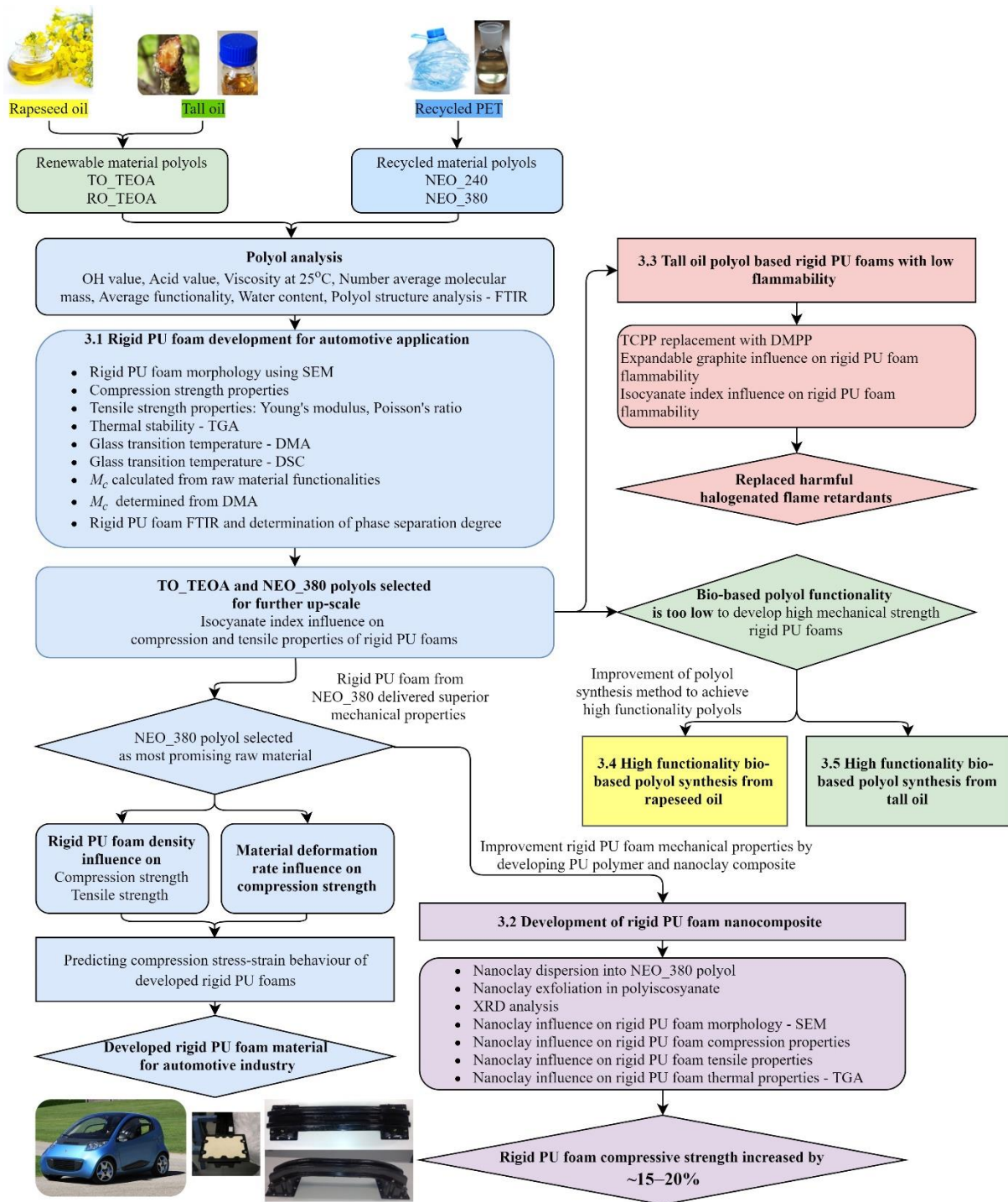


Figure 1. The workflow of Doctoral Thesis.

Aim of the doctoral thesis:

To develop rigid PU foam material from sustainable raw materials with increased mechanical properties and to develop novel polyol synthesis method from renewable materials available in Northern Europe.

Tasks of the Doctoral Thesis

1. To develop high-density rigid PU foam material from bio-based polyols.
2. To develop high-density rigid PU foam material from APP polyols obtained from recycled PET.
3. To test mechanical and thermal properties of the developed high-density rigid PU foams and assess their viability as impact absorption material for automotive industry applications.
4. To reinforce developed high-density rigid PU foams with montmorillonite nanoclay particles to increase the mechanical properties of the composite.
5. To develop low-density rigid PU foam as a thermal insulation material from renewable feedstock with low flammability characteristics by replacing harmful halogenated flame retardants with intumescent flame retardant alternative.
6. To develop a synthesis method for high functional bio-based polyols from RO and TOFA.

Thesis statements to be defended

1. APP polyols are more suited for structural high-density rigid PU production when compared to polyols obtained from TO and RO.
2. Montmorillonite nanoclay filler increases compression properties of rigid PU foams.
3. Halogenated flame retardants are not required to develop highly flame retardant rigid PU foam thermal insulation.
4. RO and TOFA are well suited for high functional bio-based polyol synthesis.

Scientific novelty

1. Demonstration of sustainable material viability for the development of structural engineering materials with high-performance requirements.
2. Replacement of halogenated flame retardants with more sustainable alternatives.
3. RO based high functionality polyol synthesis method has been developed by combining oxirane ring opening reaction with transesterification/transamidation reactions with polyfunctional alcohols, and synthesised polyols have been used for rigid PU foam thermal insulation material development
4. Development of TOFA epoxidation method using innovative heterogeneous phase catalysts such as ion exchange resin and immobilised Lipase enzyme.
5. TOFA epoxidation has been modelled using heterogeneous phase reaction model that can be used for synthesis parameter optimization.

Practical significance

1. Developed high-density rigid PU foam materials that can be applied as a structural material in various engineering solutions especially in the automotive industry.
2. Developed high-efficiency thermal insulation material from renewable raw materials with increased fire resistance performance, which is suitable for civil engineering applications.
3. Developed high functionality bio-based polyols can be applied as a crosslink reagent in various PU materials.

Approbation of PhD thesis in Scopus indexed articles

Paragraph 3.1

- **M. Kirpluks**, U. Cābulis, M. Kurańska, A. Prociak, Three Different Approaches for Polyol Synthesis from Rapeseed Oil, *Key Eng. Mater.* 559 (2013) 69–74. doi:10.4028/www.scientific.net/KEM.559.69.
- **M. Kirpluks**, U. Cabulis, A. Ivdre, M. Kuranska, M. Zieleniewska, M. Auguscik, Mechanical and Thermal Properties of High-Density Rigid Polyurethane Foams from Renewable Resources, *J. Renew. Mater.* 4 (2016) 86–100. doi:10.7569/JRM.2015.634132.
- **M. Kirpluks**, U. Cabulis, J. Andersons, G. Japins, K. Kalnins, Modeling the Effect of Foam Density and Strain Rate on the Compressive Response of Polyurethane Foams, *SAE Int. J. Mater. Manuf.* 11 (2018). doi:10.4271/05-11-02-0014.
- E. Cischino, Z. Vuluga, C.E. Ezeiza, I.L. Benito, E. Mangino, J. De Claville Christiansen, C.-G. Sanporean, F. Di Paolo, **M. Kirpluks**, P. Cabulis, A Concrete and Viable Example of Multimaterial Body: The Evolution Project Main Outcomes, in: *Procedia CIRP*, (2017) 300–305. doi:10.1016/j.procir.2017.03.292.
- **M. Kirpluks**, E. Cischino, U. Cabulis, J. Andersons, Rigid PUR foam impact absorption material obtained from sustainable resources, *AIP Conf. Proc.* (2019) 2139. doi.org/10.1063/1.5121686

Paragraph 3.2

- **M. Kirpluks**, L. Stiebra, A. Trubaca-Boginska, U. Cabulis, J. Andersons, Rigid closed-cell PUR foams containing polyols derived from renewable resources: The effect of polymer composition, foam density, and organoclay filler on their mechanical properties, in: K. Thakur, Vijay, M.K. Thakur, M.R. Kessler (Eds.), *Handb. Compos. from Renew. Mater.*, Scrivener Publishing LLC, 2017: pp. 313–339. doi:10.1002/9781119441632.ch31.
- U. Cabulis, **M. Kirpluks**, J. Andersons, The Effect of Montmorillonite Type Nanoparticles on Stiffness and Flammability of Rapeseed Oil Based Polyisocyanurate Foams, *Key Eng. Mater.* 559 (2013) 19–24. doi:10.4028/www.scientific.net/KEM.559.19.

Paragraph 3.3

- **M. Kirpluks**, U. Cabulis, V. Zeltins, L. Stiebra, A. Avots, Rigid Polyurethane Foam Thermal Insulation Protected with Mineral Intumescent Mat, *Autex Res. J.* 14 (2014) 259–269. doi:10.2478/aut-2014-0026.
- **M. Kirpluks**, U. Cabulis, A. Avots, Flammability of Bio-Based Rigid Polyurethane Foam as Sustainable Thermal Insulation Material, in: *Insul. Mater. Context Sustain., InTech*, 2016: p. 148. doi:DOI: 10.5772/61361.

Paragraph 3.4

- **M. Kirpluks**, D. Kalnbunde, Z. Walterova, U. Cabulis, Rapeseed Oil as Feedstock for High Functionality Polyol Synthesis, *J. Renew. Mater.* 5 (2017) 1–23. doi:10.7569/JRM.2017.634116.
- **M. Kirpluks**, D. Kalnbunde, H. Benes, U. Cabulis, Natural oil based highly functional polyols as feedstock for rigid polyurethane foam thermal insulation, *Ind. Crops Prod.* 122 (2018) 627–636. doi:10.1016/j.indcrop.2018.06.040.

Paragraph 3.5

- **M. Kirpluks**, E. Vanags, A. Abolins, A. Fridrihsone, U. Cabulis, Chemo-enzymatic oxidation of tall oil fatty acids as a precursor for further polyol production, *J. Clean. Prod.* 215 (2019) 390–398. doi:10.1016/j.jclepro.2018.12.323.

1. LITERATURE REVIEW

1.1. Polyurethane Foams in Brief

Polyurethane Material Chemistry

The main difference between polyurethane (PU) materials and other common polymers is that there is no urethane monomer. Typically the PU polymer is created in a chemical polycondensation reaction between polyisocyanate moiety containing isocyanate groups ($-NCO$) and a polyol component containing hydroxyl groups ($-OH$). This main chemical reaction is the foundation of the majority of the PU materials. However, the term “polyurethane” can be deceiving as it refers to the broad variety of different materials with different properties and applications. Polyurethanes can be soft or hard, flexible or rigid, thermoplastic or thermoset. Properties of the PU polymer matrix are derived from the chemical composition of raw materials used in the polymerization reaction. The length and the chemical nature of the moieties R_1 and R_2 depicted in Figure 1.1 play the most significant role on the properties of the final material [1].

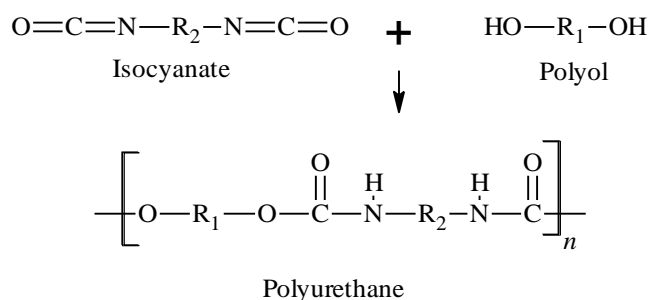


Figure 1.1. Generic urethane linkage reaction [1].

A general grasp of the raw material chemical structure influence on the characteristics of the PU materials is depicted in Figure 1.2. Thermoplastic PU materials can be obtained if the average functionality of polyols and isocyanate is selected as $f_n = 2$. Contrarily, if the average functionality of reactants is higher, more crosslinked polymer matrix will be obtained. A higher degree of branching or crosslinking will stiffen the matrix, thus more rigid, harder material will be obtained. The chains in-between the functional groups can be shorter, stiffer and/or with additional chemical interchain interaction which further stiffens overall polymer matrix. Aliphatic, as well as aromatic structure polyols and isocyanates, are utilized on an industrial scale to produce materials that we use in our modern everyday life. Due to the broad variety of PU polymer material properties, they can be found in different everyday applications such as coatings, adhesives, sealants, elastomers, rubbers, flexible PU foam in furniture, footwear and automotive industries and rigid PU foam as thermal insulation in an appliance and civil engineering applications as well as impact absorption material in sportswear and automotive sector.

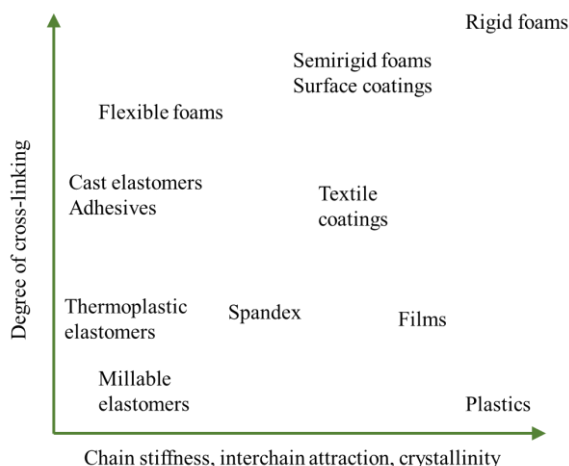


Figure 1.2. Structure-property relationship in polyurethanes [1].

Polyols

In general, polyols can be separated into two distinct groups polyether and polyester based polyols from which the vast majority produced are polyether type polyols [2]. Polyether-type polyols are obtained in an ethyl or propyl oxidation reactions by developing and extending glycol chains of starter alcohol. For rigid PU foam production, higher functionality polyols are necessary thus the starter alcohol also needs to have a high OH group functionality. Commonly glycerol with $f_n = 3$ and sorbitol $f_n = 6$ are among other glycols are used as a starter. Ethylene oxide and propylene oxide are obtained from ethylene and propylene oxidation which are a direct product of naphtha cracking process. From now on polyols obtained by propyl oxidation reaction will be referred as petrochemical origin polyols. Polyether-type polyol production scheme is depicted in Figure 1.3. By changing the starter type, reagent molar ratios and reaction conditions different molecular size glycols can be obtained. Polyol functionality and its molecular mass have a significant influence on the properties of the final material. The common characteristics of polyols that are used in PU material industry are as follows: OH value ($\text{mg}_{\text{KOH}}/\text{g}$), acid value ($\text{mg}_{\text{KOH}}/\text{g}$), viscosity ($\text{mPa}\cdot\text{s}$), number of average functionality – f_n , number of average molecular mass – M_n (Da or g/mol), and moisture content (wt. %).

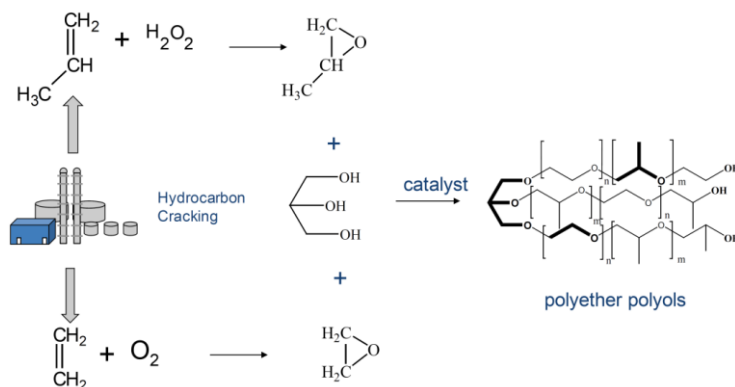


Figure 1.3. Petrochemical polyol production scheme [2].

Another type of common polyols – polyester polyols are mainly obtained in the polyesterification reaction as depicted in Figure 1.4. In PU material industry this type polyols are less common due to the more difficult production process and smaller flexibility in material formulation development. Polyester polyols take about a quarter of the total polyol market share. They are mainly applied in bulk goods industries with the well-established industrial processes, like sandwich panel production and pipe-in-pipe insulation production [2].

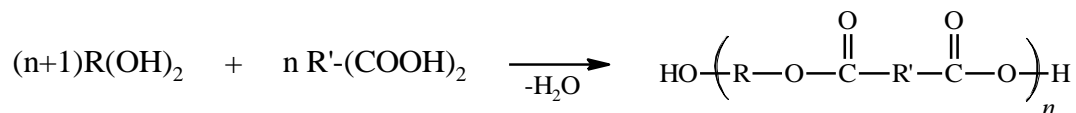


Figure 1.4. Polyester polyol production scheme [2].

The global polyol market size is expected to reach 45.17 billion USD by 2025 at an 8.5% annual growth rate during the forecast period, according to a report by Grand View Research, Inc. Polyols are expected to be applied in typical applications such as polyester resins as well as PU materials [3]. Nevertheless, there have been new developments in sustainable polyol production on an industrial scale from different bio-based feedstock as well as CO₂ based polyols [4,5]. Development of sustainable raw material origin and bio-based polyols is especially promising as their market share is expected to increase faster than common petrochemical polyol growth rate. The global *green* and bio-based polyol market was valued at 2.63 billion USD in 2015 and is projected to reach 4.71 billion USD by 2021 at a 9.5% annual growth rate. Some of the different types of sustainable origin polyols are explored in paragraph 1.2.

Polyisocyanate

PU material production would not be possible without other main polycondensation reaction component – polyisocyanate. Polyisocyanates are compounds that have at least two NCO groups in their chemical structure. The NCO group reacts with any active hydrogen, thus polyisocyanates are used for various polymer production technologies, such as polyurethanes, polyureas and polyamides. The chemical reaction of the isocyanate group with an “active hydrogen” is depicted in Figure 1.5. Isocyanate group can react with alcohols, water, carboxylic acids, amine, ureas, urethanes and amides. Furthermore, the NCO group can react with other NCO groups forming dimerization products or trimerization product – isocyanurate ring if the conditions are right. During the PU material production, several of mentioned reactions occur at the same time, thus the final polymer matrix is a copolymer with a varied chemical functionality which reflects on the material properties.

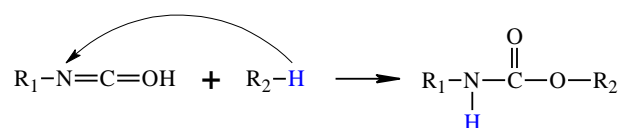


Figure 1.5. Isocyanate reaction with active hydrogen compounds [1].

For PU material industry the most important reaction is isocyanate reaction with OH groups as depicted in Figure 1.1. Another reaction especially important for rigid PU foam material

Structure and Reactivity Polyisocyanates

Aliphatic, as well as aromatic structure polyisocyanates, are employed in PU material industries. For different types of PU foams usually, aromatic type isocyanates are used, where toluene diisocyanate (TDI) is more common in flexible PU foam production, whereas methyl diphenyl diisocyanate (MDI) is used for rigid PU foam production. Both types of isocyanates have different isomers which are depicted in Figure 1.8. Furthermore, for rigid PU foams, MDI with the increased functionality is used which is achieved by polymerization of MDI.

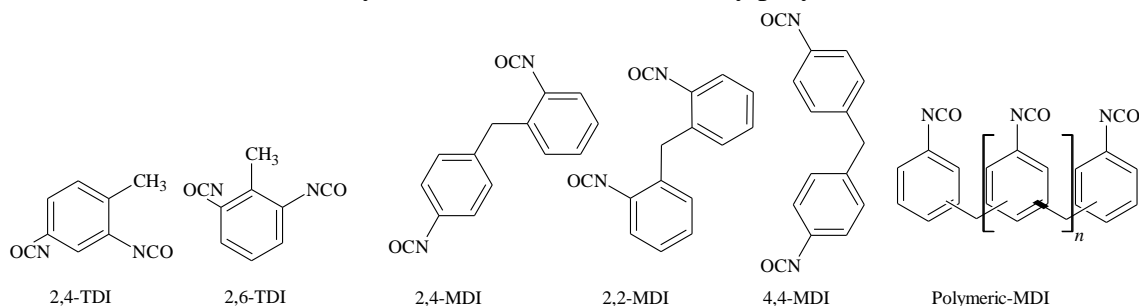


Figure 1.8. Chemical structure of different aromatic type isocyanates used for PU foam production [1]

Reactivity of Isocyanates

The structure of the compound with the active hydrogen atom significantly influences the reactivity with the NCO group thus impacting the technological process of the polymeric material development. All of the amines are much more reactive than the hydroxyl compounds. Primary hydroxyl groups are more reactive than secondary hydroxyl groups and much more reactive than tertiary or phenolic hydroxyl groups. The reactivity of NCO groups with different active hydrogen compounds is summarised in Table 1.1. The difference between different group reactivity with isocyanates must be taken into account when PU material formulation is developed.

Table 1.1. Reactivity of NCO groups with different active hydrogen compounds [2,11]

Active hydrogen compound	Functional groups	The relative reaction rate (non-catalyzed, at 25°C)
Primary aliphatic amine	R-NH ₂	1000
Secondary aliphatic amine	R ₂ -NH	200-500
Primary aromatic amine	Ar-NH ₂	2-3
Primary OH groups	R-CH ₂ -OH	1
Water	H ₂ O	1
Carboxylic acids	$\begin{array}{c} \text{O} \\ \parallel \\ \text{R}-\text{C}-\text{OH} \end{array}$	0.4
Secondary OH groups	$\begin{array}{c} \text{R} \\ \\ \text{R}-\text{CH}-\text{OH} \end{array}$	0.3
Urea groups	$\begin{array}{c} \text{O} \\ \parallel \\ \text{R}-\text{NH}-\text{C}-\text{NH}-\text{R}' \end{array}$	0.15
Tertiary OH groups	$\begin{array}{c} \text{R} \\ \\ \text{R}-\text{C}-\text{OH} \\ \\ \text{R} \end{array}$	0.005
Phenolic OH group	Ar-OH	0.001-0.005
Urethane group	$\begin{array}{c} \text{O} \\ \parallel \\ \text{R}-\text{NH}-\text{C}-\text{O}-\text{R}' \end{array}$	0.001

Chemical structure of different isocyanates also has an influence on the reactivity but not to the same level as the differences of the active hydrogen compound structures. Generally, aromatic isocyanates are more active than aliphatic structure isocyanates, among which TDI is slightly more reactive than MDI. Also, the reactivity of pMDI depends on the oligomerization degree [1].

Some isocyanates are classified as dangerous substances but not MDI. MDI is the least hazardous of the commonly available isocyanates. Nevertheless, exposure to MDI may cause skin irritation, difficulty breathing, or coughing. Further hazards may occur with contact with water. MDI is insoluble in water and the MDI and water reaction products are chemically inert [12]. Nevertheless, in the isocyanate reaction with water, CO₂ gas is released which can over pressurise the container vessel resulting in an explosion hazard. Besides, this reaction generates a relatively large amount of heat (47 kcal/mol) which can lead to further complications [7]. Main concerns regarding isocyanates come from their production process which will be described in the next paragraph.

Production of Isocyanates Applied for Rigid PU Foam Production

The most common method of preparing isocyanates involves aromatic or aliphatic amine reaction of with phosgene. The use of phosgene is exceedingly problematic considering that it has been historically used in chemical warfare. In the initial step of the amine and phosgene reaction N-substituted, carbamoyl chloride is produced. The reaction is highly exothermic and is followed by hydrogen chloride elimination. Typical phosgenation rout of MDI synthesis from petrochemical resources is depicted in Figure 1.9. Isolation of the desired isocyanate product is achieved by distillation at reduced pressure. Few alternative processes to the phosgenation rout have been developed where amine or nitro precursors are converted into isocyanates via the use of carboxylation agents. Unfortunately, they have not been implemented on an industrial scale.

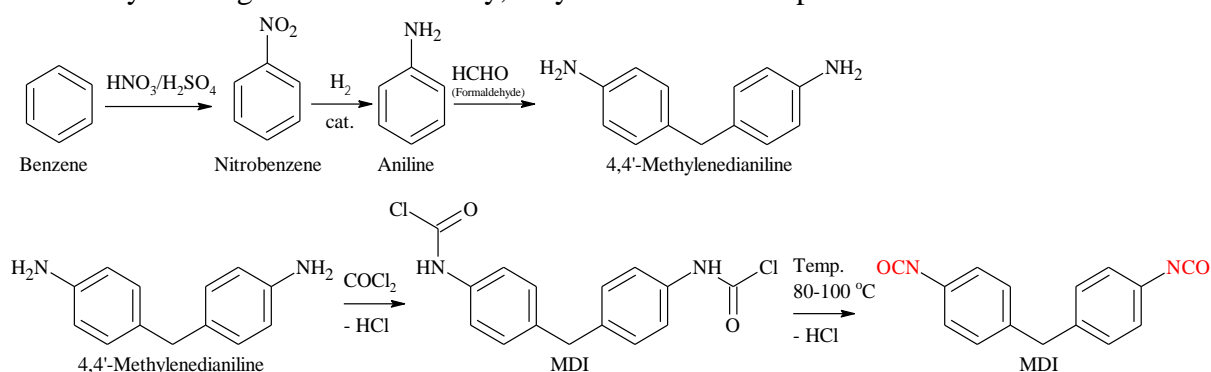


Figure 1.9. MDI manufacturing process [1]

1.2. Sustainable Polyol Development

21st is the Bioeconomy century where a great deal of effort, research and investment will be devoted to moving towards post-petroleum society. The development of advanced new materials and technologies of bio-based products is critical [13,14]. Widespread R&D activities have been conducted to develop bio-based polymeric materials and replace their petrochemical

counterparts [15]. Bio-based polyols are the most perspective way how to introduce sustainable feedstock into PU materials.

Plant oils have been considered as an alternative resource for the production of polymeric materials and have been extensively studied. By modifying plant oils, it is possible to obtain a large variety of monomers and polymers [16–18]. Although there has already been major progress, the potential of the available bio-resources in value-added sectors still needs to be maximised, and new approaches through the more complete deployment of the twelve Principles of Green Chemistry have to be delivered [19].

The global plant oil production over the last 50 years has shown a steady increase from about 23 Mt (Megaton) in 1967 to 208 Mt in 2019. Palm oil production has risen from 2 Mt in 1967 (then the 6th largest) to become the largest oil crop in 2019 with 76 Mt oil produced. Palm oil is mainly used for general food consumption. Soybean's oil production has shown an increase from 5 Mt in 1967 to 58 Mt in 2019 and now its production is the second largest in the world. Rapeseed (*Brassica napus*) is a widely cultivated crop around the world mainly due to its oil-rich seeds. In 2019, the production of rapeseed oil (RO) reached 28 Mt which is the third largest amount [20,21]. In the European Union, the changes in biofuels policy led to the decreasing use of RO for biodiesel production. Nevertheless, the European Union's consumption of RO was 9.5 Mt in 2019, from which 69.1% were used for industrial products (biodiesel, lubricants, etc.), 30.4% for domestic food consumption and 0.5% as a feed [22,23].

The main feedstock for bio-based polyol production are different natural oils, like soybean oil, palm oil, sunflower oil, corn, oil, linseed oil, olive oil, castor oil, etc. as well as animal origin oils, like fish oil [2,18]. All natural oils, except for castor oil, have to be chemically modified before they can be used for PU material production as they do not contain hydroxyl groups. A generic triglyceride structure of the natural oils is depicted in Figure 1.10. [24–26]. Two approaches for polyol synthesis from vegetable oils can be distinguished, modification of double bonds of the unsaturated fatty acids and transesterification of triglyceride backbone [27].

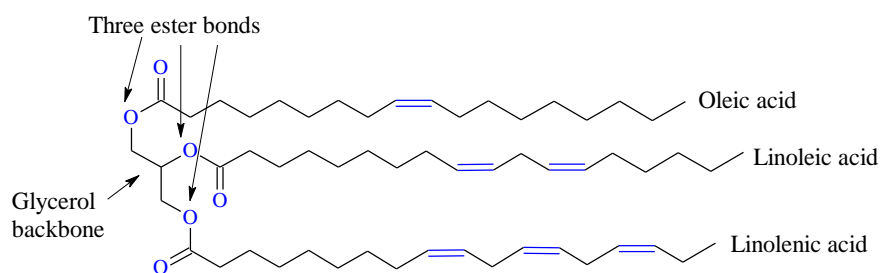


Figure 1.10. The generic structure of vegetable oil containing oleic, linoleic and linolenic acid chains.

Epoxidation and Epoxy Ring Opening of Natural Oils

Plant oil double bond epoxidation has attracted a lot of attention, as chemical reaction yields epoxides that are easily convertible intermediates and have a wide commercial use because of their varied chemical activity. Epoxides have been used as raw materials for products such as alcohols, glycols, plasticizers, high-temperature lubricants, polyols and polymers e.g., polyurethane, polyesters and epoxy resins [28,29]. The polyol production from epoxidized

vegetable oils is already a well-studied topic. Various epoxidation methods of different kind of plant oils such as soybean [30], palm, canola [31–33], castor [34], jatropha [35,36], wild safflower [37] and others [38–41] have been reported. The most widely used method in above-mentioned studies is triglyceride or fatty acid methyl ester epoxidation with *in-situ* formed peroxy-carboxylic acid, such as performic or peracetic acids, in the presence of a strongly acidic catalyst. The main disadvantage of the chemical epoxidation method is the acid-catalyzed side-reaction occurrence with oxirane rings, which leads to the formation of by-products [42]. Furthermore, the use of additional acid as an oxygen carrier means that it has to be separated from the reaction media after oil epoxidation, which, along with the use of hazardous chemicals, is not desired from the viewpoint of Green chemistry. The use of performic or peracetic acids in the epoxidation process could lead to the thermal runaway of the reaction which is highly undesired for an industrial upscale and due to safety concerns [43–45].

In recent times, various chemo-enzymatic catalysis reactions have been studied as a more sustainable approach to conventional chemical catalysis methods. One of the fields is double-bond epoxidation using a Lipase enzyme to catalyze the peroxy-carboxylic acid *in-situ* formation. The method is considered to be milder and more selective than traditional acid catalyzed *in-situ* epoxidation methods [42,46]. The most effective lipase for unsaturated bond epoxidation has shown to be *Candida Antarctica* Lipase B (Novozym® 435 – immobilized Lipase enzyme on acrylic resin beads) [47]. The main advantages of the enzyme-catalyzed epoxidation are relatively low epoxidation temperatures (30–50 °C) in comparison to chemical epoxidation at 60–100 °C, high selectivity and epoxidation conversion rate (exceeding 90 %), and reusability of the enzyme [48,49]. Furthermore, it has been reported that Lipase can catalyze a formation of fatty acid peracids, such as perstearic [50,51] and peroleic [52], which allows avoiding the use of formic and acetic acid in the epoxidation process. Although the possibility to use Lipase as a catalyst for epoxidation has been known for a while, there have been relatively few investigations into the synthesis of polyols to be further used in polyurethane production.

Structure of the acyl donor has a significant influence on the selectivity of chemo-enzymatic epoxidation of fatty acid derivatives as well as oxirane oxygen yield. Generally, higher molecular mass (C4–C18) linear alkyl chain carboxyl acids are preferred [53]. Furthermore, the rate of epoxidation is strongly dependent on the saturation degree of the carboxylic acids due to steric hindrance of molecules. Lu et al. demonstrated that saturated stearic(C_{18:0}) acid delivered 1.3, 1.5, and 2.1 times higher yields of epoxy oxygen than oleic(C_{18:1}), linoleic (C_{18:2}) and linolenic(C_{18:3}) acids respectively in chemo-enzymatic epoxidation of soybean oil methyl esters [54]. The reaction medium also influences the yields of the desired product. Enzyme catalyst activity is strongly affected by the choice of organic solvent. Non-polar solvents are preferred, although no linear correlation between the polarity of the solvent and the degree of conversion has been found [49,53,55]. Promising technology is the application of ionic liquids in the enzymatic epoxidation of fatty acid methyl esters where relative conversion to oxirane up to 89% has been achieved [56]. In this process ionic liquids act as reservoirs for the substrate and products, this decreases the substrate and product inhibition by water [55]. The benefits of using organic solvents or other components in the epoxidation process must be counterweighted

to the environmental impact derived from their production and utilization. The ideally designed process must be as simple as possible employing as little raw resources as possible. Yields of 83% for relative conversion to oxirane have been reported in a solvent-free chemo-enzymatic epoxidation of *Sapindus mukurossi* fatty acids [57]. As such, solvent-free approach delivers viable product bypassing the need for additional resources and materials.

Most frequently epoxidation with in-situ generated peroxy acid and subsequent epoxy ring opening reaction with haloacids or alcohols is used to functionalize unsaturated fatty acids [2,18,27] into polyols. The reagent used in the epoxy ring opening has the largest influence on the properties of the polyol and final PU material. Polyols with secondary OH groups and lower average functionality ($f_n=2-3$) are more suitable for elastomer and flexible PU foam production [1,58,59]. Polyols obtained from epoxy group opening with diethylenglycol (DEG) are more suitable for rigid PU foam production as they deliver higher functionality, $f_n=3-5$ [1,60,61]. Such polyols have primary and secondary hydroxyl groups in their structure. Primary hydroxyl groups are more reactive with isocyanate which makes them more useful for spray-applied rigid PU foam formulations [62,63].

Transesterification of Natural Oils

Another approach to obtain polyols from natural oils is to carry out transesterification of the ester bonds of fatty acid triglycerides using different polyfunctional alcohols. The most frequently used alcohol is glycerol (see Figure 1.11.), but several drawbacks have been reported, like low selectivity towards mono-glyceride products, separation of mono-glyceride from other reaction products which is an energy-intensive process, neutralization of homogeneous phase catalysts and high temperature requirements of the synthesis process [64,65]. The main application of such fatty acid mono-glycerides is as non-ionic surfactant used as emulsifiers in the food, detergents and cosmetics industries. Nevertheless, their application as a polyol for PU material production has also been reported [27,66,67]. Rigid PU foams produced from palm oil polyol which was obtained in the transesterification process with glycerol showed a comprehensive decrease in mechanical and thermal properties [68]. Better rigid PU foam characteristics were obtained when polyol was synthesized from glycerol polymerization and esterification of castor oil. Polyols were characterised with high functionality which delivered an increase in mechanical properties of rigid PU foam, excellent PU foam cell morphology and up to industry standard thermal conductivity of 0.0218 W/m·K [69].

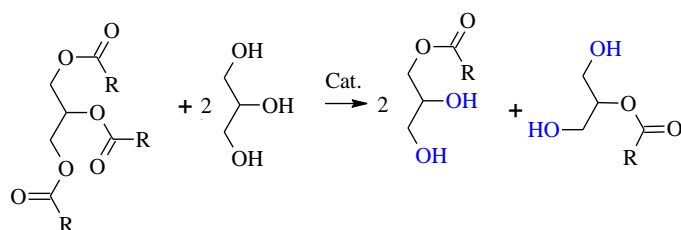


Figure 1.11. Overall simplified scheme of fatty glycerolysis [72].

Other reagents such as pentaerythritol [70] and triethanolamine (TEOA) [26] (See Figure 1.12.) have been used for natural oil transesterification aiming to obtain polyols bearing uniquely more reactive primary hydroxyl groups, such as polyols obtained from RO transesterification reaction with TEOA. They showed the potential to be used in rigid PIR foams as their flammability and mechanical characteristic improved with the increase of isocyanate index [71,72]. The replacement of petrochemical polyether-based polyols with RO based polyols showed a beneficial influence on the heat-insulating properties and significantly reduced water absorption [73]. Such polyols were used not only for the production of rigid PU foams but also for the development of spray-applied coatings [74].

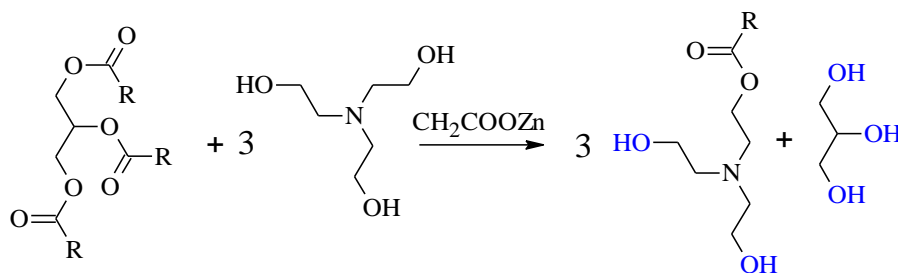


Figure 1.12. Idealised natural oil transesterification with TEOA [77].

In a similar method to TEOA, the diethanolamine (DEOA) can be used to obtain polyols from RO and other natural oils as shown in Figure 1.13. Such polyols have been successfully used for PU coating and rigid PU foam development [75]. Rigid PU foams from linseed oil polyols obtained in transamidation with DEOA showed low dimensional stability which limits their application on an industrial scale [76]. Similar polyols have been reported in phthalic anhydride resin coating application [77] and polyesteramide resins [78]. Although transamidation process provides a simple and cheap polyol synthesis method, the low functionality of the produced polyol limits its application on an industrial scale.

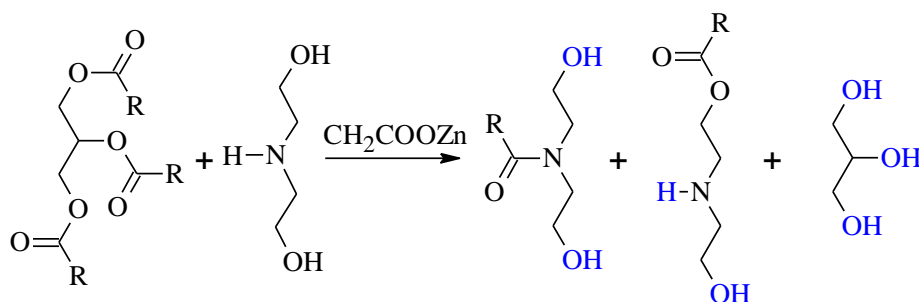


Figure 1.13. Idealised natural oil transamidation with diethanolamine [27,79].

Wood Biomass Derived Polyols

Another potential feedstock for bio-based polyol production is wood biomass which has attracted the attention of researchers as it is considered a second-generation bio-based raw material. Wood biomass contains a variety of potentially useful chemicals. Historically, the main value-added product derived from wood biomass is cellulose which is used in the paper production. The cellulose and hemicellulose fraction of the wood biomass attributes to 56 – 64 wt.% whereas other constituents like lignin and extractives account for 27–35 wt.% and

4–14 wt.% respectively [79]. After cellulose extraction, a considerable part of wood biomass is left unused which entails a positive sustainability impact if a side stream is used to develop value-added products.

Lignin Application in PU Materials

Lignin is considered as a type of bio-polymer with the highly varied chemical structure depending on the type and species of biomass feedstock as well as extraction process. In the wood material, it works as a type of glue holding together cellulose fibres enhancing the rigidity. Native lignin is a high molecular weight biopolymer composed of phenyl propanol units [80]. Various routes of lignin depolymerisation have been used to obtain lignin-based polyols. Moreover, other methods of lignin liquefaction like glycolysis, oxypropylation and hydrolysis among others have been used to obtain polyols suitable for rigid PU foam development [81].

PU foams require polyols to be in a liquid state to ensure the foaming process as well as the formation of the distinct foamed morphology of the material. Liquefied lignin via glycolysis process has been used to produce flexible PU foams applicable for furniture and automotive industries [82]. Nevertheless, liquefied lignin obtained via oxypropylation method seems to be more suitable for both, rigid as well as flexible PU foams [80,83,84].

Lignin has been also used as a solid filler in PU material development. At increased temperature lignin even works as crosslink reagent and is incorporated into PU polymer chain with a covalent bond [85]. It is possible to introduce up to 10 wt.% of solid lignin particles into flexible PU foams despite hindering of the foaming process [86]. Lignin also has been used as a filler for different rigid PU foams with varied success rate. Some authors claim that lignin in solid form works as a polyol reacting with pMDI during the rigid PU foam foaming process [87]. Nevertheless, it is not certain that the reactivity of OH groups of lignin is high enough to compete with other OH groups present in PU foam formulation. A.N. Hayati et.al. demonstrated a more appropriate way where the OH value of the polyol and lignin mixture was measured, instead of taking into account OH values of the separate polyol constituents. Analysed OH value was used in rigid PU foam formulation development. Obtained rigid PU foams showed a marginal increase of the thermal conductivity and compression strength. Nevertheless, the bio-based content of developed rigid PU foams was increased by the addition of 10 wt.% of lignin and potential commercial effect could be achieved assuming that lignin is a cheap raw material [88]. The reactivity of the lignin could be improved by lignin solvent fractionation where more pure material is obtained. PU films where lignin solvent separated fractions were used as a crosslinking reagent delivered increased Young's modulus as well as increased glass transition temperature [89]. Another, way how to improve the incorporation of lignin into PU polymer matrix is to carry out a pre-treatment of lignin functional groups [90]. The pre-polymerization of lignin with pMDI resulted in the development of good quality rigid PU foams with lignin content up to 30 wt.% [91].

The development of lignin-based polyols as well as lignin incorporation into bio-based composite materials seems to be an ongoing endeavour. Although, the upscale of proposed technologies to commercial production has not yet occurred the future is promising as more

companies start to focus on innovations in bio-economy. Most commendable is the 43 million EUR investment of BBI JU and Graanul Invest in developing bio-fractionation flagship plant in Estonia, which promises to turn sustainable hardwood residues into high purity intermediate building blocks of cellulosic sugars and high-quality lignin [92].

Tall Oil as PU Material Feedstock

Crude tall oil is a material which is generated in the wood pulp production process. The word ‘tall’ is means ‘pine’ in Swedish, which indicates that crude tall oil is mainly generated in the pulping of softwood (pine) trees. During cellulose Kraft pulping process a side stream of black liquor is produced which consists of lignin fraction, hemicellulose extractives and other inorganic substances. Black liquor contains valuable chemicals that are fed back into the pulping process. In order to do this, first, a layer of soap is removed, called crude sulphate soap. It can either be burned as process fuel or further processed into crude tall oil [93,94].

Crude tall oil is characterized as a viscous dark brown liquid with distinct ill-smelling aroma prior to refining. The typical chemical compositions of crude tall oil are 38–53 wt.% fatty acids, 38–53 wt.% rosin acids and 6.5–20 wt.% unsaponified (neutral) compounds [94]. For PU material development fatty and rosin acids are most interesting, especially fatty acids as their chemical structure bears similarity to other vegetable oils. During crude tall oil purification rosin acids, fatty acids, as well as distilled tall oil fractions, are separated. The main fatty acids in the crude tall oil are oleic and linoleic, whereas main rosin acid is abietic acid, but other acids such as pimaric acid are also found. Chemical structure of the carboxylic acids found in tall oil is depicted in Figure 1.14. The chemical composition is dependent on the species of the biomass used in the pulping process. The purified products are used in various industries as follows: *tall oil rosin* – adhesives, printing ink, rubber emulsifier; *distilled tall oil* – metalworking fluid; *tall oil fatty acids* (TOFA) – fuel additive, alkyd resins, dimer acids; *tall oil pitch and heads* mainly as process fuel in distillery [93].

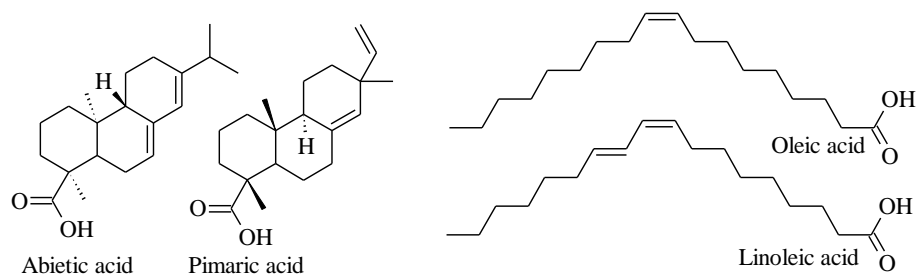


Figure 1.14. Chemical structure of rosin and fatty acids found in tall oil [97].

Crude tall oil is relatively available feedstock with a potential supply of 2.6 Mt from which about 0.85 Mt is not valorised. Moreover, crude tall oil is a relatively cheap raw material with prices ranging from 320-550 €/t [93]. The purification of crude tall oil into TOFA and distilled tall oil will add to the price of the raw material, but it will be still comparable to other vegetable oils. Despite the chemical structure similarity with other vegetable oils, application of different tall oil fractions in PU materials has not been widely studied. Tall oil fractions have been mainly used for biodiesel production [95]. It was found that tall oil does not give any additional carbon

or energy benefit over bio-diesel derived from other vegetable oil [96]. Thus refined tall oil application in polymer material industry is more appropriate as it is high-quality raw material.

Researchers from LS IWC have studied tall oil as a potential feedstock for rigid PU foam development for more than 30 years and have developed two main polyol synthesis methods. They are, amidation and esterification reactions with DEOA and TEOA respectively where obtained polyols are amides/esters of respective alcohols (TO_DEOA and TO_TEOA). The process is similar to transamidation and transesterification of RO described before. Obtained polyols have similar characteristics because the chemical structure of the polyols is also similar to RO based polyols. Crude tall oil, as well as TOFA, has been used to produce polyols suitable for rigid PU foam thermal insulation development [97]. TO_TEOA polyol has been used as a chain extender in PU elastomer development which resulted in a copolymer with better thermal stability [98]. The same polyol was used as a base polyol for fire retardant wood varnish coating development [99,100]. TO_DEOA polyol also has been used as a chain extender in PU elastomer development, but developed material had only a slight increase of the thermal stability [101]. Moreover, good quality rigid PU foam thermal insulation has been developed from the TO_DEOA polyol [102]. A somewhat unusual application of TO_DEOA polyol based rigid PU foams was in the development of support matrix for lignin-degrading microorganisms. The developed composite could sustain the growth of *Phanerochaete flavido-alba*, which is a fungus. The idea was to immobilise microorganisms for easier enzyme production and obtained results were promising [103].

Most importantly the two functional sites – carboxylic group and ethylenic unsaturation of TOFA makes it useful for the development of high functionality polyols. Furthermore, because TOFA is a mixture of free fatty acids it is possible to carry out chemo-enzymatic epoxidation without using additional carboxylic acids [104]. Obtained epoxidised tall oil fatty acids (ETOFA) can be used to produce high functionality polyols and bio-based surfactants [105]. Also, ETOFA was used as a binder for plaster type insulation applicable in building walls [106]. Different ETOFA synthesis routes are explored in the frame of this thesis (see Paragraphs 3.5).

Bio-polyols Produced on an Industrial Scale

Several bio-based polyols have already been upscaled to industrial production, like Cargill™ - soybean oil-based polyol [107], Lupranol Balance ® 50 - castor oil-based polyol [108], Novocard XFN resins - cashew nutshell oil-based polyol [109] among others. The majority of these polyols are used for the production of flexible PU foams due to the relatively high cost of bio-based polyols and higher margins of the end product. To enter into the market of rigid PU foam thermal insulation the polyol has to offer equivalent or better properties at the same or lower price than the petrochemical alternative. For spray applied rigid PU foams higher functional polyols with primary hydroxyl groups have to be developed.

A combination of epoxy ring opening and transesterification of fatty acid triglycerides could lead to higher polyol functionality which would ensure high crosslink density of PU matrix resulting in a rigid PU foam with increased mechanical properties, good dimensional stability and high ageing stability. This is investigated in Paragraphs 3.4 and 3.5 of the presented thesis.

A similar idea was explored to obtain water-soluble soybean oil-based polyols. Although polyol molecular weight was 3800–5900 Da and reported structure had plenty of primary OH groups, no PU materials were obtained [110].

PET Glycolysis

Another way how to replace petrochemical resources in PU foams is to use recycled materials. PET is one of the versatile engineering plastics which is used to manufacture textiles and bottles, as well as packaging, photographic films, video and audio tapes. A side stream of PET production, as well as post, consumed PET can be recycled to produce aromatic polyester polyols (APP) [111]. Somewhat similar to lignin, PET can be depolymerised using glycolysis method with different alcohols, such as ethylene or diethylene glycol (DEG) [112–114]. PET glycolysis with DEG is depicted in Figure 1.15 [112]. Different polymer/oligomer molecular size fractions can be obtained changing the glycolysis time and reaction conditions. Depolymerised PET then can be reused in successful replacement for one of the glycols in the alkyd [115], polyester or PU resins [116].

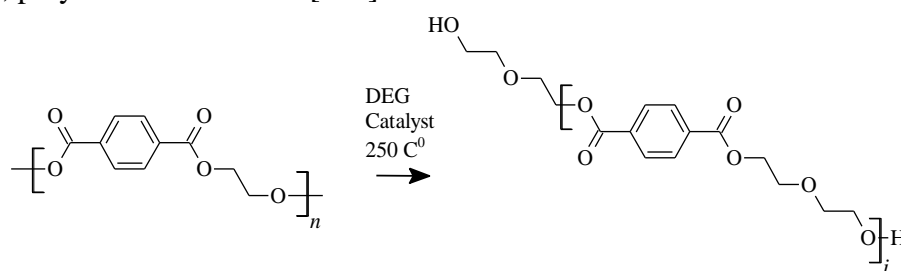


Figure 1.15. Glycolysis of PET.

The usual issue in PU foam formulations with the APP polyols is their compatibility with non-polar blowing agents like *n*-pentane, *n*-pentane and some hydrofluorocarbons. This can be solved by introducing non-polar segments into APP structure, such as vegetable oil fatty acid derivatives. Post consumed PET transesterification with castor oil was successfully achieved in the presence of zinc acetate catalyst [117]. The transesterification of PET was also done by using RO_TEOA based polyols from which good quality rigid PU foams were developed with prolonged ageing stability [118,119]. Added fatty acid moieties into polyol structure insured good compatibility with Solkane 365/227 – hydrofluorocarbon based blowing agent which was the main reason why excellent quality rigid PU foam were obtained [120]. In a similar way to RO_TEOA based polyols also TO_TEOA based polyols can be used for PET transesterification [121]. APP polyols obtained from recycled PET industrial side-stream or post-consumed waste have been successfully applied in a good quality rigid PU foam development.

1.3. Rigid PU Foam Flammability

One of the major disadvantages of rigid PU foams is their low thermal resistance, high flammability and high smoke production when burning. PU foams based on petrochemical and bio-based polyols are ignitable and can be an additional fuel source in the case of a fire disaster. This is a serious concern and restricts the PU material application [122]. The limiting oxygen

index (LOI) is the minimum concentration of oxygen in material surroundings that will support combustion of a polymer. It is measured by passing a mixture of oxygen and nitrogen over a burning specimen, and reducing the oxygen level until a critical level is reached. The LOI of non-modified PU foams is in the range of 18-20 [122–124]. Highly porous lightweight combustible foams tend to have a fast flame-spread and a high heat emission. The increasing demand for PU foams is the reason why many studies are devoted to fire retardancy [125,126].

An improvement in the thermal stability of PU foams may be achieved through the introduction of isocyanate trimerization structures into the PU matrix [71], the so-called PIR foams. The trimerization reaction of isocyanate groups is shown in Figure 1.7. Isocyanurates, from a thermodynamic point of view, are more thermally stable than urethane bonds (urethane dissociates at approx. 200 °C as opposed to 350 °C for polyisocyanurates). The thermal stability of functional moieties of isocyanate-based polymers is in the following order: isocyanurate (350 °C) > urea (250 °C) > urethane (200 °C) > biuret (135-140 °C) > allophanate (106 °C) [9,125].

PIR foams have higher fire retardancy but their broader use is limited due to price and technological difficulties. PIR foams are obtained in a large excess of isocyanate: 4-6 moles of isocyanate groups to every OH group [127]. Increased pMDI amount leads to more complicated processing equipment as the volume ratios of components are not equal. Furthermore, the isocyanate trimerization reaction occurs only at the increased temperature of the reaction mixture. Thus, PIR thermal insulation production via in-situ spray foaming is difficult and rarely used commercially [9].

Flame Retardants – Expandable Graphite

The usual solution to decrease the flammability of material is by adding different flame-retardants (FR). FR are compounds that are designed to prevent or slow the ignition of the material and/or to reduce the flame spread. Usually, they contain halogen, phosphorus or nitrogen moieties in their chemical structure. The most common and most effective FRs are so-called halogenated FRs, which have significant health risks associated with them. The main health hazards of halogenated FR are volatile compound emission from materials and toxic and hazardous gases released during the burning process [128,129]. In May 2001, the EU signed the Stockholm Convention that aims to ban organo-halogen chemicals (this includes several flame-retardants) globally. Rigid PU foam thermal insulation materials need to comply with flammability class E according to EN 13501 - fire classification of construction products and building elements standard. This is hard to achieve without using FR. Thus scientific community has put considerable efforts to find a replacement for halogenated FR in rigid PU foams.

Intumescent halogen-free FRs can be good substitutes for halogenated ones due to the formation of a protecting char layer that covers the surface of a material and limits the amount of heat reaching the polymer, slowing down the thermal degradation of the material. Furthermore, the protective char layer decreases the transition of volatile compounds into the gas phase, thus reducing the amount of fuel in the gas phase and decreasing the emitted heat of

the fire [130,131]. Moreover, the intumescent layer makes a thermal barrier, protecting the foam core from high temperature and is used as a smoke suppressant [132,133]. Expandable graphite (EG) can be used as a good substitute for halogenated liquid FR in rigid PU/PIR foams [134,135].

EG has a special graphite flake structure, i.e. stacked layers of hexagonal sp^2 hybridized carbon structures. Intercalated EG with H_2SO_4 is shown in Figure 1.16. EG material can be treated with sulphuric acid, nitric acid or acetic acid, which are intercalated into the graphite crystalline structure between carbon flakes. When heat is applied the acid releases gas that expand or exfoliate the graphite particles.

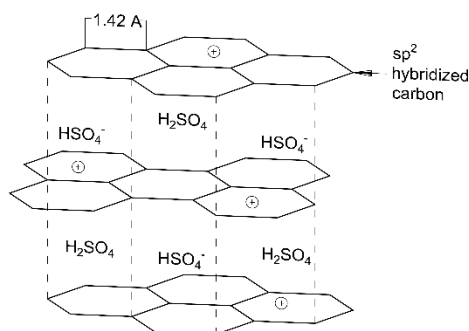
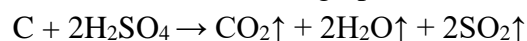


Figure 1.16. Generic structure of EG intercalated with H_2SO_4 [135].

High temperatures cause the oxidation of graphite in the following reaction with H_2SO_4 :



The released gases cause the expansion of graphite, which acts as a physical barrier for the heat and mass transfer from and into polymer material [136]. Volatile compound reduction in gas phase means less fuel for the burning process. Also, limiting the heat transfer to material means longer degradation of the polymer matrix, which in result limits the volatile compound release. Ultimately, the carbon char layer prevents the PU/PIR foams from burning [137,138]. An additional benefit of such FR is the reduction of smoke as the protective char layer also stops particulate escape into the airflow.

EG keeps most of the natural graphite attributes, such as low price and high porosity, making it very useful as functional carbon materials that can be applied in various fields of the polymer industry as FR [139]. EG addition with loads over 20 wt.% into rigid PU foams with an apparent density of 35 kg/m^3 gives a significant improvement in the fire resistance of the materials [140]. Nevertheless, EG as an FR is most effective at slightly higher rigid PU/PIR foam apparent densities, up to 100 kg/m^3 [129,133]. For some rigid PU/PIR foams the addition of 10 wt.% resulted in an increase of LOI from 19.2 to 31.8 and decrease of the peak of heat release rate in cone calorimeter test from 200 to 101 kW/m^2 [123]. Even for structural high-density rigid PU foam EG showed a significant decrease of flammability properties while only slightly decreasing mechanical properties [141]. The size of EG particles influences the flame retardant efficiency. EG particles of a smaller size did not produce enough char to cover the whole surface of the burning sample, resulting in a poor flame retardant properties of rigid PU/PIR foams [142].

Although EG can replace halogenated FR and significantly decrease the flammability of polymer materials, there is a crucial drawback regarding thermal insulation materials. Graphite is an excellent heat conductor, so with the addition of EG into PU/PIR foams, the thermal conductivity of the material rises, which is a highly undesired property for thermal insulation material [142]. To avoid the above-mentioned disadvantages, intumescent fabric (IF - non-woven glass fibre filled with EG) can be used as an FR solution. Recently, several researchers have investigated the fire behaviour of the foam/fabric combination [143,144] using a cone calorimeter, but it was done only for flexible PU foams. The idea was to test the fire behaviour of mattresses for automotive and furniture cushions. The results have shown that such fabric is a viable flame-retardant solution. Another, approach to reduce the effect of EG on the increase of the thermal conductivity of rigid PU/PIR foams is to reduce the distribution of the EG particles in the polymer mass. This was achieved by initial encapsulation of EG particles in melamine-formaldehyde resin microcapsules [145–147]. To sum up EG seems highly effective replacement for halogenated FR in rigid PU/PIR foams.

2. MATERIALS AND METHODS

2.1. High-density Rigid PU Foam Development from Sustainable Raw Materials

Polyols from Sustainable Raw Materials Used for Rigid PU Foam Development

This study is a direct continuation of M. Kirpluks master thesis where several bio-based polyol synthesis methods were developed. Furthermore, the Doctoral Thesis was carried out in a frame of several EU funded research projects. As such, the development of sustainable rigid PU foam material was based on different bio-based polyols as well as polyols obtained from recycled raw material – PET. In the frame of Doctoral Thesis, the synthesis of the bio-based / recycled polyols was not covered, because it was based in earlier work. The synthesis of bio-based polyol from rapeseed oil is depicted in Figure 2.1 and the synthesis of bio-based polyol from tall oil is depicted in Figure 2.2. The characteristics of used polyols from sustainable raw materials are described in Chapter 3.1. Materials used for polyol synthesis and analysis are summarised in Table 2.1.

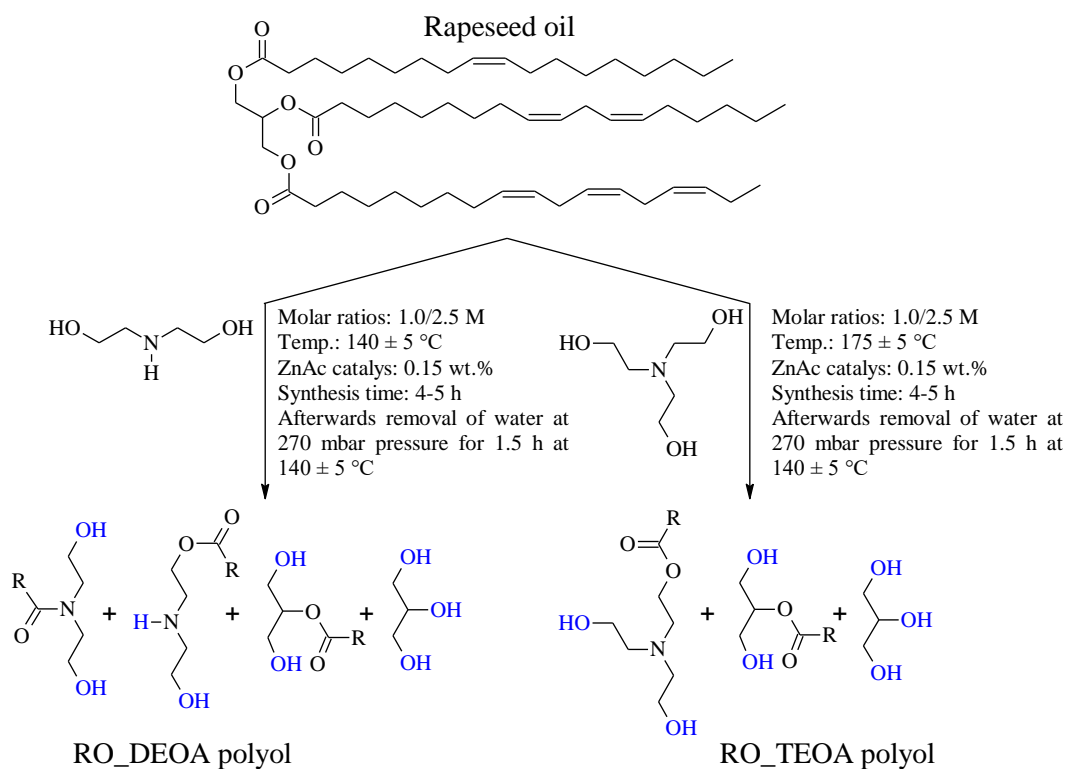


Figure 2.1. Synthesis of bio-based polyol from rapeseed oil by transamidation and transesterification methods

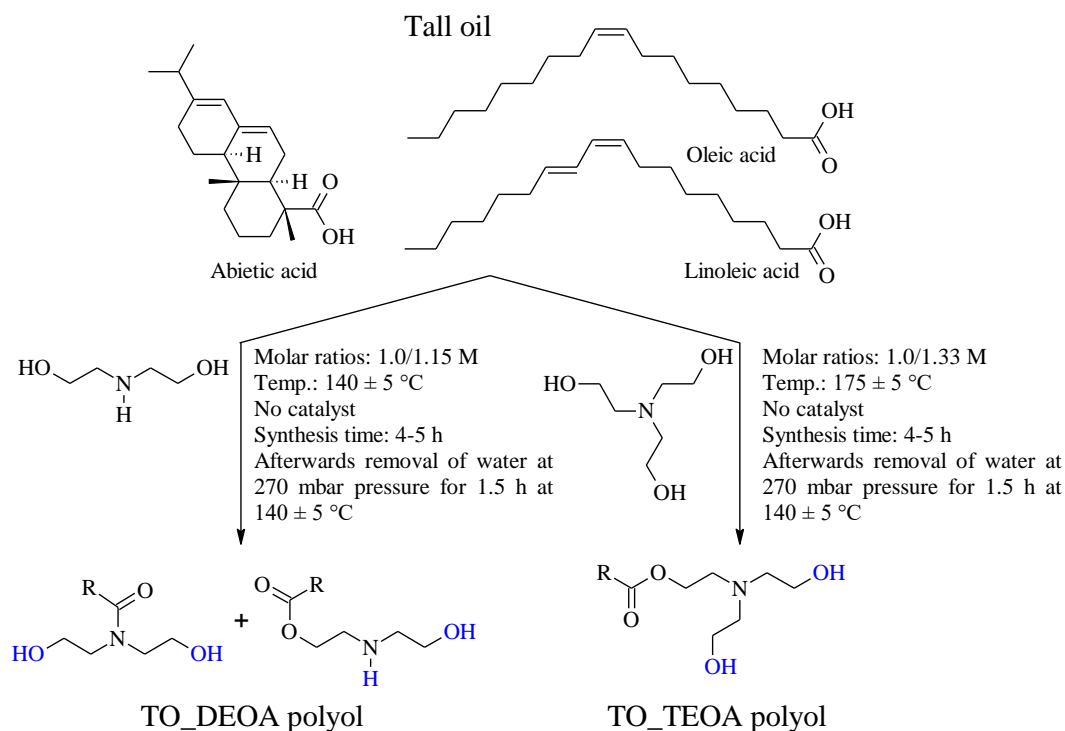


Figure 2.2. Synthesis of bio-based polyol from tall oil by amidation and esterification methods

Table 2.1

Materials for Bio-polyol synthesis and analysis

Material	CAS number	Characteristics	Producer
Rapeseed oil (RO)	8002-13-9	Iodine value = 117 I ₂ mg/100 g sample Acid value = 2.1 mg KOH/g, Saponification value = 192 mg KOH/g Fatty acid composition: 62 % oleic acid, 21 % linoleic acid, 11% linolenic acid, and 6% of saturated fatty acids.	Iecavnieks & Co Ltd. Latvia.
Distilled tall oil (TO) tradename "FOR-20"	8002-26-4	Fatty acid content – 79-81% Rosin acid content – 19-21% Unsaponifiables content - 3%	Forchem OY, Finland.
Distilled tall oil fatty acids (TOFA) tradename "FOR-2"	61790-12-3	Fatty acid content: > 96% Rosin acid content: max. 2.1% Unsaponifiables content: max 2%	Forchem OY, Finland.
Diethanolamine (DEOA)	111-42-2	Reagent grade, 99.2%	Huntsman, the Netherlands
Triethanolamine (TEOA)	102-71-6	Reagent grade, 99.2%	Huntsman, the Netherlands
Diethylene glycol (DEG)	111-46-6	ReagentPlus®, 99%	Sigma-Aldrich
Glacial acetic acid	64-19-7	Glacial, ReagentPlus®, ≥99%	Sigma-Aldrich
Hydrogen peroxide	7722-84-1	purum p.a., ≥35 %	Sigma-Aldrich
Acidic ion exchange resin (Amberlite IR-120 H)	39389-20-3	Appearance: Yellow-brown moist spherules, particle size (0,3-1,1 mm): ≥ 90	Sigma-Aldrich
Sulphuric acid (H ₂ SO ₄)	7664-93-9	≥97.5%	Sigma-Aldrich
Hanus solution	n.a.	For determination of iodine number c(IBr) = 0.1 mol/l Titripur®	Sigma-Aldrich
Zinc acetate dihydrate	5970-45-6	Reagent grade, > 98%	Sigma-Aldrich
4-(dimethylamino)pyridine	1122-58-3	reagent plus, ≥ 99%;	Sigma-Aldrich

(DMAP)			
Acetic anhydride	108-24-7	puriss, $\geq 99\%$	Sigma-Aldrich
Dichloromethane	75-09-2	puriss.p.a., ACS reagent;	Sigma-Aldrich
Ethyl acetate	141-78-6	puriss, 99.5%;	Sigma-Aldrich
<i>N,N</i> -dimethylformamide (DMF)	68-12-2	ACS reagent, $\geq 99,8\%$;	Sigma-Aldrich
Potassium hydroxide	1310-58-3	puriss, $\geq 85\%$	Sigma-Aldrich
Potassium iodide	7681-11-0	ACS reagent, $\geq 99\%$	Sigma-Aldrich
Tetraethylammonium bromide	71-91-0	reagent grade, 98 %	Sigma-Aldrich
Perchloric acid	7601-90-3	ACS reagent, 70%	Sigma-Aldrich
Sodium sulfate anhydrous	7757-82-6	puriss	Sigma-Aldrich

Rigid PU Foam Sample Production

Rigid PU Foam Sample Preparation in Open-top Mould

The polyol component was obtained by weighing all necessary components (*green* polyols, Lupranol 3422, catalyst, blowing agent, surfactant and flame retardant) and stirring them for 1 min by a mechanical stirrer at 2000 rpm. Reagents used for polyol component preparation are summarized in Table 2.2. PU foams were prepared after conditioning the polyol component at room temperature for at least 2 hours in a sealed container to de-gas the mixed in the air.

The polyisocyanate (pMDI) and a polyol component were weighed and mixed by a mechanical stirrer at 2000 rpm for 15 sec. An appropriate amount of the reactive PU mass was poured into the open-top mould and the PU foam was cured at 50 °C in an electric oven for 2 hours.

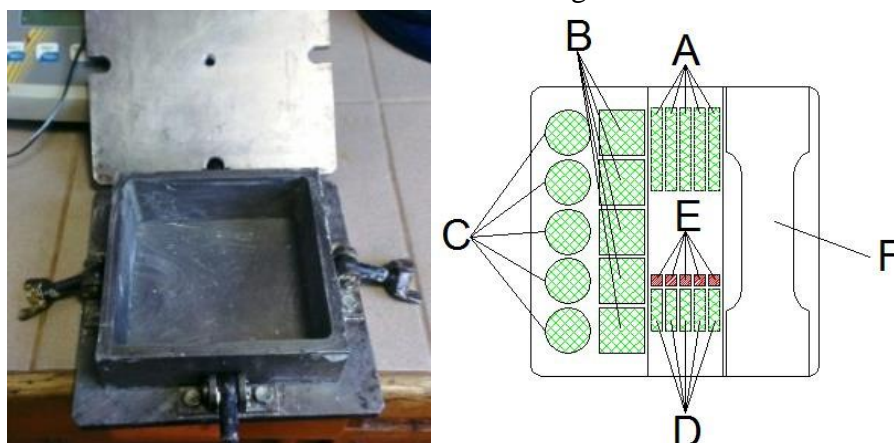
Table 2.2

Materials used for rigid PU foam development

Material	CAS number	Characteristics	Producer
TCP	13674-84-5	Flame retardant based on 1-chloro-2-propyl phosphate	Lanxess, Germany
Solkane® 365/277	n.a.	A blend of 86-92% of 1,1,1,3,3 pentafluorobutane and 8-14% of 1,1,1,2,3,3,3-heptafluoropropane	Solvay Special Chemicals, Germany
Lupranol® 3422	n.a.	A higher functional polyether polyol based on sorbitol, OH value 490 mg KOH/g	BASF, Germany
Polycat® 5	3030-47-5	Tertiary amine catalyst based on pentamethyldiethylenetriamine	Air Products Europe Chemicals, Netherlands
PC CAT TKA 30	n.a.	30 wt.% potassium acetate in DEG	Air Products Europe Chemicals, Netherlands
Niax Silicone L-6915	n.a.	Silicone based surfactant	Momentive Performance Materials Inc., Germany
NP-10	63469-23-8	The reactive delayed action time amine-based catalyst based on 1,1'-[[3-(Dimethylamino)propyl]imino]bis(2-propanol)	Momentive Performance Materials Inc., Germany
Desmodur 44V20L (pMDI)	101-68-8	Polymeric 4,4'-diphenylmethane diisocyanate. The average functionality is 2.8 to 2.9 and NCO content 30.5-32.5 wt%.	Covestro, Germany

Rigid PU Foam sample Production in a Stainless Closed Type Steel Mould

The polyol component was obtained as described in the paragraph above. The pMDI and the polyol component were weighted and mixed by a mechanical stirrer at 2000 rpm for 15 sec to prepare PU foams. Afterwards, the reacting mixture was poured into a stainless steel mould that was preheated to 50°C and placed on a balance. An appropriate amount of the reacting PU mass was poured into the mould and then the mould was sealed. The lid of the mould was kept in place by four steel eye bolts with M12 thread that are embedded into the bottom lid of the mould. The mass of the reacting mixture was chosen to obtain PU foams with an approximate desired apparent density. The air was able to escape from the mould through the opening in the top of the mould's lid, which was closed after all air escaped. Afterwards, PU foams were cured at 50 °C for 2 h. At that point, the mould was cooled to the room temperature and PU foams were removed and conditioned for at least 24 h. Then, the samples for tests were cut out according to the respective standards. The samples were cut from the inner part of the PU foam block at least 10 mm from PU foam block walls. This insured that the integral skin of the PU foam block did not have an effect on sample properties. Samples were prepared in a stainless steel mould to adjust the apparent density of the material. The stainless steel mould and generic sample placement in the PU foam block are shown in Figure 2.3.



- A - Samples for DMA test (12mm x 40 mm x 5 mm)
- B - Compressive strength parallel foaming directions (cylinder dimensions:R-11mm;h-22mm)
- C - Compressive strength perpendicular foaming directions (cylinder dimensions:R-11mm;h-22mm)
- D - Samples for TMA test perpendicular to foaming direction (5mm x 5mm x 20mm)
- E - Samples for TMA test parallel to foaming direction (5mm x 5mm x 20mm)
- F - Tensile strength and Young's modulus (25mm x 55mm)

Figure 2.3. The stainless steel mould, the PU foam block and generic sample placement

2.2. Rigid PU Foam Nanocomposite Development

Nanoclay Additives Used for Rigid PU Foam Reinforcement

In the frame of the Doctoral Thesis, rigid PU foams were reinforced with two different modified nanoclay particles. The goal was to increase the mechanical properties of developed materials. For this purpose, two commercially available nanoparticles were used: Cloisite 15A and Cloisite 30B. Both of them are modified montmorillonite nanoparticles which characteristics summarised in Table 2.3.

Table 2.3.

Two different nanoclay: Cloisite 15A and Cloisite 30B characteristics

Nanoparticle	Organic modifier	Modifier concentration	Moisture	Weight loss on ignition	Density	Interplanar distance
Cloisite 15A	2M2HT*	125 meq/100g clay	<2%	43%	1.66 g/cm ³	31.5 Å
Cloisite 30B	MT2EtOH*	90 meq/100g clay	<2%	30%	1.98 g/cm ³	18,5 Å

2M2HT: dimethyl, dehydrogenated tallow, quaternary ammonium

HT – hydrogenated tallow

MT2EtOH: methyl, tallow, bis-2-hydroxyethyl, quaternary ammonium

T – Tallow

Cloisite 15A nanoclay has larger interplanar distance but no reactive groups in the organic modifier. The reactive OH group of Cloisite 30B could mean better interaction between polyol and nanoclay surface due to the polarity. Nanoparticles were dispersed into NEO 380 polyol and following nanoclay contents were investigated 0 %; 1 %; 2 %; 3 %; 5 %; 10 % and 20 % in polyol mass. Furthermore, the same content of nanoclay was dispersed into polyisocyanate component of rigid PU foam – pMDI. Following nanoclay content in rigid PU foams: 0 %; 0.25 %; 0.5 %; 0.76 %; 1.29 %; 2.68 %; 5.83 % were investigated. Methods used to disperse nanoclay particles and experimental workflow is depicted in Figure 2.4.

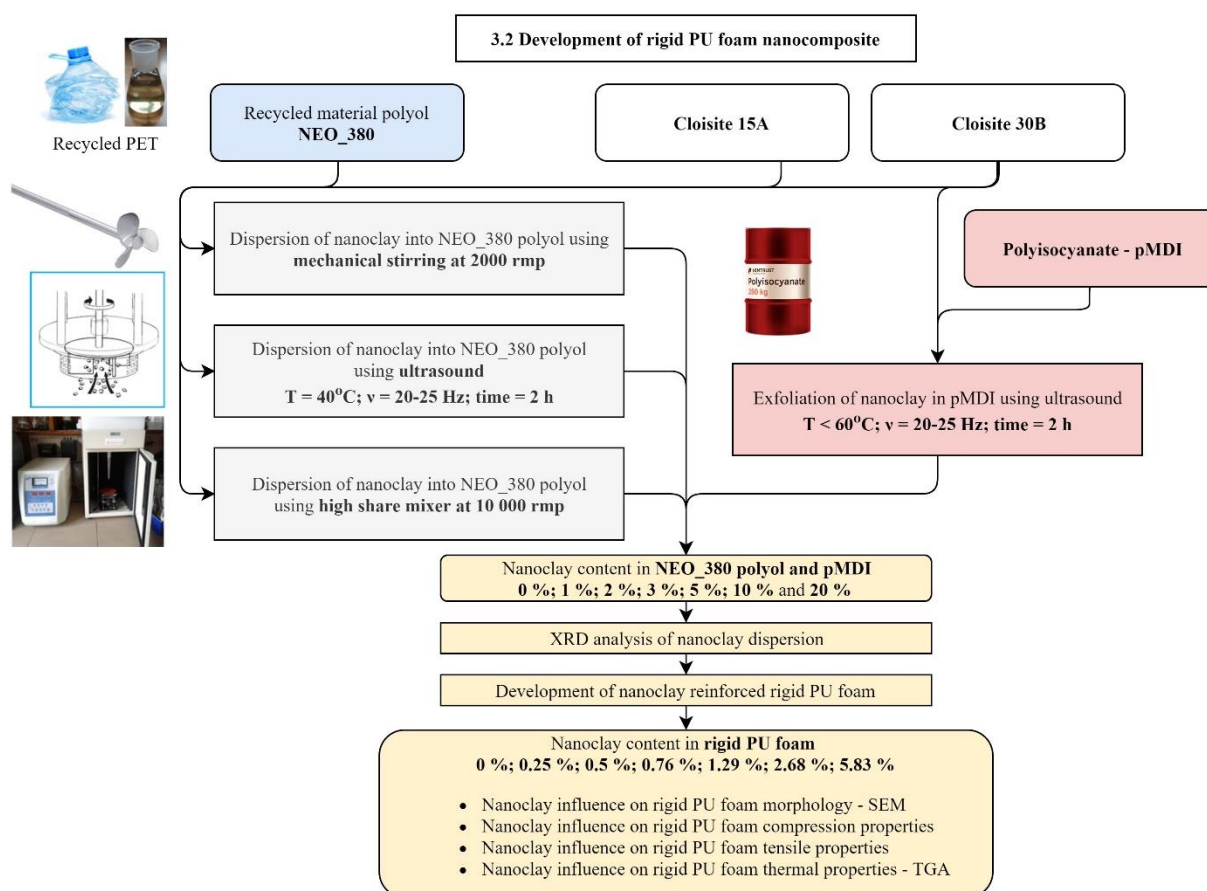


Figure 2.4. The workflow of nanoclay introduction into rigid PU foam structure and its influence on the foam characteristics.

X-ray Diffraction Analysis of Nanoparticle Dispersions in Polyols

The degree of intercalation of the polyol in organoclay layers was evaluated via the basal spacing by X-ray diffraction (XRD). The XRD patterns of organoclay-polyol samples were obtained by a Bruker D8 Advance diffractometer, produced by Bruker AXS GmbH, equipped with a scintillation counter detector, using Ni-filtered copper radiation ($\text{CuK}\alpha$) at 0.15418 nm wavelength. The organoclay-polyol samples were spilled into sample holders and excess of the samples was removed with a flat slide. The diffractometer tube voltage and current amounted to 40 kV and 40 mA, respectively. The divergence slit was set to 0.6 mm, and the anti-scattering slit - to 8.0 mm. The diffraction patterns were determined at a scan speed of 1 s/0.02° from 0.8° to 13° in the 2 θ scale.

2.3. Development of Low Flammability Rigid PU Foam Thermal Insulation Composite

In 3.3 paragraph of results and discussion, the flammability of rigid PU foams was decreased by adding non-halogenated flame retardants (FR) dimethyl-propyl-phosphate (DMPP) as well as expandable graphite (EG). Furthermore, a composite rigid PU foam was developed where one side of the material was protected with glass fibre non-woven intumescent fabric (IF). The non-halogenated FRs were compared to conventional additive FR tris(chloropropyl)phosphate (TCPP). The workflow of low flammability rigid PU foam thermal insulation development is depicted in Figure 2.5 where the different samples with respective FR loadings are listed as well as the different tests and flammability analysis used to evaluate FR performance.

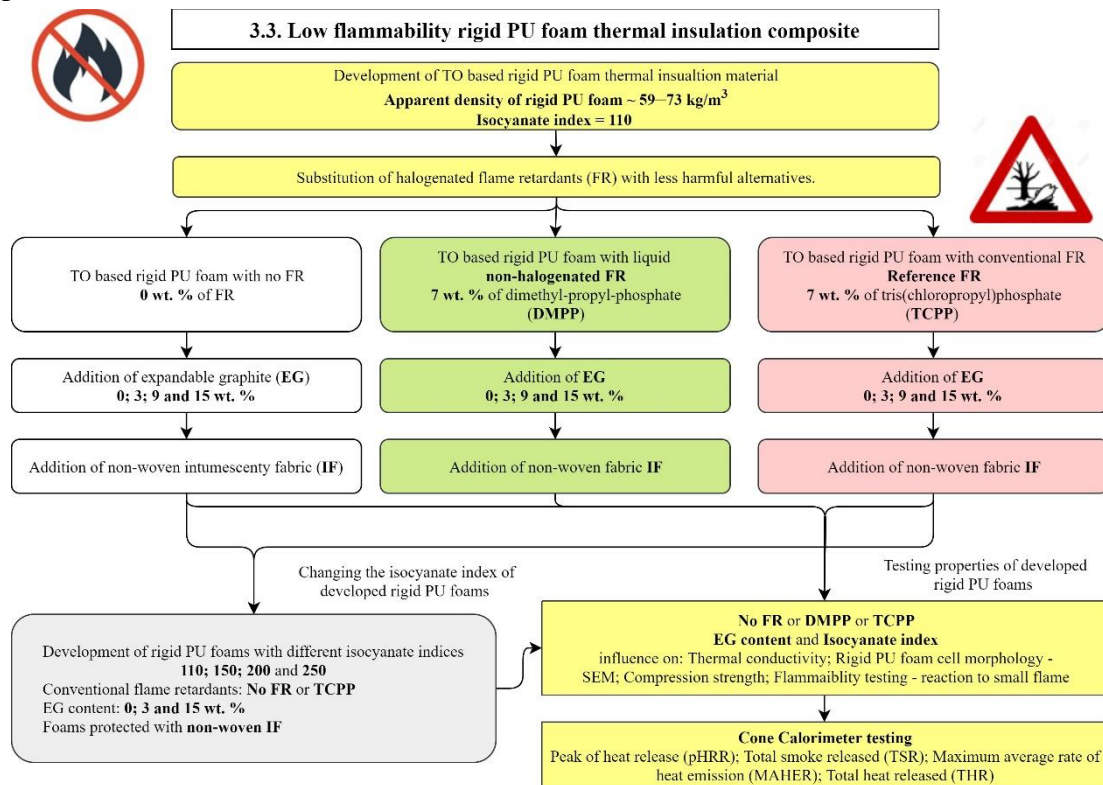


Figure 2.5. The workflow of low flammability rigid PU foam thermal insulation development

2.4. High Functionality Bio-based Polyol Synthesis from RO

The bio-based polyol synthesis methods from RO described in Figure 2.1 were improved by combining the oxirane ring opening reaction with the transamidation/transesterification process to obtain high functionality polyols. The viability of developed high functionality polyols was tested by developing rigid PU foam thermal insulation material and testing its common characteristics, such as compression strength, thermal conductivity and foaming technological parameters. The workflow of the research described in paragraph 3.4 is depicted in Figure 2.6.

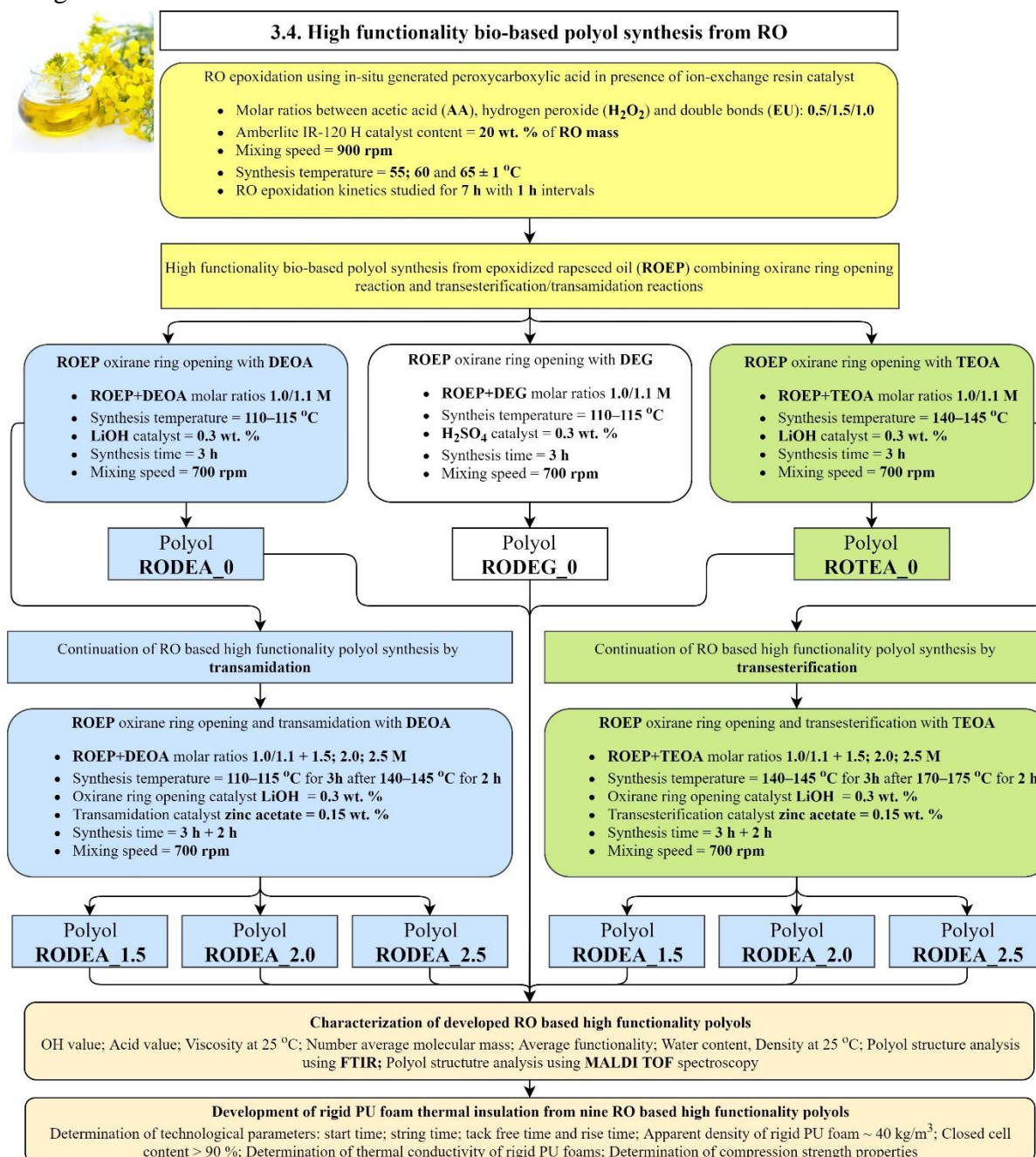


Figure 2.6. The workflow of high functionality polyol development from RO

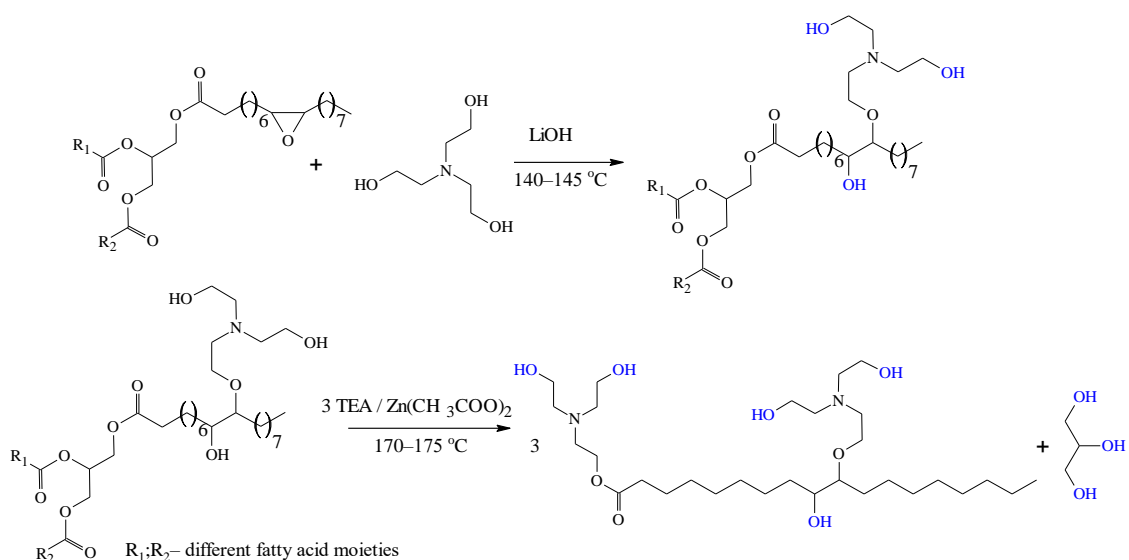


Figure 2.8. Idealized ROEP epoxy ring opening and transesterification with TEOA.

Developed RO based high functionality polyols were used to obtain rigid PU foam thermal insulation material. The described rigid PU foam formulations (Table 2.4) were designed to obtain foams with apparent density $\sim 40 \text{ kg/m}^3$. Usually, the components of rigid PU foam formulation are conditioned at room temperature before foam production. Formulations based on ROTEA polyol had to be cooled down to $+10 \text{ }^\circ\text{C}$ before foam production as they were too fast at room temperature which shows the catalytic activity of the ROTEA polyol.

Table 2.4

Polyol formulation and renewable material content in PU foams.

Polyol formulation, pbw	RO DEG	RODEA 0	RODEA 1.5	RODEA 2.0	RODEA 2.5	ROTEA 0	ROTEA 1.5	ROTEA 2.0	ROTEA 2.5
Green Polyol					100.0				
Cross-linkage reagent (Lupranol 3422)					33.3				
Flame retardant (TCPP)					21.3				
Blowing reagent (water)					2.9				
Blowing agent (Solkane 365/277)					17.3				
Tertiary amine catalyst (Polycat 5)	1.3	0.9	0.9	0.9	0.9	-	-	-	-
Potassium acetate 30%	1.8	0.9	0.9	0.9	0.9	-	-	-	-
Surfactant					2.0				
Polyisocyanate (pMDI)	189.8	255.2	296.0	299.4	307.3	215.0	245.3	252.3	254.6
Isocyanate index					130				
Renewable materials in PU foam, %	22.6	19.3	16.1	15.5	14.9	19.5	16.1	15.3	14.7

2.5. TOFA Epoxidation

Different parameter influence on the TOFA epoxidation process was studied in the frame of this Doctoral Thesis. Three different catalysts were used, such as H_2SO_4 , ion exchange resin

Amberlite IR 120 as well as enzymatic catalyst *Novozym 435*. Furthermore, other synthesis parameters, such as Acetic acid content, H_2O_2 content and molar ratio as well as temperature influence on the TOFA epoxidation was investigated. Different catalysts were compared to select TOFA epoxidation method with the highest relative conversion to oxirane, also the regeneration of the *Amberlite IR 120* catalyst was studied to confirm its commercial viability. The TOFA epoxidation kinetics were evaluated using a mathematical model based on a surface reaction mechanism. The overall workflow of TOFA epoxidation is depicted in Figure 2.9.

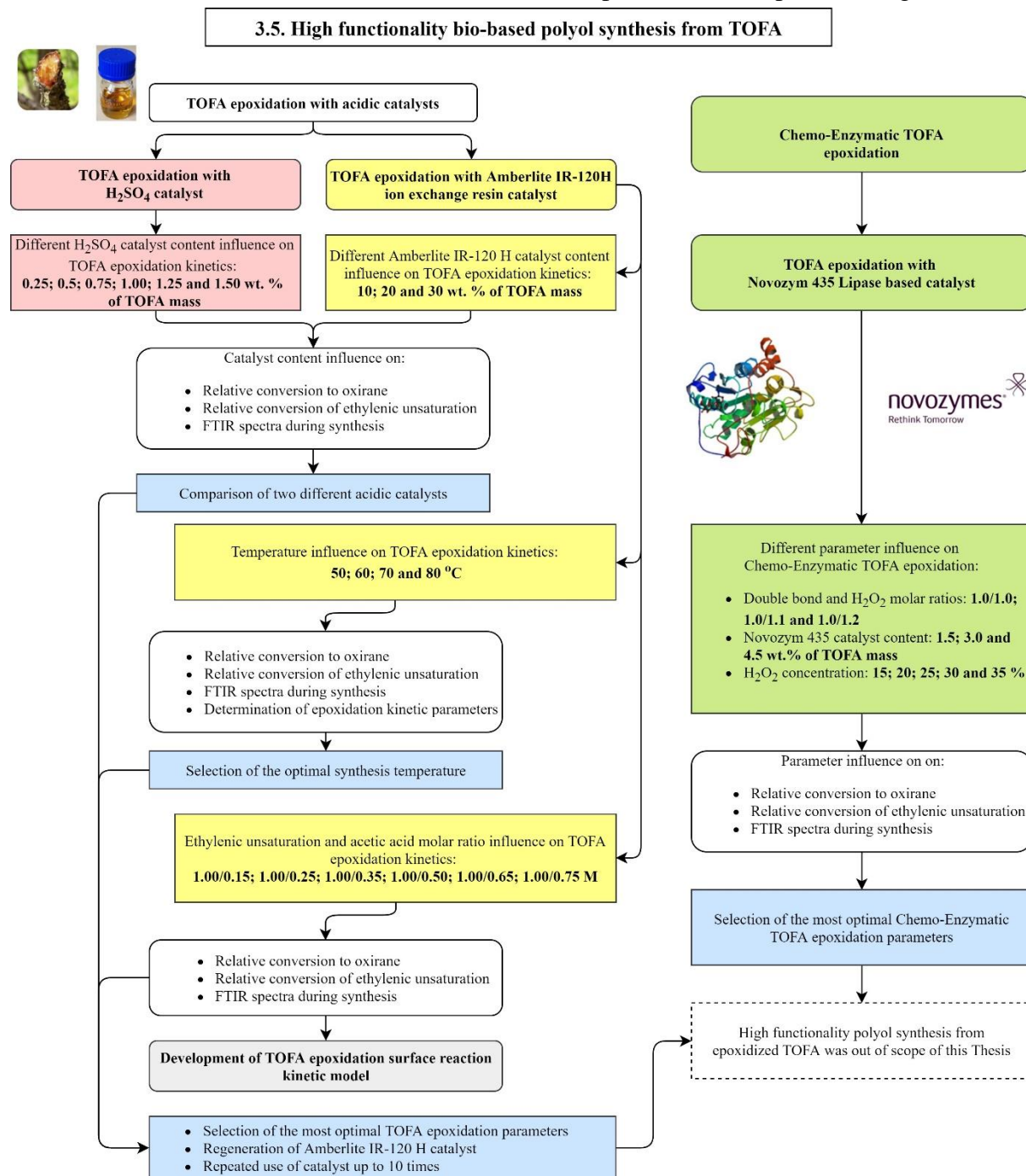


Figure 2.9. The workflow of TOFA epoxidation as a precursor for high functionality polyol synthesis

2.6. Polyol Analysis Methods

The different methods and equipment used to characterise polyols are listed in Table 2.5.

Table 2.5

Analysis methods of polyols, polyol synthesis products and intermediates

Analysis method	Determined characteristic	Equipment	Relevant standard
Titrimetric	OH value	Laboratory burette, volume 25 mL, accuracy ± 0.03 mL	DIN 53240-2
	Acid value		DIN 53402
	Iodine value		ISO 3961:2013
	Epoxy group content (OO_{ex}); the content of oxirane oxygen		ASTM D1652-11
	Polyol moisture	Denver Instrument Model 275KF automatic titration equipment	An alternative method to DIN 51777
Viscosity	Viscosity	Thermo Scientific HAAKE (Medium-High Range Rotational Viscometer).	
Gel permeation chromatography (GPC)	Number-average molecular weight (M_n) and number-average functionality (f_n) of the synthesized polyols	GPC from Knauer equipped with refractive index detector (Detector RI) and polystyrene/divinylbenzene matrix gel column with a measurement range up to 300000 Da at eluent tetrahydrofuran eluent flow of 0.8 mL/min was used to analyse synthesized polyols.	
Fourier transform infrared (FTIR) spectroscopy	Polyol chemical structure	Thermo Fisher Nicolet iS50 spectrometer at a resolution of 4 cm^{-1} , 32 scans. The FTIR data was collected using an attenuated total reflectance technique with a ZnSe and Diamond crystals.	
Mass spectroscopy	Polyol chemical structure	The MALDI-TOF mass spectra were acquired with an Ultraflex, Bruker Daltonics, Bremen, Germany. The spectra were taken as the sum of 30000 shots with a DPSS Nd: YAG laser (355 nm, 1000 Hz). The specimens were prepared by the dried droplet method. The sample solution (10 mg/mL), DHB (2,5-Dihydroxybenzoic acid; 20 mg/mL) used as the matrix and sodium trifluoroacetate (NaCF_3COO ; 10 mg/mL) as a cationization agent in THF were mixed at a volume ratio of 4:20:1.1 μL , and the mixture was deposited on the ground-steel target plate. The drop was dried in the ambient atmosphere.	

From the determined oxirane content, the percentage of relative conversion to oxirane (RCO) was calculated by Equation [36,37,39]:

$$RCO = \left[\frac{OO_{ex}}{OO_{th}} \right] \times 100 \quad (2.1)$$

where RCO is the relative conversion to oxirane, %. OO_{ex} is the experimentally determined content of oxirane oxygen, % and OO_{th} is the theoretical maximum oxirane content in 100 g of oil, which was calculated to be 8.90 % using Equation 2.2 [36,37,39]:

$$OO_{th} = \left[\frac{(IV_0/2A_i)}{100+(IV_0/2A_i) \times A_o} \right] \times A_o \times 100\% \quad (2.2)$$

where A_i (126.9) and A_o (16.0) are the atomic weights of iodine and oxygen respectively and IV_0 is the initial iodine value of TOFA.

The unsaturated bond conversion (UBC) was calculated by Equation 2.3:

$$\text{UBC} = \frac{(EU_i - EU_{ex})}{EU_i} \times 100 \% \quad (2.3)$$

From the determined relative conversion to oxirane (Equation 2.1.) and TOFA unsaturated bond conversion (Equation 2.3.) the selectivity (S) of TOFA epoxidation reaction was calculated by Equation 2.4 [151]:

$$S = \frac{\text{RCO}}{\text{UBC}} \times 100 \% \quad (2.4)$$

The polyols' f_n was calculated based on hydroxyl values, and M_n as seen from Equation 2.5 [60].

$$f_n = \frac{M_n \cdot \text{OH}_{val}}{56110} \quad (2.5)$$

where f_n is the number-average functionality; M_n is the number-average molecular weight; OH_{val} is the hydroxyl value of polyol.

2.7. Rigid PU Foam Characterization Methods

Different methods and equipment used to characterise developed rigid PU foam are summarised in Table 2.6

Table 2.6

Equipment used for rigid PU foam characterization and relevant testing standards

Determined characteristic	Equipment
Rigid PU foam apparent density	Digital callipers, resolution 0.01 mm; laboratory balance, resolution 0.001 g; testing according to ISO 845:2006
Rigid PU foam foaming technological parameters	Rigid PU foam formulation was optimized using FOAMAT equipment. This equipment measures foaming parameters (cream time, gel time, end time and track free time). Furthermore, the kinetics of the foaming process is represented as a change of the foam height, the temperature in the foam core, the pressure fluctuations at the base of the mould and change of dielectric polarization of the foamed material.
Compression strength	Zwick/Roel 11000 N testing machine, testing according to ISO 844:2014
Tensile strength	Zwick/Roel 11000 N testing machine, testing according to ISO 1926:2005
Closed cell content	Equipment developed at LS IWC, testing according to ISO 4590:2016
Thermal conductivity	Linseis HMF 200, measurement range 0 °C to +20 °C, testing according to ISO 8301.
Scanning electron microscope (SEM) imaging	Tescan TS 5136 MM SEM with a secondary electron (SE) detector. Before the SEM investigation, samples with a size of 1x1x0.2 cm were cut and sputtered with a gold layer using an Emitech K550X sputter coater (current 25mA, coating time 2 min). Obtained data and images were processed with Vega TC software.
Rigid PU foam chemical structure analysis using FTIR spectroscopy	Thermo Fisher Nicolet iS50 spectrometer at a resolution of 4 cm ⁻¹ , 32 scans. The FTIR data was collected using an attenuated total reflectance technique with a ZnSe and Diamond crystals.
Glass transition temperature determination using dynamic mechanical analysis (DMA)	Mettler Toledo DMA/SDTA 861e equipment in the compression regime. DMA was performed using a constant frequency of 1 Hz and an amplitude of 20 μm. A heating rate of 3°C/min and a temperature range between -50°C and 200°C were also used. The glass transition temperature (T_g) from DMA analysis was considered as a peak point of tan (δ).
Thermal degradation of PU foams was analyzed by thermogravimetric analysis (TGA).	Discovery TGA equipment from TA instruments. Foam samples of 10 ± 1 mg were placed on platinum scale pans and heated in an air or nitrogen atmosphere at 10 °C/min in a temperature range between 25 – 1000 °C. Data

	processing was performed using the OriginPro 8.5.1. and TA Instruments Universal Analysis 2000 v4.5A software.
Flammability analysis - Cone Calorimeter	The reaction to the 35 kW/m ² heat flux was tested using an FTT Dual Cone Calorimeter from Fire Testing Technology Ltd. The peak heat release rate (pHRR, kW/m ²); time to pHRR (TTP, s); ignition time (IT, s); time to flame out (FOT, s); total smoke release (TSR, m ² /m ²) and the maximum average rate of heat emission (MARHE, kW/m ²) were determined according to the ISO 5660 - 1:2015 standard.
Flammability analysis – reaction to flame source	Single-Flame Source Test (Ignitability Apparatus) from Fire Testing Technologies, UK. Developed rigid PU/PIR foams were tested according to ISO 11925-2:2010 standard where the material is subjugated to direct impingement of flame. The foam sample was exposed to a small propane flame which was applied at a 45 ° degree angle at the bottom of the sample. The propane flame was applied for 15 sec after which the flame source was removed from the sample surface and the material was allowed to burn autonomously for additional 15 sec. During the test time following events were recorded: did the sample ignited; did the flame tip reached a 150 mm mark and at which time; was there a flame out of the burning sample; was there a formation of flaming droplets.

Rigid PU Foam Cell Size and Cell Density Determination from SEM Images

To clarify the shape, average size of cells, cell size distribution and anisotropy coefficient, images were taken in parallel and perpendicular directions to foam rise. Cells in cross-section images were measured both lengthwise and breadthwise. For each sample, more than 200 cells were measured. To determine cell size distribution, the number of cells in the 20 μm interval was divided by the total number of cells. Anisotropy coefficient was calculated using. Eq. 2.6.

$$R = \frac{\sum_{i=1}^n \frac{h}{l}}{n} \quad (2.6)$$

where h – cell size lengthwise; l – cell size breadthwise; n – total number of cells.

The SEM images were analyzed by the software ImageJ. Using this software, the cell density (N_f) was determined by the number of cells per unit volume of foam, which was calculated using Eq. 2.7 [152] .

$$N_f = \left(\frac{n \cdot M^2}{A} \right)^{3/2} \quad (2.7)$$

where n – the number of cells in the micrograph; M - the magnification of the micrograph; A - the area of the micrograph (cm²).

Rigid PU Foam Degree of Phase Separation Analysis Using FTIR

FTIR absorption spectra of the stretching vibrations of the –C=O group in the range of 1760–1650 cm⁻¹ were analysed. The intensity of individual signals was determined with a split of the multiplet peak of the carbonyl band via Gauss curve fitting using Omnic Spectra 2.0 software. The degree of the carbonyl groups participating in hydrogen bonding can be described by the carbonyl hydrogen bonding index, $R_{C=O}$, as given in Eq. 2.8. Based on the intensity of the peaks, $R_{C=O}$ index was calculated, defining the participation of urethane and urea groups forming hard segments, linked with the hydrogen bond of –C=O groups [153,154]

$$R_{C=O} = \frac{A_{B1} + A_{B2}}{A_{F1} + A_{F2}} \quad (2.8)$$

where: A_{B1} , A_{B2} - the respective surface areas of peaks from vibrations bound with the hydrogen bond of the carbonyl groups of urea (B1) and urethane (B2) bonding. A_{F1} , A_{F2} - the respective surface areas of peaks from vibrations unbound with the hydrogen bond of the carbonyl groups of urea (F1) and urethane (F2) bonding.

Moreover, the degree of phase separation (DPS) was obtained from Eq. 2.9.

$$DPS = \frac{R_{C=O}}{1 + R_{C=O}} \quad (2.9)$$

The changes in carbonyl hydrogen bonding and DPS affect the properties of PUs, as presented in the work by Pretsch and Jakob [155,156], as well as Ryszkowska *et al.* [152,156].

With the use of the results of multiplet band distribution, the participation of urethane bonds (U_1), urea bonds (U_2) and allophanate bonds (A_L) in hard segments were also calculated using equations below:

$$U_1 = \frac{\Sigma A_{1i}}{\Sigma A_i} \quad (2.10) \quad U_2 = \frac{\Sigma A_{2i}}{\Sigma A_i} \quad (2.11) \quad A_L = \frac{\Sigma A_{3i}}{\Sigma A_i} \quad (2.12)$$

where: U_1 , U_2 , A_L are contributions of urethane (1), urea (2) and allophanate groups (3); A_{1i} , A_{2i} , A_{3i} are the absorbance of carbonyl groups of urethane (1), urea (2) and allophanate groups (3), respectively and A_i is the absorbance of carbonyl groups in the 1760 cm^{-1} and 1650 cm^{-1} region from carbonyl in the hard segment.

3. RESULTS AND DISCUSSION

3.1. High-density Rigid PU Foam Development from Sustainable Raw Materials

Sustainable Polyols Used for High-density Rigid PU Foam Development

The main goal of this study was to obtain material that can be suited for the development of impact absorption element of an electric vehicle. This was done as a part of European Union's FP7 project EVolution where LS IWC was tasked to develop sustainable material based rigid PU foams. Thus different bio-based and recycled material based polyols were investigated for the development of the high-density rigid PU foam structural material. The workflow of this chapter is depicted in Figure 1.

The most significant properties of the polyols used in the development of high-density rigid PU foams are presented in Table 3.1. For the development of high-density rigid PU foams, two different polyols from renewable raw materials were used TO_TEOA and RO_TEOA which were synthesized at LS IWC [26,101,103]. APPs used in this study were produced by Neo Group, Lithuania. The main business of this company is the production of PET granules and PET bottles. The side stream of those commodities contains PET dust and other industrial waste, which is directly transferred into a glycolysis reactor where it is converted into APP. Glycolysis of the PET side stream is done using DEG. Changing the technological parameters and the catalyst amount, two different grade APPs are produced [157]. Described polyols were used to formulate high-density rigid PU foam systems which are covered in the next paragraph.

Table 3.1

Technical characteristics of polyols obtained from sustainable resources.

Polyol type		OH value, mgKOH/g	Viscosity at 25°C, mPa·s	Acid value, mgKOH/g	M_n , g/mol	f_n	Water content, %
Bio-based polyols	TO_TEOA	342	280 ± 25	< 5	391	2.4	0.24
	RO_TEOA	301	190 ± 25	< 5	474	2.6	0.05
Recycled APP polyols	Neopolyol 240 (NEO 240)	258	5000 ± 500	< 5	683	3.1	0.04
	Neopolyol 380 (NEO 380)	366	3500 ± 500	< 5	505	3.3	0.12

The chemical structure of the used polyols was studied by Fourier transform infrared spectroscopy (FTIR). FTIR spectra of polyols from renewable materials and recycled raw materials are depicted in Figure 3.1. The broad peak at 3444-3385 cm^{-1} indicates the presence of -OH groups in all of the polyols. TO_TEOA and RO_TEOA polyol showed the =C-H vibration of the double bond at 3008 cm^{-1} . TO_TEOA and RO_TEOA polyol FTIR spectra were similar as expected, due to a similar process of the polyol synthesis. Tertiary amine group stretching vibrations are seen at 1043-1042 cm^{-1} . The presence of the tertiary amine groups in the structure of TO_TEOA and RO_TEOA polyols explain the autocatalytic properties of the polyols [26,158–160].

The chemical structure of NEO 240 and NEO 380 polyols is different. Similar to bio-based polyols a broad peak of –OH group was identified at 3444 - 3429 cm^{-1} . In contrast to polyols from bio-based resources, the NEO 240 and NEO 380 has an aromatic ring structure which gives distinctive signals. The C-H stretching vibration between 3000 - 2700 cm^{-1} is different from bio-based polyol FTIR spectra as it contains alkyl as well as arene groups. The aromatic ring C-H bond in plane and out of plane bending vibrations were identified at 1130 cm^{-1} and 734 cm^{-1} , respectively. A further indication of the para-substituted phenyl ring is identified as peaks of C=C stretch of the phenyl ring and vibrations of H atom attached to phenyl ring at 1506, 1455, and 1021 cm^{-1} which are not present for bio-based polyols. Furthermore, the C – O – C stretching vibration of ester groups is seen at 1282 cm^{-1} . All polyols showed a C=O bond stretching peak at 1760 – 1665 cm^{-1} [116,159,161,162].

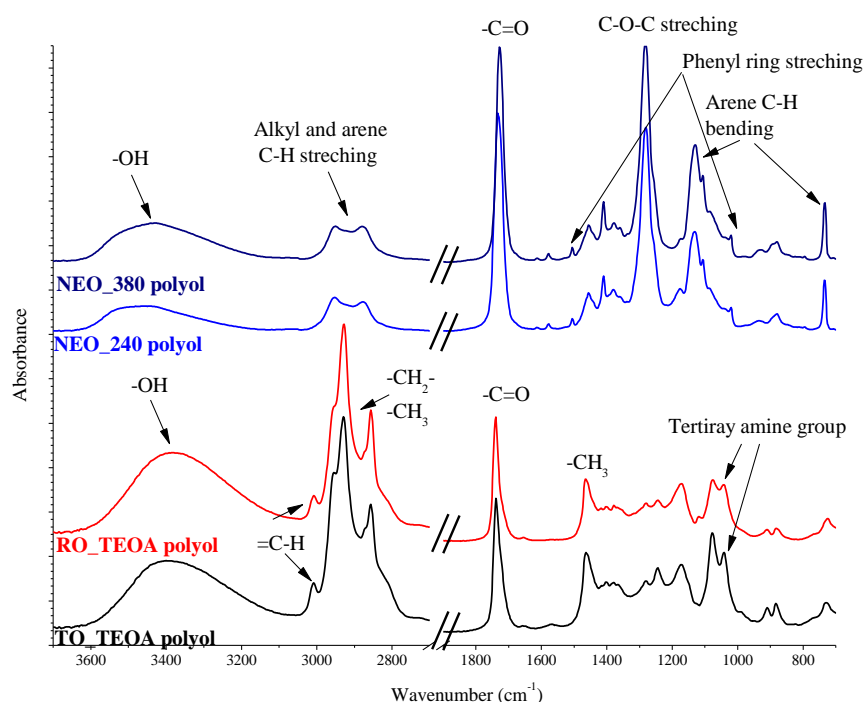


Figure 3.1. FTIR spectra of bio-based polyols (TO_TEOA and RO_TEOA) and polyols obtained from recycled PET (NEO 240 and NEO 380)

High-density Rigid PU Foam Formulations

To compare the different polyols, isocyanate index was chosen 160 for all PU foam formulations. Isocyanate index is the ratio of the equivalent amount of isocyanate used relative to the theoretical equivalent amount times 100. Developed rigid PU foam formulations are depicted in Table 3.2. Sustainable material content was calculated based on the mass of renewable/recycled materials used in PU foam formulation. Stoichiometric ratios of tall oil and rapeseed oil in polyols were taken into account as well as approximate sorbitol content in Lupranol 3422. Unfortunately, the APP polyol producer NeoGroup did not disclose the PET content in the APP polyol. The information they provided said that 50 % of the APP polyols are derived from recycled PET. This approximation was taken into account for recycled

material content calculations. The technological parameters of the developed formulations were determined from the cup tests from which the free rise density and closed-cell content samples were cut (see Table 3.2 – technological parameters and PU foam properties). Furthermore, the molecular weight between two crosslinking points (M_c) was calculated based on proposed formulation and average molecular mass of the polyols and their average functionality using method proposed by U. Stirna et.al. [2,62].

Table 3.2

Polyol formulation, renewable material content in PU foams, technological parameters, free rise density, closed-cell content and M_c of PU foams.

Polyol formulation	TO_TEOA polyol	RO_TEOA polyol	NEO 240	NEO 380
Green Polyol	80.0			
Cross-linkage reagent, Lupranol 3422	20.0			
Flame retardant, TCPP	20.0			
Blowing reagent, water	1.0			
Reactive catalyst, PC CAT NP 10	0.3	0.3	1.6	1.6
Surfactant, NIAX Silicone L6915	2.0			
Polyisocyanate	184	189	150	193
Isocyanate index	160	160	160	160
<i>Formulation characteristics</i>				
Renewable/recycled materials in PU foam, %	26	26	29	25
<i>Technological parameters</i>				
Cream time, s	50	25	27	25
String time, s	115	50	45	45
Tack free time, s	180	80	58	60
End time, s	120	95	60	60
<i>PU foam properties</i>				
Free rise, apparent density, kg/m ³	140	155	161	145
Closed cell count,%	96	99	91	99
The apparent density of moulded PU foams, kg/m ³	203	203	208	210
M_c , g/mol	552	536	499	453

High-density rigid PU foam samples were obtained in the stainless steel mould as described in paragraph 2.1. This was done to ensure the uniformity of the different formulations. The targeted density of the rigid PU foams was 200 kg/m³ which was achieved with acceptable deviations. It can be seen that despite the equal amount of blowing agent (water) the free rise density of the foams is not equivalent. It was not possible to change the blowing agent amount, because that would change the chemical composition of the PU polymer matrix as water reacts with the isocyanate. Furthermore, the different apparent free rise densities would not allow comparing the mechanical properties of the foams.

The rigid PU foam formulations based on bio-based polyols had significantly lower catalyst amount than the APP based systems (0.3 to 1.6 pbw – Table 3.2). The tertiary amine groups of the bio-based polyols have a catalytic effect on PU formation reaction. A higher catalyst content

would lead to too fast system and it would not be possible to pour the foaming material into the mould.

To comply with the Green Chemistry principles a reactive catalyst – dimethylaminopropyldipropanolamine (PC CAT NP-10 from Nitroil) was chosen for the rigid PU foam development. Its chemical structure is depicted in Figure 3.2. The reactive catalyst would react with isocyanate and become a part of PU polymer matrix, thus reducing VOC emission from rigid PU foam. Usually, catalysts are the most expensive component of a PU foam formulation, furthermore, they are one of the contributors to the VOC emissions from the material [163]. This is why it is important to find the most optimal catalyst amount in PU foam formulation. An excess of the catalyst will increase the cost of PU foam material with minimal benefits to the reactivity.

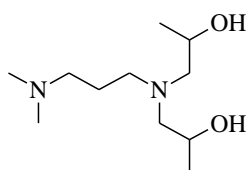


Figure 3.2. Dimethylaminopropyldipropanolamine – reactive PU catalyst

The NEO 380 polyol formulation from Table 3.2 was used to optimise the catalyst content. PC CAT NP-10 was the sole catalyst used and following pbw in the polyol component were tested: 0.4; 0.9; 1.2; 1.6; 1.9 and 2.2 pbw. This corresponds to 0.31; 0.70; 0.93; 1.24; 1.46 and 1.69 wt.% of the polyol component. As expected the increase of the reactive catalyst content increased the cream time and the foaming speed of the formulations depicted in Figure 3.3. The increase in the foaming speed was not linear and after 1.24 % (1.6 pbw) it did not increase by a significant amount. Moreover, there was a small difference in the PU foam curing at catalyst contents between 1.24–1.96% (Figure 3.3c)

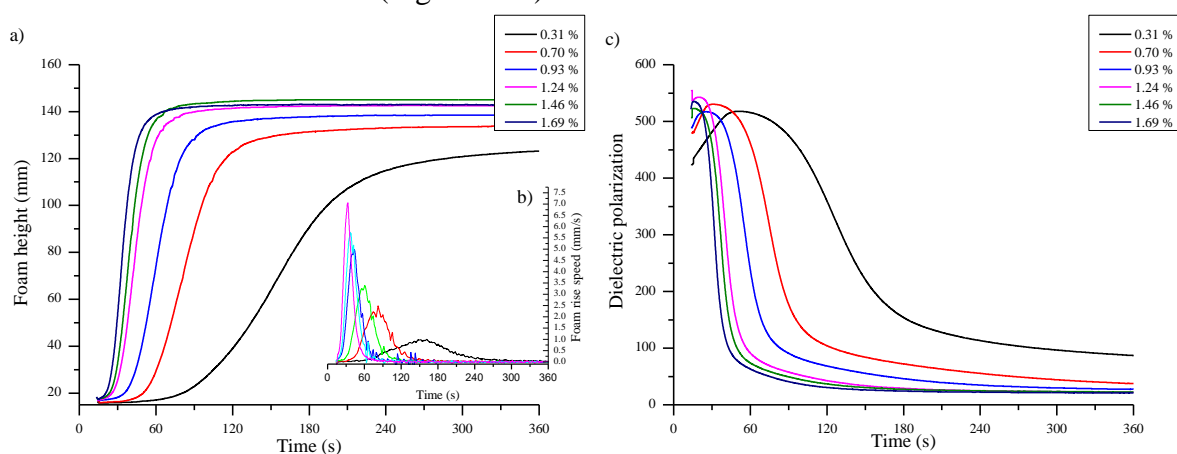


Figure 3.3. Dimethylaminopropyldipropanolamine catalyst content influence on the PU foam a) height, b) foam rise speed and c) dielectric polarisation

The curing of the rigid PU foam material is depicted as a change of the dielectric polarization (Figure 3.3c). The industry requires fast curing systems as prolonged production cycles of the moulded materials increase the production costs. This specific formulation was designed for automotive industry application. Usual demoulding time for such application is

between 15–20 min. For this study material was cured for 2 h because sometimes material had some swelling after faster demoulding. This was especially noticeable for rigid PU foam formulations that were based on the polyols obtained from renewable resources. It can be explained by the low functionality of the polyols which leads to a smaller degree of crosslinking of the polymer matrix.

For further upscale of the developed formulations, a catalytic composition must be improved to achieve desired fast demoulding times of the material. One of the ways how this can be achieved is by using a delayed-action catalyst, like a commercial catalyst PC CAT® DBU TA from Niax which is 1,8-Diazabicyclo[5,4,0]undecene blocked with 2-ethylhexanoic acid. The release of 1,8-Diazabicyclo[5,4,0]undecene from the acid complex during the rigid PU foaming can be seen in Figure 3.4 as a rapid change in the dielectric polarization when the temperature of the system reached 74 °C. Furthermore, the release of the catalyst corresponds with a peak of the PU foam rise speed. This formulation is an example of how the developed rigid PU foam material could be improved and the technological parameters could be tailored for an individual needs of the end producer. In the scope of the Doctoral Thesis PC CAT NP 10 was used as a sole catalyst for high-density rigid PU foam formulations because a rapid curing system was not required. Final optimization of the formulation highly depends on the needs of the end producer, experiments with the delayed reaction catalysts show the versatility of the developed material.

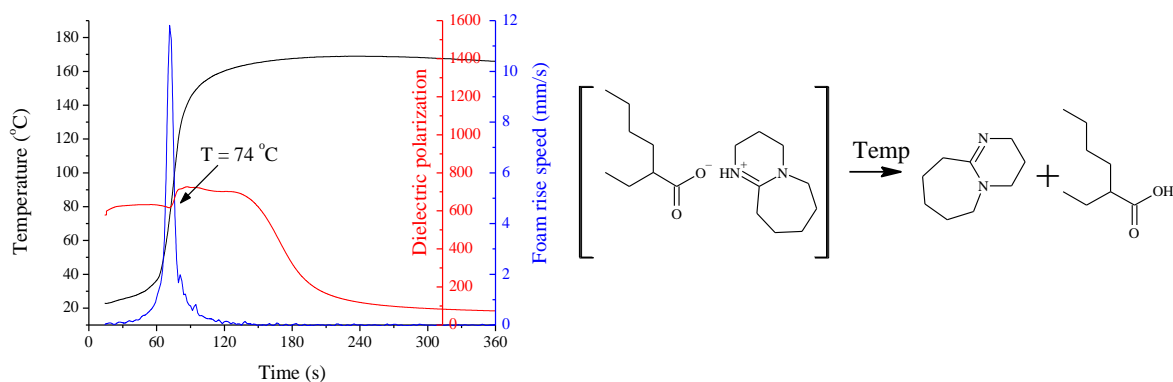


Figure 3.4. The effect of 1,8-Diazabicyclo[5,4,0]undecene delayed action catalyst on the reactivity of the rigid PU foam

Different Sustainable Polyol Influence on High-density Rigid PU Foam Cell Morphology

SEM was used to obtain images of the developed high-density rigid PU foams from which average cell length, width and anisotropy index were determined (Table 3.3). It can be seen that the polyol type did not influence the isotropic properties of the PU foams. The average anisotropy coefficient across all types of polyols used to develop rigid PU foams was 0.98 ± 0.03 . The stainless steel mould constrained the PU foam rise thus the foam cells could not elongate parallel to the foaming direction. Nevertheless, there was a noticeable difference in cell density of PU foams which were based on the NEO 380 APP polyol. The SEM images of the developed rigid PU foams from renewable and recycled resources and their cell size distribution histograms are shown in Figure 3.5 and Figure 3.6 respectively.

Table 3.3

Cell dimensions and coefficient of anisotropy for obtained PU foams from different polyols.

Polyol type	Cell length, μm	Cell width, μm	Anisotropy coefficient	Cell density, $\text{cells}/\text{cm}^3 \cdot 10^{12}$
TO polyol	158 \pm 33	165 \pm 34	0.96 \pm 0.02	1.360
RO polyol	252 \pm 42	268 \pm 45	0.94 \pm 0.02	0.323
NEO 240	155 \pm 23	153 \pm 21	1.01 \pm 0.02	1.550
NEO 380	123 \pm 21	123 \pm 21	1.00 \pm 0.02	5.180

It can be seen that foams from RO/TEOA polyol have the largest cells as well as the most broad/uneven cell size distribution. Further results will indicate that the large cell size of rigid PU foams based on RO_TEOA polyol directly influence the mechanical properties. The idealised chemical structure of TO_TEOA and RO_TEOA should be similar (See Figure 2.1 and Figure 2.2). The slight difference in the viscosity of the polyols (280 $\text{mPa}\cdot\text{s}$ and 190 $\text{mPa}\cdot\text{s}$), as well as glycerine that is formed during the transesterification reaction, could be the main contributors for the cell size difference. Furthermore, the precise chemical composition of the RO_TEOA polyol has not been studied. It is unclear to what degree the triglyceride molecules have been trans-esterified and what is the content of diglyceride moieties is in the obtained polyol. The diglyceride structures are a problem for rigid PU foam development as they disrupt the polycondensation reaction thus decreasing the cross-linkage of the PU foam matrix.

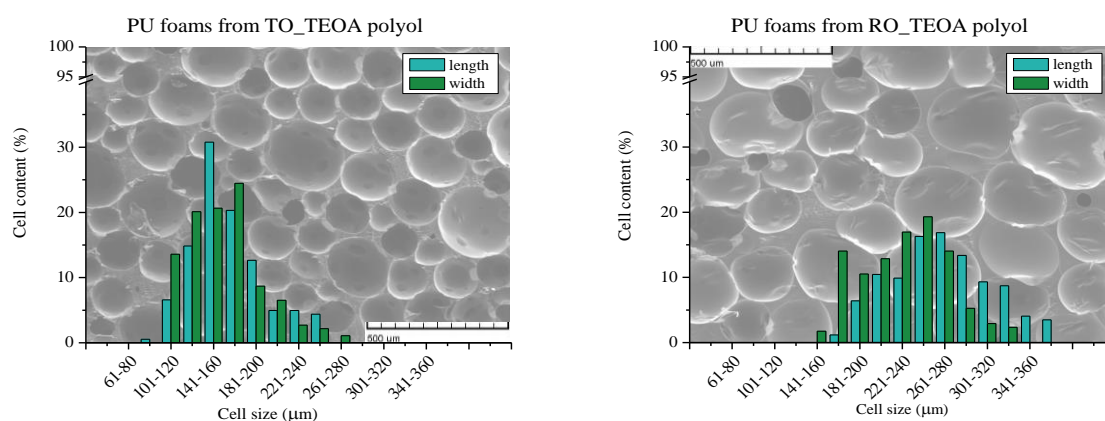


Figure 3.5. SEM images of high-density rigid PU foams from bio-based polyols

When compared to PU foams from bio-based polyols PU foams from recycled PET-based polyols showed smaller cell size and more uniform cell size distribution as seen in Figure 3.6. The high repeatability and even structure of rigid PU foam from recycled PET polyol was one of the reasons that this material was selected for further investigations.

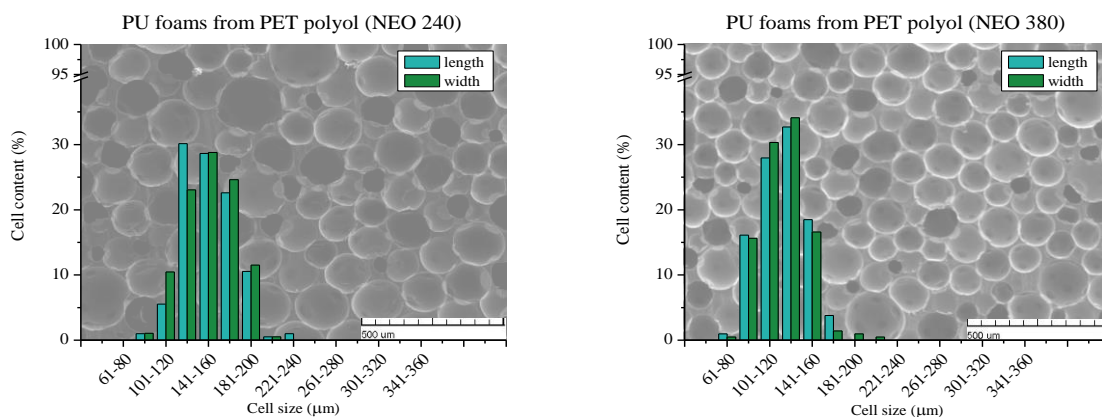


Figure 3.6. SEM images of high-density rigid PU foams from recycled PET-based polyols

Mechanical Properties of High-Density Rigid PU Foams

Rigid PU foams obtained from bio-based resources (TO_TEOA and RO_TEOA) were compared to the two APP polyols from recycled PET (NEO 240 and NEO 380). Common characteristics of rigid PU foam were compared to select the most viable polyol for further investigations and up-scale.

The Compression Strength of PU Foams from Sustainable Polyols

Compression strength was measured parallel and perpendicular to the foaming direction to confirm the isotropic properties of developed materials. It must be noted that isotropic properties of the foamed material are more dependent on the foam production method and mould design than on material formulation. Compression strength and Young's modulus of developed PU foams are shown in Figure 3.7. The apparent density of tested foams was $206 \pm 3 \text{ kg/m}^3$ and $202 \pm 5 \text{ kg/m}^3$ parallel and perpendicular to the foaming direction. Developed rigid PU foam showed almost isotropic mechanical properties which correlate with the measured cell size distribution of the foams (Figure 3.5 and Figure 3.6). The slight deviation from ideal isotropic material is explained by the difference in apparent densities of the samples. Rigid PU foam does not have perfect apparent density distribution through the whole material. Foam near the mould walls tends to increase its density, this results in the relatively high standard deviation of the mechanical characteristics [164].

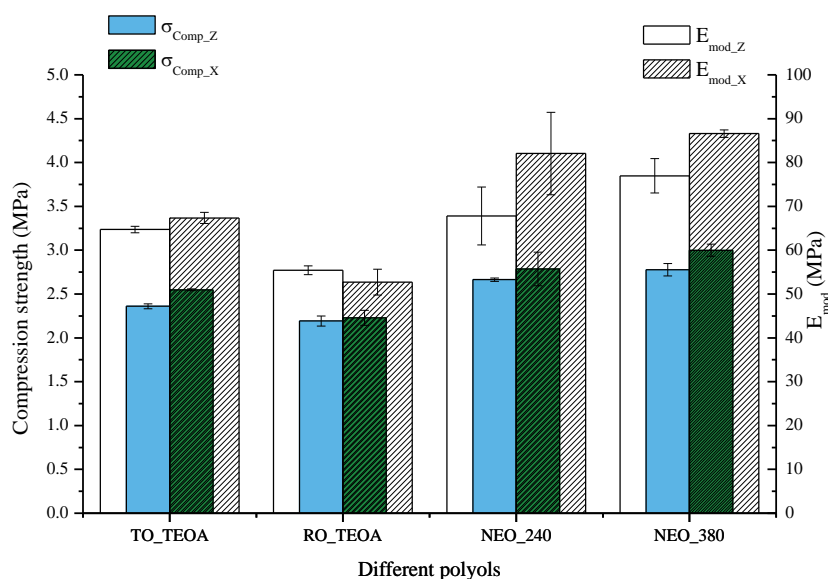


Figure 3.7. Compression strength and Young's modulus of rigid PU foams from sustainable polyols measured parallel (Z) and perpendicular (X) to foaming direction

There is a slight difference in compression strength (~15–21 %) and Young's modulus (~22–39 %) between rigid PU foams obtained from bio-based polyols and APP polyols. APP polyol based rigid PU foams exhibit higher mechanical stiffness and load-bearing capability. The main reason for the different mechanical properties is the different chemical structure of base polyols as other factors influencing rigid PU foam mechanical properties were the same for the set of experiments (apparent density; isocyanate index; blowing agent content; foaming and curing conditions). Aromatic ring structure delivers higher stiffness of the polymer matrix as aromatic chains are less flexible than aliphatic structures. Furthermore, the difference in the mechanical properties of the developed foams can be explained by the different molecular weight of links between two crosslinking points – M_c . Rigid PU foams obtained from TO_TEOA and RO_TEOA polyols had lower compression strength and Young's modulus than APP based PU foams which correlates with the M_c of different PU polymer matrices. Higher compression performance of NEO_380 polyol based foams is explained by higher aromaticity of polymer matrix due to APP polyol structure. Further investigations of the developed rigid PU foams are explored in the publication by M. Kirpluks et.al. [165] where several models of rigid PU foam mechanical properties are proposed to predict Young's modulus, Poisson's ration and strength as a function of porosity and apparent density. The bio-based polyols showed the lowest mechanical strength value also when neat monolithic (solid) PU polymer was obtained.

Tensile Strength of PU Foams from Sustainable Polyols

Tensile strength tests showed similar results to compression strength tests. Tensile strength, Young's modulus, Poisson's ration and apparent density of rigid PU foams from sustainable polyols are shown in Table 3.4. Rigid PU foams developed form APP polyols have slightly higher tensile strength and Young's modulus than foams based on bio-polyols. The difference of tensile properties of developed rigid PU foams is explained by the same factors as in the

previous paragraph (aromatic structure of APP polyols and higher crosslink density of polymer matrix – M_c). Elongation at break and Poisson's ratio was similar between developed materials.

Table 3.4

Tensile strength, Young's modulus, Poisson's ratio and apparent density of rigid PU foams from sustainable polyols

Polyol type	Apparent density	Young's modulus	Tensile strength	Elongation at break	Poisson's ratio
	kg/m ³	MPa	MPa	%	
TO polyol	203 ± 1	122 ± 7	3.08 ± 0.04	4.8 ± 0.4	0.49 ± 0.13
RO polyol	203 ± 2	90 ± 8	2.18 ± 0.32	3.7 ± 0.3	0.34 ± 0.02
NEO 240	207 ± 3	138 ± 6	3.22 ± 0.20	4.9 ± 0.4	0.34 ± 0.11
NEO 380	202 ± 3	132 ± 8	3.34 ± 0.05	6.3 ± 0.5	0.31 ± 0.08

Thermal Properties of PU Foams from Sustainable Polyols

Thermal Stability of PU Foams from Sustainable Polyols

Thermal degradation of polymer material is directly related to the chemical structure of the polymer matrix. The thermal degradation in air atmosphere of developed rigid PU foams is depicted in Figure 3.8. Four distinct steps of thermal degradation can be separated which are listed in Table 3.5. Thermal degradation steps were determined from peaks of mass loss which were analysed using multiple Gauss peak fit tool in OriginPro software, because of overlapping of the different peaks.

The initial step of mass loss (T_1 and $T_{5\%}$) can be attributed to the release of the additive flame retardant TCPP, unreacted isocyanate/polyols, water moisture and other VOCs. This peak was the same for all samples at 201–203 °C. Furthermore, it was possible to confirm the release of TCPP by testing rigid PU foam samples which were obtained without using this flame retardant. Mass loss step of TCPP release is not present for TGA curves of rigid PU foam with no TCPP (see Figure 3.9).

Both rigid PU foams obtained from bio-based polyols had a thermal degradation step T_2 at 262 °C which is attributed to the degradation of the long aliphatic dangling chains. The structure of bio-based polyol has reactive OH groups at the end of the fatty acid chain [26,103,157]. Thus fatty acid chain moiety is not part of the PU polymer matrix. APP polyol based rigid PU foam did not have this thermal degradation step which confirms that it is related to the fatty acid dangling chain decoupling.

Rigid PU foams start to decompose at 200 °C by the scission of hard segments (polyurethane and polyurea bonds) of PU polymer network. This process happens with no mass loss, hence it is not visible in TGA analysis. The next stage of degradation T_3 at 296–312 °C is related to the oxidative degradation of the polyol component which is a result of hard segment degradation [134,166]. APP polyols are more thermally stable as such they degrade at a slightly higher temperature than aliphatic polyols 305–312 °C to 296–304 °C.

The last degradation stage T_4 is attributed to the decomposition of heavy aromatic groups of PU foam materials like isocyanurate rings and pMDI component. For all samples, it was at the same temperature range of 562–569 °C (see Table 3.5).

Table 3.5

Thermal stability properties for rigid PU foams, temperatures of different stages of PU foam degradation [°C].

Polyol type	T_{onset}	$T_{5\%}$	$T_{25\%}$	$T_{50\%}$	T_1	T_2	T_3	T_4
TO polyol	143	191	281	479	202	262	296	562
RO polyol	151	201	297	474	203	262	304	569
NEO 240	150	203	289	485	201	-	312	565
NEO 380	148	196	310	511	203	-	305	567

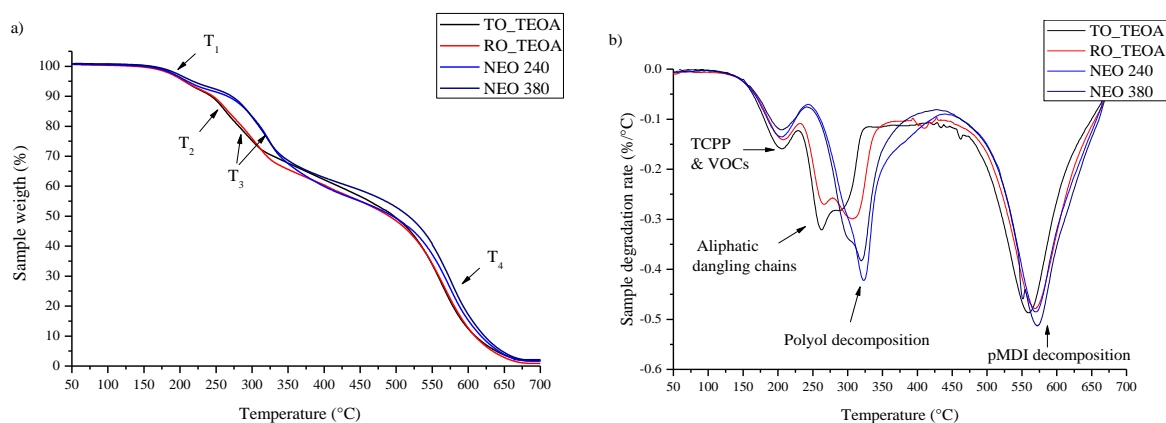


Figure 3.8. Thermal degradation of PU foams from sustainable polyols a) TGA mass loss curves b) DTG analysis

The higher thermal stability of rigid PU foam obtained from APP polyols is distinctly seen for samples with no TCPV. The onset point of the polyol degradation step is 229 °C for rigid PU foam from bio-based polyols whereas for rigid PU foam from APP polyols it is 274 °C.

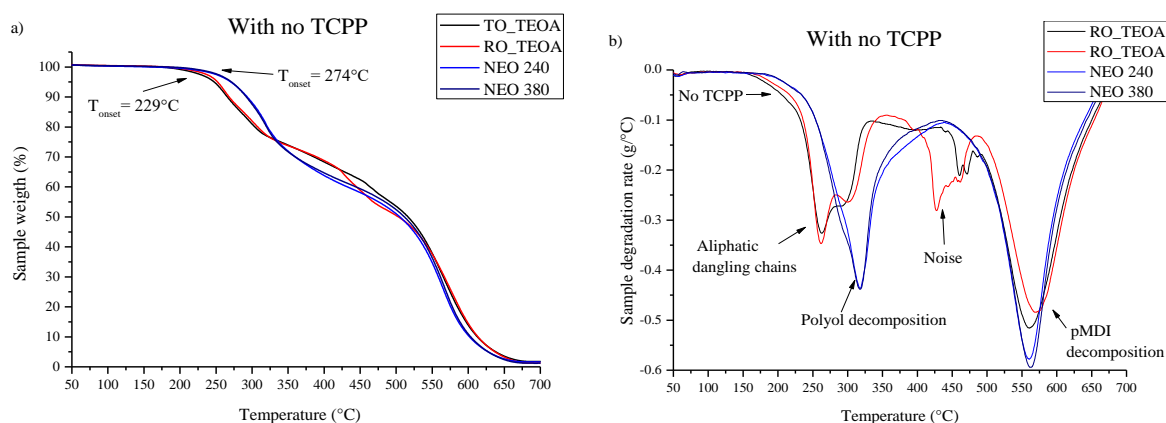


Figure 3.9. Thermal degradation of PU foams from sustainable polyols with no TCPV a) TGA mass loss curves b) DTG analysis

The Glass Transition Temperature of PU Foams from Sustainable Polyols

For polymers, one of the most important characteristics is the glass transition temperature (T_g) which is a temperature region where polymer an amorphous substance transfers from hard, glassy material to a soft, rubbery material. Contrary to crystalline materials T_g is not a distinct thermodynamic transition like melting/crystallisation temperature but a temperature region,

sometimes up to 50 K wide. Different factors can influence the T_g of PU materials, like hard segment content, the crosslink density of polymer matrix, different plasticisers as well as the chemical structure of raw materials (polyols, isocyanate – aliphatic/aromatic) [167].

A distinct change of polymer materials properties during heating can be used to express the T_g of rigid PU foams. Dynamic mechanical analysis (DMA) measures the response of a given material to an oscillatory deformation (here in compression) as a function of temperature. DMA results are composed of three parameters: a) the storage modulus (E'); b) the loss modulus (E''); and c) $\tan \delta$; the ratio (E'/E''), useful for determining the occurrence of molecular mobility transitions, such as the glass transition temperature T_g [168]. A rapid change of rigid PU foam mechanical properties is not desired from the material application point of view. Thus a temperature region before the decrease of E' can be described as an operational region which is most important for the developed materials [167]. Damping, the dissipation of energy under a cyclic load - $\tan \delta$ can also be used for T_g determination of rigid PU foams as the change of E' can be difficult to evaluate [169–171].

Differential Scanning Calorimetry (DSC) among other methods is used for T_g determination. The heat capacity of the polymer is different before and after the glass transition temperature. The heat capacity of polymers is usually higher above T_g . DSC is a valuable method to determine T_g . The temperature in the middle of the inclined region is taken as the T_g as depicted in Figure 3.11 [74,154,171].

For this work, the T_g of developed rigid PU foams was determined using DMA and DSC analysis methods. The summary of obtained T_g results is depicted in Table 3.6. Interpretation of obtained results is problematic as they do not correlate with calculated M_c values in case of rigid PU foam obtained from bio-based polyols. Furthermore, there is a noticeable discrepancy between T_g obtained using the DMA method and T_g obtained from DSC curves. Usually, the difference between these two different methods is about 10-20 K [167]. For developed rigid PU foams from renewable raw materials, it is much higher. The drop of E' and $\tan \delta$ can differ up to 25 K which is accurate for rigid PU foams developed from APP polyols but not for rigid PU foams from bio-based polyols [167]. It should be mentioned that another method for T_g determination - Thermo Mechanical Analysis (TMA) was used, but it was observed that it is not sensitive enough to evaluate T_g of the developed rigid PU foams.

Table 3.6

T_g of developed rigid PU foams from sustainable raw materials

Polyol type	Drop of E' , °C	$\tan \delta$, °C	DSC T_g , °C	M_c , mol/g
TO polyol	51	142	105	551
RO polyol	77	146	109	536
NEO 240	71	113	103	499
NEO 380	91	136	108	453

Looking closer into E' and $\tan \delta$ curves (see Figure 3.10) of developed rigid PU foams explains why the T_g values have such discrepancies. Rigid PU foams obtained from APP polyols have a typical and noticeable drop of E' and one distinct peak of $\tan \delta$, whereas rigid PU foams obtained from bio-based polyols do not. The E' curve has two or more steps as seen in Figure 3.10 a), also $\tan \delta$ peak has two or more overlapping peaks. Such DMA results are

indicative for the non-homogenous polymer matrix. Several glass transition steps could be occurring and their influence on mechanical properties of the material overlaps in a broad temperature region. Noteworthy is the observation that E' for rigid PU foams obtained from RO_TEOA polyols is lower than for foams obtained from TO_TEOA polyol and this correlates with the mechanical properties described in paragraph 3.1.

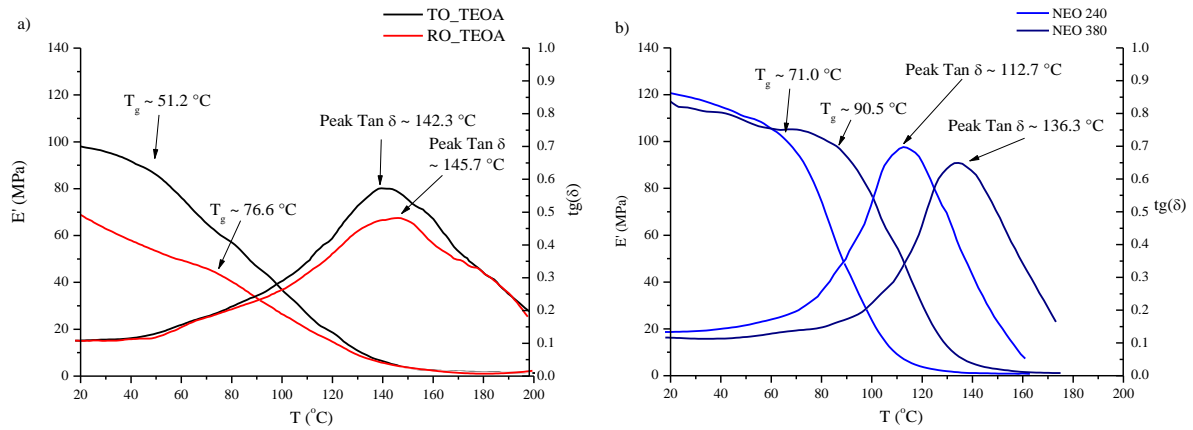


Figure 3.10. DMA data of E' and $\text{Tan } \delta$ of PU foams from a) bio-based polyols b) APP polyols

A similar conclusion can be made from DSC curves of developed rigid PU foam depicted in Figure 3.11. Rigid PU foams from APP polyols have more distinct glass transition step at 102.5 °C for NEO 240 polyol and 108.0 °C for NEO 380 polyol. Whereas for rigid PU foams obtained from bio-based polyols the heat capacity change step is barely detectable and the midpoint of step is very much dependent on how the linear regions before and after step are placed. Such DSC curves confirm that rigid PU foams from bio-based have a non-homogeneous polymer matrix. This is due to the nature of used bio-based polyols as they are a mixture of different substances. Materials with a broad functionality distribution usually display a broad glass transition as a result of superimposed glass transitions of network sections with low, medium, and high cross-linking density.

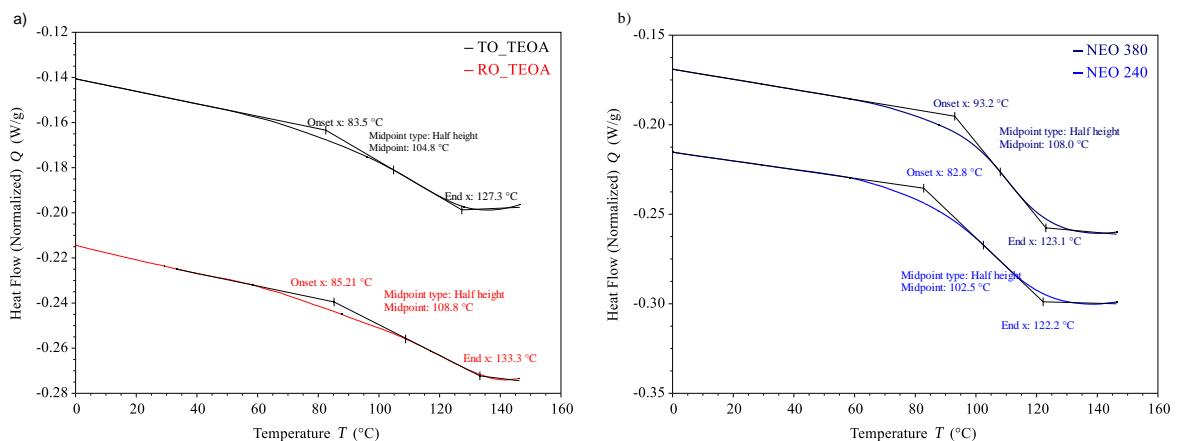


Figure 3.11. DSC data of PU foams from a) bio-based polyols b) APP polyols

In summary, the T_g of developed high-density rigid PU foams was evaluated using two different methods DMA and DSC. Rigid PU foams obtained from bio-based polyols showed

where f is the functionality of the reactant and C_f is the concentration of the reactant with the functionality f , expressed as moles per cubic centimetre of the final polymer. There is no ($f=2$) term in the sum because difunctional reactants do not form junction points [172]. The expression 3.1. was further evolved by L.W. Hill to calculate the crosslink density of the polymer matrix that does not agree with the ideal case of 100% conversion of all functional groups.

$$v_e = \frac{(2p-1)}{2} \sum_{f=3}^{\infty} f \cdot C_f \quad (3.2)$$

where p is defined as a fractional conversion. In case of $p=1.00$, all functional groups of the initial monomers have reacted and there are no dangling chains and no unreacted compounds that are dissolved into the polymer matrix.

Another parameter characterising crosslinked polymer matrix is the molecular weight between cross-links (M_c). In literature, there are several different interpretations of this parameter. L.W. Hill [172] proposed that:

M_c - is the total sample weight that contains one mole of elastically effective network chains [g/mol].

When v_e and M_c definitions are compared it can be concluded that the polymer matrix density ρ is reciprocal and M_c can be expressed as:

$$M_c = \frac{\rho}{v_e} \quad (3.3)$$

In this case, the density ρ of the polymer matrix can be cancelled out by expressing the concentration of the elastically effective networks in weight (vs. volume):

$c_f = C_f/\rho$ – moles of f functional reactant per gram of final polymer. Inserting new concentration into Eq. 3.2 an equation for M_c calculation is obtained:

$$M_c = \frac{\rho}{v_e} = \frac{\rho}{\frac{(2p-1)}{2} \sum_{f=3}^{\infty} \rho \cdot f \cdot c_f} = \frac{1}{\frac{(2p-1)}{2} \sum_{f=3}^{\infty} f \cdot c_f} \quad (3.4)$$

Equation 3.4 is useful because it allows to calculate M_c without experimental determination the density of the polymer matrix. Which is extremely useful for foams as the determination of polymer matrix density is close to impossible for the foamed morphology of the material. The Eq. 3.4 is valid only for p values in the 0.75-1.00 range, furthermore, it is assumed that no compounds have been incorporated in-between polymer chains as a solution.

The M_c can be expressed by two additional equations:

$$M_c^{B\&H} = \frac{M_0}{(p \cdot f_0 - 2)} \quad (3.5)$$

, where $M_0 = \sum_{i=1}^{\infty} \frac{n_i \cdot M_i}{n_i}$ and $f_0 = \sum_{i=1}^{\infty} \frac{n_i \cdot f_i}{n_i}$; n_i – number of moles of reactant i and M_i – molecular weight of reactant i [172]. A. Fridrihsone et al. had a similar approach [74] and expressed M_c as:

$$M_c^{A.F.} = \frac{\sum_{i=1}^{\infty} m_i}{\sum_{i=1}^{\infty} \frac{(f_i - 2) \cdot m_i}{M_i}} \quad (3.6)$$

, where m_i is the mass of individual reactants.

The M_c derived from equations 3.5 and 3.6 are different than 3.4 as they consider crosslink the same as a branch point. Whereas in Eq. 3.4 the crosslink is taken to be the same as elastically effective network chain [172].

Furthermore, the crosslink density and molecular mass between crosslinks can be obtained from experimental DMA data. The relationship between the rubbery plateau of the DMA test and crosslink density is:

$$v_e = \frac{G'}{R \cdot T} \cong \frac{E'}{3R \cdot T} \quad (3.7)$$

$$M_c^{DMA} = \frac{\rho \cdot R \cdot T}{G'} \cong \frac{3\rho \cdot R \cdot T}{E'} \quad (3.8)$$

, where G' is the shear modulus of rubbery plateau [Pa], E' –modulus of the rubbery plateau in tensile measurement [Pa]; ρ – density of polymer matrix [g/cm^3]; R – ideal gas constant [$\text{J}/\text{mol} \cdot \text{K}$]; T - the temperature of the rubbery plateau of G' and E' [K].

For this work, the M_c was calculated using described equations. The M_c from Eq. 3.4 has to be critically evaluated because this equation is designed for an ideal network of crosslinks, which rigid PU foam is not. There are unreacted groups which were noticed in FTIR spectra described in next paragraph, furthermore, the polymer matrix contains sol fraction of unreacted compounds like flame retardant, blowing agent, catalysts and surfactants, not to mention the dangling chains of the bio-based polyols. In the case of bio-based polyols for M_c calculation according to Eq. 3.4 the bio-based polyols were considered having an average functionality of $f_n=2$ to comply with their idealized chemical structure depicted in Figure 3.12.

The polymer matrix of all four rigid PU foam formulations was obtained in the not foamed form (solid material) and Young's modulus of the solid polymer was obtained from tensile test stress-strain curves [165]. Unfortunately, it was not possible to obtain good quality DMA curves for the monolithic (solid) polymer samples. Solid PU was too crosslinked and developed inner stresses during the curing process. When the material was heated above glass transition temperature the inner stresses were released and the samples started to crack developing noise signals in DMA curves. For M_c calculation according to Eq. 3.8 it is necessary to obtain G' or E' of the rubbery plateau of the material. The E' of the rubbery plateau of the polymer matrix was derived from the DMA data of rigid PU foam samples seen in Figure 3.10. It was assumed that a direct proportion between E' storage modulus in glassy state and E' of the rubbery plateau is the same for solid polymer as well as for foamed material. The different M_c measurements are summed up in Table 3.7.

Table 3.7

The storage modulus of rigid PU foams in rubbery plateau from DMA test (E_F), the storage modulus of solid PU polymer in rubbery plateau from DMA test (E_S), the temperature of the rubbery plateau (T), different M_c of rigid PU foam formulations.

Polyol type	E_F' , Pa	E_S' , Pa	T, K	M_c^{DMA} , g/mol	M_c , g/mol	$M_c^{B\&H}$, g/mol	$M_c^{A.F.}$, g/mol
TO_TEOA	1990	$1.88 \cdot 10^7$	429	568	405	468	552
RO_TEOA	1600	$1.86 \cdot 10^7$	429	590	413	463	536
NEO 240	1717	$2.20 \cdot 10^7$	405	550	333	456	499
NEO 380	1626	$2.78 \cdot 10^7$	433	391	303	418	453

Surprisingly the calculated M_c using various methods are in good agreement between each other. As expected the M_c calculated using L.W. Hill method have smaller values than $M_c^{B\&H}$. Furthermore, the M_c^{DMA} which is only one obtained from experimental data is very close to the

calculated M_c values. The M_c of both bio-based polyols is very similar due to similar chemical structure of the polyols. The $M_c^{A.F.}$ are 552 and 536 g/mol in case of TO_TEOA and RO_TEOA polyols respectively. For the rigid PU foams from APP based polyols the $M_c^{A.F.}$ are 499 and 453 g/mol in case of NEO 240 and NEO 380 polyols respectively. When the different M_c values are compared it is seen that both bio-based foams have higher M_c than APP based rigid PU foams, thus lower crosslink density. This confirms the conclusion that the higher crosslink density of APP based rigid PU foams delivers better mechanical properties. Furthermore, the polymer matrix of APP based PU foams is further reinforced due to the aromatic ring structure of the NEO 240 and NEO 380 polyols.

Chemical Structure of Rigid PU Foams from Sustainable Polyols

FTIR analysis was done to confirm the chemical structure of developed rigid PU foam materials. Analysed FTIR spectra are depicted in Figure 3.13. Signals in the range of $3337 - 3330 \text{ cm}^{-1}$ are the result of symmetric and asymmetric stretching vibrations of the N-H groups present in urethane groups. At 2926 cm^{-1} and 2854 cm^{-1} , symmetric and asymmetric CH_2 stretching vibrations were observed for rigid PU foams obtained from bio-based polyols. Presence of these distinct peaks confirms that obtained PU foams contain alkyl chains that were introduced from fatty acid moieties of bio-based polyols. Rigid PU foams from APP polyols had a broad peak at 2904 cm^{-1} which is a result of overlapping signals of alkyl and arene group C-H stretching. A small but distinct peak of unreacted isocyanate $-\text{NCO}$ group asymmetric stretching was identified at 2277 cm^{-1} for all samples. All rigid PU foam showed a C=O bond stretching peak at $1705-1712 \text{ cm}^{-1}$. Distinct conjugated C=C bond vibration of aromatic rings was identified at 1595 cm^{-1} . The peaks at 1510 cm^{-1} and 1307 cm^{-1} were attributed to the in-plane N-H bending and NCO stretching of the urethane group. Isocyanate trimerisation products were confirmed by C-N stretching vibrations seen at 1410 cm^{-1} [173–176].

There were several distinct differences between rigid PU foams obtained from bio-based polyols and APP polyols. First, previously mentioned alkyl chains seen as symmetric and asymmetric CH_2 stretching at 2926 cm^{-1} and 2854 cm^{-1} were more distinct for foams obtained from bio-based polyols. APP polyol based rigid PU foams had C-O-C stretching vibration doublet peak at 1267 cm^{-1} and 1100 cm^{-1} of aromatic ester group introduced by phthalic acid derivatives which were not present for foams from bio-based polyols. Furthermore, APP polyol based rigid PU foams had a very distinct peak of skeletal deformation, $\gamma(\text{CH})$, the vibration of the benzene ring at 730 cm^{-1} [115,116,159,161,162].

FTIR spectra analysis showed that rigid PU foams had high urea group content, compared to other PU materials due to the used blowing agent – water. The hydrogen bond index and degree of phase separation were very similar between all of the developed rigid PU foams. This is because all foams had the same isocyanate index thus amount of urethane groups in the polymer matrix should be the same. The similar degree of phase separation indicated that the different mechanical characteristics of rigid PU foam are caused by the inherent nature of polyols used. The aromatic groups present in NEO_240 and NEO_380 deliver higher rigidity of PU polymer matrix as well as higher thermal stability, thus they should be considered for application where mechanical characteristics of developed material are vital.

Isocyanate Index Influence on Mechanical Properties of Rigid PU Foams

Based on results obtained in previous paragraphs two best polyols have been selected for further material development. TO_TEOA and NEO_380 polyols were compared as a potential base component for sustainable rigid PU foam development. TO_TEOA polyol showed the most stable properties and highest mechanical properties when compared to RO_TEOA polyol, so it was chosen as bio-based polyol for further testing. Likewise, NEO-380 polyol delivered better characteristics when compared to NEO_240 polyol, so it was chosen as a recycled feedstock based polyol. Based on previous formulations (Table 3.2) rigid PU foams with different isocyanate indices (100-200) were developed to determine isocyanate index influence on the mechanical properties of developed materials. Foams were produced using stainless steel mould to obtain isotropic material with similar apparent densities of $\rho = 200 \pm 10 \text{ kg/m}^3$.

PU elastomers and flexible PU foams are produced with isocyanate index 100-110, which corresponds to the stoichiometric ratios of OH/NCO groups of 1.0/1.0 to 1.0/1.1. Rigid PU foams are developed in a variety of different isocyanate indices ranging from 110 up to 500 [6,71,178]. The isocyanate index is chosen to tailor desired properties of developed material for a specific application. There is no single approach for which the isocyanate index is better. It is dependent on the end application of the material and the production technology. Typical spray foaming equipment for rigid PU foam thermal insulation material development is mixing components at 1/1 volume ratios, thus this will be the deciding factor for isocyanate index of the developed formulation. Sandwich panel production equipment or reaction injection moulding (RIM) equipment usually has variable mixing ratios of the component. In this case, the isocyanate index influence on the properties of the developed materials will factor the selection of the final formulation.

Compression strength results for TO_TEOA based rigid PU foams are depicted in Figure 3.15. It is seen that compression strength and compression modulus increased with the increase of the isocyanate index. The increase is somewhat linear in boundaries of isocyanate index up to 200 and is caused by the addition of polyisocyanurate ring structures into PU polymer matrix. The higher crosslinking density due to shorter chains between isocyanurate rings causes stiffening of the material. A similar conclusion was made by I. Javni et al. where rigid PU foams with isocyanate index up to 350 were obtained using polyols based on propylene oxide. [178]

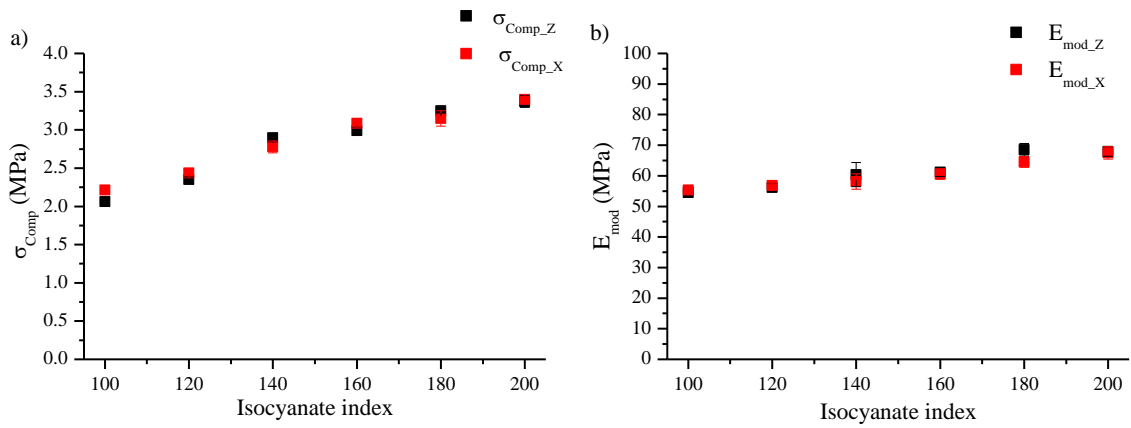


Figure 3.15. Isocyanate index influence on a) compression strength and b) Young's modulus of rigid PU foam based on TO_TEOA polyol

Similar results are seen for rigid PU foams based on NEO_380 polyol which are depicted in Figure 3.16. Although, the increase of compression strength, as well as Young's modulus, is not as prevalent as in the case of TO_TEOA polyol. This is due to the aromatic structure of the NEO_380 base polyol as polyisocyanurate rings only slightly increase the stiffness of already rigid APP chains.

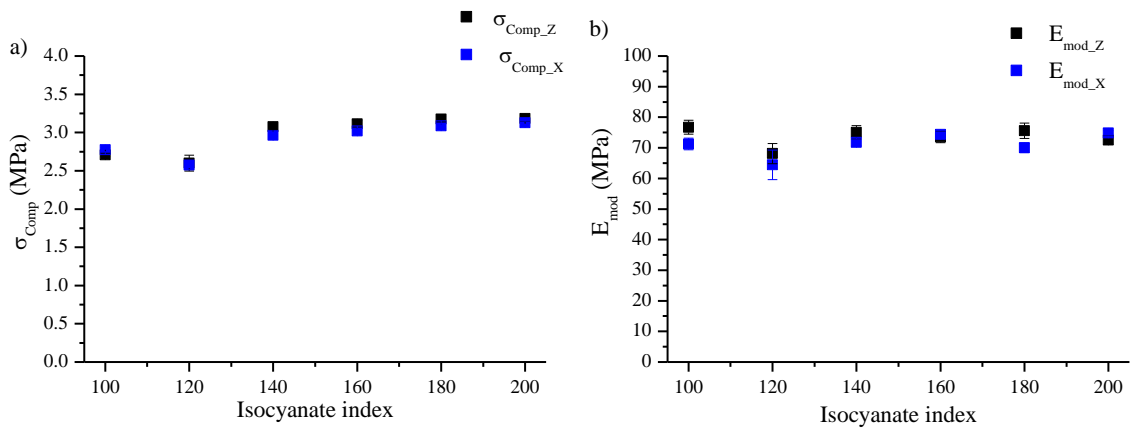


Figure 3.16. Isocyanate index influence on a) compression strength and b) Young's modulus of rigid PU foam based on NEO_380 polyol

There is also a linear dependency of the tensile properties of rigid PU foams ($\rho = 200 \pm 10 \text{ kg/m}^3$) with different isocyanate indices which is depicted in Figure 3.17. This investigation showed most convincingly that rigid PU foams based on APP polyol NEO_380 have better mechanical properties which are the targeted characteristics of materials developed in the frame of this Doctoral Thesis.

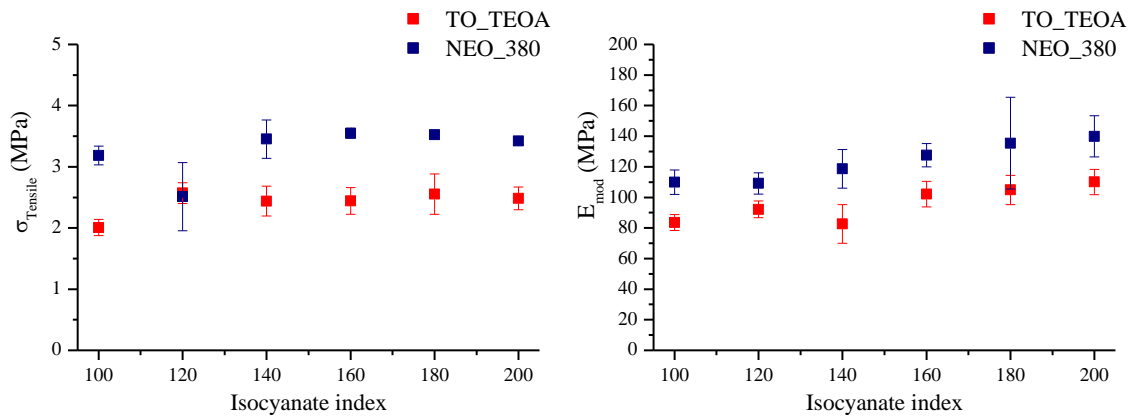


Figure 3.17. Isocyanate index influence on a) tensile strength and b) Young's modulus of rigid PU foam based on TO_TEOA and NEO_380 polyols

Investigation of isocyanate index influence on the mechanical properties of rigid PU foams showed that APP polyol NEO_380 delivers superior mechanical properties. This raw material was chosen for further development of high-density rigid PU foam. LS IWC task in project EVolution was to develop impact absorption core material for the automotive industry. The implementation of bio-based raw materials in the end product was not the only priority. A possibility for up-scaling of the technology was also considered. The NEO_380 is already produced on an industrial scale from PET waste products, thus quality control issues, as well as production capacity problems, have been already answered. Furthermore, NEO_380 can be considered a sustainable raw material, because it is produced from industrial PET waste.

Density Influence on Mechanical Properties of Rigid PU Foams

Rigid PU foams are employed as an impact absorption material in the automotive industry due to their high energy absorption capacity while maintaining low apparent density. High mechanical properties at low apparent densities allow reducing the weight of the car part while fulfilling safety requirements of the vehicle. For impact absorption application rigid PU foams with apparent density ranging from 30 to 400 kg/m³ have been employed [179,180]. For precise development of impact absorption material as well as modelling of rigid PU foam filled car part it is necessary to measure the stress-strain response of developed rigid PU foams.

In the frame of this thesis, rigid PU foams in vast apparent density range between 50 – 600 kg/m³ have been developed. The density of the rigid PU foams based on NEO 380 polyol was varied by modifying rigid PU foam formulation depicted in Table 3.2. To reach lower densities than the free rise density of described formulation of 145 kg/m³ a physical blowing agent was added (Solkane 87/13) 4–10 pbw in the polyol component. Higher densities were achieved by a high degree of overfilling the stainless steel mould, more reacting mass was poured into the mould. The physical blowing agent was used to keep the same polymer matrix as the chemical blowing agent – water would change the composition of the polymer structure. Obtained experimental data for compression yield strength and compression elastic modulus (Figure 3.18) closely correlates to a power-law function $\sigma_{comp} \sim \rho^{1.75}$ and $E_{comp} \sim \rho^{1.68}$. Obtained relations are similar to previously reported by M.C. Hawkins et al. [181] and S.H. Goods [182].

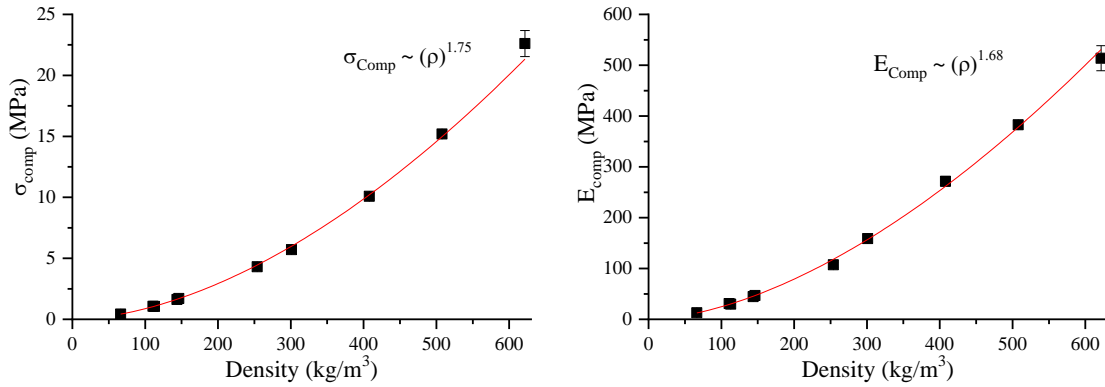


Figure 3.18. Density influence on compression yield strength and elastic modulus of rigid PU foam from NEO 380 polyol

Rigid PU foam apparent density influence on the tensile stiffness and strength is depicted in Figure 3.19. Similar to compression strength results the experimental data can be closely approximated by a power-law relation $\sigma_{max} \sim \rho^{1.30}$ and $E_{mod} \sim \rho^{1.75}$. Obtained mechanical characteristics are comparable to the commercial materials obtained from petrochemical feedstock with similar apparent densities. Furthermore, developed formulations showed slightly superior tensile strength and Young’s modulus than commercial rigid PU foams produced by NECUMER GmbH, Germany [183] and PUR 240 from Utah Foam Products, Inc. [184].

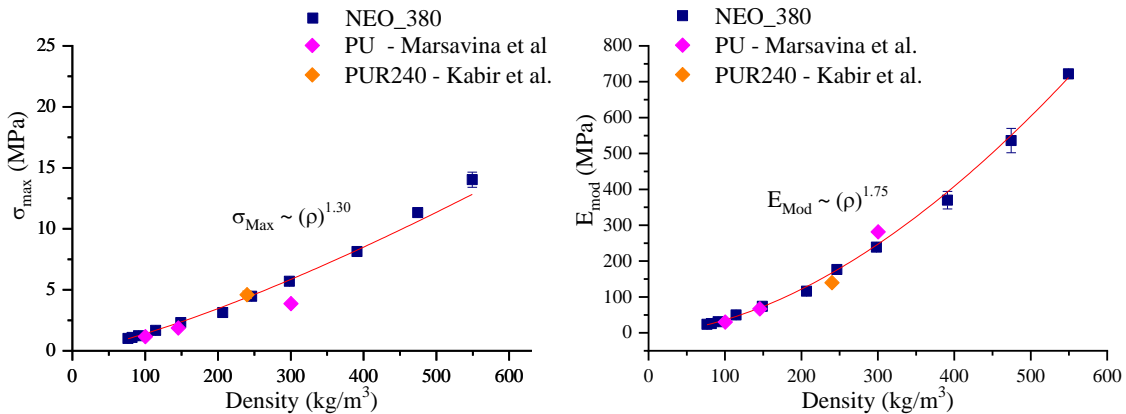


Figure 3.19. Apparent density influence on tensile strength and Young’s modulus of rigid PU foam from NEO 380 polyol

More in-depth analysis of analytical relations describing the tensile strength and Young’s modulus of foams as a function of apparent density has been described in the paper by M. Kirpluks *et.at.* [165]. Higher density foams were modelled according to continuum models where a strut-based unit cell models were used for lower density rigid PU foams. The continuum models describe rigid PU foams as a composite containing spherical [185], concave [186] or convex inclusions [187]. In strut-based unit cell models rigid PU foams are described as cubic unit cell [188,189] or more realistic Kelvin cell [190] which is closer to realistic foam morphology. Analytical models reasonably accurate describe rigid PU foam tensile properties at different apparent densities.

High Strain Rate Deformation Testing of Rigid PU Foams

The mechanical characteristics of foams are strongly affected by their apparent density as well as strain rate during mechanical deformation. The design of structural parts with an impact mitigation functionality is generally performed using numerical simulation codes by employing the finite element modelling (FEM) for crash simulation. As input data for such simulations, compressive stress-strain diagrams of foams are utilized. The compression stress-strain diagrams for developed rigid PU foams at different apparent densities at quasi-static strain rates were described in previous paragraphs. The FEM of the crash simulation needs input data of the rigid PU foam behaviour at high strain rates. A model of strain-rate and density-dependent stress-strain response that could be calibrated against a limited set of test data would allow reducing the number of actual foam tests needed to optimise material properties for car impact absorption part development

Split Hopkinson Pressure Bar Test of Rigid PU Foams

A Split Hopkinson Pressure Bar (SHPB) is an instrument for testing the stress-strain response of materials at high strain rates (10^2 - 10^4 s⁻¹). The classical method is testing in compression mode and the modern technique dates back to 1949 [191]. SHPB has been used to test the energy absorption of different materials at high strain rates [192–194]. The general idea of SHPB is to measure the elastic strain impulse propagation through a solid material with known properties of sound wave propagation through solid material. SHPB schematic with specimen sandwiched between two long elastic pressure bars, each of which is instrumented at its midpoint with a strain gage is depicted in Figure 3.20 [195].

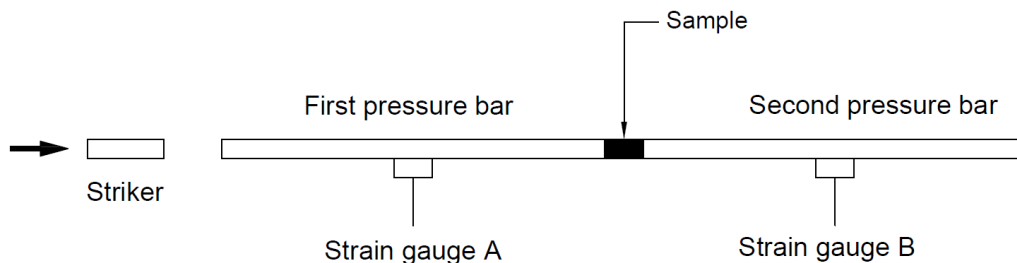


Figure 3.20. A typical configuration of SHPB

There exist several configurations of SHPB setups that can test different materials at high strain rates in compression, tensile and torsion modes. In the EVolution project, one of the partners: the Danish Technology Institute tested at LS IWC developed rigid PU foams using torsion SHPB testing equipment depicted in Figure 3.21.

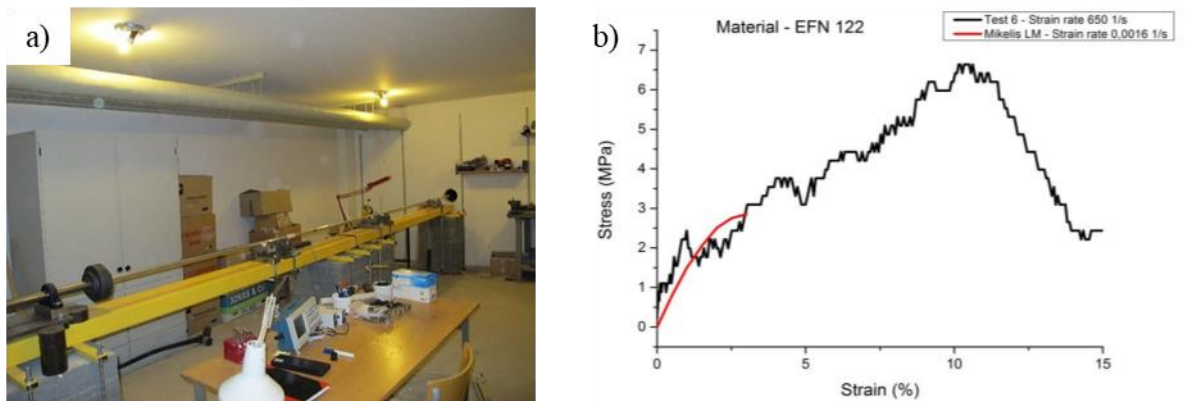


Figure 3.21. a) SHPB setup at the Danish Technology Institute, b) SHPB stress-strain curve obtained at a strain rate of 650 s^{-1} .

The SHB equipment was reconfigured to improve dynamic range and accuracy, as well as new sample geometries. Aluminium incident and transmission bars were replaced with new Ti alloy (Ti-6Al-4V) bars allowing greater input torque and angular velocity. The bars were 3 m long, 18 mm diameter, which requires precise alignment and the SHPB recalibration. The sample geometry for soft specimens requires careful optimisation because of strong reflections of the travelling pressure wave on the interface between bar and sample. The rigid PU foam samples described below were machined from foam cylinders using a specially ground parting tool designed to avoid creating stress concentrations at the specimen tube/flange interface. The optimisation of the sample geometry was key to obtaining reproducible results. Unfortunately, it was not possible to develop a testing procedure for the rigid PU foams. It was not possible to obtain reproducible results using Split-Hopkinson Pressure Bar due to the high amount of noise signals resulting from the travelling pressure wave on the interface between the bar and the sample. In Figure 3.21 are depicted stress-strain curves of NEO_380 based rigid PU foams with an apparent density of $200 \pm 10 \text{ kg/m}^3$ tested at quasi-static strain rates of 0.0016 s^{-1} and 650 s^{-1} (SHPB test result).

Rigid PU Foam High Strain Rate Compression Test

The results obtained from SHPB testing of rigid PU foam were not satisfactory for the FEM analysis of the automotive part design. Another approach was investigated to obtain stress-strain curves of developed rigid PU foams. The stress/strain curve data at high strain rates were obtained by modifying the CEAST 9340 Drop Tower (Instron) equipment. Usually, this equipment is used to test puncture impact behaviour according to ISO 6603-2:2000 standard. The testing rig is shown in Figure 3.22. b) where the compression of the PU foam sample is achieved by the impact of the sample against a steel plate. Obtained stress-strain curves are shown in Figure 3.22. c). A testing system with a 16 kN load cell was used for dynamic compression tests. Foam specimens were attached to the striking head by an oil-based adhesive and crushed against the horizontal surface of a rigidly fixed steel plate at a speed of 4 m/s, which translates into engineering strain rate, experienced by the specimen upon impact, of ca. 180 s^{-1} . The variation of impact force, striker speed, and displacement during the contact of the foam specimen with the steel plate were recorded. The impact absorption brakes were put up

so that the striker was stopped by them at a displacement corresponding to about an 80% compressive engineering strain of the foam specimen. The engineering strain was evaluated based on the striker displacement.

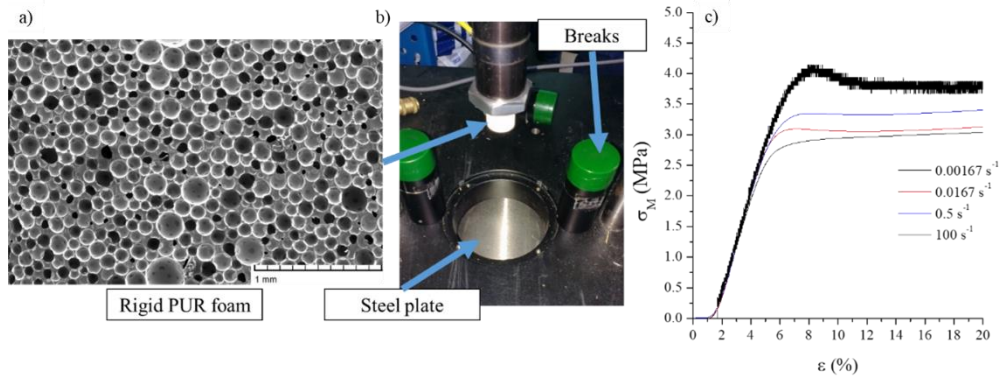


Figure 3.22. a) isotropic cell structure of the developed rigid PU foams b) testing setup, c) obtained stress/strain curves of rigid PUR foams at different strain rates

Predicting Compression Stress-Strain Behaviour of Developed Rigid PU Foams

An analytical model of compression stress-strain response of rigid PU foams could be calibrated against a limited set of test data. This would allow reducing the number of tested samples of actual rigid PU foams needed for design of the automotive part. Several models of compressive stress σ as a function of strain ε have been proposed (Eq. 3.9). Furthermore, a multiplicative factor g allows to correct the model for different strain rates $\dot{\varepsilon}$.

$$\sigma(\varepsilon) = f(\varepsilon)g(\dot{\varepsilon}). \quad (3.9)$$

Explicit analytical relations for the parameters of $f(\varepsilon) = f(\dot{\varepsilon}, \rho)$ as functions of foam density ρ have been considered by Avalle M. et. al. and Liu Q. et. al. [196,197]. Such an approach makes it possible to predict the compressive response of foams at densities different from those against which the model has been calibrated.

To apply Equation 3.9 for predicting rigid PU foam compression strength properties the functions $f(\varepsilon)$ and $g(\dot{\varepsilon})$ need to be specified. Furthermore, function parameter dependency on rigid PU foam density must be accounted for. The analytical form of $f(\varepsilon)$ is expressed in Equation 3.10 [180].

$$f(\varepsilon) = A \left(1 - e^{\left(-\frac{E}{A} \varepsilon \cdot (1-\varepsilon)^m\right)} \right) + B \left(\frac{\varepsilon}{1-\varepsilon} \right)^n. \quad (3.10)$$

The parameters E , A and B can be interpreted as Young's modulus, the plateau of plastic deformation and modulus of densification respectively. Whereas the exponents m and n are density independent material characteristics. The parameters E , A and B dependency from rigid PU foam density is described by a power-law function, therefore they can be expressed using the following Equations:

$$E(\rho) = C_E \left(\frac{\rho}{\rho_S} \right)^{k_E}; \quad A(\rho) = C_A \left(\frac{\rho}{\rho_S} \right)^{k_A}; \quad B(\rho) = C_B \left(\frac{\rho}{\rho_S} \right)^{k_B}. \quad (3.11; 3.12; 3.13)$$

The C_E , C_A and C_B are pre-factors with the dimension of stress and k_E , k_A and k_B designate the respective exponents, and ρ_S is the density of monolithic (solid) PU polymer matrix.

The strain rate effect on compression properties of rigid PU foams was described by Nagy et. al. [198] as depicted in Equation 3.14.

$$g(\dot{\varepsilon}) = \left(\frac{\dot{\varepsilon}}{\dot{\varepsilon}_0}\right)^{a+b\cdot\varepsilon}. \quad (3.14)$$

Results presented by D.A. Apostol et.al suggest that exponent parameters a and b have relatively modest variation with PU foam density [199]. For simplification it was assumed them to be linear functions of density:

$$a(\rho) = C_a + k_a \frac{\rho}{\rho_S}. \quad (3.15)$$

$$b(\rho) = C_b + k_b \frac{\rho}{\rho_S}. \quad (3.16)$$

Inserting Equation 3.10 and 3.14 into 3.9 an expression for engineering stress as a function of strain, strain rate and foam density was obtained:

$$\sigma(\varepsilon) = \left(A \left(1 - e^{\left(-\frac{E}{A}\varepsilon \cdot (1-\varepsilon)^m\right)} \right) + B \left(\frac{\varepsilon}{1-\varepsilon} \right)^n \right) \left(\frac{\dot{\varepsilon}}{\dot{\varepsilon}_0} \right)^{a+b\cdot\varepsilon}. \quad (3.17)$$

Equation 3.17 has seven different parameters, five describing the response at a reference strain rate $\dot{\varepsilon}_0$ (Equation 3.10) and two for the strain rate effect (Equation 3.14). All of the parameters except m and n exponents are density-dependent parameters described by power-law or linear function containing two material constants C_i and k_i . A minimal set of experiments must be performed to calibrate the Equation 3.17. A compression test of foams of two different densities at two different strain rates (i.e. reference strain rate and another one).

Rigid PU foams with two different densities of 113 ± 1 and 311 ± 3 kg/m³ were tested at quasi-static strain rates of $\dot{\varepsilon}_0 = 0.00167$ s⁻¹ (10 %/min; 2 mm/min) according to standard procedure ISO 844:2014. The stress-strain response of tested rigid PU foams was used to determine the values parameters of Equation 3.10 by minimizing the relative squared errors between the model and experimental data. The density-independent exponents of Equation 3.10 amounted to $n = 1.85$ and $m = -25.16$, whereas the density dependent parameters are summarised in Table 3.9. It was assumed that the density of monolithic (solid) PU polymer matrix was $\rho_S = 1210$ kg/m³ [200].

Table 3.9

Optimized values of density-dependent parameters for power-law functions based on rigid PU foam compression tests at 0.001674 s⁻¹ strain rate.

Parameter	E (Eq. 3.11)	A (Eq. 3.12)	B (Eq. 3.13)
C, MPa	1735	70.8	72.4
k	1.74	1.84	2.31

The approximation of the experimental data using Equation 3.10 was successful as depicted in Figure 3.23. The model reasonably well agrees with the experimental curves in broad rigid PU foam density range 113–513 kg/m³. Using this model it should be possible to fine-tune the apparent density of rigid PU foams required for the development of impact absorption vehicle part.

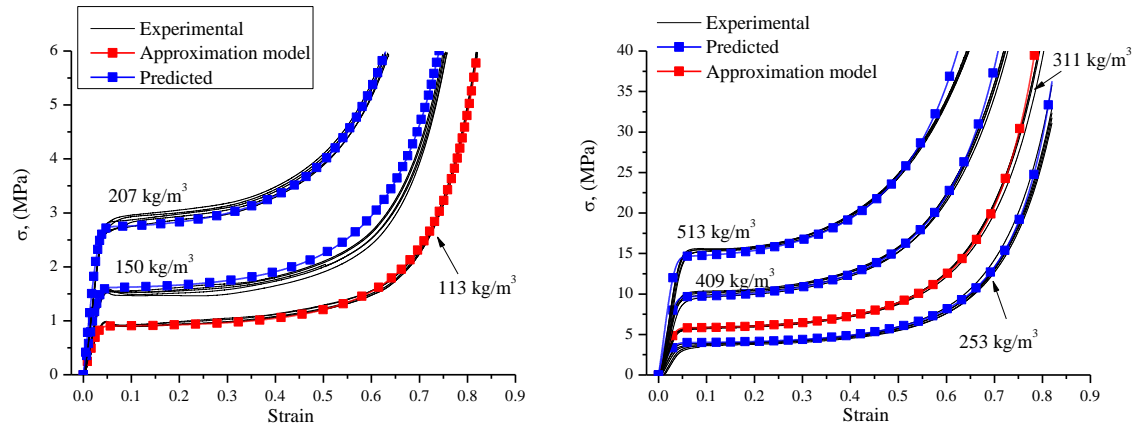


Figure 3.23. Experimental stress-strain curves of rigid PU foams with different densities for strain rate $\dot{\epsilon} = 0.00167 \text{ s}^{-1}$ (10 %/min), an approximation of data and predicted stress-strain curves using Equation 3.10

The strain rate effect on PU foam compression strength was evaluated after parameters of Equation 3.10 were established for reference strain rate tests. Experimental data from tests at $\dot{\epsilon} = 0.167 \text{ s}^{-1}$ (1000 %/min; 200 mm/min) were used for the rigid PU foams with the same apparent density as before. First, the parameters $a(\rho)$ and $b(\rho)$ were determined by minimizing the sum of squared errors between the experimental data and model values. Then, the parameters C_a , C_b and k_a , k_b were obtained using estimated values of $a(\rho)$ and $b(\rho)$. Obtained results are presented in Table 3.10.

Table 3.10

Optimized values of density-dependent parameters for linear functions based on rigid PU foam compression tests at 0.00167 s^{-1} and 0.167 s^{-1} strain rates.

Parameter	a (Eq. 3.11)	b (Eq. 3.12)
C, MPa	0.0438	0.0307
k	-0.0575	-0.144

The approximation of rigid PU foam stress-strain curves at a strain rate of $\dot{\epsilon} = 0.167 \text{ s}^{-1}$ (1000 %/min) also agrees with the experimental data as depicted in Figure 3.24. Furthermore, it was possible to predict the stress-strain curves at different apparent densities (150; 207; 253; 409 and 513 kg/m^3). Obtained coefficients of Equation 3.17 allow to predict stress-strain response of rigid PU foam at different densities as well as at different strain rates. Even, for higher strain rates of $\dot{\epsilon} = 0.5 \text{ s}^{-1}$ (3000 %/min; 600 mm/min) the model agreed with the experimental data as depicted in Figure 3.25.

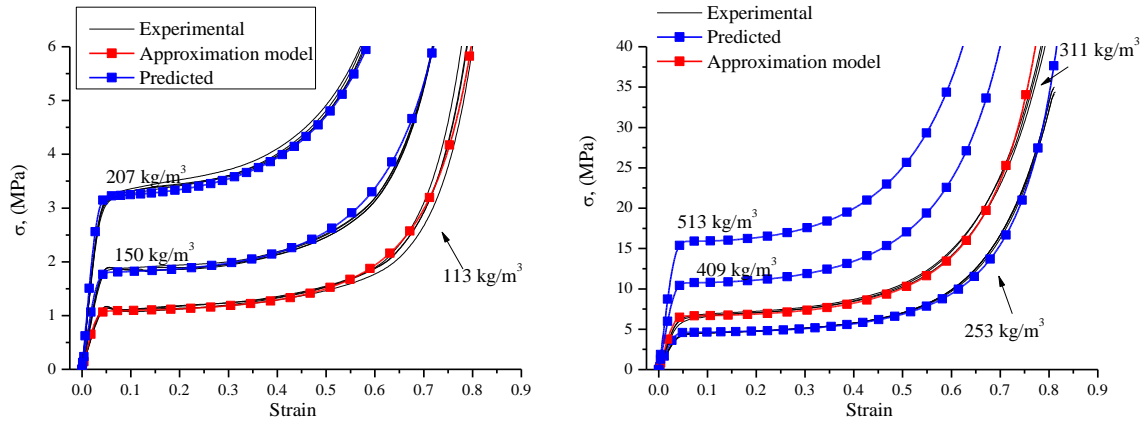


Figure 3.24. Experimental stress-strain curves of rigid PU foams with different densities for strain rate $\dot{\epsilon} = 0.167 \text{ s}^{-1}$ (1000 %/min), an approximation of data and predicted stress-strain curves using Equation 3.17

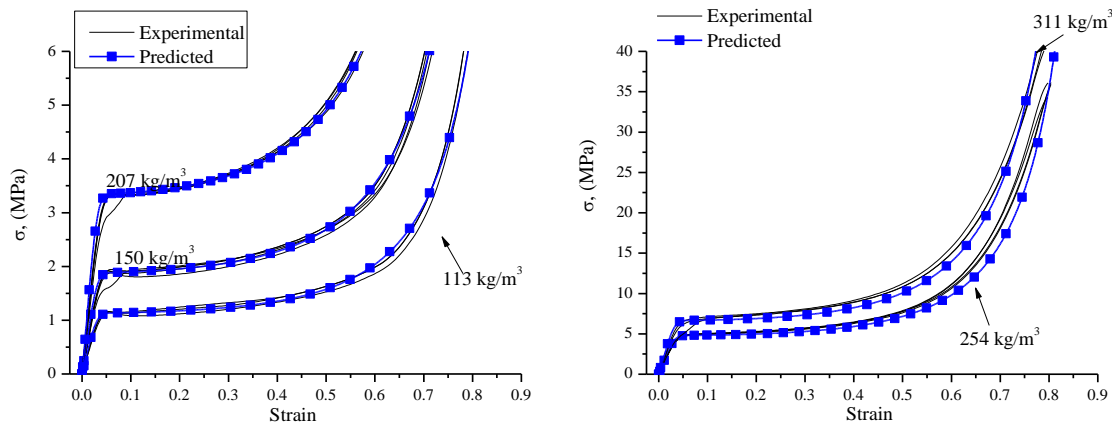


Figure 3.25. Experimental stress-strain curves of rigid PU foams with different densities for strain rate $\dot{\epsilon} = 0.5 \text{ s}^{-1}$ (3000 %/min) and predicted stress-strain curves using Equation 3.17

The data obtained from dynamic compression of rigid PU foam using CEAST 9340 Drop Tower (Instron) equipment relatively well agreed with the proposed model as depicted in Figure 3.26 a). It was difficult to optimise the speed of the striker and to choose the force gauge because the collected data contained a lot of noise signals. Nevertheless, the developed technique allowed to obtain stress-strain curves of rigid PU foams at relatively high strain rates (up to 180 s^{-1} ; 3.6 m/s) which is not possible using standard mechanical analysis testing equipment. The results of dynamic compression of rigid PU foams validated the proposed model at high strain rates so it can be a useful tool to be used in FEM analysis. More in-depth analysis of the model and its deviation from experimental results can be found in the paper by M.Kirpluks et.al [180]. To compare the different density and strain rate influence on material impact absorption ability, it is advantageous to evaluate values of absorbed energy at the same strain, which is represented as the area under the stress-strain curve [201]. For this study, rigid PU foams were evaluated until the strain of 0.6 which corresponds with the end of plastic deformation of the material. The absorbed energy of rigid PU foams depicted in Figure 3.26 b) shows that the density of the material has a significant influence on the impact absorption properties of the material and that the rigid PU foams are only lightly strain rate sensitive.

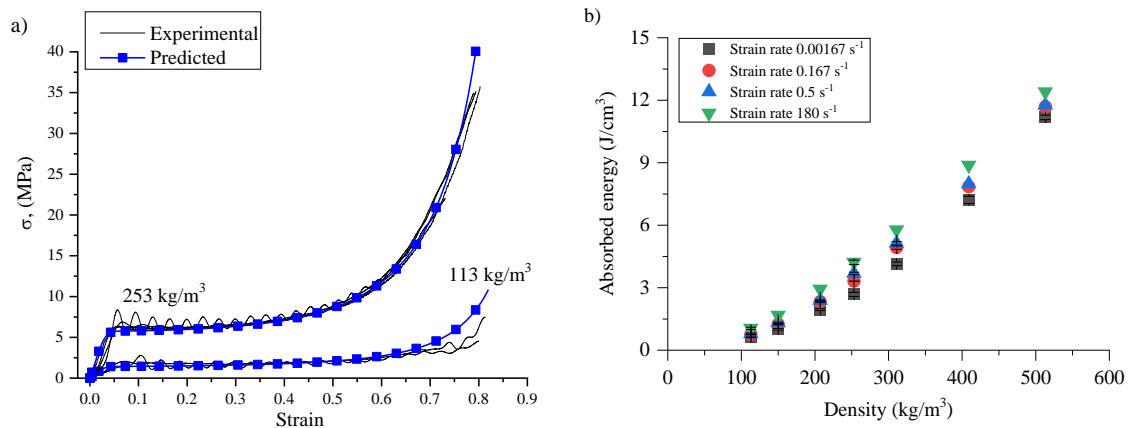


Figure 3.26. a) Experimental stress-strain curves of rigid PU foams with different densities for strain rate $\dot{\epsilon} = 180 \text{ s}^{-1}$ (3.6 m/s) and predicted stress-strain curves using Equation 3.17 and b) absorbed energy of developed rigid PU foams till 0.6 strain of material at different densities and strain rates.

Development of Impact Absorption Demonstrator for The Automotive Industry

Introduction to EU FP7 Project Evolution

Global trends toward CO₂ reduction and resource efficiency have significantly increased the importance of lightweight materials over the last years. The European Commission (EC) has set severe targets for average new car CO₂ emissions of 95 g/km by 2020, and by 2030 EC aims to reduce CO₂ emissions down to 75 g/km [202]. Weight reduction of the vehicle directly decreases the energy consumption and subsequently reduces the CO₂ emissions. Additional reduction of the CO₂ emissions could be achieved by the use of materials that are obtained from the renewable or recycled feedstock, like PU foams [203].

The weight reduction is particularly important for electric vehicles whose broader implementation is crucial to reduce the CO₂ emissions. Currently, the battery costs and the expected range of the vehicle are the most limiting factors for the slow rate of Full Electric Vehicle (FEVs) adoption for a larger consumer base. As a rough estimation, considering the battery costs for the year 2015, each slot of vehicle weight reduction of 50 kg implies a battery cost decreasing of about 500 €/car. This cost reduction can compensate for the additional cost due to light weighting, contributing to market penetration of EVs [204].

The Body in White (BiW) is the heaviest vehicle element, representing about 40% of total vehicle weight, hence the implementation of lightweight measures here appears effective. The project EVolution stands for “The Electric Vehicle revOLUTION enabled by advanced materials highly hybridized into lightweight components for easy integration and dismantling providing a reduced life-cycle cost logic”. Project EVolution finished in November 2016 and was a result of a cooperation between 24 partners from 11 different European Union (EU) countries, intending to demonstrate the sustainable production of a fully electric 600 kg vehicle. EVolution project was principally based on Pininfarina Nido concept which is fully electric and is an A-segment car conceived as a multifunctional rolling chassis plus a non-structural upper frame [205,206]. The Nido FEV and the Nido BiW concept is shown in Figure 3.27.

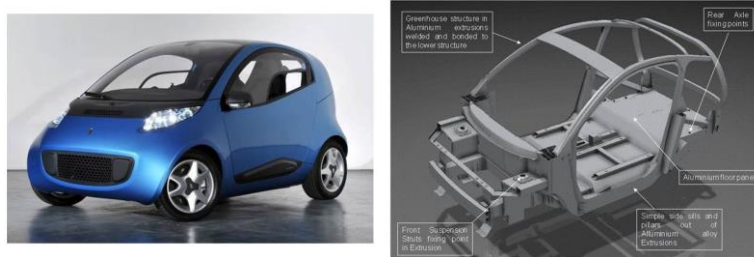


Figure 3.27. Nido concept (left) and Nido BiW (right)

EVolution project was focused on some specific car body areas. Different demonstrators were designed using lightweight materials to achieve 50% weight saving over existing steel equivalent. Selected demonstrators were: the underbody, the side door, the front crossbeam, the structural node (shotgun system) and the front mechanical subframe. Previous fully aluminium BiW of the Nido was redesigned to integrate the demonstrators, following the approach to lightweight everywhere reinforcing only where it is necessary while accomplishing structural performances, crashworthiness included.

Latvian State Institute of Wood Chemistry (IWC) was one of the partners cooperating in EVolution project to design novel rigid PU foam material for impact absorption used in the front crossbeam of the vehicle. Rigid PU foams were developed from sustainable resources, polyols obtained from vegetable oils and recycled PET. Rigid PU foams were developed in a broad range of the apparent densities ($50\text{--}600\text{ kg/m}^3$) and their mechanical properties were investigated to select the material that is the best suited for the core of the impact absorption element. The performance of the designed concept in vehicle crash was evaluated using FEM and subsequent crash test of the developed front crossbeam. To develop a good model, the data of the material mechanical deformation behaviour at high strain rates were acquired. The high strain rate compression tests were carried out by modifying puncture impact testing equipment to obtain stress-strain curves of foam material at $100\text{--}300\text{ s}^{-1}$ strain rates.

Development of the Nido EV Front Bumper – Crossbeam

Front bumpers designed from metal components are most commonly used in the automotive industry. Fully polymer structural front bumper beam could lead to significant weight reduction over its steel counterpart. Previously, in EU Seventh Framework Programme (FP7) project Nanotough [206], developed nanoclay (NC) and glass fibre (GF) reinforced polypropylene (PP) crossbeam was further modified to facilitate rigid PU foam impact absorption material. The Nanotough front bumper concept had a high toughness, but its stiffness did not fulfil the impact requirements, so additional impact absorption material was introduced. The proposed design was analyzed using ECE94 Full Front Crash simulations with the support of Pininfarina.

The new beam design consisted of two components, front and rear beam shell members and a core of rigid PU foam. Additional crash boxes made from NC and GF reinforced PP filled with rigid PU foams were developed and the whole system was tested for impact absorption. The proposed front crossbeam design is shown in Figure 3.28.

The target weight saving was set 50% over existing steel equivalent, which was achieved. The crash test results underlined the potentiality of this solution in terms of raw materials, processes and performances.

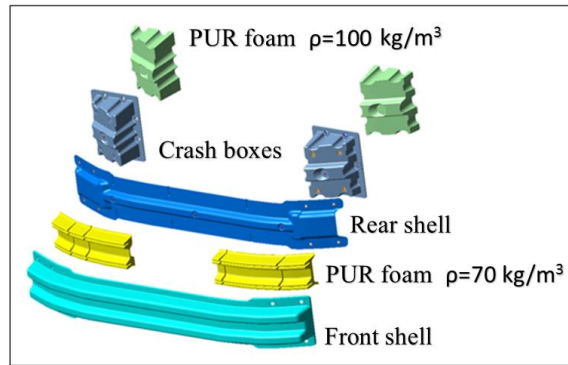


Figure 3.28. Evolution front crossbeam demonstrator concept

The Manufacturing Process

Starting from the background knowledge and the results obtained within the Nanotough project, partner ICECHIM together with partners from Alborg University proposed a new polymer material composition as a combination of two key solutions from nanotechnology and advanced materials field [206,207]. Therefore, the composition of the new polymer material was specially tailored using a special nano silicate additive (PP with 30-50% GF) which was used by partner FPK-BATZ. The nano silicate was embedded into a PP matrix to obtain a smart masterbatch. The masterbatch composition and the optimum ratio between components enabled its use directly in the extrusion-injection process of the FPK-BATZ products. An increase of 300% of impact resistance was observed when masterbatch was used in comparison to virgin PP. The stiffness and mechanical strength did not decrease due to a synergistic effect between the components [206].

FPK-BATZ produced the PP parts (front shell, rear shell and crash boxes) using NC and GF reinforced PP masterbatch by injection moulding. Different foam feeding tests were carried out by LS IWC on part geometry, to define the filling strategy and the PP/PU adhesion. A series of metallic inserts were introduced into all parts to improve joint strength into plastic parts and to avoid creep or stress relaxation.

Front and rear shell members were bonded together with a Polyurethane-based two-component adhesive, after plasma treatment of the surfaces, then the crossbeam and the crash boxes were bolted together, obtaining the complete demonstrator shown in Figure 3.29. The produced demonstrator was subjected to a physical crash test based on ALLIANZ protocol. The tests were focused on analyzing the impact resistance of the new structural component. Results were promising and showed that the proposed design has similar impact absorption properties than the steel front bumper counterpart.



Figure 3.29. Evolution Front Bumper Crossmember demonstrator prototype and the technological mock-up with integrated demonstrators

Summary of the Project Evolution

Proposed design elements of Nido demonstrated an interesting lightweight solution that could be implemented in modern vehicles. Proposed BiW of the Nido is estimated to be 113 kg versus 160 kg of the initial full aluminium baseline at the start of the project and more than 50 % lighter than the steel counterpart. Finite element analysis of the virtual full vehicle indicated good structural behaviour, considering EU standards of crash homologation and global static and dynamic performances.

A technological mock-up representing the full vehicle environment was conceived and manufactured by Pininfarina to demonstrate the part assemblies and showcase the project solution as shown in Figure 3.29. The production costs together with savings made from lightweight solution implementation are in line for a medium vehicle production volumes ($\geq 30,000$ units/year).

The project demonstrated that it is possible to implement sustainable materials where high-performance requirements are demanded. Rigid PU foam formulations obtained from recycled PET showed high stability and good mechanical properties. Recycled PET polyols could be used to replace aromatic polyester polyols obtained from petrochemical materials.

Conclusions of High-Density Rigid PU Foam Development

- Bio-based, as well as APP based polyols, were suitable raw material for the development of high-density rigid PU foams
- Bio-based polyols deliver lower mechanical properties of developed material due to lower functionality which decreased the crosslink density of PU polymer matrix
- The aromatic structure of APP polyols improved the mechanical properties of developed rigid PU foams.
- The crosslink density of polymer matrix and aromaticity of polyols directly correlated with the higher thermal stability of APP polyol based rigid PU foams.
- APP polyol NEO_380 was suitable to develop rigid PU foam in a broad apparent density range (50-600 kg/m³).

- The density influence on rigid PU foam mechanical properties was approximated by a power-law function.
- Mathematical model of apparent density and deformation strain rate influence on the stress-strain response of developed rigid PU foam was calibrated to predict compression behaviour of foams in a relatively broad range of densities ($\sim 100\text{-}500 \text{ kg/m}^3$) and strain rates ($0.00167\text{-}180 \text{ s}^{-1}$).
- Developed rigid PU foam formulations were successfully implemented into impact absorption crossbeam of Nido EV vehicle.
- A scale part of the front bumper cross member and crash boxes filled with developed rigid PU foam was produced and tested in vehicle crash tests.
- Materials developed in the frame of this Doctoral Thesis were useful to fulfil the goals of EU FP 7 project EVolution.

3.2. Rigid PU Foam Nanocomposite Development

Addition of nanoparticles into the polymer matrix can significantly change the properties of the end composite. Reinforcement of polymer matrix usually is done to increase the mechanical properties of the material or to obtain other beneficial properties. Filling a rigid PU foam polymer matrix with nanoclay affects both the morphology and mechanical properties of the material. Well-dispersed nanoclay particles serve as nucleation sites promoting the bubble formation which leads to a reduction of cell size of foams [208,209]. Furthermore, the nanoclay particles inside the cell walls work as a gas barrier, reducing the gas diffusivity through the foam. T.Widy&C.Macosko demonstrated that addition of nanoclays into rigid PU foam structure can decrease the gas permeability up to 82%. The strong reduction in permeability is caused by the reduction of cell size as well as gas barrier effect of nanoclay particles [210–212]. Such an effect is important for the longevity of the thermal insulation as it will allow prolonging the ageing of the thermal insulation material [213].

Paragraph 3.2 of presented Doctoral Thesis describes the increase of the mechanical properties of previously developed high-density rigid PU foam by reinforcing their structure with nanoclay particles. To enhance the physical and mechanical properties of rigid PU foams without detrimentally affecting their morphology, filling with nanoparticles was carried out by dispersing them either in the polyol or isocyanate component. Different dispersion methods were compared and their effect on intercalation/exfoliation of the layered structure of nanoclays were investigated. Furthermore, the nanoclay effect on the thermal properties of the PU foam composite was investigated by TGA analysis.

Two commercially available organoclays from Southern Clay Products, Inc. were used as fillers to produce PU nanocomposite foams. The clays, Cloisite 15A and Cloisite 30B are purified natural montmorillonites (MMTs) modified as follows: Cloisite 15A was modified by a dimethyl dehydrogenated tallow quaternary ammonium having a cation exchange capacity of 125 meq/100g, while Cloisite 30B was modified by a methyl tallow bis-2-hydroxyethyl ammonium with a concentration of 90 meq/100g clay. The Cloisite 15A organoclay had a larger interplanar distance, 3.15 nm (cf. 1.85 nm for Cloisite 30B) according to manufacturer's data.

APP Polyol and Nanoclay Dispersion

Three different dispersion methods were investigated to achieve stable nanoclay particle dispersion into NEO_380 polyol. Furthermore, nanoclay was dispersed into the polyisocyanate component using high share mixer. It was done to achieve exfoliated nanoclay dispersion. Prepared nanoclay dispersions were used to produce rigid PU foam and nanoclay composite samples.

The easiest method for nanoclay dispersion into polyol is simple mechanical stirring. Unfortunately, such approach did not deliver stable and well-dispersed system. Mechanical stirring was not sufficient enough to break larger agglomerates. They were visible to the naked eye so this most definitely cannot be considered a nanodispersion.

Dispersion with ultrasound was achieved by applying ultrasound over short periods; 5 s of active time and 5 s of the passive period to reduce heating of mixture. The temperature limit

was set to 40 °C and was controlled by a water bath. Ultrasound frequency was chosen 20 – 25 Hz and dispersion was done over 2 h period. The end result was homogenous milky mass with no visible agglomerates. Picture of equipment used is depicted in Figure 3.30.



Figure 3.30. Ultrasound dispersion equipment and obtained samples

High share mixer is turbine type mixing equipment that is similar to mechanical stirrer equipped with mesh net around its blades. The high-intensity mixing is achieved by high share forces developed when mixer`s blades move close to the steel mesh. Common mechanical stirring is done at mixer speeds of 100–2000 rpm. Whereas, high share mixer disperses nanoparticles at mixing speed up to 10 000 rpm. Similar to the three roll mill, developed share stress could be sufficient enough to exfoliate the nanoclay sheet structure. The significant increase of temperature, up to 100 °C due to share stresses was controlled by a cold water bath. High share mixer and setup used is depicted in Figure 3.31.

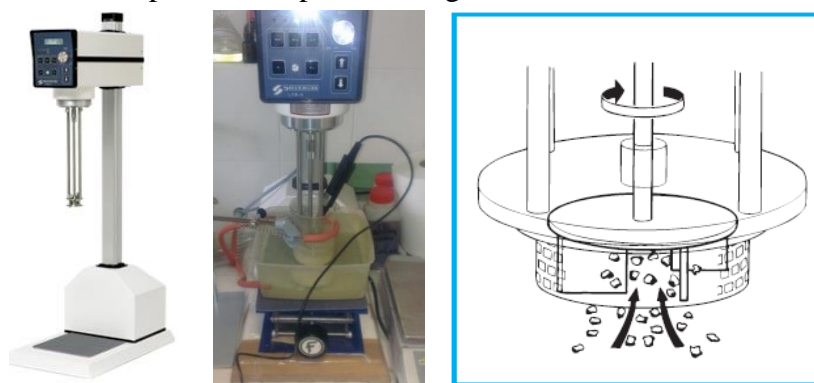


Figure 3.31. High share mixer, used setup and principle schematics

Samples of Cloisite 15A and Cloisite 30B nanoclay dispersed in NEO_380 polyol with high share mixer are depicted in Figure 3.32. Obtained polyol dispersions were homogenous, almost transparent. Polyol itself was not clear so it was hard to judge the influence of nanoclay on the transparency of the polyol. At higher nanoclay loads of 10, 20 wt.% of polyol mass the particles could not be dispersed sufficiently due to the significant increase of mixtures viscosity.

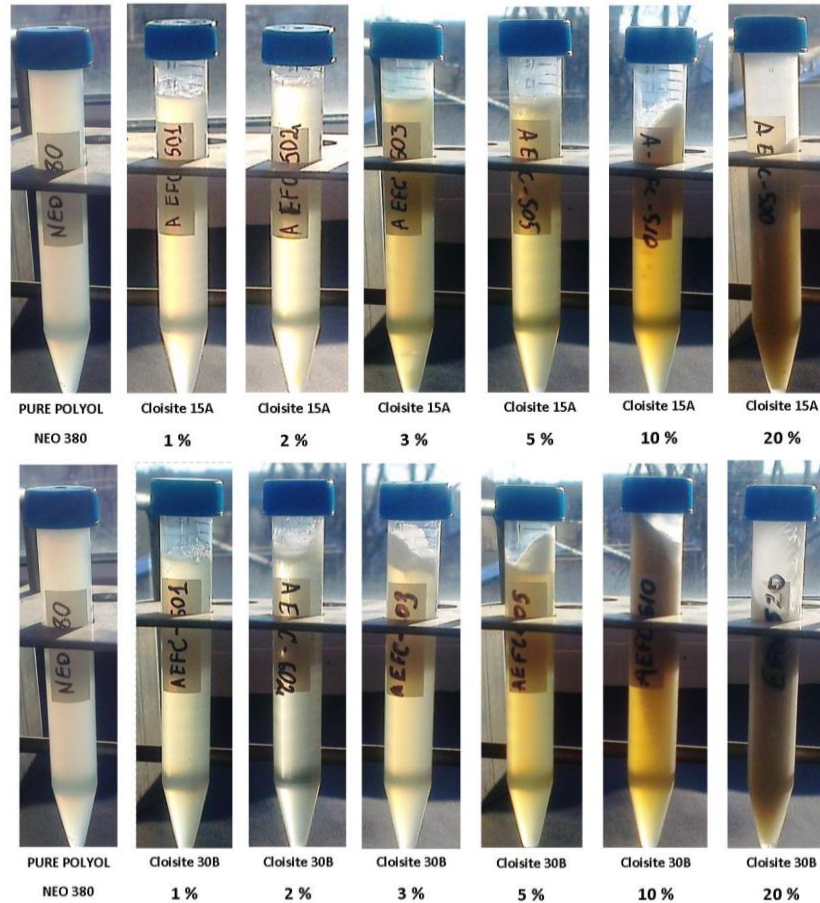


Figure 3.32. Cloisite 15A and Cloisite 30B dispersions in APP based NEO_380 polyol

X-Ray Diffraction Analysis of Nanoparticle Dispersions in Polyols

The efficiency of mechanical reinforcement with nanoclay is determined by the degree of dispersion, intercalation, and/or exfoliation of the filler. The latter can be evaluated by an XRD analysis, allowing estimation of the basal distance, D , in clay particles by Bragg's law [131,195]:

$$n \cdot \lambda = 2D \sin \theta \quad (3.18)$$

, where λ is the wavelength of X-ray radiation, D is the spacing between diffractive lattice planes, and θ is the measured diffraction angle corresponding to an n^{th} peak. The results based on the XRD patterns for Cloisite 15A are depicted in Figure 3.33 and the calculated values of spacing between diffractive lattice planes are presented in Table 3.11. It can be seen that 1 wt.% of nanoclay is a too small amount to be able to detect the effect of the mixing method on the dispersion quality. The peaks are barely noticeable and it is difficult to tell if nanoparticles have been exfoliated or there are too few signals to distinguish diffraction of lattice planes. The diffraction peaks of 5 wt.% Cloisite 15A dispersion in polyol have shifted to the left, which indicates a change in spacing between diffractive lattice planes. Nevertheless, the nanoclay particles have not been exfoliated as the diffraction signals are visible. The distance between Cloisite 15A clay lattice plates increased from 3.15 nm to 3.79 nm upon dispersion in the NEO_380 polyol.

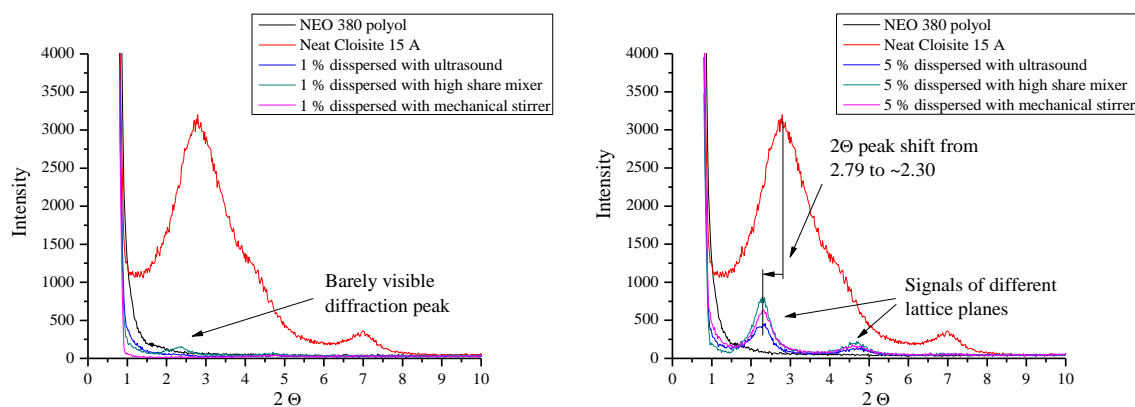


Figure 3.33. X-ray diffraction spectra for Cloisite 15A 1% and 5% dispersion in NEO 380 polyol

Table 3.11

X-ray diffraction peaks and interlamellar distances for Cloisite 15A nanoclay dispersed in NEO_380 polyol

	Peaks	2θ	D, Å
Neat Cloisite 15A	1	2.79	31.62*
1 wt.% Cloisite 15A dispersed by ultrasound	No peaks	-	-
		-	-
5 wt.% Cloisite 15A dispersed by ultrasound	1	2.30	38.40
	2	4.68	37.69
1 w% Cloisite 15A dispersed by high share mixer	1	2.34	37.75
	2	4.72	37.38
5 wt.% Cloisite 15A dispersed by high share mixer	1	2.30	38.40
	2	4.67	37.85
1 wt.% Cloisite 15A dispersed by mechanical stirring	No peaks	-	-
		-	-
5 wt.% Cloisite 15A dispersed by mechanical stirring	1	2.32	38.08
	2	4.68	37.69

* 31.5 Å – from product technical datasheet

Similar results were obtained for Cloisite 30B dispersion in NEO_380 polyols. The low concentration Cloisite 30B nanoclay dispersion of 1 wt.% gave signals that were marginally distinguishable from background noise as depicted in Figure 3.34. Whereas at 5 wt.% Cloisite 30B dispersion the first diffraction peak 2θ shifted from 4.74 to 2.32 which corresponds to an increase of distance between lattice planes from 1.85 nm to 3.76 nm. Different diffraction peak 2θ angles and distance between lattice planes of different Cloisite 30B dispersions in NEO_380 polyol are presented in Table 3.12.

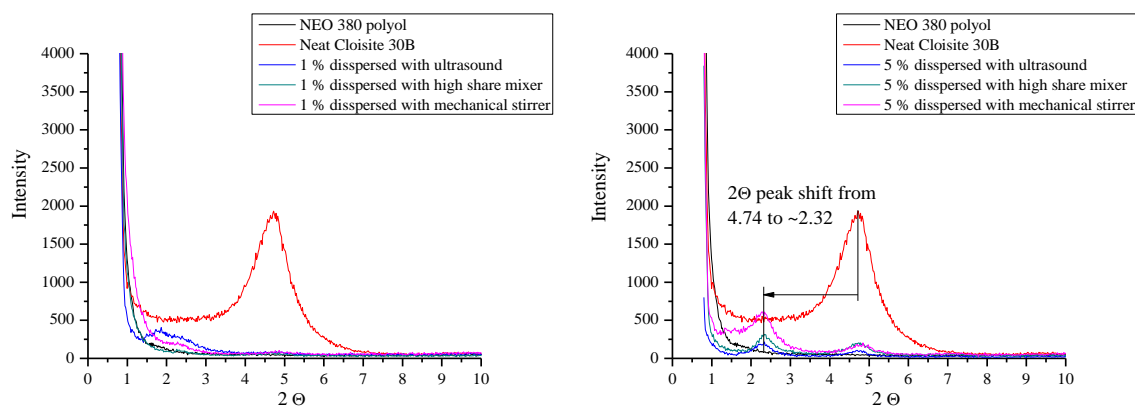


Figure 3.34. X-ray diffraction spectra for Cloisite 30B 1 wt.% and 5 wt.% dispersion in NEO 380 polyol

Table 3.12

X-ray diffraction peaks and interlamellar distances for Cloisite 30B nanoclay dispersed in NEO_380 polyol

	Peaks	2 Θ	D, Å
Pure Cloisite 30B		4.74	18.61*
1 wt.% Cloisite 30B dispersed by ultrasound	1	1.83	48.36
	2	2.32	38.08
5 wt.% Cloisite 30B dispersed by ultrasound	1	2.32	38.08
	2	4.90	36.03
1 wt.% Cloisite 30B dispersed by high share mixer	1	2.30	38.40
	2	4.65	38.01
5 wt.% Cloisite 30B dispersed by high share mixer	1	2.34	37.75
	2	4.76	37.07
1 wt.% Cloisite 30B dispersed by mechanical stirring	No peaks are seen	-	-
5 wt.% Cloisite 30B dispersed by mechanical stirring	1	2.32	38.08
	2	4.84	36.47

* 18.5 Å – from product technical datasheet

Nanoclay dispersion trials showed that the dispersion method does not influence the change of the distance between lattice planes. In both nanoclay samples, the distance between lattice plates increased. In the case of Cloisite 15A from 31.5 Å to 37.9 Å and in case of Cloisite 30B from 18.5 Å to 37.6 Å. This indicates that the type of organic modifier of the montmorillonite has little influence on the intercalation/exfoliation of the nanoclay in the polyol. It was observed, that dispersions with Cloisite 30B are much more stable and nanoclay sediments at a much slower rate. The increased stability of the Cloisite 30B dispersions could be explained by the formation of hydrogen bonds of the nanoclays organic modifier and the carboxyl groups of the NEO_380 polyol. All three dispersion methods of both Cloisite 15A and Cloisite 30B nanoclays into NEO_380 polyol are depicted in Figure 3.35. The image depicts that the X-ray diffraction spectra of the different dispersions are similar, thus it can be concluded that the mixing method does not influence the intercalation of the nanoclay. Furthermore, the exfoliation of the nanoclay lattice structure has not been achieved.

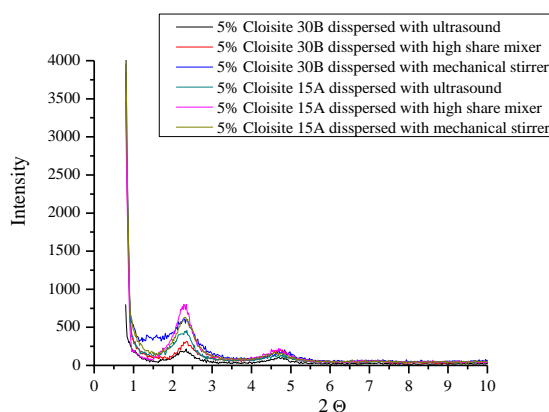


Figure 3.35. X-ray diffraction spectra for 5 wt.% of Cloisite 30B and Cloisite 15A dispersions in NEO_380 polyol

Exfoliation of Cloisite 30B Nanoclay in Isocyanate

Exfoliation of the nanoclay lattice layers could be achieved by introducing major elastic forces in-between the nanoclay layers that overcome opposing electrostatic and van der Waals forces. This was reported by J.H. Park and S.C. Jana where exfoliation of different nanoclays was achieved by curing reaction of epoxy resins [214]. A similar approach could be used for polyurethane materials where raw materials like pMDI, polyol, and/or catalysts are diffused inside the interlayer spacing of nanoplatelets of clay in presence/absence of a suitable solvent. A successful exfoliation of Cloisite 30B nanoclay in the isocyanate component of rigid PU foams was reported by P.Mondal and D.Khakhar [209]. During subsequent polymerization, the polymer chains grow leading to the expansion of interlayer spacing and exfoliation of nanoplatelets in the polymer matrix. In this process, the intercalation or exfoliation of the nanoplatelets is highly dependent on the compatibility between the interlayer modifier and raw materials or pre-polymer [215].

The organic modifier of the Cloisite 30B contains OH groups that are reactive with isocyanate. The exfoliation of Cloisite 30B was done by adding the nanoclay particles into a pMDI component of rigid PU foam formulation. Two different Cloisite 30B contents of 4.7 wt.% and 10 wt.% were evaluated. The reaction between OH and NCO groups was catalysed by adding 0.05 wt.% of dibutyltin dilaurate urethane formation catalyst. The X-ray diffraction spectra of exfoliated Cloisite 30B nanoclay are depicted in Figure 3.36. Cloisite 30B dispersion in the pMDI component is much different than nanoclay dispersion in NEO_380 polyol. Even at high Cloisite 30B nanoclay load of 10 wt.% the diffraction peaks disappeared which indicated the exfoliation of the layered structure of the Cloisite 30B. Obtained exfoliated dispersion was used to prepare rigid PU foam and nanoclay influence on the mechanical properties of the rigid PU foam was investigated.

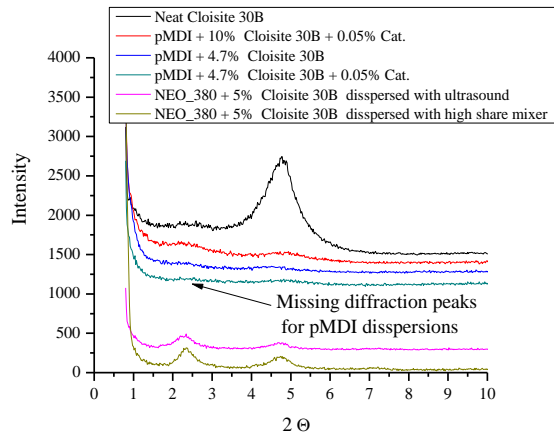


Figure 3.36. X-ray diffraction spectra for Cloisite 30B dispersions in pMDI and NEO_380 polyol

Morphological Properties of PU Foams Modified With Nanoclay

Cloisite 15A nanoclay influence on the morphological properties of rigid PU foams were investigated at several different filler contents, 0,00; 0,50; 1,29; 2,68 and 5,83 wt.% in rigid PU foam by mass. Furthermore, Cloisite 30B was also investigated at 0.50 wt.% and 0.75 wt.%. Nanoclay was dispersed using ultrasound sonification method. The average cell size distribution histograms for the Cloisite 15A filled rigid PU foams, as well as the measured average cell size, are depicted in Figure 3.37.

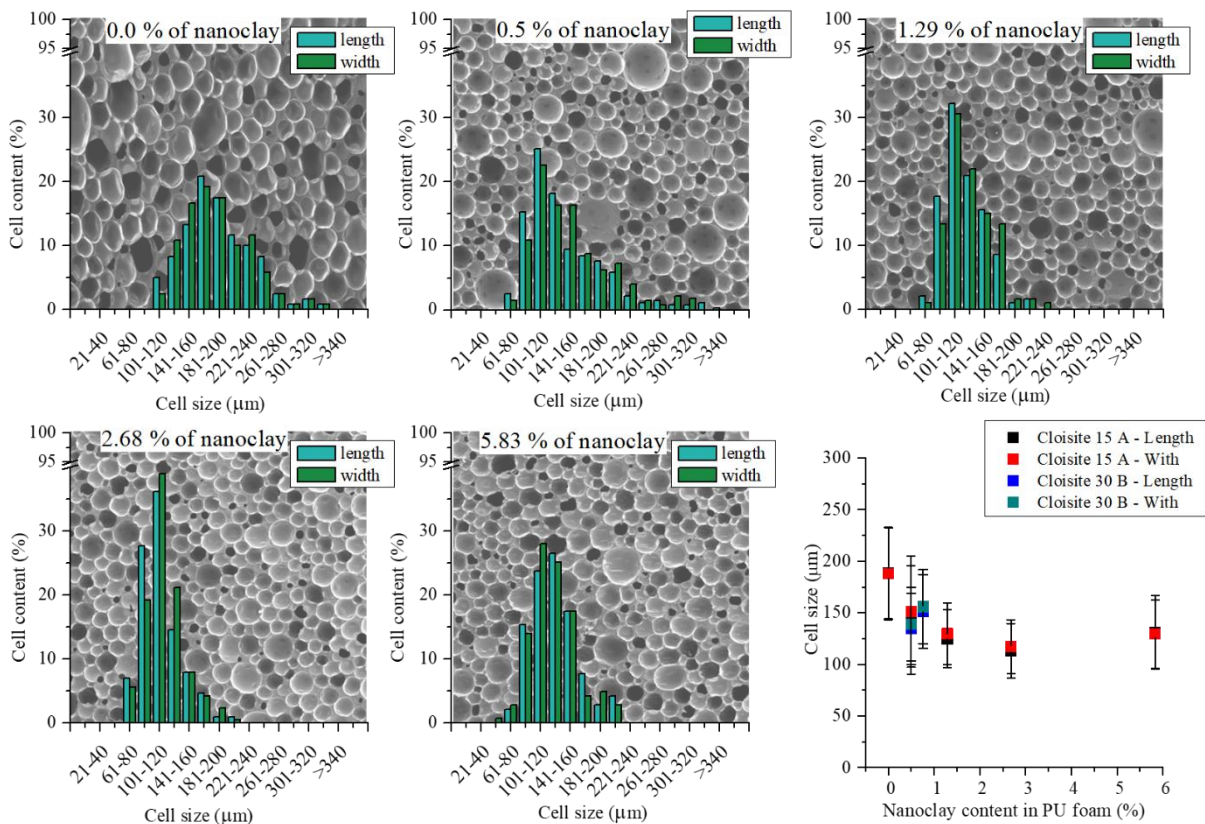


Figure 3.37. The cell size distribution of rigid PU foams filled with Cloisite 15A nanoclay

The addition of nanoclay into rigid PU foam structure did not disturb the isotropic cell structure. The anisotropy coefficient was in-between 0.95–1.02 for all of the measured samples. Nanoclay addition into rigid PU foam matrix decreased the average cell size from 188 to 113 μm for the neat rigid PU foam and 2.68 wt.% nanoclay content respectively. The decrease of cell size can be explained by the nucleation effect of gas micro-bubbles on the surface of the nanoparticles thus increasing cell count and decreasing overall cell size. The decrease of average cell size was similar for Cloisite 15 A and Cloisite 30 B nanoclay fillers. Which indicates that the organic modifier of the nanoclays does not influence cell formation of rigid PU foams. At higher nanoclay loads above 2.68 wt.% the decrease of the cell size reached a plateau. A similar trend of rigid PU foam cell size decrease was observed by M. Thirumal et. al. where Cloisite 30B was used as a filler [216]. Addition of nanoclay filler into rigid PU foam formulation significantly increased component viscosity. This introduces several technological issues for material production. At higher viscosities, it was difficult to sufficiently mix the polyol and isocyanate components. Furthermore, higher viscosity of the reacting mass hinders foam growth and formation of uniform material [217].

Mechanical Properties of Rigid PU Foams Modified with Nanoclay

Nanoclay dispersion method, as well as the two different nanoclay filler influence on the mechanical properties, were determined by compression and tensile tests at quasi-static strain rates. The X-ray diffraction analysis showed that Cloisite 30B nanoclay is exfoliated in dispersion in isocyanate (see Figure 3.36.). Thus, compression properties of the developed rigid PU foams with Cloisite 30 B dispersion in the isocyanate component were also tested. The targeted apparent density of tested rigid PU foams was 200 kg/m^3 . The samples were obtained in stainless steel mould according to the procedure described in paragraph 2.1. The apparent density of the produced samples deviated by $200 \pm 15 \text{ kg/m}^3$, thus compression strength test results were normalized to the average density of 200 kg/m^3 according to the power-law function described previously (see paragraph 3.1).

The Compression Strength of Rigid PU Foams Filled with Nanoclay

The simplest way to introduce nanoclay into rigid PU foams is to disperse the filler into polyol component by mechanical stirring. This approach was tested for Cloisite 15A nanoclay filler and compression strength and Young's modulus results are depicted in Figure 3.38. Introduction of Cloisite 15 A nanoclay filler into rigid PU foam polymer structure slightly increased the compression strength and stiffness of the material. Cloisite 15A loading beyond 1.29 wt.% was not continued as it was not expected that the mechanical stirring dispersion method would result in improvement of the mechanical properties, which was not the case. Further results will show that the dispersion method has little influence on the change of the rigid PU foam mechanical properties. Nevertheless, the mechanical stirring of Cloisite 15 A was not desirable, because it does not result in a uniform/stable dispersion, which influenced the foam formation and growth. Furthermore, the undispersed agglomerates introduced micro-size defects in the rigid PU foam structure which decreased the homogeneity of the material. This resulted in much higher deviations between parallel samples in the compression strength

test results seen in Figure 3.38. The dotted line in Figure 3.38 represents mechanical properties of the neat rigid PU foam.

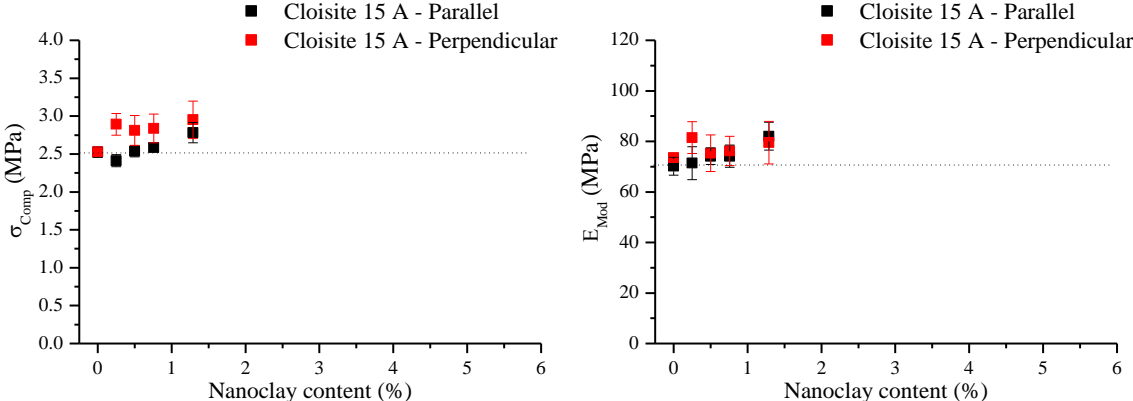


Figure 3.38. Compression strength and Young’s modulus of rigid PU foams filled with Cloisite 15A dispersed in NEO_380 polyol using a mechanical stirrer

When Cloisite 15A nanoclay particles were dispersed using ultrasound the dispersion was much more homogeneous which is reflected on the rigid PU foam mechanical properties. The standard deviation between parallel samples was lower than for samples where Cloisite 15A was dispersed using the mechanical stirrer (see Figure 3.39). The increase of the compression properties was similar with an initial increase almost proportional to the nanoclay loading. At relatively low Cloisite 15A loading of 1.29 wt.% the compression strength and Young’s modulus increased by 19 % and 10 % relative to the neat material of rigid PU foam. Parallel to the foaming direction mechanical properties increase was not so distinct. Furthermore, developed rigid PU foams showed slight anisotropic properties of compression strength. Contrary to the typical rigid PU foams compression strength perpendicular to the foaming direction was higher than when tested parallel to the foaming direction. Rigid PU foam samples were obtained in a closed mould to obtain isotropic material. Inevitably there are bound to be defects and deviations from ideal - isotropic scenario due to hand mixing of components and hand pouring of the material. Rigid PU foam seems to be stronger when tested perpendicular to the foaming direction. This is due to rigid PU foam flow in the mould. When the reacting mass reached the lid of the foam, the material continues to flow to the sides of the mould.

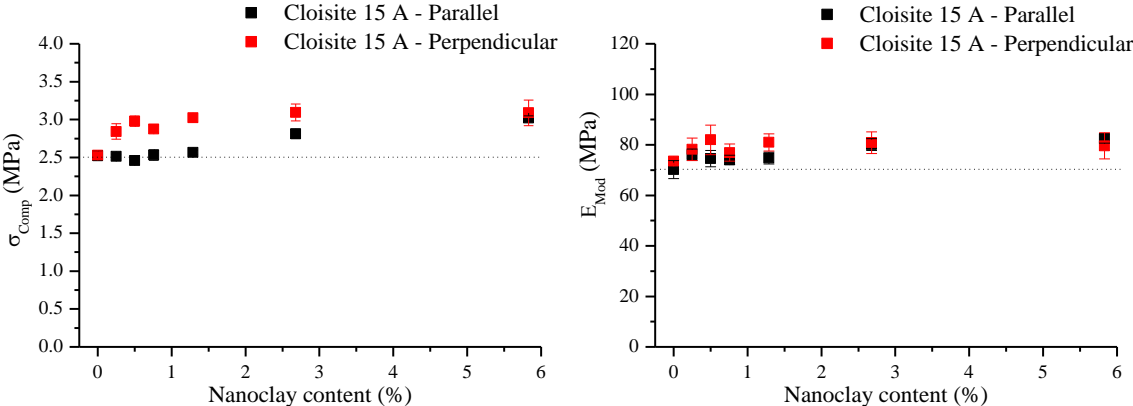


Figure 3.39. Compression strength and Young’s modulus of rigid PU foams filled with Cloisite 15A dispersed in NEO_380 polyol using ultrasound

Rigid PU foam filled with Cloisite 30B nanoclay filler which was dispersed with ultrasound showed a similar increase of the compression properties to Cloisite 15A as depicted in Figure 3.40. The initial increase of mechanical properties was proportional to nanoclay loading followed by plateau at nanoclay loadings above 2.68 wt.%. At 2.68 wt.% of Cloisite 30B nanoclay content compression strength and Young’s modulus was increased by 25 % and 17 % relative to the neat material when tested perpendicularly to the foaming direction.

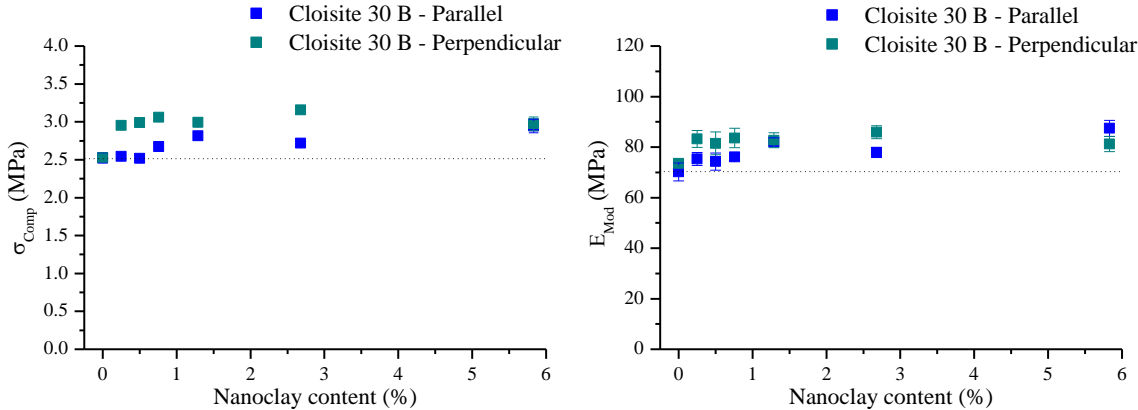


Figure 3.40. Compression strength and Young’s modulus of rigid PU foams filled with Cloisite 30B dispersed in NEO_380 polyol using ultrasound

Different shape sonotrode was tested to achieve better dispersion of Cloisite 30B nanoclay in NEO_380 polyol. Obtained compression strength and Young’s modulus results are depicted in Figure 3.41. Obtained dispersion was clearer which indicated better dispersion of the nanoclay agglomerates. Nevertheless, higher efficiency sonotrode did not result in a higher increase of compression properties. At 1.29 wt.% of Cloisite 30B, compression strength and Young’s modulus increased by 17 % and 14 % respectively relative to the neat material when tested perpendicular to the foaming direction. Higher efficiency sonotrode could influence NEO_380 polyol by scission of ester bonds of polyol structure. Unfortunately, this was not confirmed by any analytical methods.

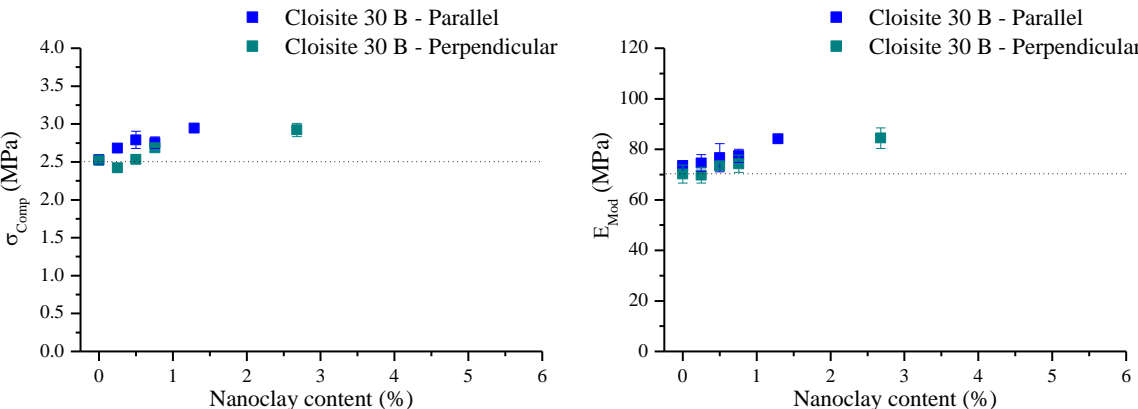


Figure 3.41. Compression strength and Young’s modulus of rigid PU foams filled with Cloisite 30B dispersed in NEO_380 polyol using ultrasound (different sonotrode)

High share mixer dispersion method showed the most promising results as discussed in the previous paragraph. Unfortunately, seemingly better dispersion of nanoclay in NEO_380 polyol

did not result in a much higher increase of rigid PU foam compression properties. Compression strength and Young's modulus of Cloisite 15A and Cloisite 30B dispersed with high share mixer are depicted in Figure 3.42 and Figure 3.43 respectively. The highest increase of compression strength of 23 % and Young's modulus of 29 % was observed for 2.68 wt.% of Cloisite 30B dispersion. The compression properties of rigid PU foams filled with nanoclay which was dispersed using high share mixer showed close to isotropic characteristics for both types of filler. This was explained by a better dispersion of nanoclay particles and increased followability of the material in the sample preparation process.

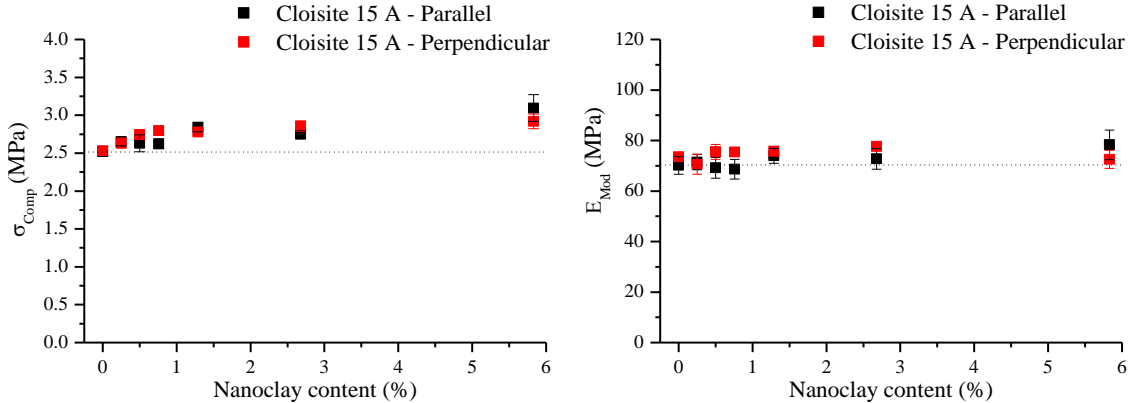


Figure 3.42. Compression strength and Young's modulus of rigid PU foams filled with Cloisite 15A dispersed in NEO_380 polyol high share mixer

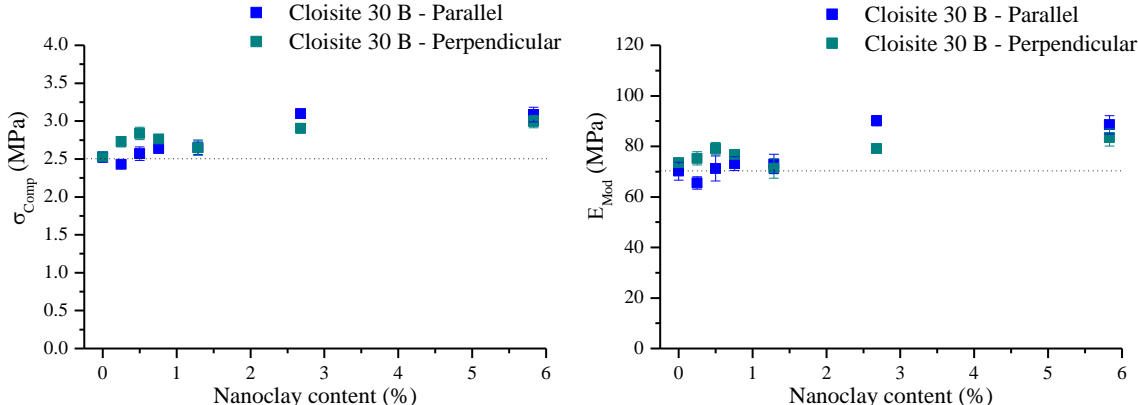


Figure 3.43. Compression strength and Young's modulus of rigid PU foams filled with Cloisite 30B dispersed in NEO_380 polyol high share mixer

X-ray diffraction analysis of Cloisite 30B dispersion in the isocyanate component showed that the nanoclay filler was exfoliated (see Figure 3.36.). An exfoliated nanoclay filler should yield a higher increase of the mechanical properties at lower nanoclay loading [168,215]. Compression strength and Young's modulus of rigid PU foam where Cloisite 30B was dispersed in the isocyanate component is depicted in Figure 3.44. The increase of mechanical properties of the rigid PU foam is noticeable at much lower Cloisite 30B content. At 0.25 wt.% the compression strength and Young's modulus was increased by 10 % and 16 % respectively. The best results were achieved for 1.29 wt.% of Cloisite 30B content at 17 % and 20 % increase of compression strength and Young's modulus respectively. Exfoliation of Cloisite 30B helped

to achieve an increase of mechanical properties at low nanoclay loadings. Nevertheless, the maximum increase of the mechanical properties was not higher than for samples where nanoclay was dispersed into NEO_380 polyol.

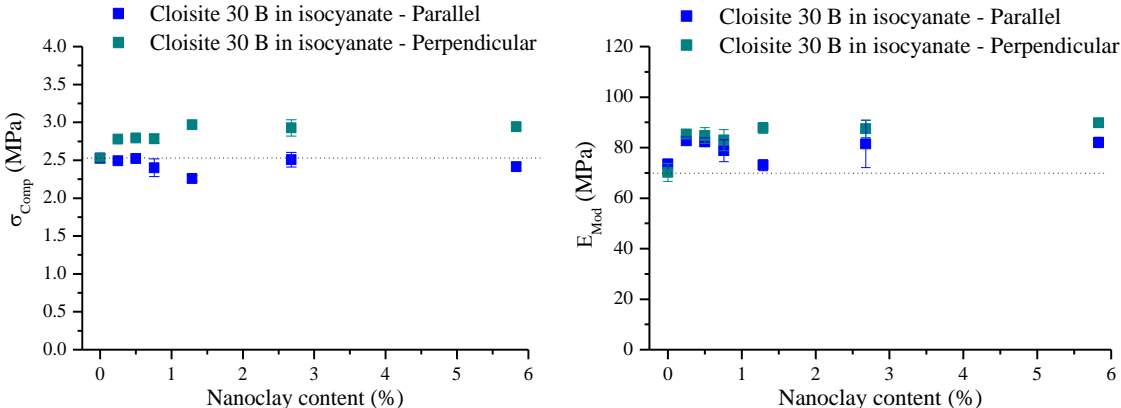


Figure 3.44. Compression strength and Young’s modulus of rigid PU foams filled with Cloisite 30B dispersed in isocyanate

To drive the exfoliation process a reaction of the Cloisite 30B organic modifier and pMDI was catalyzed using dibutyltin dilaurate catalyst. Rigid PU foams obtained from this pMDI showed a significant increase of Young’s modulus which is depicted in Figure 3.45. At 0.76 wt.% of Cloisite 30 B Young’s modulus was increased by 35% when compared to the neat material. Unfortunately, the same increase was not observed for the compression strength of rigid PU foam. The added catalyst not only promotes the exfoliation of the Cloisite 30B nanoclay but also promoted the side reactions of the pMDI isocyanate groups. This was observed as an increase in the viscosity of the pMDI component. The pMDI oligomerization products have much stiffer chain linkages which contribute to the increase of Young’s modulus. Nevertheless, the increased viscosity of the material did not allow to obtain good quality rigid PU foam as seen from the compression strength results.

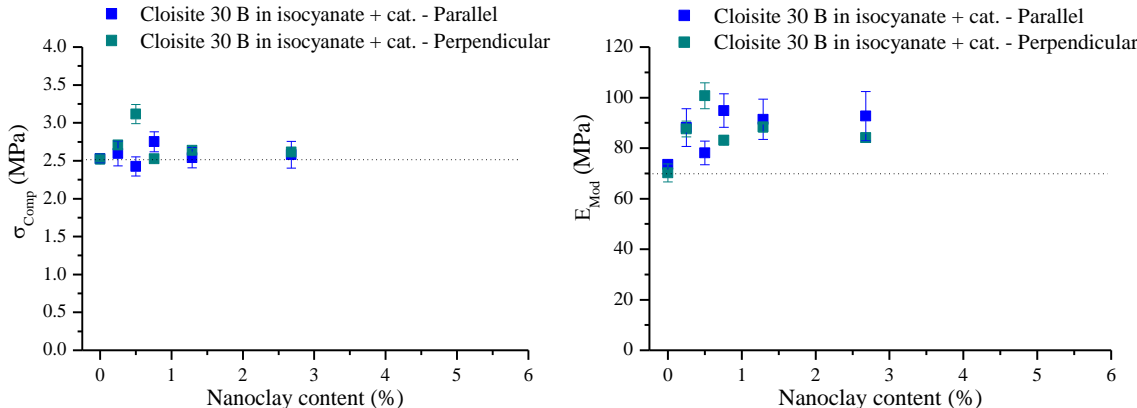


Figure 3.45. Compression strength and Young’s modulus of rigid PU foams filled with Cloisite 30B dispersed in isocyanate with added catalyst

All nanoclay dispersion methods showed a similar increase of compression strength and Young’s modulus of developed rigid PU foam samples. Cloisite 30B showed slightly better performance as rigid PU foam reinforcement filler than Cloisite 15A due to the presence of OH

groups in the organic modifier of the nanoclay. At 1.29–2.68 wt.% of Cloisite 30B compression strength was increased by 15–24 % and Young’s modulus by 13–29 %. Exfoliated Cloisite 30B nanoclay allowed to achieve similar increase of mechanical properties at lower filler loadings of ~0.25-0.76 wt.%. Achieved increase of the compression properties corresponds to literature data. Nevertheless, achieved increase of the compression properties is not significant enough to counterweight the technological difficulties what the preparation of the nanocomposite implies.

Tensile Strength of Rigid PU Foams Filled With Nanoclay

Both nanoclay fillers were dispersed in NEO_380 polyol by ultrasound sonification as well as high share mixer. Tensile strength test results were normalized to an average apparent density of 200 kg/m³ according to power-law function discussed paragraph 3.1. Obtained tensile fracture strength and Young’s modulus results are depicted in Figure 3.46. Addition of nanoclay filler did not increase tensile properties of rigid PU foam. Obtained foams become more brittle with reduced toughness and tensile strength. The change of rigid PU foam morphology due to the presence of the nanoclay filler contributes to the reduction of foam tensile toughness. Furthermore, the tensile strength of the monolithic (solid) polymer may also be adversely affected by the nanofiller in the case of its agglomeration [218,219]. More in-depth analysis of the reduction of Mode I fracture toughness is discussed in paper by M.Kirpluks et.al [165].

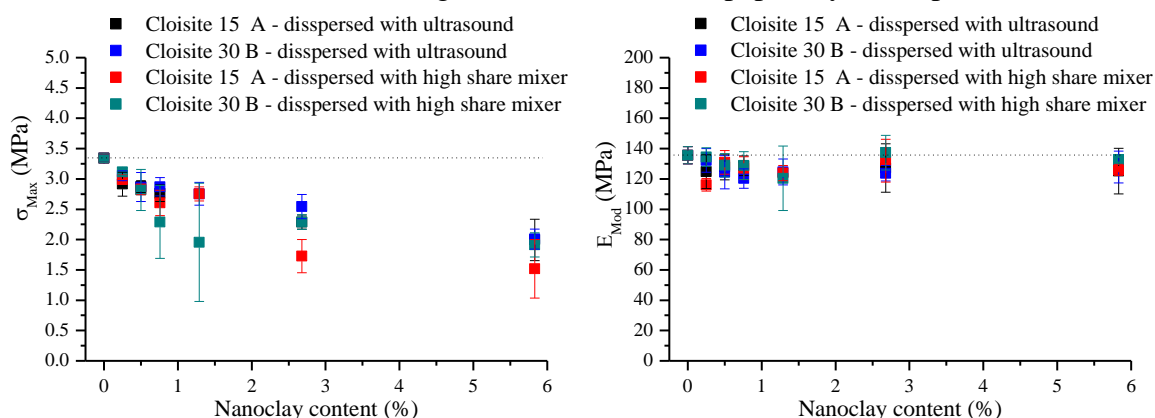


Figure 3.46. Tensile strength and Young’s modulus of rigid PU foams filled with Cloisite 15A and Cloisite 30B dispersed in NEO_380 polyol

Thermal Properties of PU Foams Modified With Nanoclay

Cloisite 15A and Cloisite 30B nanoclay influence on rigid PU foam thermal stability were evaluated by TGA analysis. The same nanoclay loadings as before were tested. Mass loss and rigid PU foam degradation rate curves of rigid PU foam filled with Cloisite 15A and Cloisite 30B are depicted in Figure 3.47 and Figure 3.48 respectively. Neither of nanoclay type influenced the thermal stability of developed rigid PU foams. Both of nanoparticles work as a solid filler and no covalent bond is formed between nanoclay and PU matrix that would increase thermal stability. The only difference between the neat material and nanoclay composites is in the increased final residue of the material which corresponds to the nanoclay loadings.

This does not mean the nanoclay particles can’t work as a flame retardant. Relatively low loading of Cloisite 30 B nanoclay can significantly decrease a flame spread rate of the rigid PU foam and increase LOI [216,220]. A significantly better increase of thermal stability of PU

material was achieved by M. Berta et. al. where Cloisite 30B was exfoliated into PU elastomer matrix [221]. A similar observation of what is presented in this thesis was observed by Z. Xu et.al. where different nanoclay fillers did not influence the thermal stability of rigid PU foams. Whereas a significant decrease of material flammability was achieved in the cone calorimeter test [222].

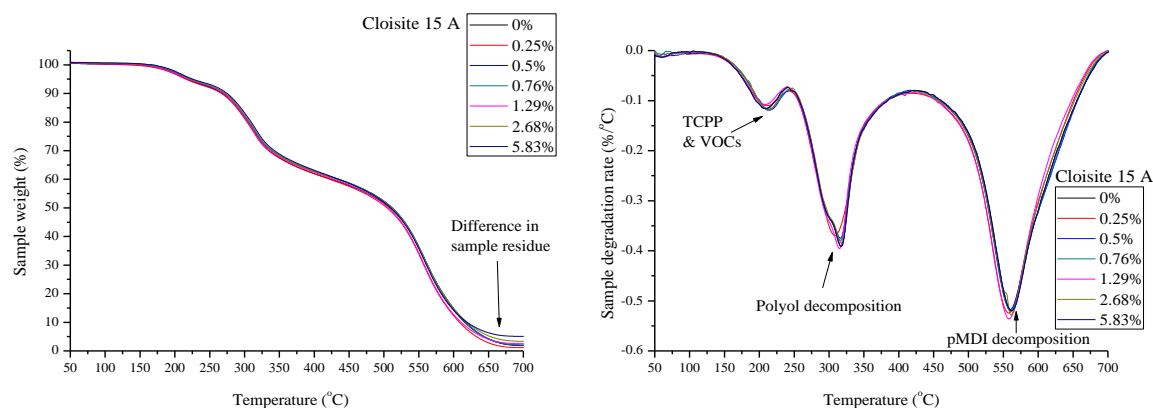


Figure 3.47. Thermal degradation of rigid PU foams filled with Cloisite 15 A nanoclay

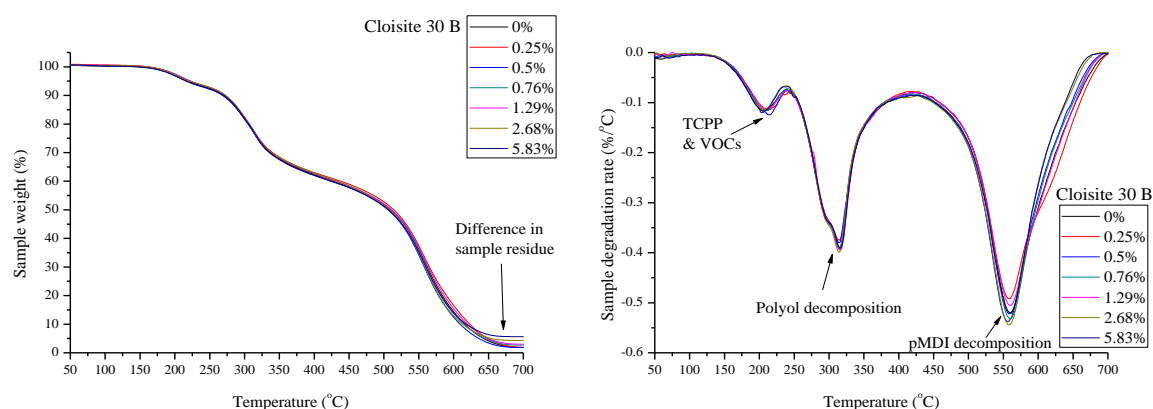


Figure 3.48. Thermal degradation of rigid PU foams filled with Cloisite 30 B nanoclay

Conclusions of Rigid PU Foam Nanoclay Composite Development

- Two different nanoclay fillers were introduced into developed rigid PU foam structure;
- Three different nanoclay dispersion methods into NEO_380 polyol have been evaluated;
- Cloisite 30B nanoclay has been exfoliated in isocyanate component of rigid PU foams;
- Nanoclay addition into rigid PU foam structure decreased average cell size due to the nucleation effect of gas microbubbles during the foaming process;
- Nanoclay type did not influence morphological changes of rigid PU foams;
- Both nanoclay types increased rigid PU foam compression strength, an average increase of 15–20% of compression strength was achieved at 1.29 –2.68 wt.% of nanoclay content;
- Nanoclay dispersion method into NEO_380 had little effect on rigid PU foam compression properties.
- Exfoliation of Cloisite 30B nanoclay allowed to achieve the same compression strength increase at lower nanoclay content of 0.25–0.76 wt.%;

- Tensile strength was significantly decreased with the addition of nanoclay filler due to the change of rigid PU foam morphology;
- Thermal stability of rigid PU foam was not changed by the addition of nanoclay filler. Possible decrease of flammability could be achieved but was not studied in the frame of this thesis.

3.3. Low Flammability Rigid PU Foam Thermal Insulation Composite

TO Polyol Based Rigid PU Foams with Low Flammability

Results described in this paragraph were performed in the frame of COST Action MP1105, FLARETEX: “Sustainable flame retardancy for textiles and related materials based on nanoparticles substituting conventional chemicals”. In the frame of this project, alternative flame retardants were explored to replace halogenated flame retardants in bio-based rigid PU foam thermal insulation material. Several different options were investigated to replace commercially commonly used tris(chloropropyl)phosphate (TCPP). An additive dimethyl-propyl-phosphate (DMPP) was used as a direct replacement in typical rigid PU foam formulations. Furthermore, a composite material containing expandable graphite (EG) filler was developed by introducing EG particles in rigid PU foam matrix and by developing the layered sandwich structure of rigid PU foam and intumescent flame retardant non-woven fabric (IF). The effect on the flammability of developed rigid PU foams with more sustainable flame retardants was studied using Cone Calorimeter (ISO 5660-1:2015) equipment and single-flame source test according to ISO 11925-2:2010 standard. Rigid PU foam formulation developed during M.Kirpluks master thesis was used as a base material to test the novel flame retardants. The main polyol in this rigid PU foam formulation was obtained from TOFA using amidation process with DEOA as described in paragraph 2.1. Obtained results will show that non-halogenated flame retardants can yield significant reduction of rigid PU foam flammability.

The neat formulation of TOFA_DEOA polyol based rigid PU foam was modified by adding the different flame retardants into the polyol component. Conventional, liquid flame retardants TCPP and DMPP were compared at 7 wt.% of rigid PU foam mass. The EG flakes were also added into the polyol component. A homogenous mixture was achieved by the mechanical stirring of the components at 2000 rpm. A possible synergistic effect between PIR groups and non-halogenated flame retardants was studied by changing the isocyanate index of the rigid PU foams (indices of 110; 150; 200 and 250 were tested). A sandwich like composite where rigid PU foam is protected by non-woven IF was obtained by producing samples in a stainless steel mould. The bottom of the mould was lined with the intumescent non-woven fabric and reacting rigid PU foam mass was poured on top of it. The long start time of the foam formulation ($\tau_{\text{cream}} \sim 35$ s) insured good adhesion between the intumescent non-woven fabric and rigid PU foam. No additional adhesive was necessary which shows the potential of this technology in the state of art rigid PU/PIR continuous panel production. Different types of developed rigid PU foam samples are depicted in Figure 3.49.

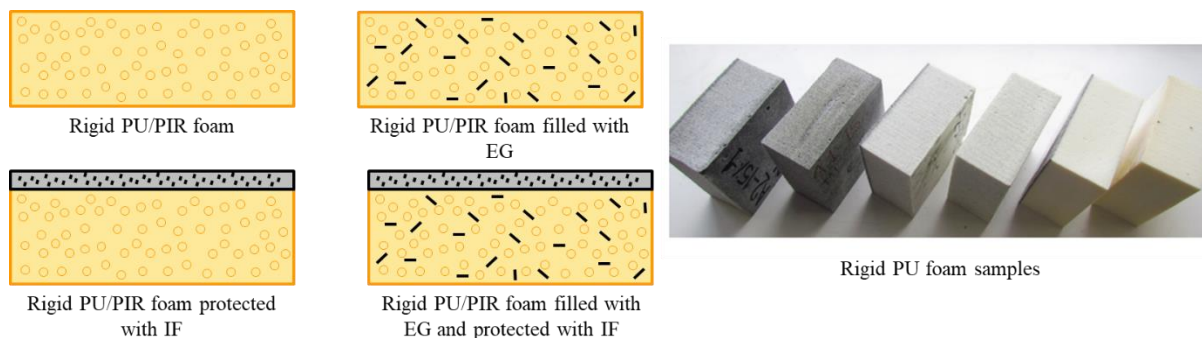


Figure 3.49. Rigid PU foam sample types used for flammability analysis

Thermal Conductivity of the Developed Rigid PU/PIR Foams

The main characteristics of any thermal insulation material are thermal conductivity (λ) and thermal resistance. Figure 3.50 shows the measured λ for the rigid PU foam obtained from the TOFA_DEOA polyol and filled with different amounts of EG particles. The isocyanate index of these samples was 110. The λ of rigid PU foams containing EG loadings of 0; 3; 9; and 15 wt.% are compared for rigid PU foams without liquid flame retardant (see Figure 3.50a) and with 7 wt.% of DMPP (see Figure 3.50 b). Furthermore, the λ of rigid PU foam composites containing non-woven IF layer was also measured. It can be seen that non-woven IF layer has no effect on the λ value of the rigid PU foams but there is a clear increase of λ with the addition of EG. Graphite is a good heat conductor, thus it is no surprise that the λ value increased. Furthermore, the EG particles disrupt the cell morphology of rigid PU foams further decreasing the efficiency of the insulation material. The λ value of the neat rigid PU foams with no DMPP FR was 24.44 mW/m·K, which is considered acceptable for the material that could be used in civil engineering. Unfortunately, the addition of DMPP increased λ value up to 28.74 mW/m·K. The increase of λ value with the addition of DMPP is explained by plasticization and decrease of the overall crosslink density of the rigid PU foam polymer matrix as explained in paragraph 3.1. Most of the conventional additive liquid flame retardants decrease the glass transition temperature of the PU polymer matrix [171]. The rapid jump of the λ value can be explained by CO₂ emission from closed cells of rigid PU foam and its substitution with air (O₂ and N₂). Such effect is highly undesirable because, at λ value of 28.74 mW/m·K, the thermal insulation properties of the developed rigid PU foams are comparable to XPS/EPS. Rigid PU foams cannot compete with XPS/EPS in terms of price and bio-based feedstock will not counterweigh the price/performance of increased λ value. It must be mentioned that the closed-cell content of all developed rigid PU foams was above 90 %. The substitution of CO₂ or another gas (blowing agent) with air in conventional PU foams is a slow process and takes years [223]. However, even with a λ value of 28.74 mW/m·K, the developed rigid PU foams are an efficient thermal insulation material that can be applied in civil engineering. A similar increase of the λ value (from 26 to 28 mW/m·K) was observed by L. Gao et al. for EG and diethyl ethyl phosphonate filled rigid PU/PIR foams [224].

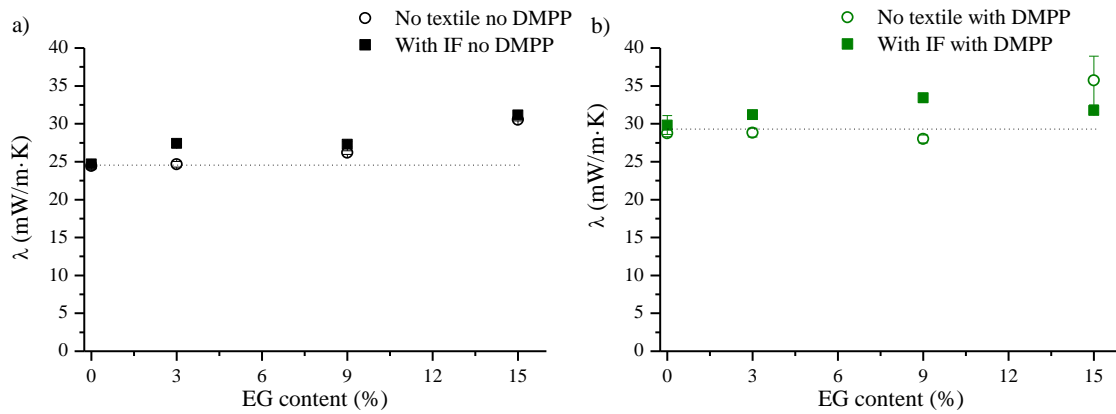


Figure 3.50. Thermal conductivity of rigid PU foams (II-110) protected with IF: a) with no liquid FR and with EG; b) with DMPP as FR and EG.

For thermal insulation application, rigid PU foams with different isocyanate indices are produced. The exact isocyanate index is dependent on the application type and rigid PU foam production technology. The isocyanate index influence on λ value of rigid PU/PIR foam with different EG content is depicted in Figure 3.51. Similar to samples with liquid flame retardant, for rigid PU foams with different isocyanate indices, non-woven IF had little influence on the λ value of the developed materials. The λ values increased with increased EG content. The lowest measured λ value of 22.80 mW/m·K was for rigid PU/PIR foam with the highest isocyanate index (250). Due to the cyclotrimerization reaction, shown in Figure 1.7, the crosslinking density of the polymer matrix increased. Crosslinked PU/PIR polymer matrix reduces the CO₂ diffusion through cell walls. The λ value of 22.80 mW/m·K can be considered up to industry quality standards of a rigid PU/PIR foam thermal insulation material.

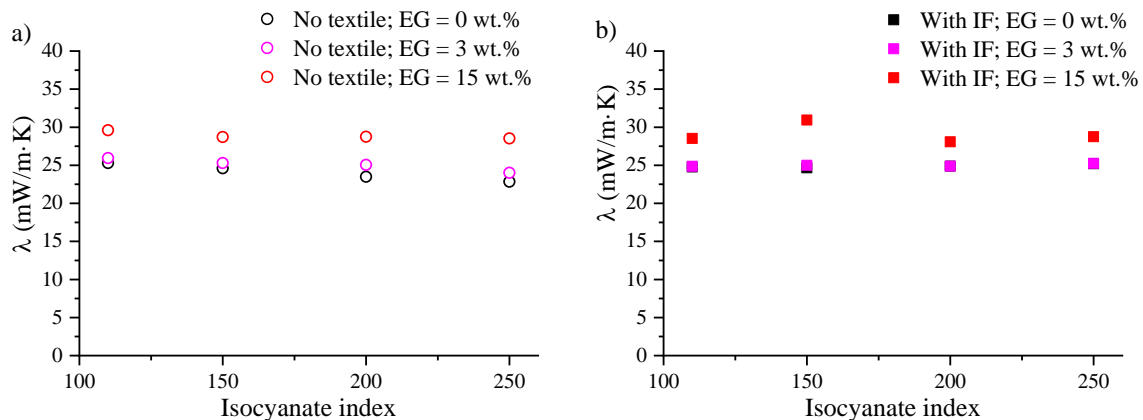


Figure 3.51. Thermal conductivity of rigid PU/PIR foams with different isocyanate indices and different EG content: a) with no IF; b) protected with IF.

Mechanical and Morphological Properties of the Developed Rigid PU/PIR Foams

The addition of EG particles into rigid PU/PIR foam structure disrupted the cell morphology of the foam which resulted in a previously mentioned increase of the thermal conductivity. Furthermore, bulky and heavy EG particles increased the viscosity of the rigid PU/PIR foam reacting mass during the foaming process, which increased the apparent density of the material.

The disruption of the foam morphology is the main reason for the decrease of the compression strength of the foam. The apparent density, compression strength and Young's modulus for rigid PU foams filled with EG particles are depicted in Table 3.13. The compression properties were tested in parallel (Z) and perpendicular (X) to the foaming direction. Addition of DMPP increased the rigid PU/PIR foam density from 59 to 68 kg/m³. The blowing agent in the formulation was not changed, thus its relative content in the formulation was decreased with the addition of DMPP. The rigid PU/PIR foams were water blown, so a change of blowing agent amount would change the polymer matrix of the tested material.

Table 3.13

Apparent density, compression strength and Young's modulus for rigid PU foams with no liquid flame retardant but with EG and for PU foams with DMPP and EG

Foam characteristic	Rigid PU foams based on TO polyol with no liquid FR			
	0	3	9	15
Density, kg/m ³	59 ± 2	60 ± 2	62 ± 3	66 ± 4
Compression strength Z, MPa	0.38 ± 0.04	0.36 ± 0.03	0.35 ± 0.02	0.29 ± 0.03
Young's modulus Z, MPa	9.4 ± 1.5	8.7 ± 1.6	8.7 ± 0.8	7.1 ± 1.2
Compression strength X, MPa	0.22 ± 0.03	0.24 ± 0.02	0.21 ± 0.02	0.22 ± 0.02
Young's modulus X, MPa	4.2 ± 1.0	4.4 ± 0.7	4.1 ± 0.5	4.6 ± 0.6
	Rigid PU foams based on TO polyol with DMPP			
Density, kg/m ³	68 ± 2	70 ± 2	73 ± 3	69 ± 2
Compression strength Z, MPa	0.35 ± 0.03	0.45 ± 0.03	0.32 ± 0.03	0.32 ± 0.02
Young's modulus Z, MPa	7.4 ± 1.0	11.5 ± 1.6	7.0 ± 1.3	8.4 ± 0.6
Compression strength X, MPa	0.26 ± 0.01	0.35 ± 0.02	0.24 ± 0.01	0.17 ± 0.01
Young's modulus X, MPa	4.2 ± 0.3	6.8 ± 0.7	4.3 ± 0.3	2.5 ± 0.4

The compression strength and Young's modulus of rigid PU/PIR foams with different isocyanate indices and different EG content is depicted in Figure 3.52. The increase of isocyanate index increased the mechanical properties of the developed insulation material similar to results discussed in paragraph 3.1. At isocyanate index of 200, the highest values of compression strength and Young's modulus were achieved, 0.49 MPa and 10.34 MPa, respectively when tested parallel to the foaming direction. The increase of mechanical properties can be attributed to the increase of the crosslinking density and aromaticity of the developed rigid PU/PIR foams. At higher isocyanate index mechanical properties did not increase further. This can be explained by the sub-optimal catalyst package of the formulation. Although potassium acetate - catalyst promoting polyisocyanurate ring formation was added, further work on formulation optimization should be performed. Furthermore, the laboratory foaming conditions are not ideal for the PIR foam development as the process requires high temperature for the foam curing. Tested foams had distinct anisotropic properties where samples tested perpendicularly to the foaming direction showed lower mechanical properties, which is typical for rigid PU/PIR foams. Similar to previous results, the addition of EG particles in rigid PU/PIR foams decreased mechanical properties due to the disruption of the cell morphology.

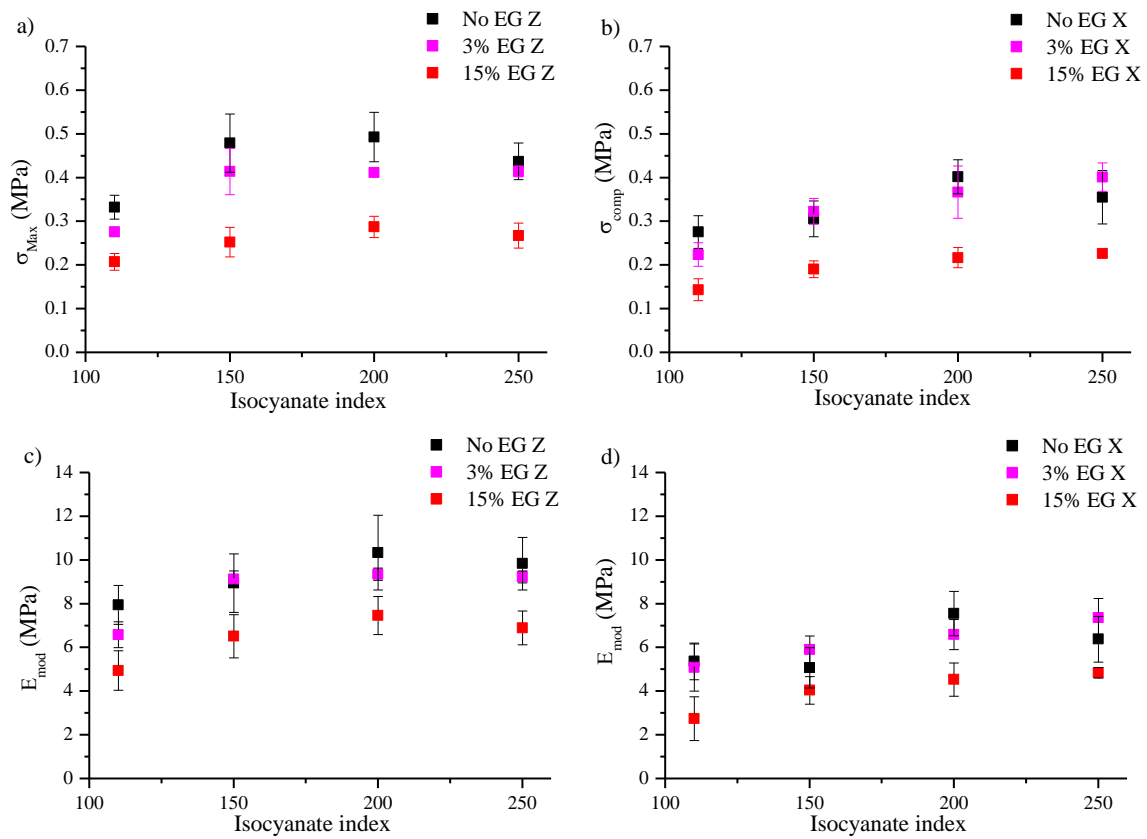


Figure 3.52. Compression strength a) parallel and b) perpendicular to the foaming direction; Young's modulus c) parallel and d) perpendicular to the foaming direction.

Developed composites had good surface adhesion between EG particles and rigid PU/PIR foam polymer matrix (see Figure 3.53.). The SEM images depict the disruption of the even cell structure of rigid PU/PIR foams by EG particles. Unfortunately, the cell size distribution analysis was not performed for the developed rigid PU/PIR foams as it was out of the scope of FLARETEX project.

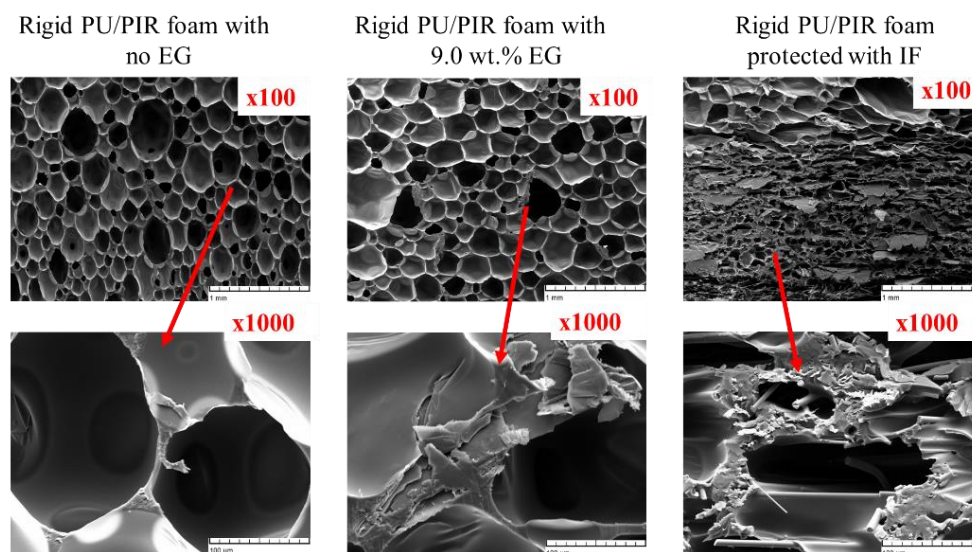


Figure 3.53. SEM images of neat rigid PU/PIR foams, PU/PIR foams filled with 9% EG and intumescent non-woven fabric and rigid PU/PIR foam composite.

The main objective of this study was to obtain rigid PU/PIR foams with decreased flammability without losing superior thermal insulation properties. This was done by protecting one side of the PU foam material with non-woven IF, as shown in Figure 3.49. Reacting foam mass was poured on top of the non-woven IF which insured good adhesion of the foam material to the glass fibres. The adhesion layer of the composite is depicted in Figure 3.53. It can be seen that the rigid PU/PIR polymer matrix is incorporated into the glass fibre structure of the non-woven fabric. Some rigid PU/PIR foam cells are undoubtedly formed in-between glass fibres. No additional adhesive was necessary for the developed composite.

Flammability of Developed Rigid PU/PIR Foams

The cone calorimeter test gives a significant amount of information about the flammability of the tested materials and their reaction to the heat flux. This test is a useful technique to compare different materials and gain an initial idea of how a material will react in a fire disaster scenario. In the cone calorimeter test, the material is subjected to the constant radiant heat flux $q_{\text{ext}} = 0\text{--}100 \text{ kW/m}^2$, where the flux of 35 or 50 kW/m^2 is most commonly used [224–226]. The small sample size of 100x100x50 mm makes this technique particularly useful to compare and optimize materials as for the Single Burning Item (EN 13823:2010) test much bigger samples are required [227]. The cone calorimeter test gives an initial idea of how a material will behave in an open fire scenario. Common material characteristics that are obtained during this test are kinetic curves of the heat release rate (HRR), time to ignition (TTI), total heat released (THR), the peak of heat release rate (pHRR), total smoke release (TSR), and the maximum average rate of heat emission (MARHE). pHRR can be used to compare materials provided that the test setup conditions are kept constant for all tested samples (sample thickness, sample holder, distance from the heater, heat flux, airflow, etc.). Furthermore, the kinetic curves of the HRR give an excellent idea about material flammability as the data monitors sample behaviour through the whole burning process.

A comparison of HRR curves of rigid PU foams obtained from the TO_DEOA polyol filled with different amounts of EG and two different conventional liquid additive flame retardants (TCPP and DMPP) is depicted in Figure 3.54. The addition of EG into PU foams decreased pHRR from 327 to 103 kW/m^2 when no other flame retardant was used. There was no synergistic effect between EG and DMPP or TCPP because the pHRR of PU foam samples with 15 wt.% of EG and 7 wt.% of liquid FR did not decrease below 103 kW/m^2 . Nevertheless, DMPP had a significant effect on rigid PU foam flammability reduction where pHRR was reduced from 327 to 179 kW/m^2 . Also, the THR was decreased from 55.3 to 28.2 kW/m^2 when DMPP was added to the neat rigid PU foam. Unfortunately, the addition of DMPP to the rigid PU foam increased the λ value of the material which reduces the commercial feasibility of the developed insulation material. Surprisingly, the addition of TCPP to the rigid PU foams did not significantly reduce the pHRR (327 kW/m^2 – for neat material to 355 kW/m^2 for TCPP filled rigid PU foam). Nevertheless, the effect of TCPP was seen in the reduction of THR where it was reduced from 55.3 to 28.5 kW/m^2 when compared to the neat material. Also, the TSR was decreased from 2832 to 1283 m^2/m^2 . The comparison of similar amounts of the three different

flame retardants (7 wt.% of DMPP and TCPP vs 9 wt.% of EG) is depicted in Figure 3.54d and it unmistakably shows that EG performs on the level of conventional flame retardants if not better.

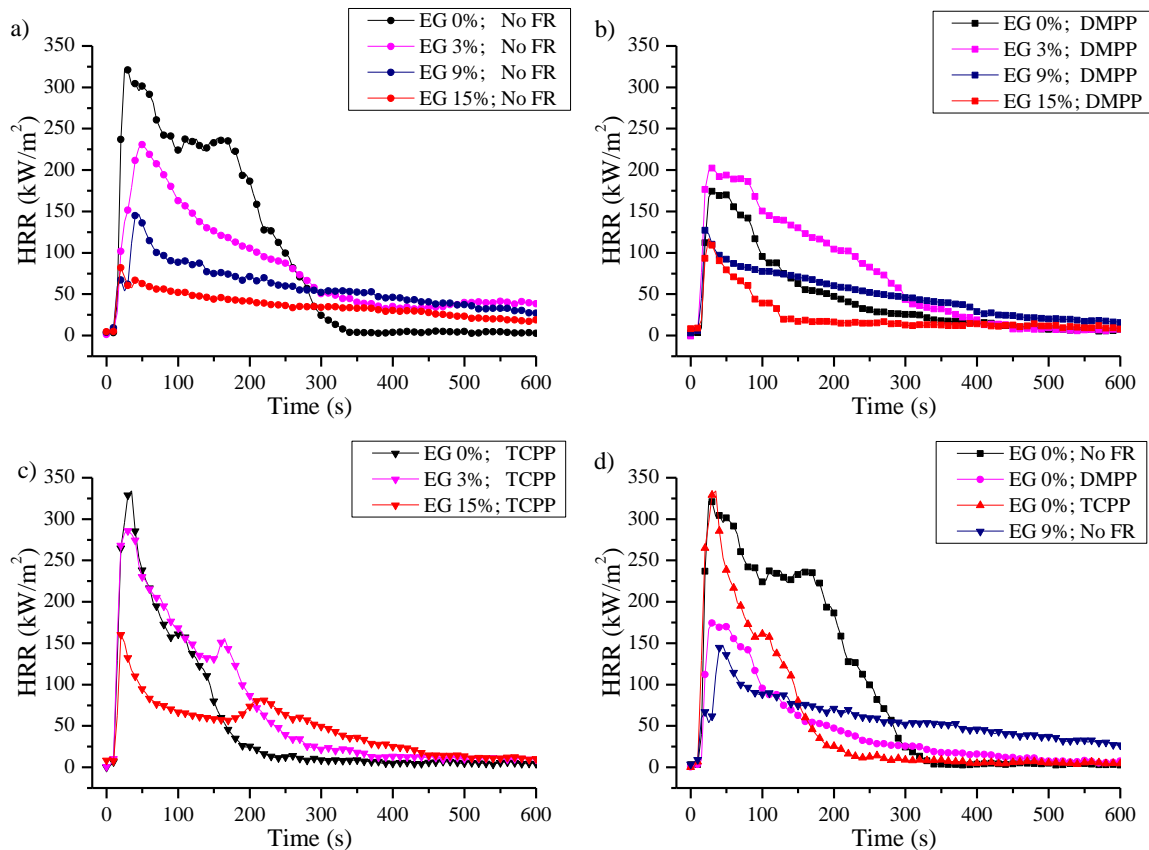


Figure 3.54. HRR curves of PU foam based on TO polyol with II-110, different amount of EG and a) no conventional liquid FR, b) 7 wt.% DMPP, c) 7 wt.% TCPP and d) comparison between three FRs.

The addition of trimerization products of isocyanate groups into the PU/PIR polymer matrix increases its thermal stability and decrease flammability, which is depicted as a smaller area under the HRR curve in Figure 3.55a. The increase of the isocyanate index from 110 to 250 decreased pHRR from 355 to 305 kW/m². The increase of the isocyanate index prolonged the burning of PU/PIR foam but the material burned with less intensity. Figure 3.55b depicts HRR curves of PU/PIR foams protected with IF. There was no heat release detected because the material did not ignite during the test time when subjugated to a heat flux of 35 kW/m². The unwoven intumescent fabric did what it was designed to do and formed a protective char layer on top of the rigid PU/PIR foam. Figure 3.55 depicts images of PU/PIR foams during the cone calorimeter test. The IF formed a thick char layer on top of the PU/PIR foam that stopped the thermal degradation of the PU/PIR polymer matrix. The unwoven intumescent fabric gives excellent flame protection while keeping low thermal conductivity values as seen in Figure 3.50 and Figure 3.51b.

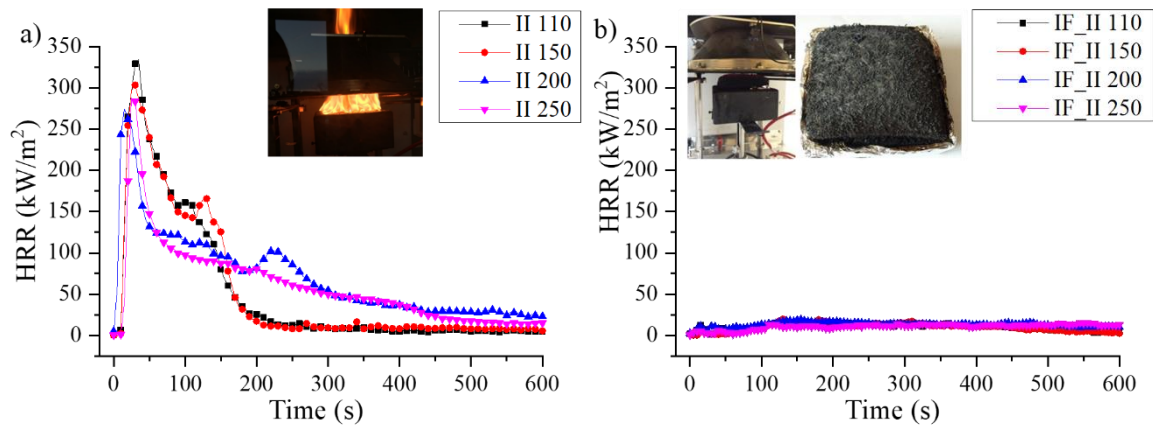
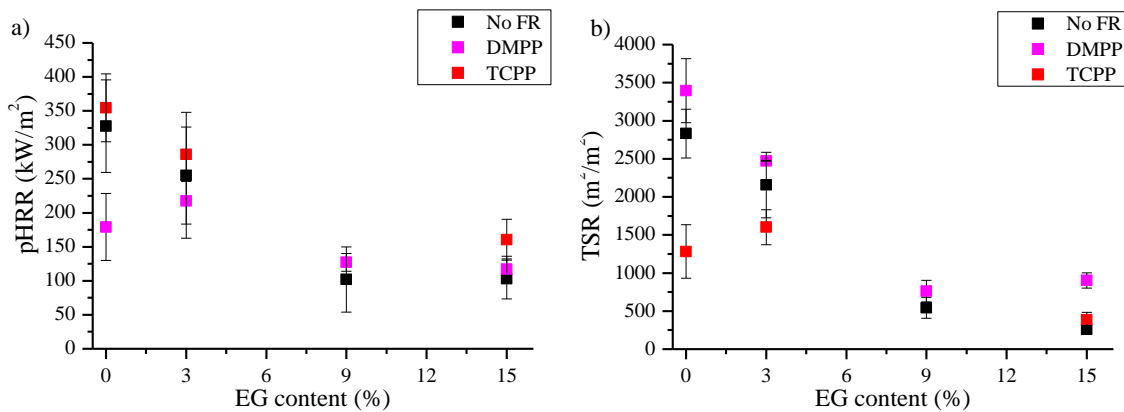


Figure 3.55. Rigid PU/PIR foam HRR curves: a) foams with different isocyanate index; b) PU/PIR foams with IF protection.

Most significant flammability characteristics data (pHRR, TSR, MAHER and THR) after the cone calorimeter test of TO_DEOA polyol based rigid PU foams with the isocyanate index 110 and different amounts of EG are summarized in Figure 3.56. The conventional liquid flame retardant TCPP showed the smallest effect on PU foam flammability when compared to DMPP. A simplified interpretation of the cone calorimeter data can be done comparing the maximum average rate of heat emission (MAHER) coefficient. This index is deduced from the maximum of HRR, which is often considered to be one of the most important fire hazards. However, this coefficient can be used to compare the materials tested under the same conditions. It can be seen that the most significant reduction of MAHER is for samples with 9 and 15 wt.% loads of EG and that only DMPP decreases MAHER for samples with no EG. In summary, EG significantly decreased the flammability of PU foams.



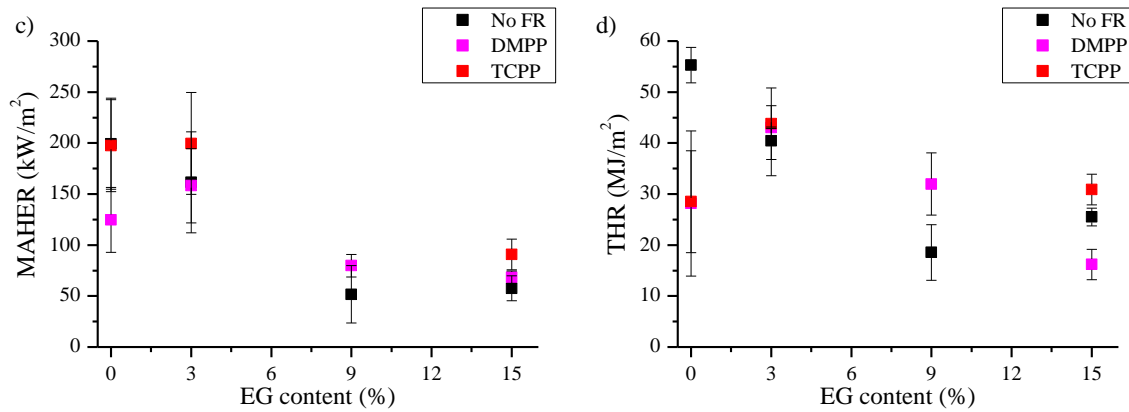


Figure 3.56. a) pHRR; b) TSR; c) MARHE; d) THR of PU foam with different loads of EG and two different conventional liquid FRs.

As mentioned, the samples with non-woven IF did not ignite, so the flammability characteristics were exceedingly low. For samples with no non-woven IF, the pHRR decreased with the increase of the isocyanate index, which correlates with the statement that cyclotrimerization groups are more thermally stable. Similarly to the case of the PU foam with an isocyanate index of 110, the addition of EG decreased pHRR and MAHER. The pHRR and MAHER coefficients of rigid PU/PIR foams with different isocyanate indices, and with and without non-woven intumescent fabric fire protection are depicted in Figure 3.57.

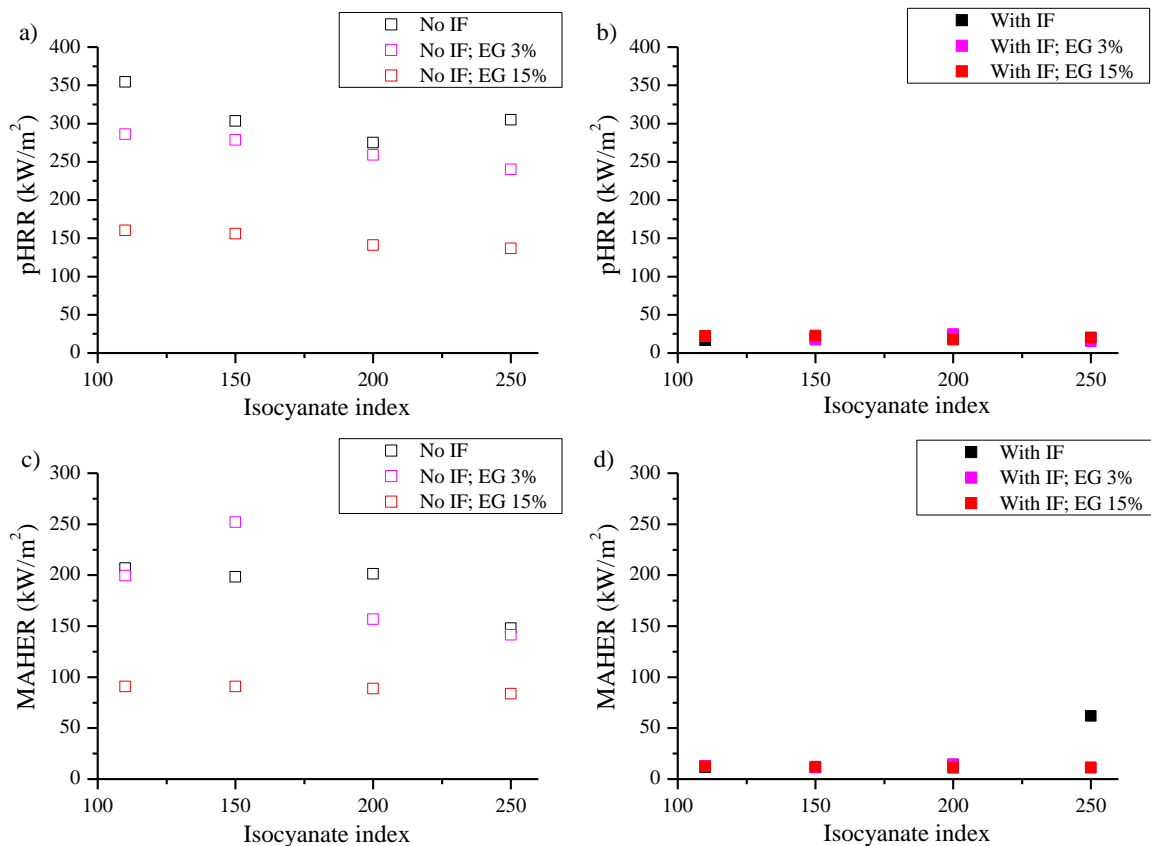


Figure 3.57. pHRR for rigid PU/PIR foams: a) with no IF, b) with IF and MAHER, c) with no IF and d) with IF.

Smoke is an important fire hazard as the majority of human victims in a fire disaster happen due to poisoning with toxic gases. The cone calorimeter gives little information about the chemical consistency of the smoke. The data obtained from the test represents the solid particle amount in the smoke produced while the sample is burning. TSR data of rigid PU/PIR foams with different isocyanate indices and different EG amount is depicted in Figure 3.58. It can be seen that the addition of EG and the increase of the isocyanate index significantly decreased the amount of the produced smoke. The non-woven IF did not stop the smoke release from the rigid PU/PIR foam composite. Although the smoke was with no fire its amount was comparable to the burning samples with no non-woven IF. Peculiar is the observation that at 15 wt.% of EG there was no difference in smoke release in between different isocyanate indices. At 15 wt.% of EG, the flammability of the rigid PU/PIR foams is reduced so much that there is no difference between the chemical structure of the polymer matrix. This indicates that low isocyanate index rigid PU foam together with EG flame retardant could be applied for applications where high flame retardancy requirements are demanded, such as public building thermal insulation [228].

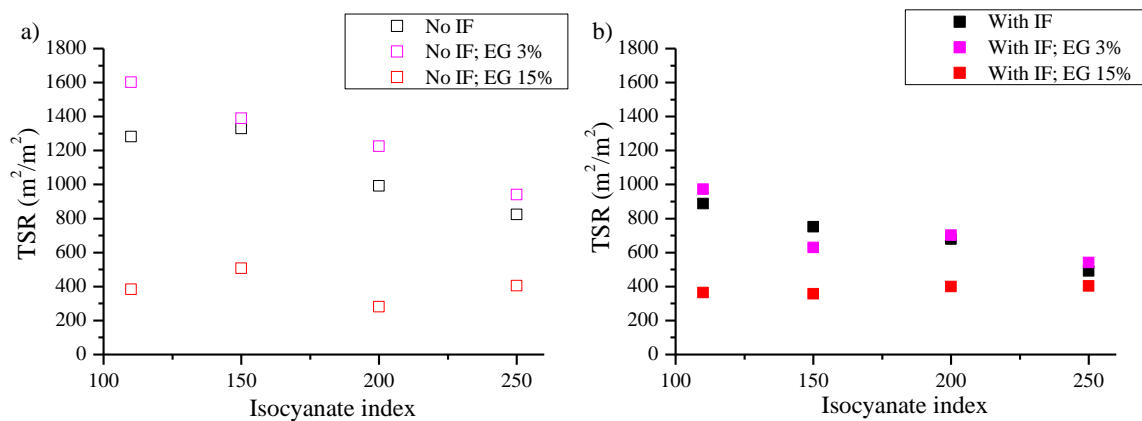


Figure 3.58. The total smoke released of rigid PU/PIR foams: a) with no IF; b) with IF.

Reaction to Fire of Developed Rigid PU/PIR Foam

One of the simplest flammability tests is material analysis according to EN 11925-2:2010 standard. The test takes place inside a test chamber where the test specimen is mounted vertically. The test specimen is subjected to edge and/or surface exposure from a propane gas flame. During the test, time of ignition, burning droplets and whether the flames reach the top marking of the test specimen within a prescribed time period, is registered. The top marking is positioned 150 mm from the flame application spot. This is the most basic test which is required for materials used in civil engineering. Reaction to fire test is required to classify building materials according to European fire classification of construction products (EN 13501-1:2018) Euro-class E. Such products are capable of resisting, for a short period, a small flame attack without substantial flame spread. Furthermore, the test gives information on flaming droplet formation. To satisfy Euro-class E the material has to be subjected to the small flame for 15 sec. To reach a higher reaction to fire class material has to satisfy EN 11925-2:2010 standard conditions under flame application time of 30 sec. After successful EN 11925-2:2010 test

material must be tested according to the Single Burning Item (SBI) test in accordance with EN 13823:2010 which will classify material for Euro-class D, C, or B [226,229].

In frame of this Doctoral Thesis developed rigid PU/PIR foams were tested according to EN 11925-2:2010 standard to pass the test for Euro-class E. Samples were subjugated to a small propane flame for 15 sec after the small flame application rigid PU/PIR foam was allowed to burn for additional 20 sec after which the sample was extinguished if that was necessary. The main criteria of the reaction to fire test is whether the flame of the burning sample reached the 150 mm mark. The samples were also weighted after the test and the mass loss in wt.% was compared. Furthermore, the height of the rigid PU foam damaged by the flame was measured by a simple ruler. Obtained results are summarized in Table 3.14. The main conclusion is depicted by colouring in green the cells of the samples that have passed the test. Addition of 3 wt.% of EG into rigid PU/PIR foam allows passing the reaction to a flame test. Only rigid PU/PIR foam with an isocyanate index of 110 and 3 wt.% of EG did not pass the test. At 3 wt.% of EG, the rigid PU/PIR foams barely pass the test which is represented in the height of the foam damaged by flame. With the increase of the EG content rigid PU/PIR foam becomes less and less flammable, which correlates with Cone Calorimeter test results discussed previously. The reaction to the small flame test showed that the addition of 7 wt.% of TCPP will not ensure flame retardancy of the material. This was unexpected as TCPP is one of the most commonly used flame retardants. Most likely the inherent chemical structure of the TO_DEOA polyol used to prepare foams does not allow to develop flame-retardant material. The dangling chains introduced into PU/PIR polymer matrix from tall oil fatty acids are easily split off during the thermal degradation of the material. The aliphatic structure of the dangling chains works as an excellent fuel to sustain the burning of the rigid PU/PIR foam. A comparison of the thermal stability of rigid PU foams developed from aliphatic (TO_TEOA) and aromatic (NEO_380) polyols was discussed in paragraph 3.1.

Table 3.14

Test results of the reaction to a small flame for rigid PU/PIR foams.

Isocyanate index of the rigid PU/PIR foam	EG content in rigid PU/PIR foam, wt.%	Mass loss after test, wt.%	Did flame reach the 150 mm mark, Yes/No	Height of the rigid PU/PIR foam damaged by flame, mm
110	0	3.6	Yes	195
150		1.9	Yes	158
200		1.4	Yes	151
250		1.5	No	115
110	3	9.6	Yes	165
150		1.5	No	148
200		1.0	No	104
250		1.1	No	73
110	9	0.7	No	48
150		0.8	No	58
200		0.9	No	51
250		1.0	No	36
110	15	0.9	No	47
150		0.8	No	48
200		0.9	No	43
250		1.0	No	37

Pictures of tested rigid PU/PIR foam after reaction to small flame test are depicted in Figure 3.59. The pictures show most convincingly the difference between flammability of rigid PU/PIR foams with different loadings of EG. Also, there is a noticeable difference in flammability of rigid PU foam with 3 wt.% EG and different isocyanate indices. Rigid PU/PIR foam with an isocyanate index of 250 has a smaller area damaged by the flame than rigid PU/PIR foams with an isocyanate index of 150. The visual difference is significant even according to the test both samples have passed Euro-class E requirements. It must be mentioned that none of the tested rigid PU/PIR foam samples did form flaming droplets during the reaction to a flame test. Rigid PU/PIR foam is a thermoset material which does not lose its rigidity during a fire like EPS/XPS foam thermal insulation.

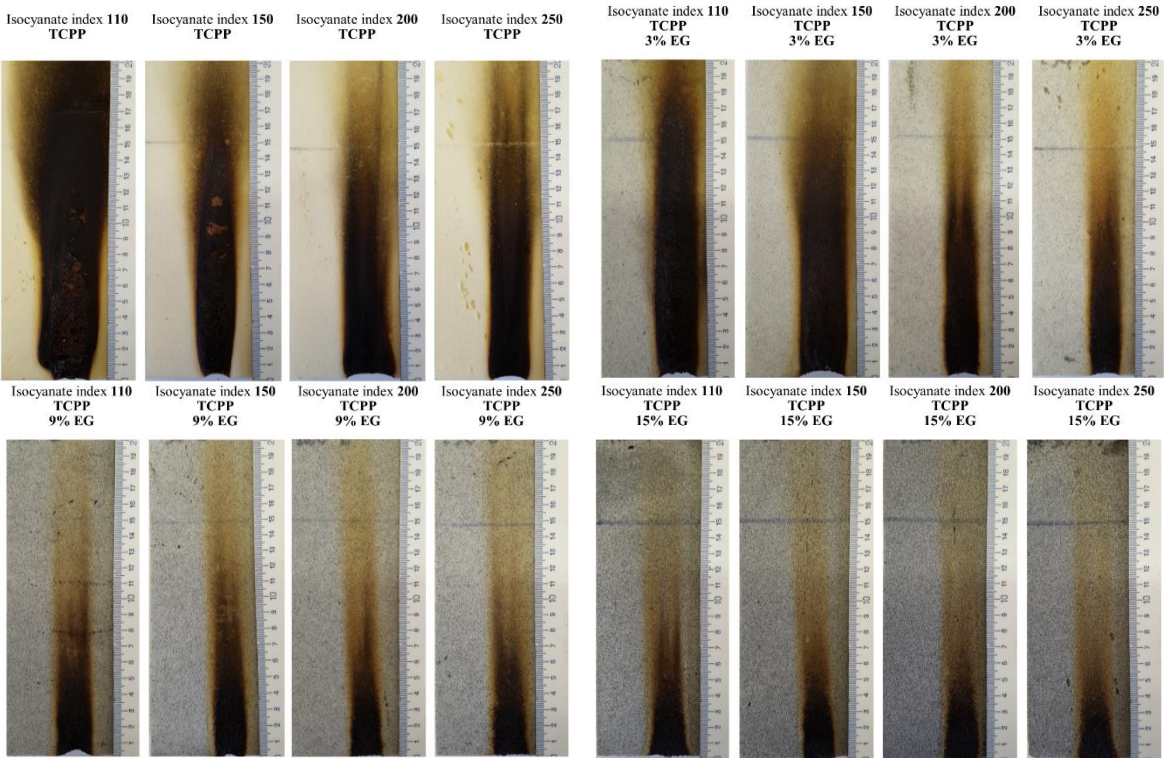


Figure 3.59. Rigid PU/PIR foam samples after reaction to small fire test with different isocyanate index: 110-250; EG content: 0-15 wt.% and TCPP content of 7 wt.%.

Visually most distinguishing influence of EG flame retardant is depicted in Figure 3.60. At isocyanate index 110 the rigid PU foam does not pass the reaction to a flame test, but the addition of EG flame retardant allows to do it. Furthermore, the fourth sample in the picture is rigid PU foam covered with unwoven intumescent fabric. The picture depicts excellent flame retardant properties of the composite.

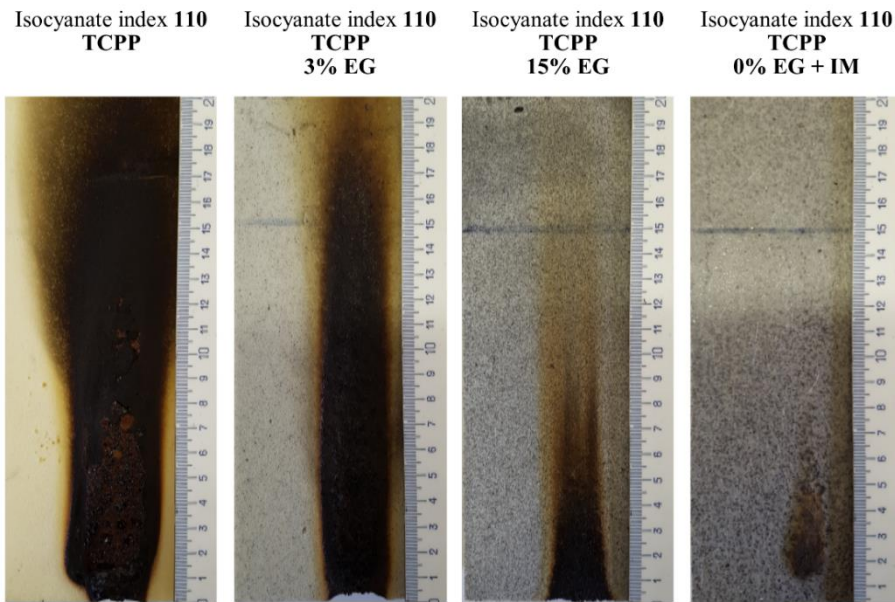


Figure 3.60. Comparison of rigid PU/PIR foam samples after reaction to the small fire test.

Summary of Low Flammability Rigid PU/PIR Foam Development

This study showed flammability properties of rigid PU/PIR foams obtained from TO_DEOA polyol which is synthesised from tall oil. The bio-based polyol is a suitable substitution for petrochemical materials, as the main characteristic of thermal insulation material, λ was at 22.0 mW/m·K, which is considered the industry standard for this type of material.

This study also showed a novel method of replacing liquid halogenated flame retardants with intumescent flame retardant for rigid PU/PIR foams using flexible, thermally expandable non-woven IF and EG. The addition of non-woven IF into rigid PU/PIR foams would be easily up-scalable in production of sandwich-type panels. The study of SEM images showed that no additional adhesive was needed as the unwoven intumescent fabric is incorporated into the rigid PU/PIR foam structure. The synergy between two types of liquid flame retardants (TCPP and DMPP) and additive EG was investigated but no significant improvement in flame retardancy was detected. At lower loads of EG, only DMPP showed the reduction of the heat release of rigid PU/PIR foams during burning. The conventional flame retardant, as well as EG, increased the thermal conductivity of the developed rigid PU/PIR foams. When a flame retardant composite with non-woven IF was tested no increase of thermal conductivity was detected. Furthermore, additive flame retardants decreased the physical-mechanical properties and disrupted the cell morphology of rigid PU/PIR foams. Thus the non-woven intumescent fabric is the most perspective solution to ensure flame retardancy of rigid PU/PIR foam on an industrial scale for sandwich panel production. Nevertheless, rigid PU/PIR foam filled with 15 wt.% of EG and 7 wt.% of the conventional liquid DMPP delivered excellent flame retardancy properties which could be considered to test higher European fire classification of building materials, up to class B. EG content of 15 wt.% provided the lowest peak of heat release in the cone calorimeter test of 102.9 kW/m². Although EG provided excellent flame

retardancy properties, the increase in thermal conductivity from 22.80 to 35.72 mW/m·K would not be acceptable for commercial use of this material. Therefore, non-woven IF is the best option as it not only stopped material from igniting in the cone calorimeter test but also did not influence the thermal conductivity of the developed rigid PU/PIR foams.

Conclusions of Low Flammability Rigid PU Foam Development

- TO_DEOA polyol which was obtained from distilled tall oil was suitable to develop rigid PU/PIR foam thermal insulation material with low thermal conductivity value of 22.80 mW/m·K.
- Rigid PU/PIR foams with isocyanate indices of 110-250 were developed and their flammability was tested.
- Flame retardancy of the developed rigid PU/PIR foams was insured by the addition of different flame retardants. Two conventional liquid flame retardants, TCPP and DMPP were compared to an additive flame retardant, EG flakes. Furthermore, a sandwich type composite of rigid PU/PIR composite and non-woven IF was developed.
- Addition of EG particles into rigid PU/PIR foams increased the thermal conductivity of the thermal insulation material, which is a negative aspect.
- Non-halogenated flame retardant DMPP showed better flame retardancy properties than commonly used TCPP.
- EG additive flame retardant was superior when compared to DMPP and TCPP and no synergistic effect between the additive and liquid flame retardants was determined.
- Best flame retardancy properties were achieved for the non-woven IF and rigid PU/PIR foam composites, where samples did not ignite in Cone Calorimeter test when exposed to a heat flux of 35 kW/m².

3.4. High Functionality Bio-Based Polyol Synthesis from RO

Rapeseed oil (RO), as well as tall oil (TO), can be used as renewable and abundant feedstock for bio-based polyol synthesis. The simplest way how to introduce OH groups into natural oil structure is by employing the one-step method of transamidation/transesterification or amidation/esterification with TEOA and DEOA respectively. Bio-based polyol synthesis by these methods was previously studied in the frame of M. Kirpluks graduate and master's thesis [230]. Results discussed in paragraph 3.1 indicated that polyols obtained in the one-step methods do not deliver rigid PU foams with comparable mechanical properties to foams obtained from APP polyol. Furthermore, polyol synthesis from RO epoxidation and subsequent oxirane ring opening with DEG resulted in rigid PU foams that had much higher compression strength and higher thermal stability [231]. Double bond epoxidation and epoxy ring opening is an excellent way to introduce additional functional OH groups into the chemical structure of fatty acid moieties [35]. One of the goals of this Doctoral Thesis was to improve on the one-step bio-based polyol synthesis to obtain polyols with higher functionality which would deliver better mechanical and thermal properties of rigid PU foams. A general approach improving the one step bio-based polyol synthesis method from RO would be to combine the epoxidation of the double bonds and epoxy ring opening with transesterification/transamidation process. This would result in bio-based polyols with increased functionality and additional beneficial properties derived from the chemical structure of the oxirane ring opening reagent. Epoxy ring opening with TEOA and DEOA reagents would introduce tertiary amine moieties into the chemical structure of the bio-polyol delivering auto-catalytical properties increasing the reactivity of the rigid PU foam formulation which was demonstrated by A. Fridrihsone et.al [232].

RO Epoxidation and Temperature Influence on the Epoxidation Process.

The acetic acid (AA) was chosen as an oxygen carrier in epoxidation reaction instead of formic acid because it has been shown by S. Dinda et al. that this acid despite the slower formation of oxirane has a higher ultimate degree of conversion to oxirane. Also using formic acid would result in a higher amount of undesired side products [39]. The temperature influence on epoxidation rate of RO was investigated for three different temperatures 55; 60 and 65 °C. V.V. Goud et al. showed that ion exchange resin is a suitable replacement for H₂SO₄ in the epoxidation reaction as a catalyst and the process can be carried out without the use of a solvent [36]. The most common solvent for such reaction is toluene, but it has to be separated from epoxidized oil before the next step of the polyol synthesis. Also, several hazards can be related to toluene, carcinogenicity being one of them. Thus solvent-free polyol synthesis method will result in a cheaper final product and it will agree with green chemistry principles. Use of Amberlite IR-120H ion exchange resin acidic catalyst also simplified RO epoxidation because the catalyst was removed by simple filtration. The change of the relative conversion to oxirane (RCO) degree was calculated according to Equation 2.1 over synthesis time and is depicted in Figure 3.61.

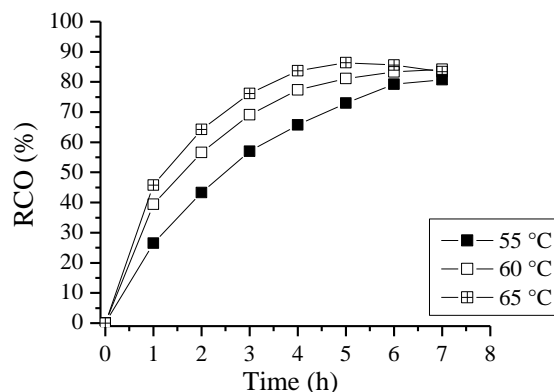


Figure 3.61. Temperature influence on double bond conversion into oxirane rings.

The highest relative epoxy group yield of 86.4 % was achieved at 65 °C after 5 h of synthesis but afterwards epoxy group content started to decrease. The decrease of epoxy groups is explained by different side reactions suggested by P.K. Gamage et al, P.D. Meshram and others [37,39,233,234] which are shown in Figure 3.62.

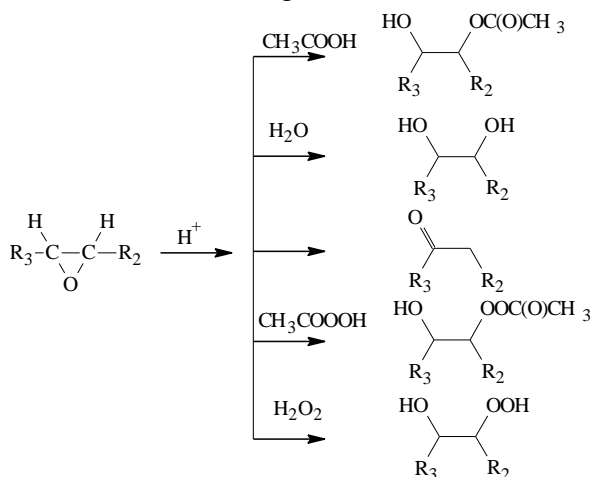


Figure 3.62. Possible side reactions during epoxidation [36].

The epoxidation process was also monitored by FTIR spectroscopy where C-O-C oxirane ring stretching vibrations were identified at 830-820 cm^{-1} [235]. The epoxy group absorption peak increased during the synthesis process as depicted in Figure 3.63. A slight decrease in its intensity was observed in the case of epoxidation at 65 °C after 5 h synthesis mark. This correlates with a conversion degree (see Figure 3.61.) results and confirms side reaction occurrence. Although the highest conversion of double bonds into epoxy groups was achieved at 65 °C the synthesis at 60 °C is preferable due to the more controllable reaction process. After 5 h of RO epoxidation at 60 °C, the relative conversion degree was 81.1 % and after 7 h it was 84.2 % which is still comparable to 86.4 % of 65 °C synthesis.

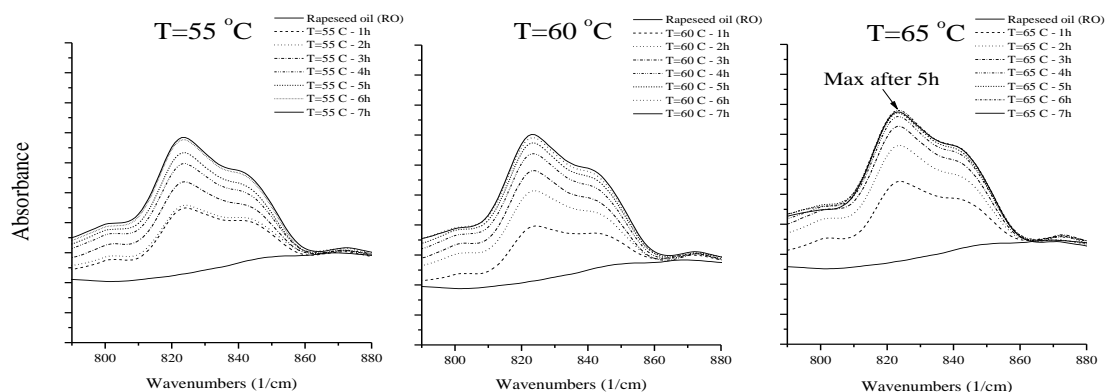


Figure 3.63. FTIR spectra of epoxy group absorption peak increase over RO epoxidation at 55; 60 and 65 °C.

Obtained results are similar to V.V. Goud et al. presented results of jatropha oil epoxidation [36]. Jatropha oil's chemical structure is similar to RO thus no significant difference between results was expected. The yield of oxirane rings was noticeably higher than for cotton oil and RO epoxidation in the presence of H_2SO_4 catalyst showing the additional advantage of solid phase ion exchange resin catalyst [39,234]. Also, P. Meshram et al. presented a design of a pilot-scale chemical reactor for such catalyst use in the up-scaled process [37]. Nevertheless, the stability of this type of catalyst in repeated use must be studied before this technology can be further up-scaled. Because this catalyst is intended for bio-based product use different impurities of natural oils could react with sulphonic groups, thus reducing its activity. Also, mechanical damage to resin beads could be a potential problem.

Characteristics of High Functionality Polyols from Epoxidized RO

The nine green polyols presented in experiment plan (depicted in Figure 2.6) were characterised by the OH value, apparent viscosity, acid value, moisture content, density, f_n , M_n , M_w and RO content in polyol (Table 3.15). The OH value of RODEG reference polyol was 242 mgKOH/g which is similar to what is reported in the literature [60]. The high acid value of 8.6 mgKOH/g is due to a sulphuric acid catalyst which was not separated or neutralized. The calculated f_n of RODEG was 3.0, i.e. high enough for rigid PU foam production. The novelty of the work is the next two sets of RO based polyols RODEA 0; 1.5; 2.0 and 2.5 and ROTEA 0; 1.5; 2.0 and 2.5 where the epoxy ring was opened with DEOA and TEOA, respectively, and transamidation and transesterification of the glycerol backbone were carried out (see Figure 1.12 and Figure 1.13). The obtained polyols have a much higher OH value ranging between 471–635 mgKOH/g and 430–557 mgKOH/g in case of RODEA and ROTEA sets respectively. The calculated f_n of synthesised polyols was much higher for RODEA polyol between 4.4–5.8 than for RODEG polyol where it was $f_n = 3.0$. The f_n increased with the increase of the ratio between DEOA (or TEOA) and the triglyceride. In the case of RODEA, polyol set the viscosity was quite high 22 000 – 23 600 mPa·s, but the polyols were still suitable for rigid PU foam formulation development. The high viscosity of the RODEA polyol set is explained by the hydrogen bonding of the polar amide groups present in the polyol chemical structure. Polyols

with such high f_n are seldom used as the only component in rigid PU foam formulation. Their main application is as crosslinking reagents and their parts by weight (pbw) ratio in polyol component formulation usually is between 10-30 pbw [1]. Tertiary amine groups of synthesised polyols have autocatalytic properties that could be useful for the development of fast curing systems used for spray applied rigid PU foams.

Table 3.15

Common characteristics of developed high functionality RO based polyols

Polyol	OH val., mgKOH/g	Viscosity (20 °C), mPa·s	Acid val., mg KOH/g	W _{H₂O} , wt.%	Density at 20 °C, g/cm ³	f_n	M _n	M _w	p _d	RO content in polyol, %
RODEG	242	6 500	8.6	0.322	1.025	3.0	695	944	1.36	70.8
RODEA 0	471	22 000	<2.0	0.046	1.022	4.4	520	600	1.15	71.0
RODEA 1.5	603	23 400	<2.0	0.041	1.029	5.5	508	562	1.11	63.5
RODEA 2.0	614	23 600	<2.0	0.044	1.035	5.7	518	652	1.09	61.3
RODEA 2.5	635	23 400	<2.0	0.055	1.041	5.8	511	541	1.06	59.3
ROTEA 0	430	1 800	<2.0	0.026	1.031	3.6	467	570	1.22	63.4
ROTEA 1.5	528	2 400	<2.0	0.028	1.037	4.9	524	696	1.33	55.1
ROTEA 2.0	550	2 400	<2.0	0.039	1.045	5.5	560	744	1.33	52.8
ROTEA 2.5	557	2 400	<2.0	0.044	1.053	5.2	528	659	1.25	50.7

FTIR Analysis of High Functionality Polyols from Epoxidized RO

The chemical structure of the synthesised polyols was studied by FTIR spectroscopy. FTIR spectra of unmodified RO, RO after epoxidation and RODEG polyol are presented in Figure 3.64. Peaks at 3416–3370 cm⁻¹ indicated the presence of OH groups in the RODEG polyol. Also as expected the double bond =C-H stretching at 3008 cm⁻¹ of unmodified RO disappeared after epoxidation process. The C-O-C oxirane ring stretching vibrations were identified at 823 cm⁻¹ for ROEP and this peak disappeared after oxirane ring was opened with DEG. Also, after the epoxy group opening an ether bond C-O stretching at 1103 cm⁻¹ was observed. C=O bond stretching peak at 1742–1736 cm⁻¹ was indicative of fatty acid triglyceride structure. Peaks at ~ 2930 and ~ 2860 cm⁻¹ were identified as of -C-H₂- symmetric and asymmetric stretching.

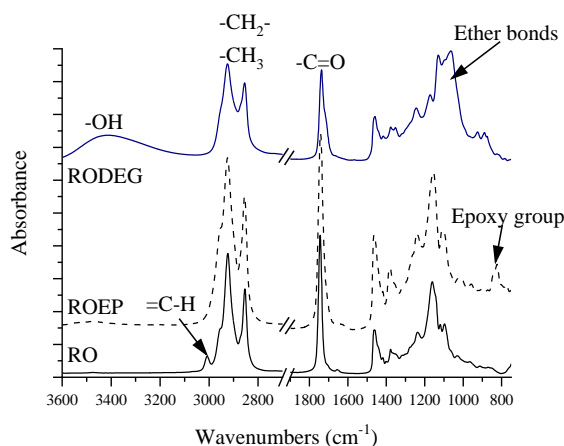


Figure 3.64. FTIR spectra of RO, ROEP and RODEG polyol.

FTIR spectra of ROEP and RODEA 0–2.5 polyols are presented in Figure 3.65a. The broad peak between 3500–3100 cm^{-1} was identified as stretching vibrations of the O-H and N-H groups. The intensity of this peak increased with the increase of DEOA ratio in polyol synthesis and correlates with the increase of OH value of tested polyols. No quantitative calibration of this FTIR analysis was done for this study. Same as for RODEG the epoxy group stretching vibration peak at 823 cm^{-1} disappeared for the analysed polyols.

FTIR spectra of ROTEA polyol are presented in Figure 3.65b. The intensity of the OH group broad peak at 3369 cm^{-1} increased with the increase of TEOA ratio in the reaction. Also, the peak of C-O stretching of ether groups at 1070 cm^{-1} and the peak of tertiary amine group stretching vibration at 1036 cm^{-1} were more noticeable. The slight shift of C=O stretching peak from 1742 cm^{-1} to 1735 cm^{-1} is explained with a change of RO triglyceride structure into TEOA fatty acid esters [159].

The most significant difference between RODEA and ROTEA polyols was the presence of amide peak at 1619 cm^{-1} for RODEA, which resulted from the transamidation reaction of fatty acid triglycerides. Similar amide group peak was also reported in the literature for polyols synthesised from RO by transamidation reaction with DEOA [25]. Moreover, the FTIR spectra of RODEA 1.5–2.5 polyols showed very weak C=O stretching peak at 1736 cm^{-1} evidencing the low content of triglyceride ester structures. The C-O stretching of ether groups and C-N stretching of tertiary amine groups from epoxy ring opening reaction were seen at 1100 – 1020 cm^{-1} . Both peaks overlap and could not be separated without further peak deconvolution.

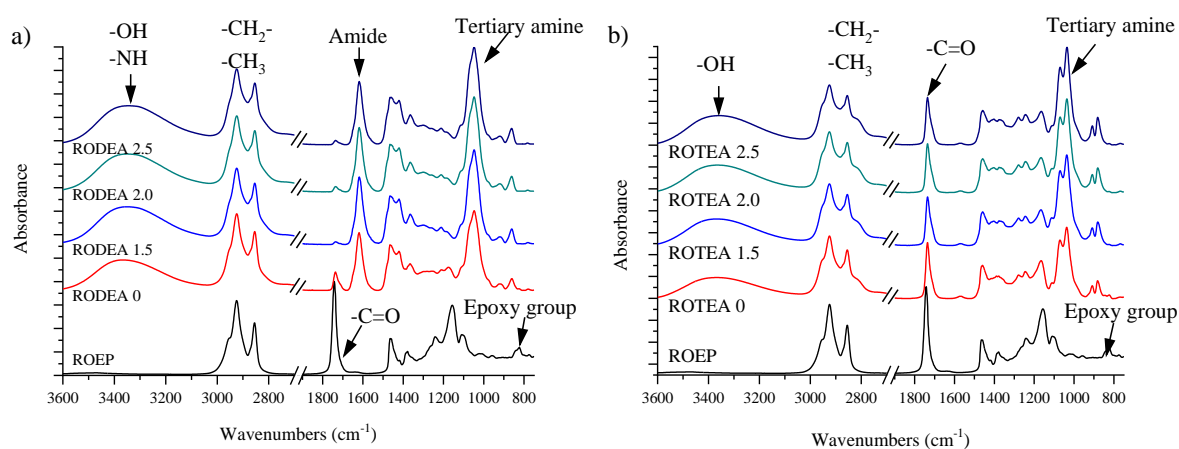


Figure 3.65. FTIR spectra of ROEP and a) RODEA 0-2.5 and b) ROTEA 0-2.5 polyols.

MALDI TOF Mass Spectrometry of RO Based High Functionality Polyols

MALDI TOF mass spectrometry was used to identify molecular ions of synthesised polyols. Parent ions were primarily MH^+ and $\text{M}\cdot\text{Na}^+$ cations. $\text{M}\cdot\text{Na}^+$ cations formed from alkyl salts in the matrix sample as well as from impurities of the synthesised polyols coming from the reagents used for polyols drying [236,237]. The absence of peaks above m/z 2000 was evidence that no higher molecular weight oligomers were formed. Several groups of parent ions were identified for all polyols corresponding to the different chemical structure of obtained

substances. Epoxy ring opening reaction in combination with several side reactions as well as transesterification reactions will contribute to a broad range of different mass peaks.

The MALDI TOF mass spectrum of RODEG polyol (see Figure 3.66) shows that the epoxy ring opening reaction with DEG took place. Simultaneously, the transesterification of ester bonds of triglyceride structure with DEG also proceeded as seen from the peak group at m/z 409–515. The peaks in this group are attributed to monoglyceride and DEG-ester fatty acid structures; e.g. the peak at m/z 501 was assigned to a product of ring opening reaction between the monoglyceride of epoxidized oleic acid and DEG and the peak at m/z 515 corresponded to the DEG ester of epoxidized oleic acid opened with DEG. Diglyceride products can be seen at m/z 796–902; e.g. the peak at m/z 888 was assigned to a ring opening reaction product between one mole of diglyceride of epoxidized oleic acid and two moles of DEG. The peak at m/z 902 corresponded to a product of ring opening reaction between two moles of DEG and one mole of diacyl ester of epoxidized oleic acid and DEG. The hypothesised polyol, a product of ring opening reaction between triglycerides of epoxidized fatty acid and DEG, is then seen at m/z 1182–1288. For instance, the peak at m/z 1273 corresponded to a product of ring opening reaction between three moles of DEG and one mole of a triglyceride of epoxidized oleic acid. The mass peaks attributed to short oligomers were observed at m/z 1568–1674. It is likely that the presence of different families of peaks is due to the association of the polymer molecules with Na^+ ions.

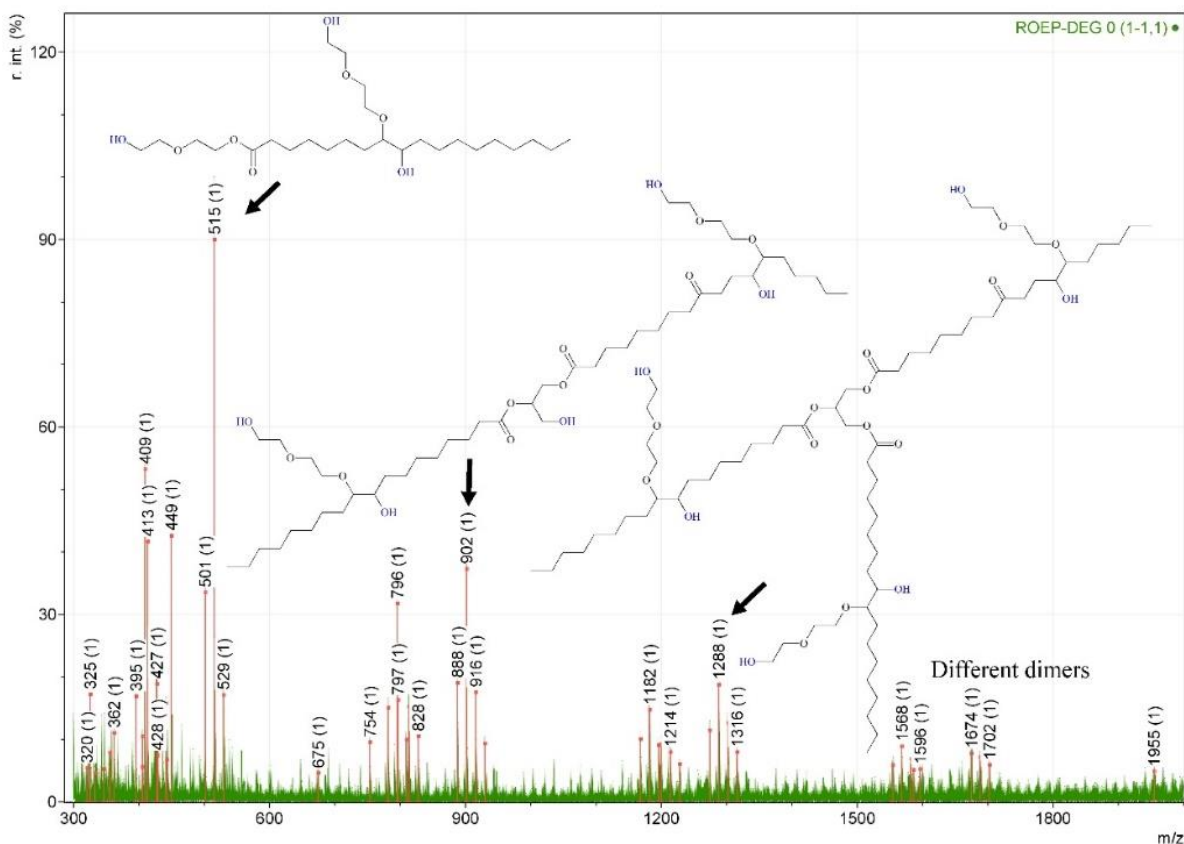


Figure 3.66. MALDI TOF spectrum of the RODEG polyol.

Similar to RODEG, the RODEA 0–2.5 polyols contained transamidation products as well as epoxy ring opening reaction products. The dominant peak at m/z 491 (see Figure 3.67.) was

attributed to MH^+ ion of the desired polyol structure from Figure 2.7. Similar structures of polyols obtained from vegetable oils have been reported although the end product contained a significant amount of oligomerization products [110]. In my case, the significantly lower molecular mass polyols were obtained with the calculated mass of 490.72 Da and theoretical functionality of 5. With the increased content of DEOA in polyol synthesis, the high molecular mass peaks decreased. The MALDI TOF mass spectrum of RODEA 2.5 polyol showed mostly peaks of transamidation products. The diglyceride of DEOA opened fatty acids were observed at m/z 742–877 and traces of the RODEA triglycerides were seen at m/z 1157–1282. It must be mentioned that without proper calibration with model substances the MALDI TOF mass spectroscopy is not suitable for quantitative product analysis and therefore in this study it was used only for qualitative identification of the obtained products.

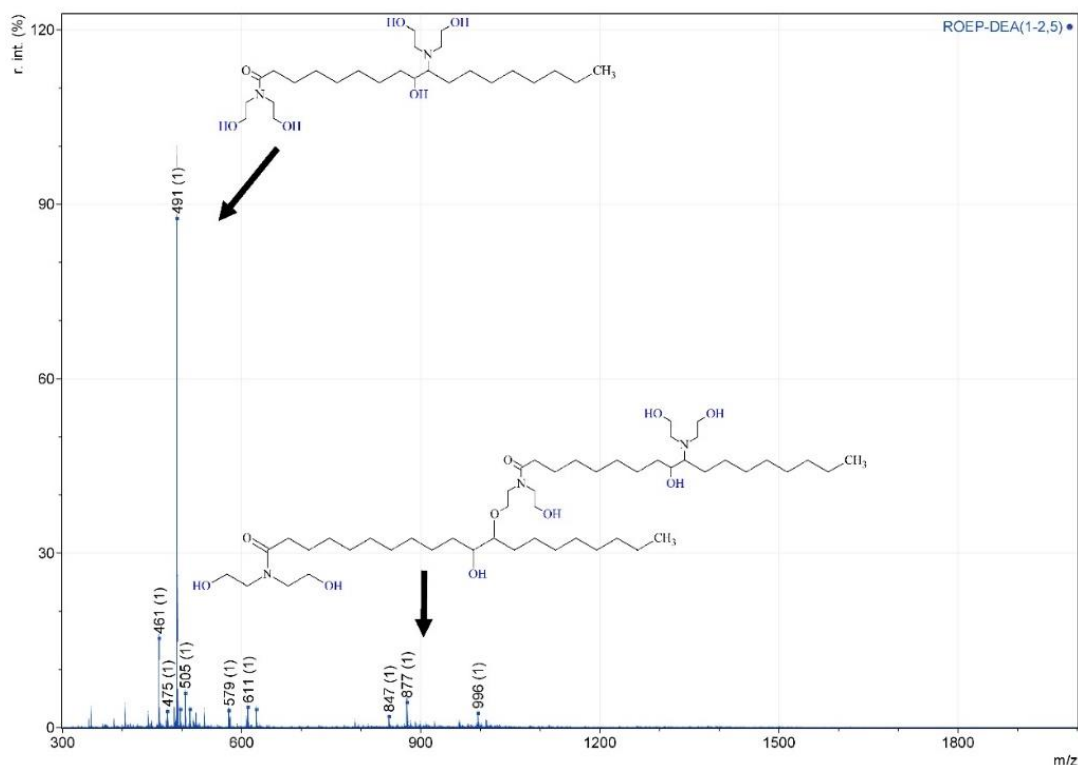


Figure 3.67. MALDI TOF spectrum of the RODEA 2.5 polyol.

The MALDI TOF mass spectrum of ROTEA 2.5 polyol (see Figure 3.68) contained the peak at m/z 580 attributed to MH^+ ion the target structure of ROTEA polyol according to Figure 2.8. However, the higher reaction temperature used for ROTEA 0–2.5 polyol synthesis led to side reactions of epoxy groups as evidenced from the presence of the peak at m/z 430, which was attributed to the oleic acid TEOA ester where the epoxy group has been converted into ketone group. It is known that the epoxy group can be converted into a variety of side products [233].

The peaks at m/z 430, 594, 711, 729, 860, 892, 1055, 1140 and 1158 were attributed to the oleic and linoleic acid TEA esters bearing ketone groups from undesired ROEP side reactions evidencing that too high temperature of ring opening synthesis was set. Moreover, the

additional side products of the ring opening reaction of ROEP with water were also identified in the ROTEA 2.5 polyol as the mass peaks at m/z 448, 729, 1055 and 1158.

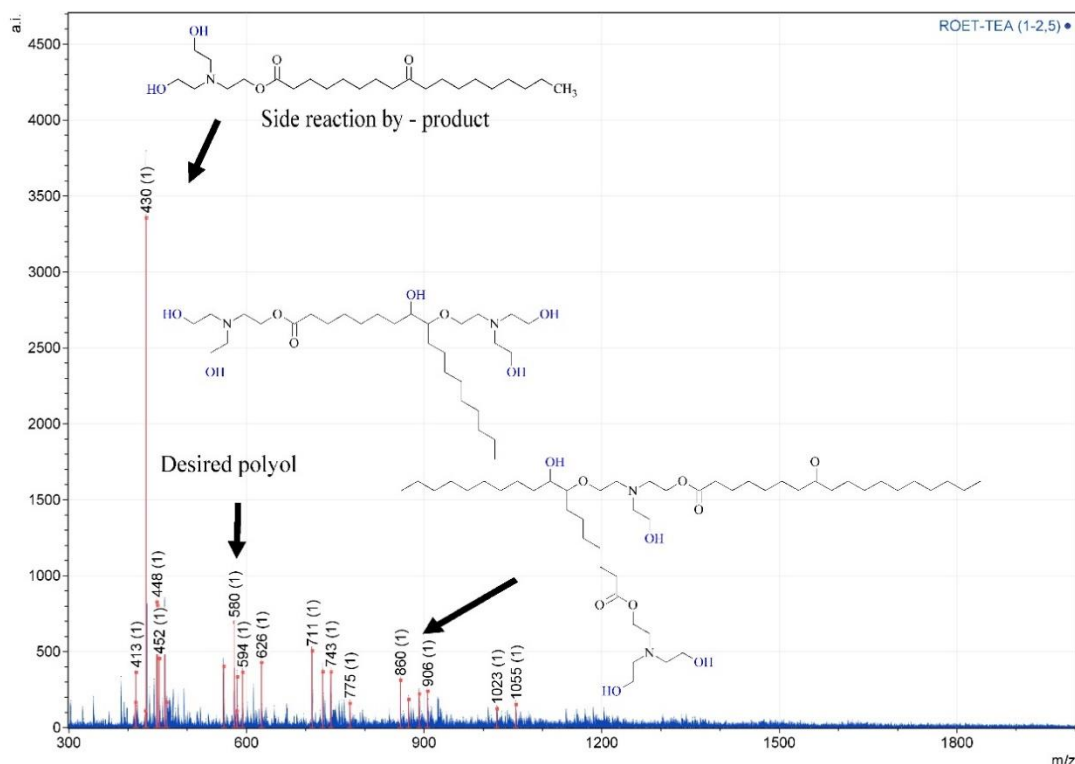


Figure 3.68. MALDI TOF spectrum of the ROTEA 2.5 polyol.

The calculated average functionality of synthesised bio-polyols (Table 3.15) was comparable to the proposed chemical structures of obtained polyols. Despite the formation of by-products in the case of ROTEA, this polyol can still be considered as high functional and suitable for rigid PU foam development. Nevertheless, further studies of obtained polyol structure and composition have to be carried out and synthesis parameters should be optimised to reduce by-product formation.

Rigid PU Foam Development from RO Based High Functionality Polyols

The synthesised polyols were used to prepare rigid PU foams according to the formulation (shown in Table 2.4) and the common characteristics of rigid PU foams were tested (Table 3.16). The PU foam formulations were developed to assess the suitability of prepared RO based polyols for further material optimization. The developed rigid PU foams had an apparent density in the range of 36–41 kg/m³, which is the common density of the thermal insulation materials. All PU foams had closed cellular structure with the closed cell content above 95 %.

No additional catalyst was used to cure the PU foam from ROTEA 0–2.5 polyols. To prepare PU foams the components had to be cooled down to 14 °C, even then the systems were much faster than in case of other polyols. This shows high autocatalytic properties of obtained polyols due to the presence of tertiary amine groups in polyol structure. ROTEA 0–2.5 polyols could be used as the crosslinking agents in fast curing systems like spray applied rigid PU foams where PU foam has to gel in 5–10 sec.

Table 3.16

Technological characteristics of rigid PU foam formulation (start time, string time, tack-free time, rise time), apparent density, closed-cell content and thermal conductivity of developed rigid PU foams.

Polyol formulation	RO DEG	RODEA 0	RODEA 1.5	RODEA 2.0	RODEA 2.5	ROTEA 0	ROTEA 1.5	ROTEA 2.0	ROTEA 2.5
<i>Technological parameters</i>									
Start time, s	17	15	15	17	18	20	17	16	15
String time, s	40	37	35	37	38	43	35	35	35
Tack free time, s	47	47	41	42	43	60	42	41	41
Rise time, s	44	42	45	48	50	55	47	46	45
Temperature of polyol system before foaming, °C	21	21	21	21	21	14	14	14	14
Apparent density of PU foams, kg/m ³	36.3	38.2	37.9	37.2	39.9	35.1	40.9	39.4	39.4
Closed cell content, %	98	95	98	98	96	93	98	98	96
Thermal conductivity, mW/m·K	21.58	23.47	21.67	22.27	23.11	23.29	21.46	21.71	21.93

Rigid PU foams from all polyols had a similar mechanical strength. The mechanical characteristics were normalised to an average PU foam density of 40 kg/m³ according to M. Hawkins (2005) to be able to compare their values [181].

The normalized compression strengths and modulus were calculated in parallel and perpendicular to the foaming direction (Figure 3.69. a, b). All prepared rigid PU foams showed decent mechanical characteristics meeting the industry standard of 0.2 MPa compression strength (in parallel to the foaming direction) for rigid PU foams with a density of 40 kg/m³.

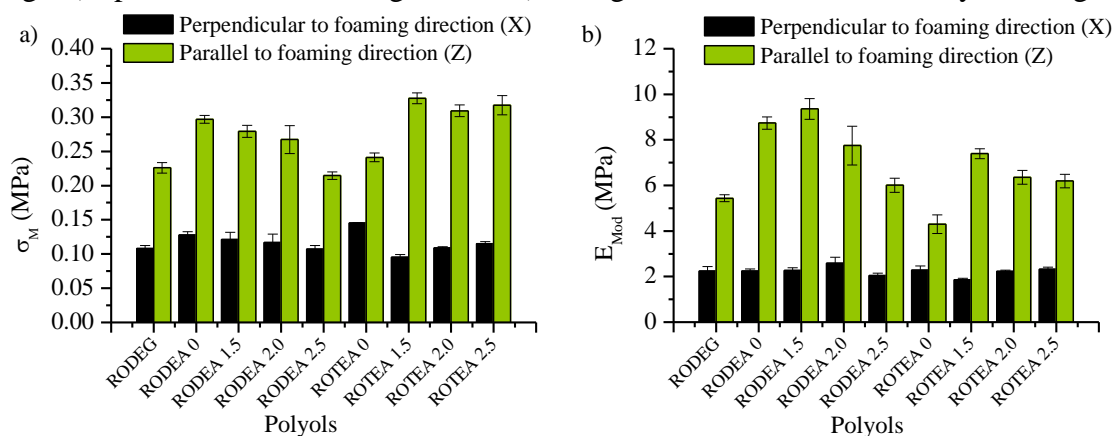


Figure 3.69. a) Compression strength and b) modulus of elasticity of rigid PU foams obtained from high functional RO polyols.

All developed rigid PU foams showed optimal thermal conductivity close to 22.0 mW/m·K (Table 3.16), typical for this type of insulation material. The prepared polyols and their influence on PU matrix, hard segment content and “ageing“ of the thermal conductivity must be further studied. These initial results are promising and showing that the novel high functional polyols could be useful in the development of high-efficiency thermal insulation materials.

Conclusions of High Functionality Polyol Synthesis from RO

- The one-step bio-polyol synthesis process was combined with RO epoxidation and epoxy ring opening to obtain high functionality polyols with $f_n = 3.6\text{--}5.8$.
- The tertiary amine groups of synthesised polyols allowed to reduce or completely remove catalysts in rigid PU foam formulations.
- The produced foams had closed cell content above 95 %, the apparent density of $\sim 40 \text{ kg/m}^3$ and thermal conductivity of $21.5\text{--}23.3 \text{ mW/m}\cdot\text{K}$.
- Obtained rigid PU foam showed excellent mechanical properties; compression strength above 0.20 MPa and compression modulus above 5 MPa in parallel to the foaming direction.
- Proposed polyols could be used as crosslinkers in rigid PU foam formulations or as a base polyol for spray applied rigid PU foams and other applications where fast curing is needed.

3.5. High Functionality Bio-Based Polyol Synthesis from TOFA

Previously developed polyols from TOFA in the one-step process by amidation or esterification with DEOA or TEOA delivered unsatisfactory properties of rigid PU foam as discussed in paragraph 3.1. Similar to RO based polyols the properties of the polyols could be improved by increasing average functionality of the polyols by epoxidation and subsequent epoxy ring opening reactions. Although vegetable oil epoxidation is a relatively well-studied topic, the epoxidation of neat fatty acids has not been studied at such detail. Majority of vegetable oils occur in nature as triglyceride esters without carboxylic acid moiety in their chemical structure. TOFA are derived from lignocellulosic biomass after the Kraft pulping process of cellulose pulp extraction [94,106]. Crude tall oil is most commonly used for heat generation in the pulp mills [238]. Nevertheless, TOFA have been reported as a potential feedstock for numerous value-added products ranging from biodiesel [95,239], wood-derived olefins for chemical industry [240], non-ionic surfactants [105], drilling and other fluids in mining industry [241] to application in polymer materials in resin production [104], plasticiser production and in PU material development [98,101]. The high amount of unsaturated bonds in the TOFA chemical structure makes it ideal feedstock for epoxidation process where afterwards oxirane rings could be used to introduce desired functional groups on to the TOFA backbone.

This chapter will explore different approaches of TOFA epoxidation. Generally, the epoxidation is done by different peroxy-carboxylic acids which can be *in-situ* generated from different organic acids and hydrogen peroxide (H_2O_2) in the presence of different catalysts. The objective of this chapter was to develop a solvent-free epoxidation method of neat TOFA and achieve high as possible double bond conversion to oxirane ring. Epoxidized tall oil fatty acids (ETOFA) would be later used for high functionality polyol synthesis. The proposed process allows for bypassing the production of intermediate products, such as TOFA methyl esters. A common epoxidation catalyst – sulphuric acid was compared to novel heterogeneous phase catalysts – ion exchange resin Amberlite IR 120 H and immobilised Lipase catalyst – Novozym® 435.

TOFA Epoxidation with Acidic Catalysts

The epoxidation of TOFA was carried out by *in-situ* generated peracetic acid from the acetic acid reaction with hydrogen peroxide in the presence of an acidic catalyst. The overall epoxidation reaction is depicted in Figure 3.70 [233,242]. The main disadvantage of the acid catalysed epoxidation method is the side-reaction occurrence with oxirane rings, which leads to the formation of by-products [42]. Unfortunately, the oxirane ring opening is also acid catalysed which leads to decreased oxirane group yield. The idealized TOFA epoxidation reaction scheme is depicted in Figure 3.70. In this work, two different acidic catalysts were compared for TOFA epoxidation process. One being homogeneous phase catalyst (H_2SO_4) and other was a heterogeneous phase catalyst (Amberlite IR 120 H). Although the catalyst type is different the general principle is similar as the epoxidation is carried out by the peracetic acid. Peracetic acid is formed in the aqueous phase of the synthesis.

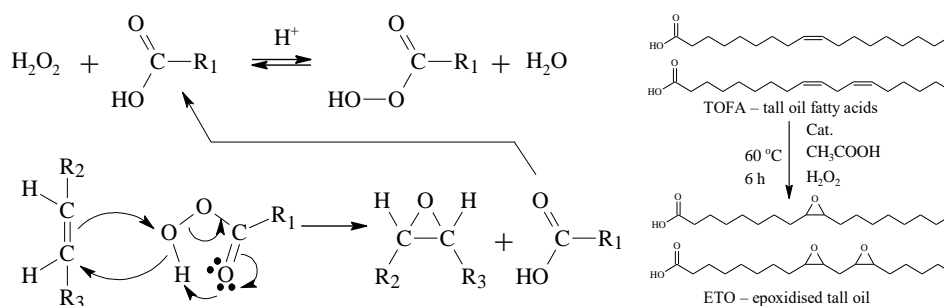


Figure 3.70. The idealized epoxidation scheme of TOFA aliphatic double bonds [241,243].

TOFA Epoxidation with a Sulphuric Acid Catalyst

During the TOFA epoxidation process with sulphuric acid as a catalyst, the degree of ethylenic unsaturation slowly decreased (EU_{ex}). The kinetic curves of increase of relative conversion to oxirane (RCO) and the decrease of relative ethylenic unsaturation (REU) at different H_2SO_4 catalyst content are depicted in Figure 3.71. The rate of iodine value/ethylenic unsaturation conversion increased with the gradual increase of the catalyst from 0.25 to 1.50 wt.%. In the case of 1.50 wt.% catalyst content after 7 hours of synthesis 88.7 % of double bonds have been oxidized. Unfortunately, the increase of RCO was not as high as for vegetable oil triglyceride epoxidation. The highest achieved RCO was 19.7 % which corresponds to 1.76 % or 1.098 mmol/g of oxirane oxygen content in TOFA. Moreover, the best result was achieved for the lowest catalyst content of 0.25 wt.%. The kinetic curves of RCO (Figure 3.71a) show that newly introduced oxirane rings are opened during the epoxidation process. The H_2SO_4 catalyse the undesired side reactions of oxirane ring cleavage with substances present in the reaction medium. This is confirmed by the increase of the rate of epoxy ring opening with the increase of H_2O_4 catalyst content.

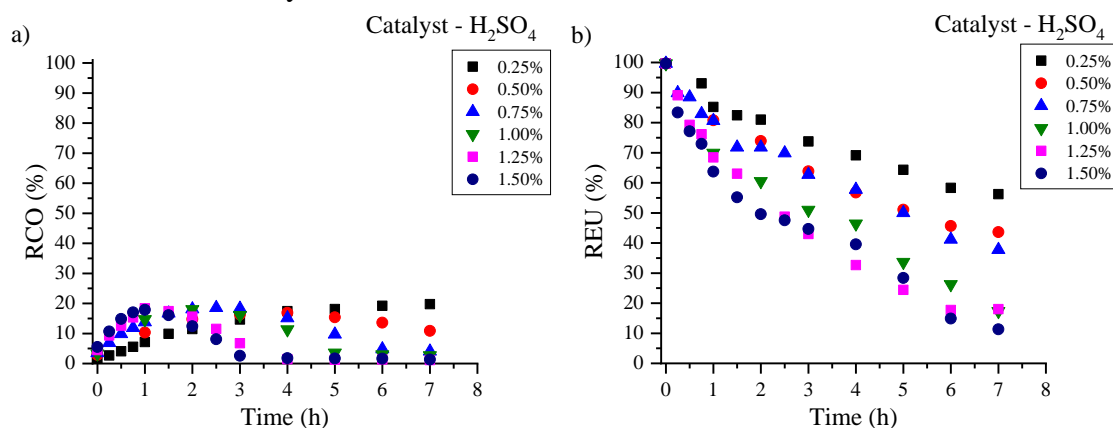


Figure 3.71. TOFA epoxidation kinetic curves, a) RCO b) REU at different H_2SO_4 catalyst contents.

The chemical structure of TOFA transformation into ETOFA during epoxidation process was studied using FTIR spectroscopy. An example of the overall FTIR spectra in the absorption range is depicted in Figure 3.72a. The double bond $=C-H$ stretching peak at 3008 cm^{-1} of unsaturated TOFA decreased while the C-O-C oxirane ring stretching vibration peak at 823 cm^{-1} increased during the epoxidation process. For TOFA, the typical absorption peaks of $-CH_2-$ symmetric stretching at ~ 2930 and asymmetric stretching at $\sim 2860\text{ cm}^{-1}$ were

identified. A close-up of the gradual decrease of the double bond stretching peak at 3008 cm^{-1} during the epoxidation process is depicted in Figure 3.73b. The double bond peak is still present after 7 hours of TOFA epoxidation, which correlates with REU data where 56.2% of initial double bonds are present (Figure 3.71b – $\text{H}_2\text{SO}_4 = 0.25\text{ wt.}\%$). The gradual increase of the C–O–C oxirane ring stretching vibration peak at 823 cm^{-1} shows the introduction of the oxirane rings into TOFA structure (Figure 3.72c) and correlates with the data of RCO (Figure 3.71a – $\text{H}_2\text{SO}_4 = 0.25\text{ wt.}\%$). The low amount of H_2SO_4 catalyst is enough to catalyse the oxirane ring opening reaction which is confirmed by the change of the $\text{C}=\text{O}$ bond stretching peak at $\sim 1730\text{ cm}^{-1}$. A single peak of the carboxyl group at 1707 cm^{-1} of neat TOFA develops a shoulder peak of an ester carboxyl group at 1737 cm^{-1} during the epoxidation process. This phenomenon is depicted in Figure 3.72d. However, in case of low H_2SO_4 catalyst content of 0.25 wt.% the oxirane ring opening was not as prevalent as for higher catalyst amounts described further.

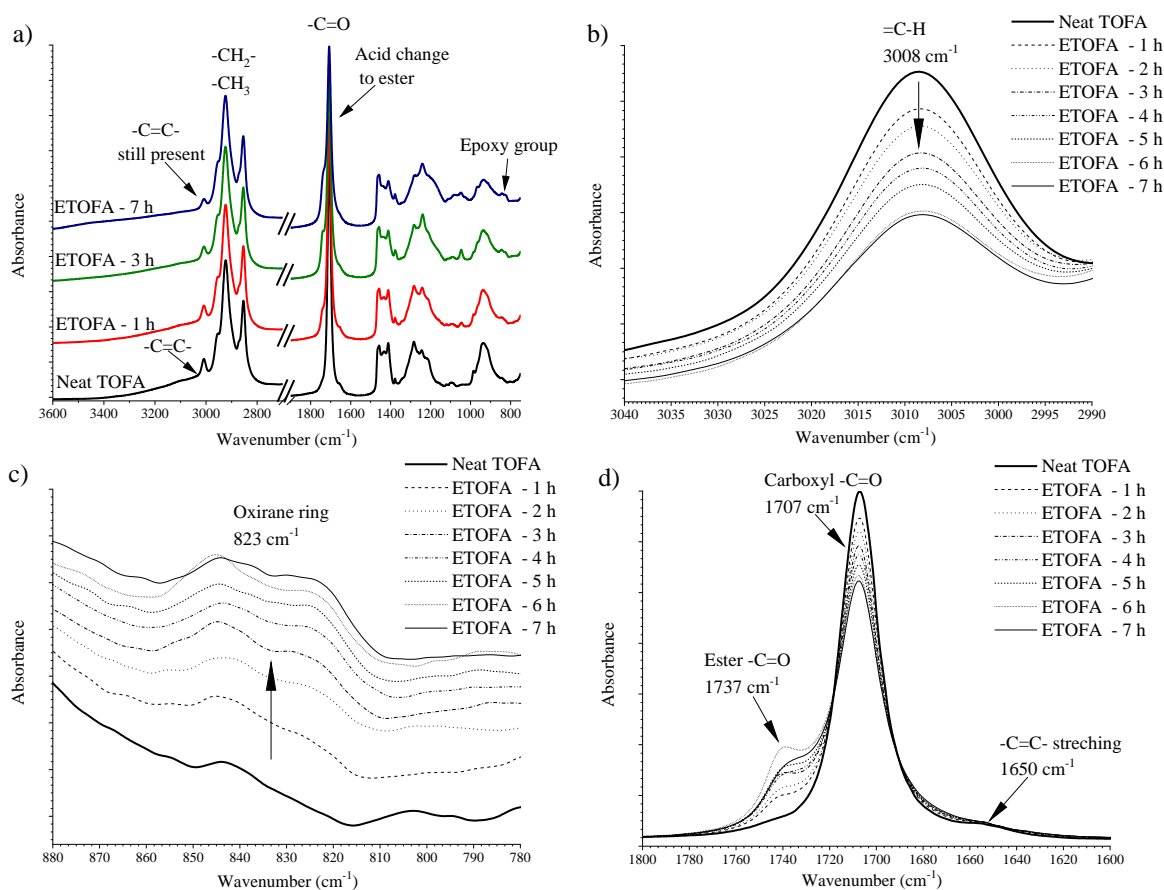


Figure 3.72. FTIR spectra during TOFA epoxidation for $\text{C}=\text{C}/\text{CH}_3\text{COOH}/\text{H}_2\text{O}_2$ 1.0/0.5/1.5; $\text{H}_2\text{SO}_4 = 0.25\text{ wt.}\%$; a) overall FTIR spectra b) change of EU absorption, 3008 cm^{-1} , c) change of OO vibration, 823 cm^{-1} , d) change of $\text{C}=\text{O}$ stretching, $\sim 1707\text{ cm}^{-1}$.

The TOFA chemical structure change during epoxidation using 1.5 wt.% of H_2SO_4 catalyst was also investigated by FTIR spectroscopy. Most important changes are depicted in Figure 3.73a. The intensity of the double bond stretching peak at 3009 cm^{-1} decreased during epoxidation process (Figure 3.73b). The decrease was more rapid and the peak was barely visible after 5 hours of synthesis when compared to synthesis with 0.25 wt.% of H_2SO_4 catalyst.

The reduction of the double bond peak intensity correlates with ethylenic unsaturation data where 11.3 % of initial double bonds are present (Figure 3.71b – $\text{H}_2\text{SO}_4 = 1.50 \text{ wt.}\%$) after 7 hours of synthesis. The double bond decrease did not contribute to the introduction of oxirane rings into the structure of TOFA as seen from C-O-C oxirane ring stretching vibration peak at 823 cm^{-1} close-ups (Figure 3.73c). The oxirane peak is visible after 1 and 2 hours of synthesis and afterwards, it disappears which correlates with the data of relative conversion to oxirane (Figure 3.71a – $\text{H}_2\text{SO}_4 = 1.50 \text{ wt.}\%$). Furthermore, the change of the $-\text{C}=\text{O}$ bond stretching peak at $\sim 1730 \text{ cm}^{-1}$ is more distinct for higher contents of H_2SO_4 (Figure 3.73d). The H_2SO_4 catalyses the oxirane ring opening reaction with water, the carboxylic groups of the TOFA as well as the acetic acid present in the reaction medium. The oxirane ring opening is also confirmed by the introduction of OH groups in ETOFA structure seen as a broad peak at $3700\text{-}3200 \text{ cm}^{-1}$ (Figure 3.73a)

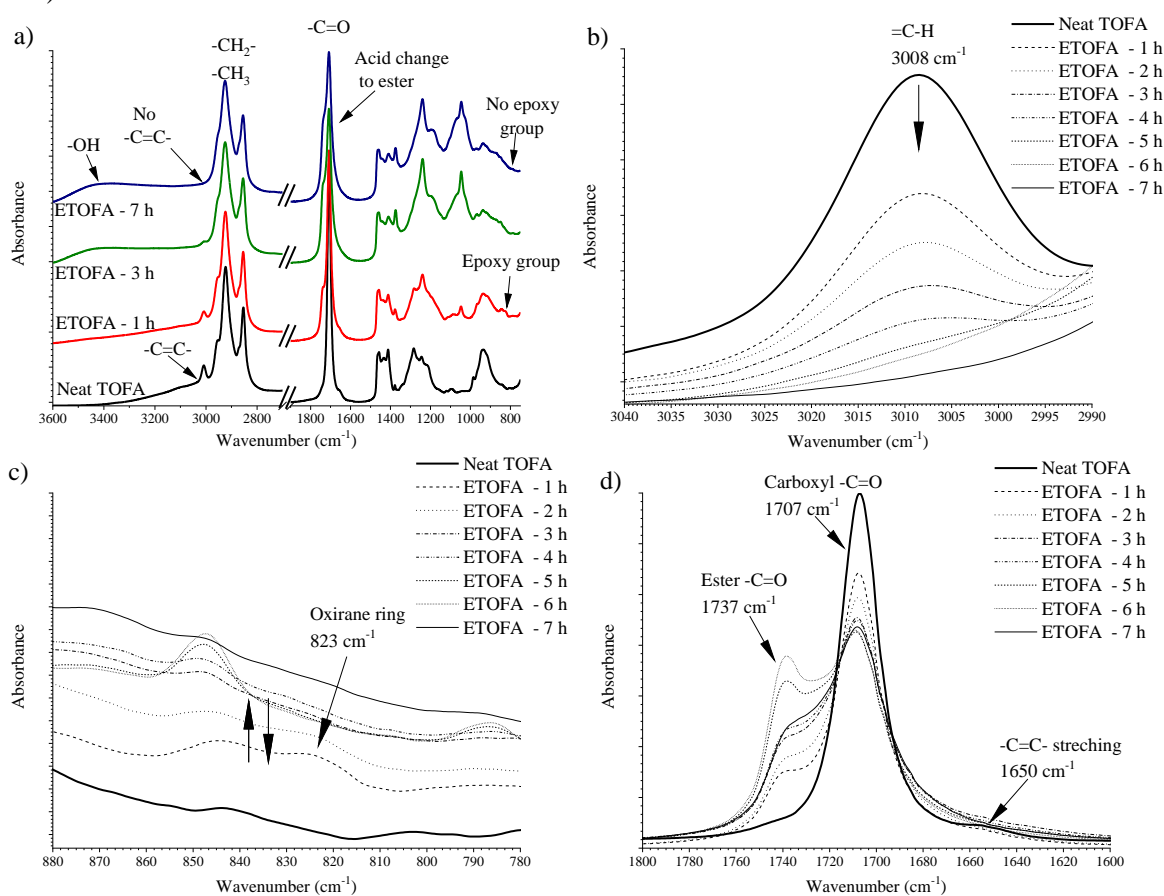


Figure 3.73. FTIR spectra during TOFA epoxidation for $\text{C}=\text{C}/\text{CH}_3\text{COOH}/\text{H}_2\text{O}_2$ 1.0/0.5/1.5; $\text{H}_2\text{SO}_4 = 1.50 \text{ wt.}\%$; a) overall FTIR spectra b) change of EU absorption, 3009 cm^{-1} , c) change of OO vibration, 823 cm^{-1} , d) change of $-\text{C}=\text{O}$ stretching, $\sim 1707 \text{ cm}^{-1}$.

Several acid-catalysed side reactions of the oxirane ring opening during epoxidation process have been reported [243,244]. Invariably, they involve an opening of the oxirane ring and, consequently, lower yields of ETOFA. Possible side reactions of acid-catalysed epoxy ring opening are depicted in Figure 3.74.

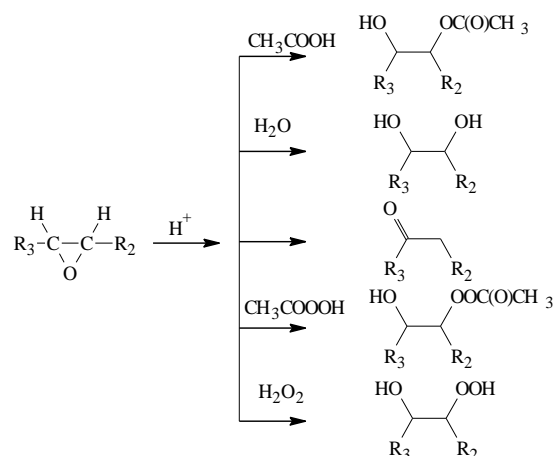


Figure 3.74. Possible side reactions during epoxidation.

The acid catalysed epoxy ring opening with nucleophilic reagents can be explained by the following mechanism (Figure 3.75). In the first step, the oxirane oxygen is protonated by the acid catalyst (Step 1). Then the carbon-oxygen bond in oxirane ring becomes weaker (Step 2) and the positive charge builds up on the electron acceptor carbon of the oxirane ring. In the next step, the nucleophilic reagent attacks the more electrophilic carbon (Step 3). In the studied system several nucleophiles are present, like water, -OH groups of different alcohols as well as the carboxylate anions of the acetic acid and TOFA. The final step (Step 4) is the deprotonation which results in the neutral side reaction product.

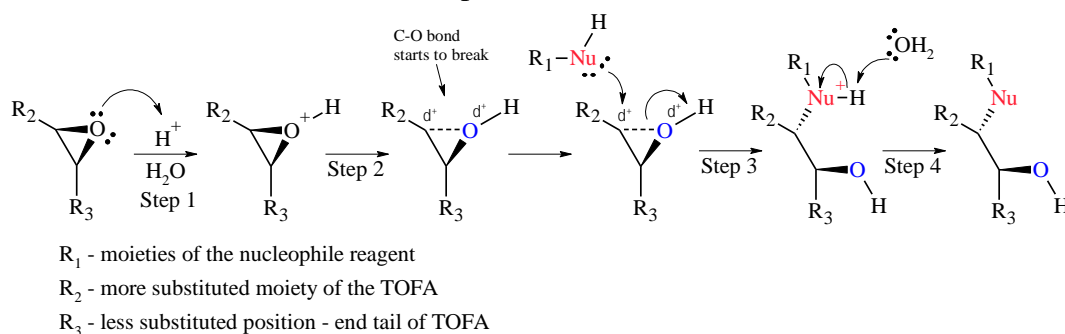


Figure 3.75. Acid catalysed epoxy ring opening.

TOFA Epoxidation with Amberlite IR-120 H Ion Exchange Resin Catalyst

Heterogeneous catalysts such as functionalized ion-exchange resins could provide several advantages. Small carboxylic acids, like acetic acid, can easily dissociate into and out of the gel-like structure of the catalyst where the formation of peracetic acid takes place. While the more bulky structure of the TOFA is less likely to penetrate the catalyst. Hence, the ETOFA is more protected from the attack of the protons which are confined inside the gel matrix. Therefore, the ETOFA epoxy ring opening during synthesis is prevented. Furthermore, a heterogeneous phase catalyst can be recovered and reused by simple filtration in a batch-type reactor. Such catalyst is also more suitable in continuous flow reactors which are more common in industrial processes.

During the epoxidation process with Amberlite IR-120 H ion exchange resin catalyst, RCO gradually increased while the REU decreased as depicted in Figure 3.76. The rate of decrease

of the REU was similar to experiments with H_2SO_4 as a catalyst where after 7 hours of synthesis the majority of double bonds have been transformed. In the case of 20 wt.% and 30 wt.% of Amberlite IR 120H catalyst after 7 hours of synthesis, 81.0 % and 86.6 % of double bonds have been transformed respectively. Using Amberlite IR 120 H catalyst the oxirane yield was much higher than in previous experiments. Oxirane group side reactions were less prevalent and 42.9 % and 45.5 % of RCO were achieved for 20 wt.% and 30 wt.% of Amberlite IR 120H catalyst after 7 hours of synthesis respectively. Catalyst content of 20 wt.% was most optimal as the further increase of the catalyst did not significantly increase the oxirane yield neither the rate of the epoxidation was boosted.

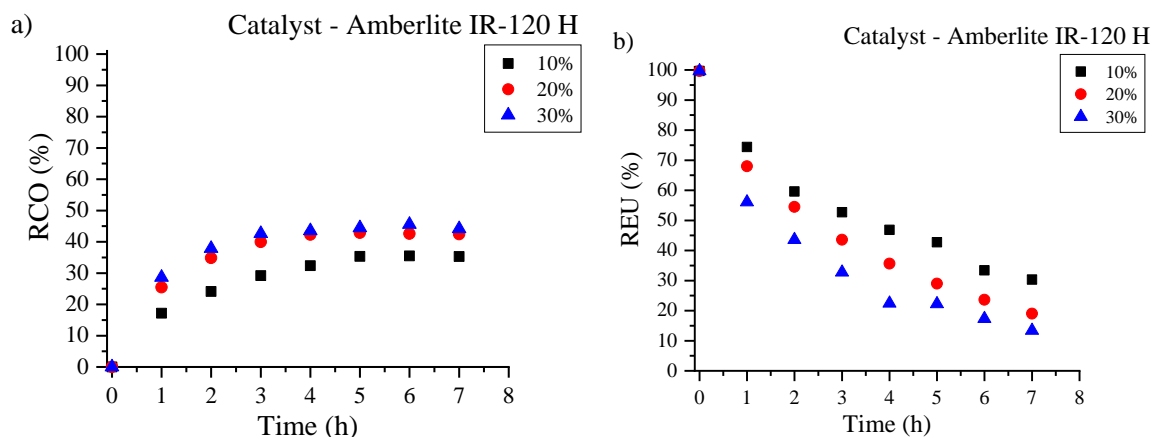


Figure 3.76. TOFA epoxidation kinetic curves, a) RCO b) REU at different Amberlite IR-120 H catalyst contents.

The chemical structure of TOFA transformation into ETOFA during epoxidation process with Amberlite IR 120 H was studied using FTIR spectroscopy. An example of the overall FTIR spectra in the absorption range is depicted in Figure 3.77a. The $=\text{C}-\text{H}$ stretching double of the bond peak at 3009 cm^{-1} of unsaturated TOFA decreased while the $\text{C}-\text{O}-\text{C}$ oxirane ring stretching vibration peak at 823 cm^{-1} increased during the epoxidation process. A close-up of the gradual decrease of the double bond stretching peak at 3009 cm^{-1} during the epoxidation process is depicted in Figure 3.77b. Similar to higher contents of H_2SO_4 (1.0–1.5 wt.%) the double bond peak disappears at the end of the epoxidation process. The gradual increase of the $\text{C}-\text{O}-\text{C}$ oxirane ring stretching vibration peak at 823 cm^{-1} shows the introduction of the oxirane rings into TOFA structure (Figure 3.77c) and correlates with the data of relative conversion to oxirane (Figure 3.76a – Amberlite IR 120 H = 20 wt.%). The side reactions of oxirane ring opening with carboxylic groups of the acetic acid as well as TOFA are confirmed by the change of the $-\text{C}=\text{O}$ bond stretching peak at $\sim 1730\text{ cm}^{-1}$ (Figure 3.77d). Although, it was not as distinct as in the case for the H_2SO_4 catalyst (Figure 3.73d). The introduction of $-\text{OH}$ stretching vibration band at $3700\text{--}3200\text{ cm}^{-1}$ confirms the oxirane ring opening as it results in the introduction of secondary OH groups into TOFA structure (Figure 3.77e).

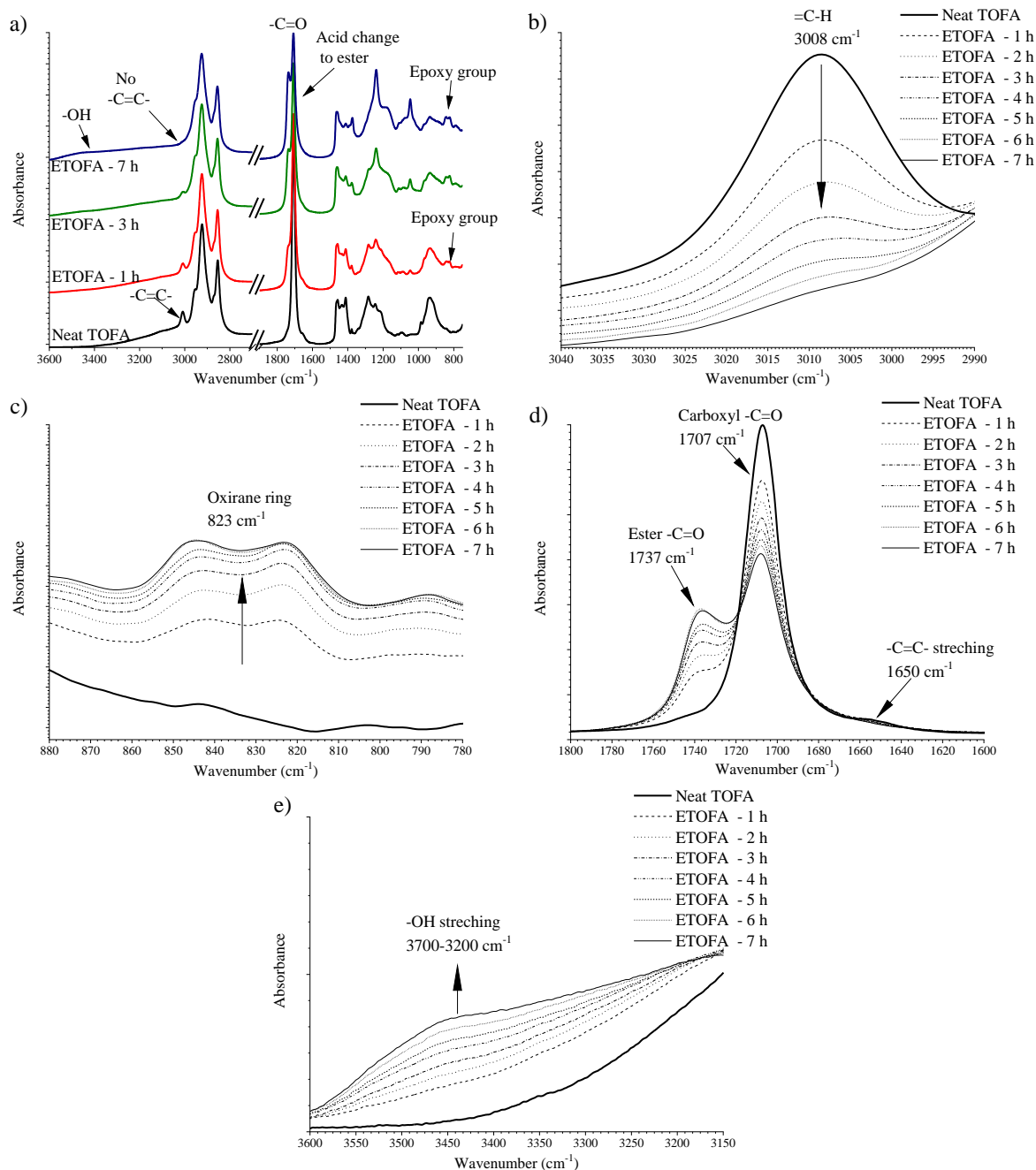


Figure 3.77. FTIR spectra during TOFA epoxidation for C=C/CH₃COOH/H₂O₂ 1.0/0.5/1.5; Amberlite IR 120 H = 20 wt.%; a) overall FTIR spectra b) change of EU absorption, c) change of OO vibration, d) change of -C=O stretching, e) change of -OH stretching.

The gel-like nature of the Amberlite IR 120H allowed to reduce the rate of oxirane ring opening side reactions because the bulky ETOFA molecules are less likely to penetrate the catalyst, thus the catalytic effect of oxirane ring protonation is removed. Nevertheless, the newly introduced oxirane rings were opened with different nucleophilic reagents present in the reaction media which is the reason for the low selectivity of the proposed epoxidation method ($S = 53.9\text{-}60.4\%$).

The comparison of the two different acidic catalysts content influence on TOFA epoxidation is depicted in Table 3.17. For the H₂SO₄ catalyst, the highest RCO was achieved after 1-2 hours

of synthesis. However, the total oxirane yield was two times lower than in the case of Amberlite IR 120H ion exchange catalyst due to the side reactions. The oxygen content of 3.82 % and 4.05 % (Amberlite IR 120H = 20 wt.% and 30 wt.%) of synthesised ETOFA is relatively high and comparable to other epoxidized natural oils [34,104,243,245]. Despite the oxirane ring opening side reaction obtained ETOFA are suitable for further polyol synthesis as well as the development of epoxide based products. Amberlite IR 120 H catalyst content of 20 wt.% was selected for further TOFA optimization as the 30 wt.% of catalyst did not result in a significant increase for RCO.

Table 3.17

Summary of the highest achieved relative conversion to oxirane and relative conversion of double bonds at respective synthesis time

	Synthesis time, h	OO _{ex} , %	RCO, %	Iodine value, g I ₂ /100g	UBC, %	S, %
Catalyst content	TOFA epoxidation with H ₂ SO ₄ catalyst					
0.25 wt. %	7	1.76	19.7	87.1	43.8	45.1
0.50 wt. %	4	1.50	16.9	88.0	48.9	39.0
0.75 wt. %	2.5	1.65	18.5	108.3	30.1	61.6
1.00 wt. %	2	1.60	18.0	92.8	39.5	45.6
1.25 wt. %	1	1.63	18.4	106.1	31.5	58.2
1.50 wt. %	1	1.54	17.4	98.7	36.3	47.8
Catalyst content	TOFA epoxidation with Amberlite IR-120 H ion exchange resin catalyst					
10 wt. %	6	3.16	35.5	51.8	66.6	53.3
20 wt. %	5	3.82	42.9	45.0	71.0	60.4
30 wt. %	6	4.05	45.5	26.8	82.7	55.1

Tall Oil Fatty Acid Epoxidation Kinetics

Temperature Influence on TOFA Epoxidation Kinetics

Determination of the kinetic parameters of the TOFA epoxidation would allow modelling the yield of the desired oxirane groups over process time. Thus it would be possible to optimise reaction parameters to achieve the maximum amount of RCO. Furthermore, the development of the TOFA epoxidation kinetic model would give an insight into chemical processes during the reaction. The temperature influence on TOFA epoxidation would allow calculating activation energy of the proposed reaction. The kinetic curves of TOFA epoxidation with Amberlite IR 120H resin catalyst at different temperatures are depicted in Figure 3.78. The increase in temperature increased the rate of REU conversion. Unfortunately, the oxirane group cleavage also increased, because the RCO started to drop after 2-3 h of synthesis time (see Figure 3.78a).

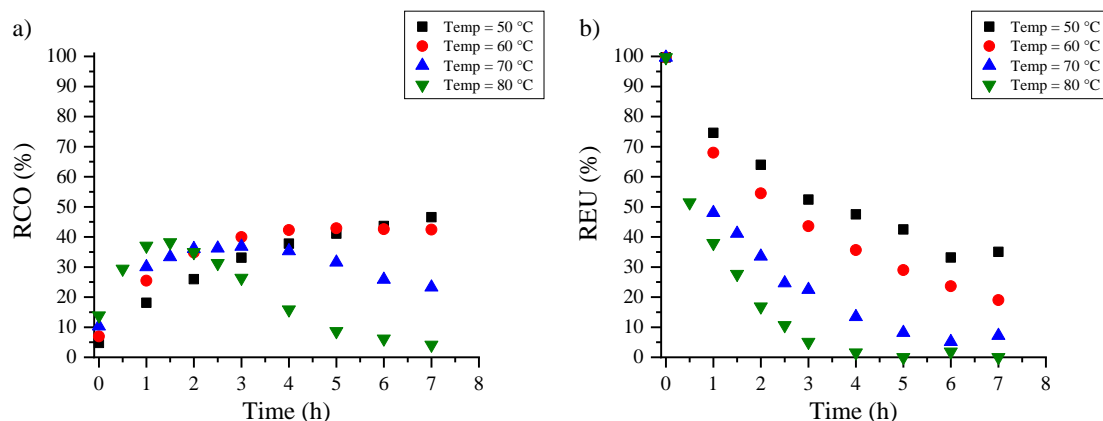


Figure 3.78. TOFA epoxidation kinetic curves, a) RCO b) REU at different temperatures.

Usually, the Arrhenius equation is used to describe the temperature dependence of the reaction rates. The rate of hydrogen peroxide decrease during epoxidation reaction is expressed by Equation 3.19. If the *in-situ* formation of peracetic acid demonstrated in reaction Scheme[1] in Figure 3.79 is considered to be rate-determining step of the TOFA epoxidation, then the reaction rate of the overall process can be expressed via relationship depicted in Equation 3.20 [32]. This model assumes that the concentration of the acetic acid stays constant during the process as it is released in the peracetic acid reaction with the double bond of TOFA. Furthermore, the degradation of newly developed oxirane rings and hydrogen peroxide should be negligible.

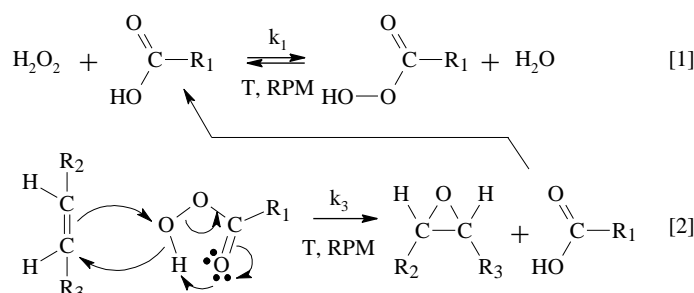


Figure 3.79. Epoxidation reaction mechanism.

$$\frac{d[\text{H}_2\text{O}_2]}{dt} = k_1[\text{H}_2\text{O}_2] \cdot [\text{AA}] \quad (3.19)$$

$$\frac{d[\text{H}_2\text{O}_2]}{dt} = k_1\{[\text{H}_2\text{O}_2]_0 - [\text{OO}]\} \cdot [\text{AA}]_0 \quad (3.20)$$

In Equation 3.20, [OO] is the oxirane oxygen content, [H₂O₂]₀ and [AA]₀ are the initial concentration of the hydrogen peroxide and acetic acid, respectively; and k₁ is the epoxidation process reaction rate constant. Integration of this equation leads to the linear relationship depicted in Equation 3.21. In this case, the ln{[H₂O₂]₀-[OO]} vs. *time* should be a straight line where the reaction rate can be estimated as a slope of the plot. Mentioned plots are presented in Figure 3.80a.

$$\ln\{[\text{H}_2\text{O}_2]_0 - [\text{OO}]\} = -k_1 \cdot [\text{AA}]_0 \cdot t + \ln[\text{H}_2\text{O}_2]_0 \quad (3.21)$$

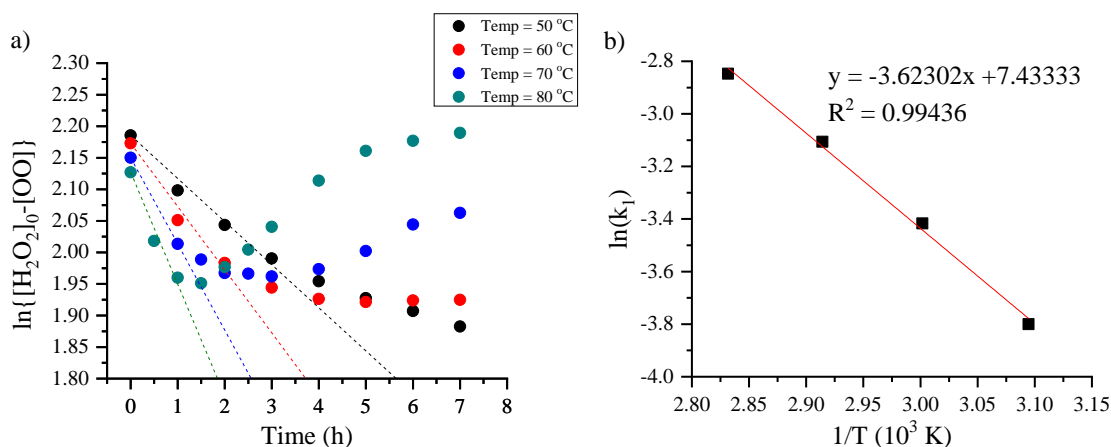


Figure 3.80. TOFA epoxidation at different temperatures a) plot of $\ln\{[H_2O_2]_0 - [OO]\}$ vs. reaction time; b) Arrhenius plot.

Unfortunately, it is seen that curves in Figure 3.80a do not have a linear relationship. This is due to the oxirane ring cleavage during the TOFA epoxidation process among other factors. At 50 °C, the curve can be considered close to linear, but for higher temperatures, they are far from the desired result. Nevertheless, a linear interpolation could be done for a few initial points as depicted by dashed lines in Figure 3.80a to obtain the reaction rate constants at different temperatures. Such approach was previously reported by several researchers for different natural oil and natural oil methyl ester epoxidation where also no linear correlation between $\ln\{[H_2O_2]_0 - [OO]\}$ vs. *time* was seen [32,39,246]. Reported studies depict natural oil epoxidation kinetics using RCO data. If the epoxidation model depicted in Equation 3.20. is true than $[OO]$ increase could be also expressed through the decrease of $[EU]$. The general assumption would be that for every mole of reacted double bond one mole of oxirane ring is obtained if there are no side reactions of oxirane ring cleavage. Because the rate-limiting step is the formation of peracetic acid i.e. the decrease of hydrogen peroxide, the rate of oxirane group introduction and the decrease of double bonds can be expressed with Equation 3.21.

$$-\frac{d[H_2O_2]}{dt} = \frac{d[OO]}{dt} = -\frac{d[EU]}{dt} \quad (3.21)$$

The $[EU]$ change over TOFA epoxidation was measured as depicted in Figure 3.78b and theoretical values of oxirane ring content calculated from a decrease of double bond content $[OO]$ were plotted as $\ln\{[H_2O_2]_0 - [OO]\}$ vs. time are depicted in Figure 3.81a. Obtained curves match linear relationship much closer than $[OO]$ results obtained from sample oxirane value titration. It is assumed that at the reaction temperatures 70 and 80 °C the reaction is finished after 3 h of epoxidation as almost all double bonds have been converted (see Figure 3.78b). The linear curve interpolation was done for data points up to 3 h for these two experiments.

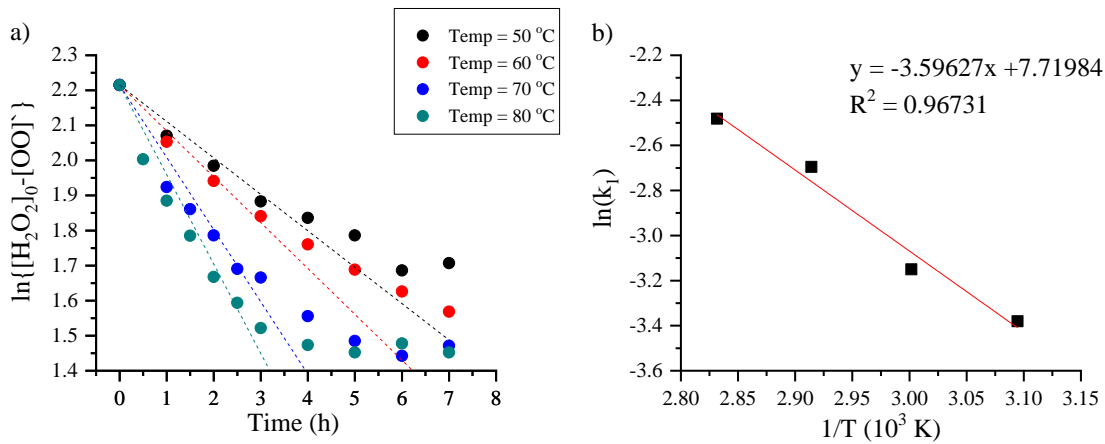


Figure 3.81. TOFA epoxidation at different temperatures a) plot of $\ln\{[H_2O_2]_0 - [OO]\}$ vs. reaction time; b) Arrhenius plot if $[OO]$ is calculated from $[EU]$ decrease.

The reaction rate constants obtained from slopes depicted in Figure 3.80a and Figure 3.81a are presented in Table 3.18. The activation energy (E_a) of the reaction was calculated from Arrhenius plots (see Fig. 3.81b and 3.82b). The enthalpy of activation (ΔH) was estimated using Equation 3.22 [39].

$$\Delta H = E_a - RT . \quad (3.22)$$

where E_a is activation energy calculated from Arrhenius plot, T [K] is temperature and R is the universal gas constant. The entropy of activation (ΔS) and free energy of activation (ΔG) was calculated using Equations 3.23 and 3.24 [39].

$$k_1 = \frac{R \cdot T}{N \cdot h} \cdot e^{\frac{\Delta S}{R}} \cdot e^{\frac{\Delta H}{R \cdot T}} . \quad (3.23)$$

$$\Delta G = \Delta H - T \cdot \Delta S . \quad (3.24)$$

where k_1 is the reaction rate constant, N is the Avogadro constant, h is the Planck's constant.

The thermodynamic properties of the TOFA epoxidation are summarised in Table 3.18. Obtained values of the thermodynamic properties are similar between the two calculation approaches. They show that the peracetic acid formation reaction is endothermic because the enthalpy of activation is positive ($\Delta H = 27$ kJ/mol) and hence an increase in the reaction temperature may lead to an increase in the conversion to oxirane oxygen. Contrary, the formation of epoxy rings is reported to be exceedingly exothermic where $\Delta H_{\text{Epoxy}} = -55$ kJ/mol, thus the whole process is exothermic [247,248]. Generated heat was matched by the thermal stabilization of the water bath. As mentioned the rate-limiting step is assumed to be the formation of the peracetic acid for which the kinetic parameters have been determined.

Table 3.18

Epoxidation rate constants, activation energy, activation enthalpy, the entropy of activation and free activation energy of the TOFA epoxidation

	Temperature [°C]	Epoxidation rate constant $k_1 \cdot 10^{-2}$ [L/(mol·s)]	Ea [kJ/mol]	ΔH [kJ/mol]	ΔS [J/(mol·K)]	ΔG [kJ/mol]
From [OO] data	50	2.2	30.1	27.3	-192.5	89.6
	60	3.3				91.4
	70	4.5				93.3
	80	5.8				95.4
From [EU] data	50	3.4	29.9	27.1	-190.1	88.4
	60	4.3				90.6
	70	6.8				92.1
	80	8.4				94.3

Although, described values of the thermodynamic properties were similar to what has been previously reported [32,39,246] the mathematical model does not represent described experimental setup. The two assumptions that the concentration of the acetic acid is constant and there are no side reactions of the oxirane ring opening are not true. Furthermore, the epoxidation rate model (Eq. 3.19.) describes the second-order reaction but studied system has several heterogeneous phases. The described model does not take into account the adsorption/desorption of reagents to the catalyst surface and the diffusion through aqueous and oil phase of the synthesis system. In the next paragraph more complex model of TOFA epoxidation has been proposed which takes into account the surface reaction on the catalyst active site as well as dissociation of the reagents in the reaction system.

TOFA Epoxidation Surface Reaction Kinetic Model

An attempt was made to apply the Eley-Rideal surface reaction mechanism to TOFA epoxidation with ion exchange resin catalyst. The Eley-Rideal mechanism was proposed by D. D. Eley and E. K. Rideal in 1938 and it is similar to the Langmuir-Hinshelwood surface reaction mechanism. The Langmuir-Hinshelwood mechanism is used to explain the interaction of surface charge carriers and excitons with adsorbed molecules that can promote surface chemical processes, whereas the Eley-Rideal mechanism is used to explain the interaction of molecules with surface-active centres that can initiate surface chemical processes [249]. In the Langmuir-Hinshelwood mechanism, both molecules adsorb to the catalyst and then undergo a chemical reaction, whereas in the Eley-Rideal mechanism only one molecule is adsorbed and the other reacts without adsorbing.

The overall reaction system of TOFA epoxidation is highly complex with three different phases of reactants. Some assumptions have to be made to simplify the determination of the reaction rate parameters of the studied process. It is assumed that TOFA do not diffuse into the porous structure of the ion exchange resin and do not adsorb to the active sites of the catalyst. Only acetic acid (AA) is adsorbed to the active site of the catalyst where it reacts with hydrogen peroxide (H₂O₂) forming peracetic acid (PA). Afterwards, the PA is desorbed from the catalyst where it is free to react with TOFA ethylenic unsaturation (EU) groups to form epoxy rings. After epoxidation of the double bonds, the AA is released. The rate-limiting step of the TOFA

epoxidation is the surface reaction which happens on the active site of the Amberlite IR 120H catalyst. There is a limited amount of oxirane group side reactions, oxirane groups are opened with water (H_2O) and AA forming glycol (G) and acyl-glycol (AG) respectively. It is assumed that mass transfer of AA and H_2O_2 to the catalyst, PA and H_2O from catalyst and PA to TOFA are much faster than the rate-limiting surface reaction step of the process, thus diffusion rates can be neglected. The idealised depiction of TOFA epoxidation process is shown in Figure 3.82.

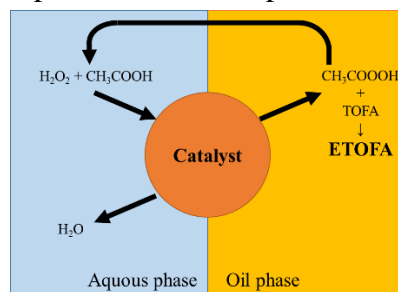


Figure 3.82. An idealised schematic of different reaction phases of the TOFA epoxidation process with heterogeneous phase Amberlite IR 120H catalyst.

The rate-limiting step of the catalyst surface reaction can be further split into three steps as depicted in Figure 3.83. In Step 1, the AA is adsorbed to the vacant site of the catalyst forming adsorbed acetic acid (AAs). In Step 2 H_2O_2 reacts with the AAs forming H_2O and adsorbed peracetic acid (PAs). In the last Step 3, the PAs is desorbed and released into the reaction medium.

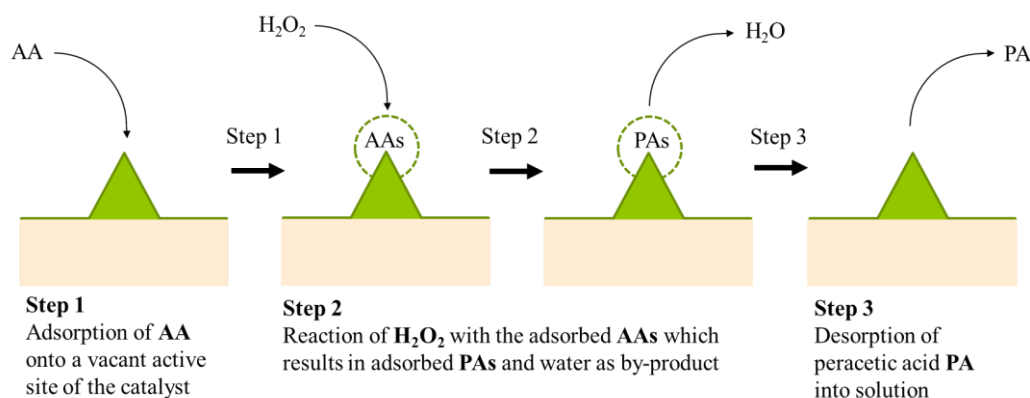


Figure 3.83. Eley-Rideal mechanism of peracetic acid formation on the surface of ion-exchange resin catalyst.

Step 1 – Adsorption of AA.

The proton of the sulphonic functional site (R_1SO_3H) of the catalyst is free to move away and protonate the carbonyl group present in the AA. As a result of the protonation of the AA, it now has the same charge as the proton and can reattach to the functional site via the process of chemisorption as depicted in Figure 3.84. The AA contacts with the vacant active sites (vs) on the surface of the catalyst and is adsorbed resulting in AAs. This is a reversible process and can be described with the adsorption and desorption reaction constants (k_a , k_a).

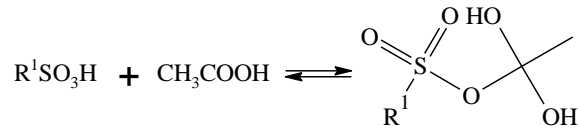


Figure 3.84. Acetic acid adsorption to the sulphonic functional site of the catalyst.

The reaction equation (Eq. 3.25) and the rate expression of non-dissociated adsorption of AA (Eq. 3.26) are as follows:



$$r_a = k_a \left([AA][vs] - \frac{[AAs]}{K_{AA}} \right). \quad (3.26)$$

where,

[AA] – acetic acid content, [mol/(100g oil)]

[vs] – vacant active site content, [mol/g(cat)]

[AAs] – adsorbed acetic acid content, [mol/(100g oil)]

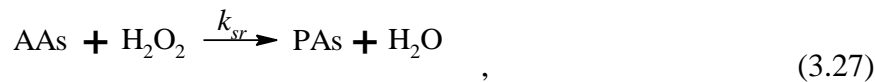
r_a – reaction rate of AA non-dissociated adsorption, [mol/(s·g(cat))]

$K_{AA} = k_a/k_{-a}$ – AA adsorption equilibrium constant, [L/mol]

k_a – AA non-dissociated adsorption rate constant, [g(cat)/(s·mol)]

Step 2. – Surface Reaction of AAs and H₂O₂.

The AAs on the catalyst surface connects with H₂O₂ and reacts forming PAs and releasing H₂O. It is assumed that the surface reaction (Eq.3.27) of AAs and H₂O₂ is non-reversible. In this case, the rate law for the PA formation according to the Eley-Rideal mechanism is described by Equation 3.28.



$$r_{sr} = k_{sr} \left([AAs][H_2O_2] - \frac{[PAs]}{K_S} \right). \quad (3.28)$$

where,

[H₂O₂] – hydrogen peroxide content, [mol/(100g oil)]

[PAs] – adsorbed peracetic acid content, [mol/(100g oil)]

r_{sr} – the rate of AAs and H₂O₂ irreversible surface reaction, [mol/(s·g(cat))]

K_S – surface reaction equilibrium constant, [L/mol]

k_{sr} – AAs and H₂O₂ surface reaction rate constant, [g(cat)/(s·mol)]

Step 3. – Desorption of PAs.

After the PAs is formed on the surface of the catalyst a reverse process to AA adsorption occurs. PA is desorbed from the catalyst surface but it can re-adsorb to a vacant active site as depicted in Figure 3.85.

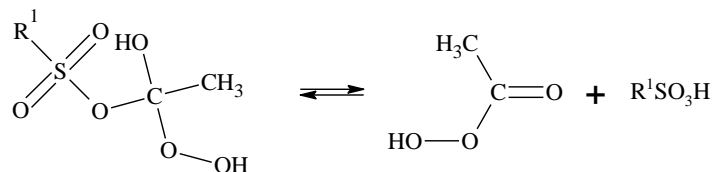


Figure 3.85. Peracetic acid desorption from the sulphonic functional site of the catalyst

The reaction equation (Eq. 3.29) and the rate expression of non-dissociated desorption of PA (Eq. 3.30) are as follows:



$$r_d = k_d([PAs] - [PA][vs] \cdot K_{PA}). \quad (3.30)$$

where,

[PA] – peracetic acid content, [mol/(100g oil)]

r_d – reaction rate of PA desorption, [mol/(s·g(cat))]

K_{PA} – PA adsorption equilibrium constant, [L/mol]

k_d – PA desorption rate constant, [g(cat)/(s·mol)]

It is highly inconvenient to measure the contents of [AAs], [PAs] and catalyst vacant active site [vs] content thus various steps are taken to eliminate them from the rate law equations. The assumption is that the surface reaction is the rate-limiting step of the process, thus adsorption and desorption reaction rate constants are quite large. In this case following ratios are approximately nil:

$$\frac{r_a}{k_a} \cong 0 \quad \& \quad \frac{r_d}{k_d} \cong 0. \quad (3.31)$$

Applying Eq. 3.31 to the rate laws of adsorption (Eq. 3.26) and desorption (Eq. 3.30) respectively following relationships for [AAs] and [PAs] are obtained:

$$[AAs] = K_{AA}[AA][vs] \quad \& \quad [PAs] = K_{PA}[PA][vs]. \quad (3.32)$$

It can be postulated that the total content of the catalyst active sites (C_t) is a sum of vacant active site content and adsorbed site content (see Eq. 3.33).

$$C_t = [vs] + [AAs] + [PAs]. \quad (3.33)$$

Inserting Eq. 3.32 into Eq. 3.33 it is possible to obtain an expression for vacant catalyst active sites:

$$C_t = [vs] + K_{AA}[AA][vs] + K_{PA}[PA][vs],$$

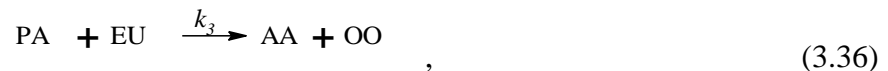
$$[vs] = \frac{C_t}{1 + K_{AA}[AA] + K_{PA}[PA]}. \quad (3.34)$$

Substituting Eq. 3.32 and Eq. 3.34 into Eq. 3.28 and keeping in mind that the reaction of peracetic production is non-reversible ($K_S \rightarrow \infty$) the general form of the rate law of Eley-Rideal surface reaction of PA formation (Eq. 3.35) where the W_{cat} is the catalyst mass ratio to TOFA mass is as follows:

$$r_{Sr} = \frac{k_{Sr} \cdot C_t \cdot W_{cat} \cdot K_{AA} \cdot [AA] \cdot [H_2O_2]}{1 + K_{AA} \cdot [AA] + K_{PA} \cdot [PA]}. \quad (3.35)$$

Epoxydation of TOFA

The released PA reacts with double bonds of the TOFA according to the previously depicted mechanism (see Scheme[2] of Figure 3.79). This is defined as a second-order chemical reaction. The rate law of the ethylenic unsaturation conversion into oxirane rings (Eq. 3.36) is depicted by Equation 3.37.



$$r_{EU} = -k_3[PA][EU]. \quad (3.37)$$

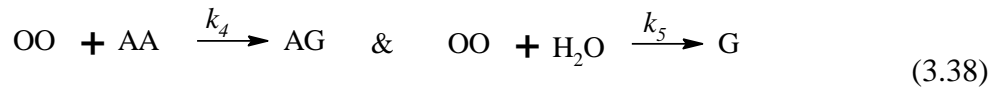
where,

[EU] – ethylenic unsaturation content, [mol/(100g oil)]

k_3 – epoxidation reaction rate constant, [100g oil/(s·mol)]

Side reactions of oxirane rings

In the ideal case, the released AA would be reabsorbed to the catalyst and the whole process would be repeated until all H_2O_2 is consumed, or all EU double bonds have been transferred into oxirane rings. However, the ion exchange resin catalyst also promotes undesired cleavage of the oxirane rings. Oxirane ring opening with AA and water have been chosen (see Figure 3.75) as the two possible side reactions (see Eq. 3.38) and their reaction rate is described by Equation 3.38 and 3.39 respectively.



$$r_{AG} = k_4[OO][AA] \quad (3.39) \quad \& \quad r_G = k_5[OO][H_2O]. \quad (3.40)$$

where,

[OO] – oxirane oxygen content, [mol/(100g oil)]

[H_2O] – water content, [mol/(100g oil)]

k_4 – reaction rate constant of the oxirane opening with acetic acid, [100g oil/(s·mol)]

k_5 – reaction rate constant of the oxirane ring opening with water, [100g oil/(s·mol)]

Summary of TOFA epoxidation model

The mechanism for the *in-situ* epoxidation of TOFA in the presence of heterogeneous phase catalyst can be summarized by several reactions that occur simultaneously. The developed model describes the surface reaction of PA formation (I) which is considered as a heterogeneous reaction and the reaction's order is considered to be 1 [36]. The desired TOFA epoxidation reaction (II) and the two undesired side reactions of oxirane ring opening (III and IV) are considered pseudo homogeneous second order reactions. The reaction equations are depicted in Figure 3.86. Furthermore, the model assumes that, in the catalytic reaction of PA formation only AA and PA are adsorbed to the catalyst active sides without dissociation, that the PA formation is irreversible and that the catalyst surface reaction is the rate-limiting step of the overall process.

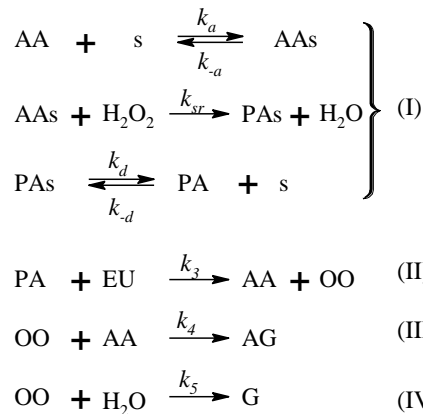


Figure 3.86. Reactions occurring during TOFA epoxidation with ion exchange resin catalyst.

The change of concentration of the different individual reagents during the TOFA epoxidation process is dependent on more than one of the reactions depicted in Figure 3.86. Furthermore, the concentration of the different reagents is not constant during the synthesis. Therefore, the rate law for the concentration change of the seven chosen reagents during the TOFA epoxidation is a system of non-linear differential equations, which is depicted in Equation 3.41. The depicted model describes the complete process of TOFA epoxidation and its solution predicts the concentration change of the reagents over synthesis time. To solve Equation 3.41 the kinetic rate and equilibrium constants have to be found beforehand.

$$\begin{aligned}
 \frac{d[H_2O_2]}{dt} &= -\frac{k_{sr}C_tW_{cat}K_{AA}[AA][H_2O_2]}{1+K_{AA}[AA]+K_{PA}[PA]}, \\
 \frac{d[AA]}{dt} &= -\frac{k_{sr}C_tW_{cat}K_{AA}[AA][H_2O_2]}{1+K_{AA}[AA]+K_{PA}[PA]} + k_3[PA][EU] - k_4[OO][AA]; \\
 \frac{d[PA]}{dt} &= \frac{k_{sr}C_tW_{cat}K_{AA}[AA][H_2O_2]}{1+K_{AA}[AA]+K_{PA}[PA]} - k_3[PA][EU]; \\
 \frac{d[EU]}{dt} &= -k_3[PA][EU]; \\
 \frac{d[OO]}{dt} &= k_3[PA][EU] - k_4[OO][AA] - k_5[OO][H_2O]; \\
 \frac{d[H_2O]}{dt} &= \frac{k_{sr}C_tW_{cat}K_{AA}[AA][H_2O_2]}{1+K_{AA}[AA]+K_{PA}[PA]} - k_5[OO] \cdot [H_2O]; \\
 \frac{d[AG+G]}{dt} &= k_4[OO][AA] + k_5[OO][H_2O];
 \end{aligned} \tag{3.41}$$

The Equation 3.41 parameters were estimated using experimental data of the decrease of ethylenic unsaturation ($[EU_{ex}]$, mol/100g oil) and the experimentally determined increase of the oxirane oxygen content ($[OO_{ex}]$, mol/100g oil) data by using constrained nonlinear multivariable algorithm. Some initial estimates of the selected thermodynamically constants ($k_{sr}C_t$; k_3 ; k_4 ; k_5 ; K_{PA} ; K_{AA}) were selected based on previous studies [36,250,251]. Then the TOFA epoxidation model was numerically solved using the fourth-order Runge-Kutta method. The nonlinear differential equation was solved using “ode45” function of MatLab R2019a software. Afterwards, an objective function of the least-squares was targeted to fit numerically calculated reagent concentrations to the experimental data. The “fmincon” function of MatLab R2019a software was used to vary the rate constants according to the Levenberg-Marquardt algorithm. Obtained rate constants of the complete TOFA epoxidation process are depicted in Table 3.19.

Table 3.19

Kinetic rate constants of complete TOFA epoxidation process using ion exchange heterogeneous phase resin catalyst

Rate constants		Unit	Values
$k_{sr}C_t$	surface reaction rate constant multiplied by the catalyst active site content	mol/(s·g(cat))	1.08
k_3	epoxidation reaction rate constant	100 g oil per s·mol	1.50
k_4	the rate constant of the oxirane opening with acetic acid	100 g oil per s·mol	0.99
k_5	the rate constant of the oxirane ring opening with water	100 g oil per s·mol	0.032
K_{PA}	peracetic acid adsorption equilibrium constant	mol/L	49.99
K_{AA}	acetic acid adsorption equilibrium constant	mol/L	0.80

A set of seven synthesis experiments were used to fit the TOFA epoxidation model. TOFA were epoxidised in following conditions: synthesis temperature – 60 °C; mixing rate 600 rpm.; ethylenic unsaturation and hydrogen peroxide molar ratios were 1.0/1.5 and Amberlite IR 120H content of 20 wt.% of oil mass was tested. The initial content of the acetic acid was varied to obtain different kinetic curves for model fitting. Following ethylenic unsaturation and acetic acid molar ratios were used: 1.00/0.15; 1.00/0.25; 1.00/0.35; 1.00/0.50; 1.00/0.65; 1.00/0.75. The different acetic acid content should not change the rate constants of the model. Obtained kinetic curves of the REU change over synthesis time are depicted in Figure 3.88 together with the fitted model which is depicted as the straight lines. Similarly, the RCO kinetic curves of TOFA epoxidation are depicted in Figure 3.87.

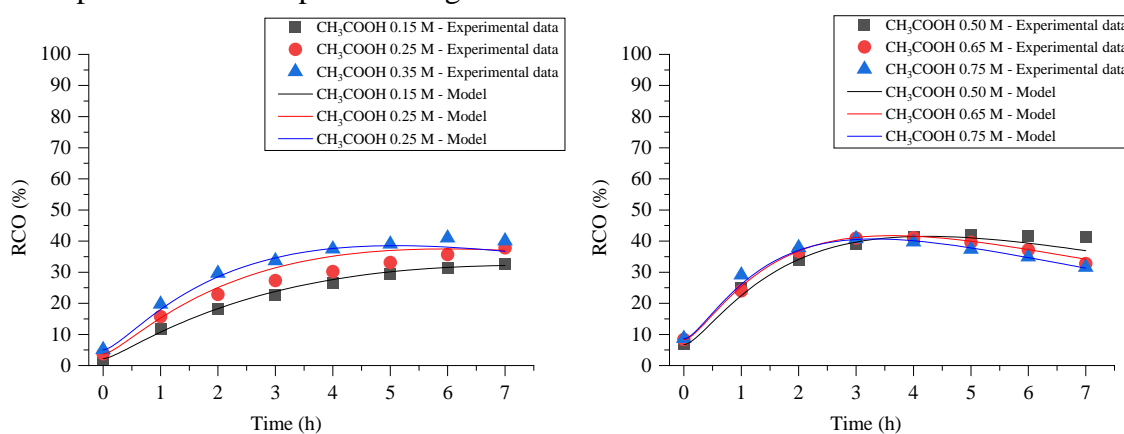


Figure 3.87. RCO kinetic curves of TOFA epoxidation.

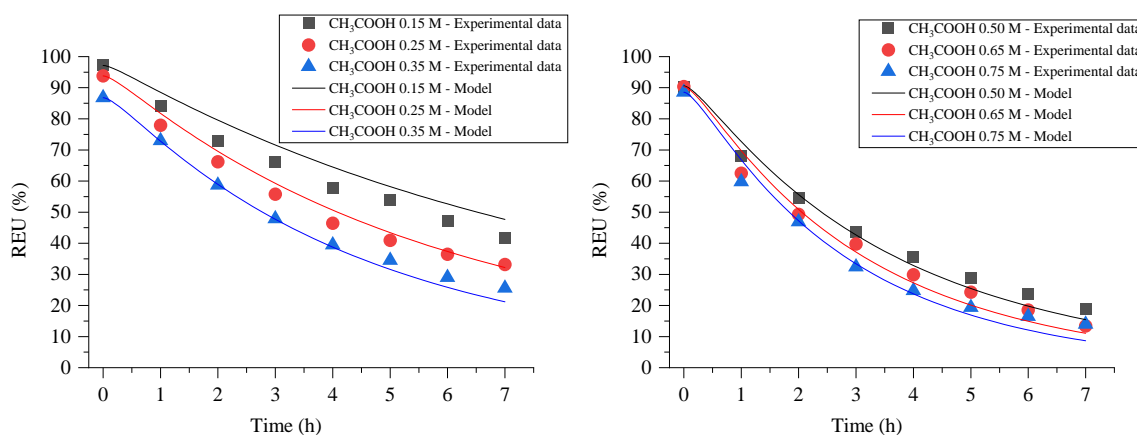


Figure 3.88. REU kinetic curves of TOFA epoxidation.

Developed TOFA epoxidation model (see. Eq. 3.41) fits relatively well to experimental data of RCO and REU. The experimental and calculated values of RCO and REU are depicted in Figure 3.89. The coefficient of determination was 0.9794 and 0.9879 in case of RCO and REU respectively. Moreover, the reaction rate parameters depicted in Table 3.19. are similar to previous studies [36,250,251]. Thus it can be concluded that the developed TOFA epoxidation model could be used for synthesis parameter optimization to find highest RCO values. The biggest drawback of the developed TOFA epoxidation model is that it is not possible to guarantee that this was the only minimum of the least square target function. Furthermore, other

minimums of the optimization function could be found outside boundaries that were set in this work. Not to mention that the TOFA epoxidation model has plenty of assumptions that do not represent the real process. Experimental data depicts that epoxy rings are opened almost at the same rate as they are introduced. Which suggests that TOFA does penetrate catalyst gel-like structure where epoxy ring opening is catalysed. Previously this type model was applied to different natural oil epoxidation, like jatropha, soybean and hemp oils [36,250,251] which have triglyceride structure and about three times larger average molecular mass than fatty acids of TOFA. Thus it is reasonable to assume that diffusion of TOFA into the catalyst could be expected. TOFA themselves are carboxylic acids that could potentially be transferred into peroxy-carboxylic acids, which could epoxidase themselves. This would further complicate the kinetic process of TOFA epoxidation. Unfortunately, these aspects were not studied in the frame of this Doctoral Thesis.

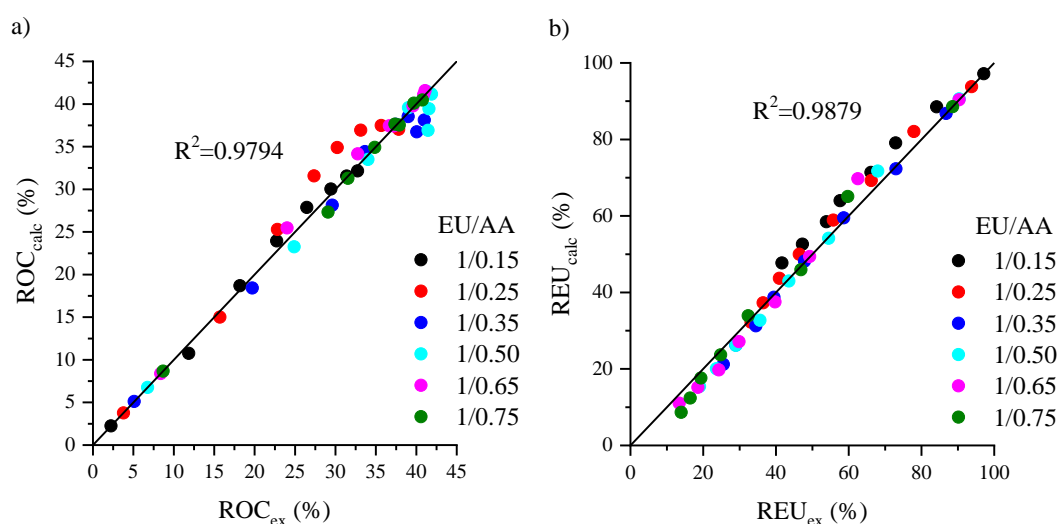


Figure 3.89. Experimental versus predicted values of RCO and REU.

Regeneration of TOFA Epoxidation Catalyst

Heterogeneous phase catalyst synthesis is only feasible if the catalyst can be recovered and reused after synthesis. Several syntheses of TOFA epoxidation were carried out where Amberlite IR 120H catalyst was regenerated after each use and reused for the next synthesis. TOFA epoxidation with following reaction conditions was selected for the catalyst regeneration trials: synthesis temperature – 60 °C; mixing rate 600 rpm.; ethylenic unsaturation, acetic acid and hydrogen peroxide molar ratios were 1.0/0.5/1.5 and Amberlite IR 120H content of 20 wt.% of oil mass were tested. After each synthesis catalyst was rinsed with ethyl acetate and warm water and then used as usual. Up to 10 repeated syntheses were carried out to determine the stability of the catalyst. The RCO and REU at the 7th hour of synthesis after 10 subsequent catalyst reuses are depicted in Figure 3.90. There was a slight drop in RCO where 41.5 % were achieved with fresh catalyst and 35.3 % were achieved after 10th reuse of the catalyst. Similarly, REU dropped from 79.0 % to 59.0 %. It is not clear if the catalyst degrades during synthesis or its purification with acetic acetate is at fault. ETOFA is highly viscous substance and its separation from catalyst beads was not easy. Nevertheless, heterogeneous phase catalysts are

not designed for the batch reactor use. A continuous flow reactor would be more effective. In such process catalyst rinsing would not be needed because the reaction would not be stopped. Further studies of catalyst stability during TOFA epoxidation are needed. They were out of the scope of the present Doctoral Thesis. This would be studied in a frame of technology upscaling project to reach industrial technology readiness level of TRL 7-9.

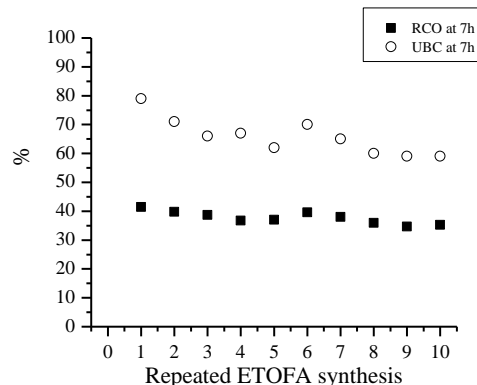


Figure 3.90. RCO and UBC at the 7th hour of TOFA epoxidation synthesis after repeated use of Amberlite IR 120H ion-exchange catalyst.

Chemo-Enzymatic TOFA Epoxidation

In the frame of this Doctoral Thesis, one more novel TOFA epoxidation catalyst was studied. The main disadvantage of the chemical epoxidation method described in previous paragraphs is the acid-catalyzed side-reaction occurrence with oxirane rings, which leads to the formation of by-products [42]. Furthermore, the use of additional acid as an oxygen carrier means that it has to be separated from the reaction media after oil epoxidation, which, along with the use of hazardous chemicals, is not desired from the viewpoint of Green chemistry. The use of performic or peracetic acids in the epoxidation process could lead to the thermal runaway of the reaction which is highly undesired for an industrial upscale and due to safety concerns [43–45]. In recent times, various chemo-enzymatic catalysis reactions have been studied as a more sustainable approach to conventional chemical catalysis methods. One of the fields is double-bond epoxidation using a Lipase enzyme to catalyse the peroxy-carboxylic acid *in-situ* formation. The method is considered to be milder and more selective than traditional acid catalysed *in-situ* epoxidation methods [42,46]. The most effective lipase for unsaturated bond epoxidation has shown to be Candida Antarctica Lipase B (Novozym® 435 – immobilized Lipase enzyme on acrylic resin beads) [47]. The main advantages of the enzyme catalysed epoxidation are relatively low epoxidation temperatures (30–50 °C) in comparison to chemical epoxidation at 60-100 °C, high selectivity and epoxidation conversion rate (exceeding 90 %), and reusability of the enzyme [48,49]. Furthermore, it has been reported that Lipase can catalyse a formation of fatty acid peracids, such as perstearic [50,51] and peroleic [52], which allows avoiding the use of formic and acetic acid in the epoxidation process. Although the possibility to use Lipase as a catalyst for epoxidation has been known for a while, there have been relatively few investigations into the synthesis of polyols for further use in polyurethane production.

In this study, second-generation feedstock – TOFA – was used as a renewable and bio-based feedstock. TOFA are produced from crude tall oil which is a side stream of wood biomass Kraft pulping processes. Crude tall oil distillation products, including TOFA, are a high-quality raw material used for various applications, from biofuels to chemical production. Distilled TOFAs are a mixture of unsaturated free fatty acids which mainly consists of oleic, linoleic, and linolenic acids [252].

The objective of this work was to develop solvent-free chemo-enzymatic epoxidation of free TOFA. The proposed process allows for bypassing the production of intermediate products, such as TOFA methyl esters, as well as simplification of the process by avoiding the use of formic and acetic acid in the epoxidation process. Obtained ETOFA can be used for the development of a variety of products, among which are high functionality bio-based polyols that are especially useful as crosslinking reagents for the development of rigid PU foam thermal insulation.

The epoxidation of TOFA was carried out by *in-situ* generated peroxy-carboxylic acids from fatty acids contained in the chemical composition of the distilled tall oil. The idealized reaction mechanism is proposed by Sun et al. [51] (see Figure 3.91a). The relatively high acidity of the TOFA mixture can lead to undesired side reactions of the fatty acid carboxyl groups with newly introduced oxirane rings resulting in dimerization and oligomerization products. The idealized TOFA epoxidation and side reaction scheme is depicted in Figure 3.91b.

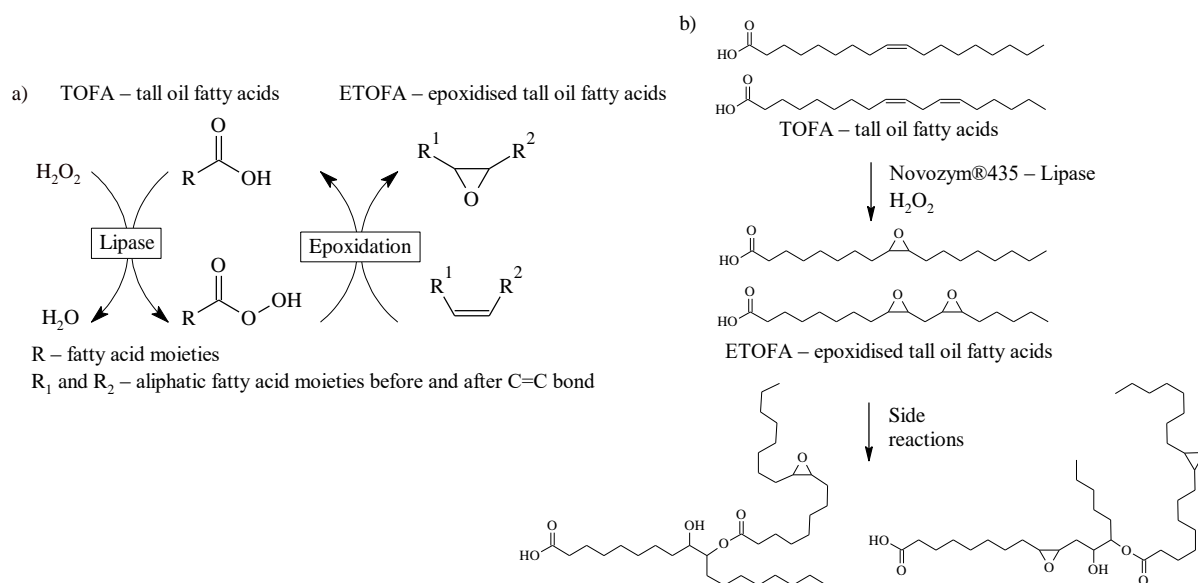


Figure 3.91. a) The idealized chemo-enzymatic epoxidation mechanism of aliphatic double bonds [51], b) TOFA epoxidation and the side reaction for oxirane ring opening.

Double Bond and Hydrogen Peroxide Molar Ratio Influence on the TOFA Epoxidation

During the TOFA epoxidation process, the oxirane group content smoothly increased as the iodine value and double bond content in the system decreased. The kinetic curves of increase of relative conversion to oxirane and the decrease of relative ethylenic unsaturation at different molar ratios between double bonds and H₂O₂ are depicted in Figure 3.92. The use of an excess of H₂O₂ did not lead to increased yield of oxirane groups when molar ratios between C=C and H₂O₂ were changed from 1.0/1.0 to 1.0/1.2. Even contrarily, the final relative conversion to

oxirane dropped slightly from 52.2 % to 45.1 % (4.65 % and 4.02 % - respective OO_{ex}). The slight decrease of reactivity with an increase of H_2O_2 content in the system can be explained by the degradation of the enzyme catalyst in the presence of H_2O_2 [253]. The highest relative conversion to oxirane was achieved for 1.0/1.0 C=C/ H_2O_2 molar ratios. For the further investigations, a slight excess of H_2O_2 at a molar ratio, 1.0/1.1 was chosen as the relative conversion to oxirane of 50.5 % (4.49 % - OO_{ex}) at the 7th hour was similar to 1.0/1.0 molar ratio experiment. This was done to ensure that H_2O_2 is always present in the system as it tends to degrade with temperature. Furthermore, the final unsaturated bond conversion was slightly higher (72.3 %) for C=C/ H_2O_2 molar ratios of 1.0/1.1. Unsaturated bond conversion reached 67.4 % for C=C/ H_2O_2 molar ratios of 1.0/1.0. The FTIR spectra showing the introduction of the epoxy ring into TOFA structure and the decrease of the ethylenic unsaturation is depicted in Figure 3.96.

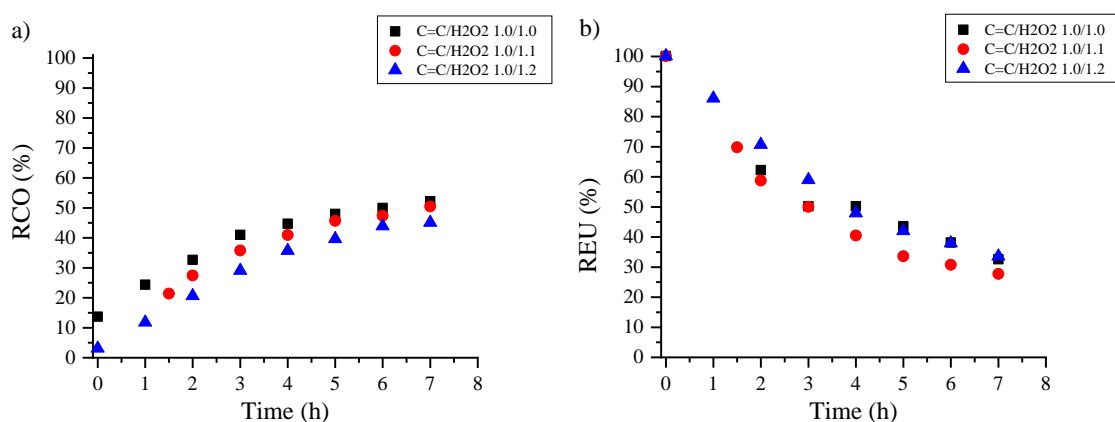


Figure 3.92. a) RCO b) REU at different double bond and H_2O_2 molar ratios ($T_{synth} = 40\text{ }^{\circ}C$; Novozym435 = 3.0 wt.%; $H_2O_2 = 20\text{ }%$).

Effect of the Novozym® 435 Content on the TOFA Epoxidation Process

The increase of enzyme load from 1.5 wt.% (w/w, relative to the weight of TOFA) to 4.5 wt.% resulted in a significant increase of relative conversion to oxirane from 35.9 to 57.8 % (3.12 % to 5.14 % of OO_{ex}), respectively, at the 7th hour of synthesis. The selectivity of the epoxidation was 74.4% after 7 hours at 4.5 % Novozym® 435 load. The kinetic curves of TOFA epoxidation with different Novozym® 435 loads are depicted in Figure 3.93. The final relative conversion to oxirane was similar, 50.5 % and 57.8 % (4.49 % to 5.14 % of OO_{ex}) for 3.0 wt.% and 4.5 wt.% catalyst load, respectively. Further increase in catalyst load was not carried out. Research carried out by Sun et al. [51] showed that catalyst loads above 3.0 wt.% would lead only to minimal increases of conversion to oxirane. Although catalyst, by definition, is required in small amounts, the cost of the catalyst is potentially one of the most significant costs for the overall process. It is desired that the catalyst amount is kept as small as possible to ensure potential industrial feasibility of the proposed technology.

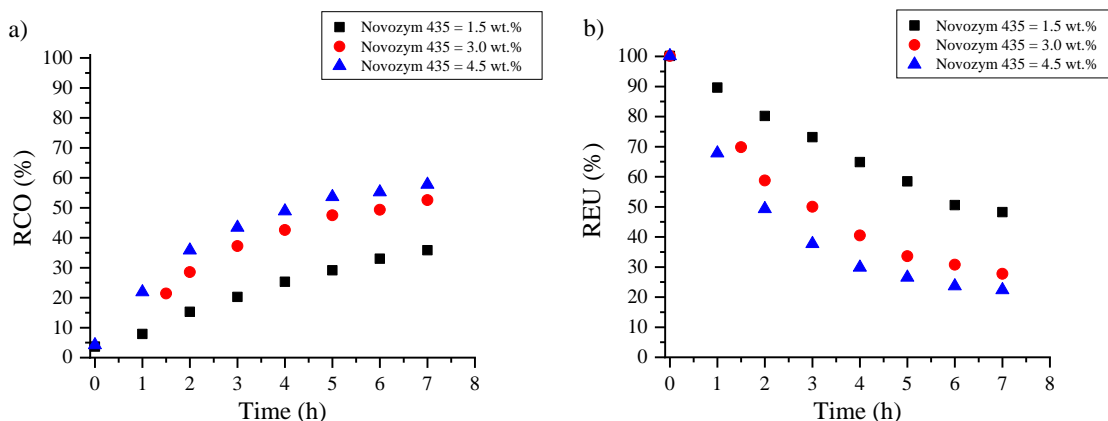


Figure 3.93. a) ROC b) REU at different Novozym® 435 catalyst content ($T_{\text{synth}} = 40\text{ }^{\circ}\text{C}$; $\text{H}_2\text{O}_2 = 20\%$; $\text{C}=\text{C}/\text{H}_2\text{O}_2 = 1.0/1.1$).

It was found that mechanical stirring is not ideal for the chemo-enzymatic epoxidation process. One of the experiments was flawed; the experiment with 1.5 w% Novozym® 435 load showed a suspiciously high conversion rate to oxirane. This effect was due to the mechanical degradation of the catalyst beads, which resulted in the increase of specific surface of the immobilized catalyst. It was identified that catalyst beads had reduced in size after the blade of the mechanical stirrer was located too close to the bottom of the flask. This is highly undesirable, as it removes the possibility of the catalyst regeneration, thus increasing the final price of the ETOFA and polyols produced from it. A possible solution is the design of a continuous flow reactor or ultrasonic reagent mixing [42,254]. The kinetic curves of the experiment with 1.5 w% of damaged Novozyme® 435 catalyst are depicted in Figure 3.94.

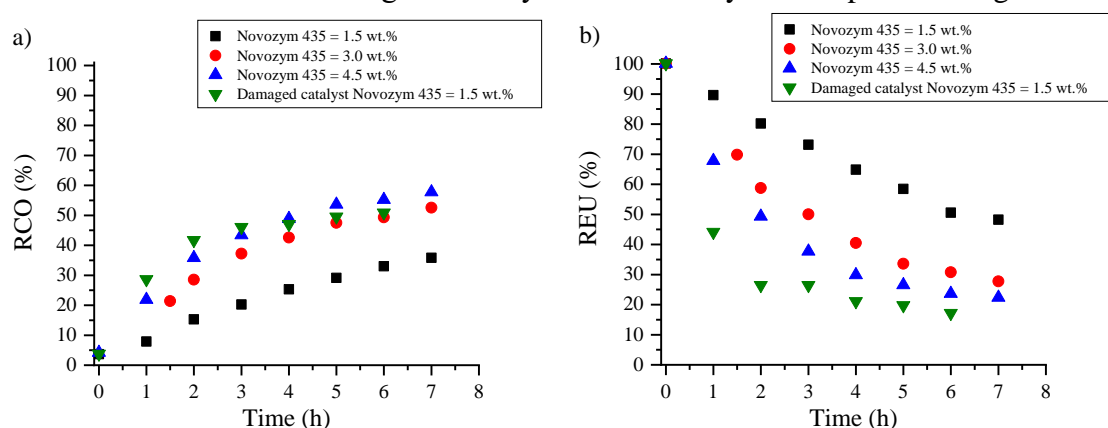


Figure 3.94. a) ROC b) REU at different Novozym® 435 catalyst content ($T_{\text{synth}} = 40\text{ }^{\circ}\text{C}$; $\text{H}_2\text{O}_2 = 20\%$; $\text{C}=\text{C}/\text{H}_2\text{O}_2 = 1.0/1.1$).

Effect of the Hydrogen Peroxide Concentration on the TOFA Epoxidation Process

In order to determine the effect of the H_2O_2 concentration on the TOFA epoxidation process, a set of experiments changing H_2O_2 concentration from 15 % to 35 % in TOFA epoxidation process was carried out (Figure 3.95), as a higher concentration of H_2O_2 could lead to degradation of the immobilized Lipase catalyst. The yield of double bond conversion to oxirane increased with the increase of H_2O_2 concentration. The highest conversion to oxirane of 67.4 % (6.00 % OO_{ex}) was obtained at 30 % H_2O_2 after 7 hours. Epoxidation using 35 % H_2O_2 was not

successful due to oxirane ring cleavage. Despite reaching the highest unsaturated bond conversion of 80.4 % at the 6th hour of synthesis the oxirane group yield stopped increasing after 5 hours and started slowly decreasing. Loss of catalyst activity at higher concentrations of H₂O₂ was not observed because the conversion rate of double bonds did not decrease at higher H₂O₂ concentrations. Nevertheless, the stability of the Novozym® 435 activity should be further studied after several synthesis cycles to ensure potential industrial feasibility of the proposed technology. The change of acid value during epoxidation process gives information about oxirane group opening with carboxylic groups of TOFA (Figure 3.95c). With the increased concentration of H₂O₂, the decrease in acid value is slightly higher. For 15 % and 35 %, H₂O₂ acid value was 135 and 130 mg KOH/g, respectively, after 7 hours. The oxirane ring opening is later confirmed by FTIR spectra (Figure 3.96d).

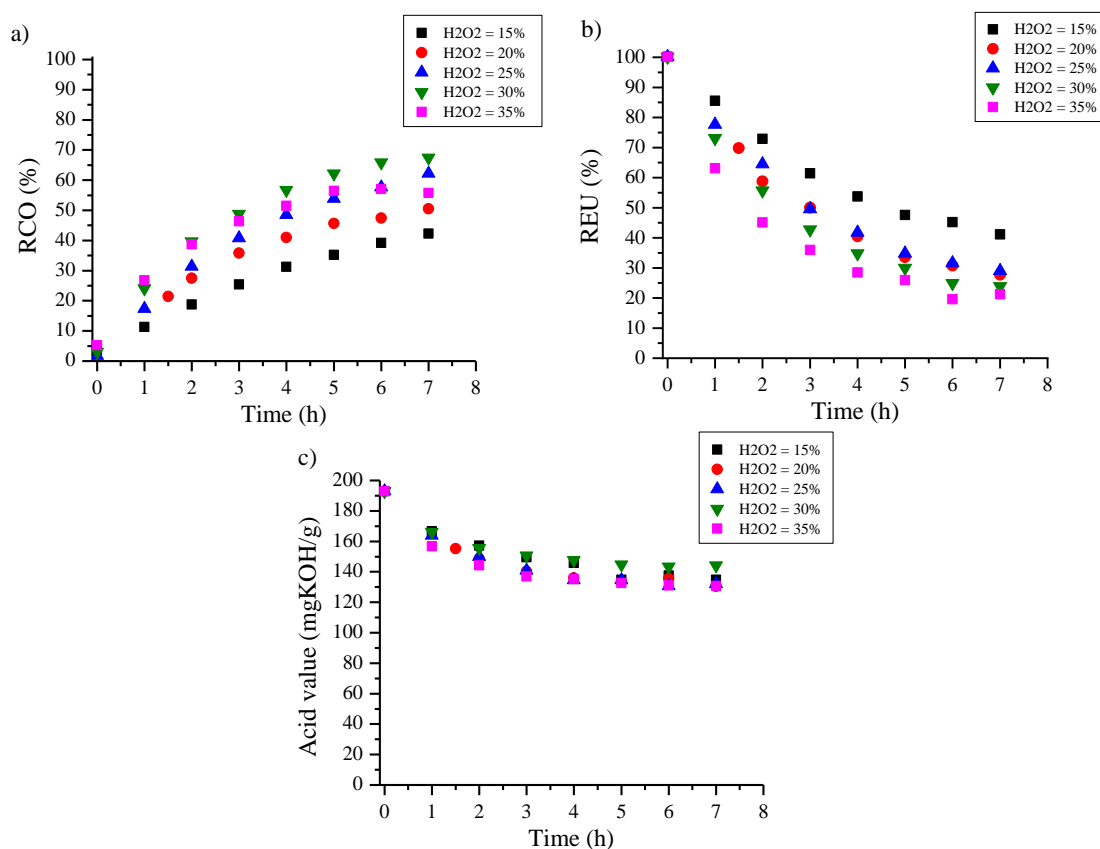


Figure 3.95. a) ROC b) REU at different H₂O₂ concentration, c) change of the acid value of the TOFA during the epoxidation process (T_{synth}=40°C; Novozym435 = 3.0 wt.%; C=C/H₂O₂= 1.0/1.1).

FTIR Analysis During TOFA Epoxidation Process

The chemical structure of TOFA transformation into ETOFA during epoxidation process was studied using FTIR spectroscopy. An example of the overall FTIR spectra in the absorption range is depicted in Figure 3.96a. The =C-H double bond stretching peak at 3008 cm⁻¹ of unsaturated TOFA decreased while the C-O-C oxirane ring stretching vibration peak at 823 cm⁻¹ increased during the epoxidation process. For TOFA, a typical absorption peaks of -CH₂- symmetric stretching at ~ 2930 cm⁻¹ and asymmetric stretching at ~ 2860 cm⁻¹ were identified. A close-up of the gradual decrease of the =C-H double bond stretching peak at

3008 cm^{-1} during the epoxidation process is depicted in Figure 3.96b. The peak almost disappears, which correlates with the measured decrease of the ethylenic unsaturation described previously (Figure 3.95b – $\text{H}_2\text{O}_2 = 20\%$). The gradual increase of the C-O-C oxirane ring stretching vibration peak at 823 cm^{-1} shows the introduction of the oxirane rings into TOFA structure (Figure 3.96c) and correlates with the data of relative conversion to oxirane.

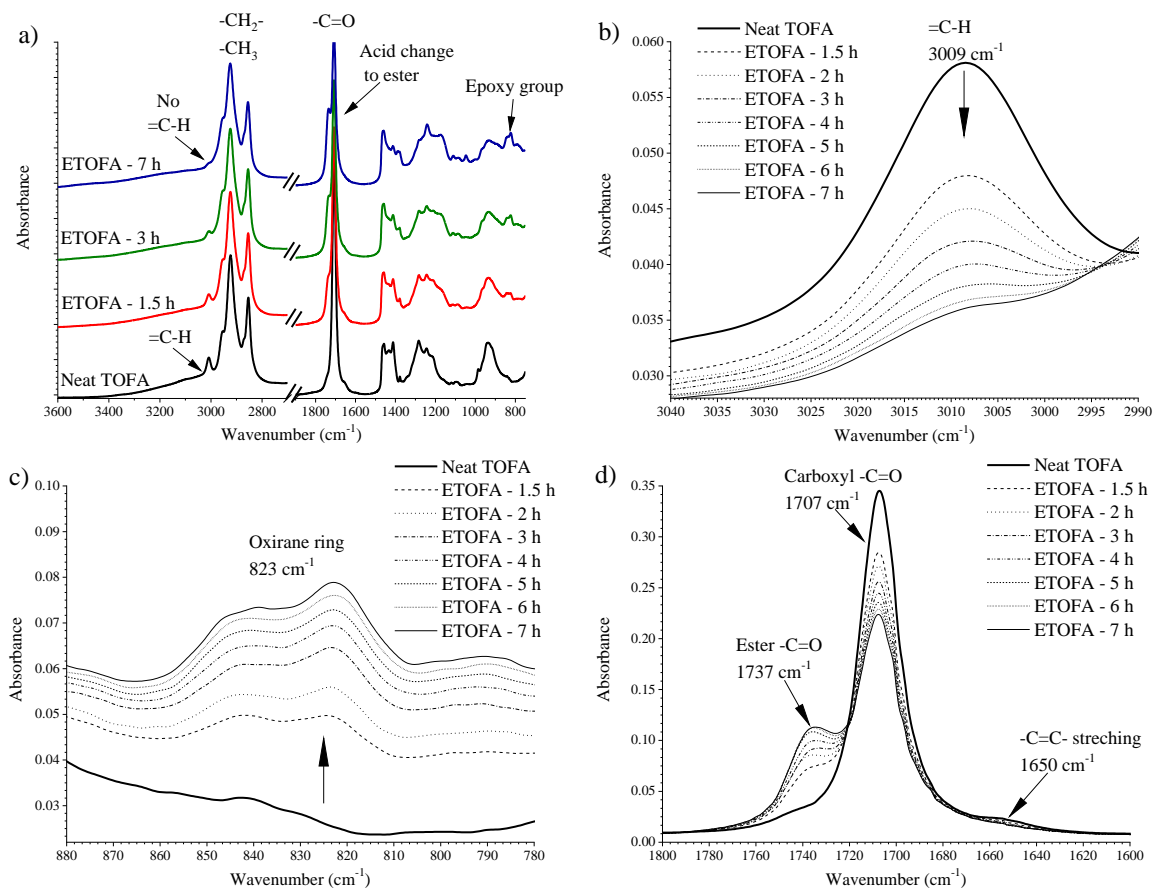


Figure 3.96. FTIR spectra during TOFA epoxidation for C=C/ H_2O_2 1.0/1.1; Novozym®435 = 3.0 wt.%; H_2O_2 = 20 % a) overall FTIR spectra b) change of EU absorption, c) change of OO vibration, d) change of -C=O stretching.

A full conversion of the double bonds into oxirane rings was not achieved. After 7 hours, about 71.0-76.1 % of double bonds were transformed. Synthesis time of 7 hours was considered optimal because at this point only minimal further conversion of the double bonds was achieved. A TOFA epoxidation for C=C/ H_2O_2 1.0/1.1; Novozym®435 = 3.0 wt.%; H_2O_2 w% = 25 % was continued for 11 hours. A marginal increase of relative conversion to oxirane from 62.2 % and 63.8 % was achieved between the 7th and 11th hours of the synthesis. The ethylenic unsaturation continued a gradual decrease and unsaturated bond conversion between the 7th and 11th hours was 71.0 % to 78.5 %. The results for 11-hour epoxidation can be found in the Annex 11 [255]. A minimal increase of oxirane groups is explained by the side reactions of the oxirane ring cleavage [233]. The carboxylic groups of the TOFA open the oxirane ring resulting in an ester bond formation and dimerization of the ETOFA. This is confirmed by the change of the -C=O bond stretching peak at ~ 1730 cm^{-1} . A single peak of the carboxyl group at 1707 cm^{-1} of neat TOFA develops a shoulder peak of an ester carboxyl group

at 1737 cm^{-1} during the epoxidation process. This phenomenon is depicted in Figure 3.96d, and it was noticeable for all studied TOFA epoxidation synthesis. The process of ETOFA dimerization is undesired because its products will increase the viscosity of the ETOFA and developed polyols. Nevertheless, this is a compromise between initial derivatization of the TOFA into TOFA methyl ester for the epoxidation process and a more streamlined process with fewer intermediate steps.

The epoxy ring opening with carboxylic groups of the TOFA is further confirmed by the change in the acid value of the TOFA (Figure 3.95c). Different H_2O_2 concentrations had a minimal influence on the epoxy ring opening with TOFA. The epoxy ring opening cleavage is considered a first-order chemical reaction [34]. The proposed side reaction is slow enough to be acceptable and obtained ETOFA could be used for further polyol development. Nevertheless, the kinetics of the oxirane ring opening with TOFA must be further studied.

TOFA epoxidation at 35 % H_2O_2 concentration showed increased cleavage of oxirane rings. Although the relative unsaturated bond conversion reached 80.4% after 7 hours, the relative conversion to oxirane remained low at 57.0 % (5.07 % - OO_{ex}). Oxirane ring cleavage results in an introduction of OH groups into the chemical structure of the ETOFA. Introduced -OH group stretching absorption is visible at $3700\text{-}3200\text{ cm}^{-1}$ band in FTIR spectra (Figure 3.97). The higher rate of oxirane ring cleavage can be explained by the localized overheating of the synthesis when higher concentration H_2O_2 is added to the mixture.

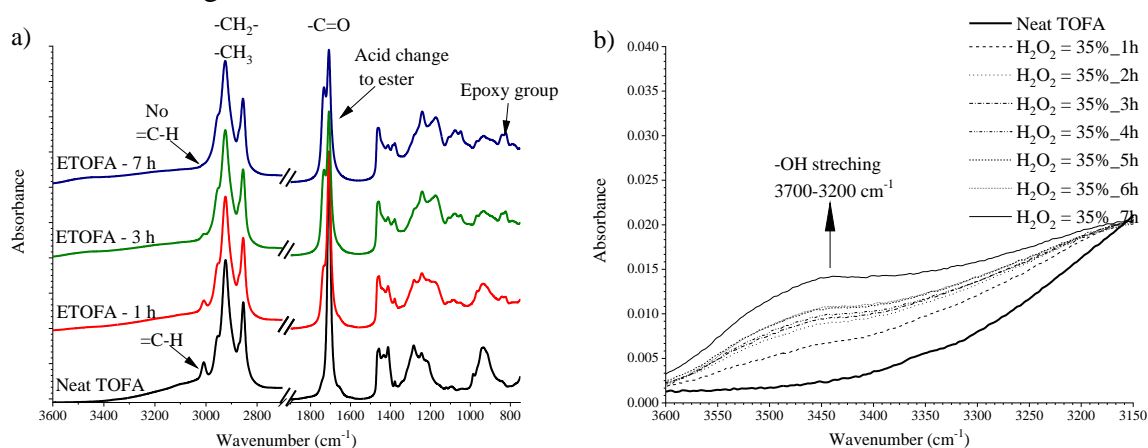


Figure 3.97. FTIR spectra during TOFA epoxidation for $\text{C}=\text{C}/\text{H}_2\text{O}_2$ 1.0/1.1; Novozym®435 = 3.0 wt.%; H_2O_2 = 35% a) change of OO vibration b) change of -OH stretching.

Overview of Chemo-Enzymatic TOFA Epoxidation

The summary of the chemo-enzymatic epoxidation of TOFA by the in-situ generation of peroxy-carboxylic fatty acids is presented in Table 3.20. An excess of H_2O_2 should be used at molar ratios $\text{C}=\text{C}/\text{H}_2\text{O}_2$ of 1.0/1.1 to achieve the higher conversion of the double bonds. Novozym®435 catalyst load of 3.0 wt.% is enough to successfully epoxidase the double bonds of TOFA. Although higher catalyst content led to higher conversion to oxirane, the increase was not significant enough to justify the use of a higher load of Novozym®435 catalyst. It is important to keep the catalyst load as low as possible because it is the most expensive

component of the synthesis. An H_2O_2 with a concentration between 20-30 % should be used, as a higher concentration H_2O_2 could lead to catalyst degradation. In the frame of this study, the catalyst regeneration was not studied. The successful regeneration of the Lipase-based catalyst is the main requirement for the development of up scalable technology. The developed process allowed to obtain ETOFA with an epoxide oxygen content of 4.49-6.00 % which is sufficient to consider this material for polyol synthesis, as well as other epoxide-based products. Obtained results are in good agreement with previous studies with a similar concept. Solvent-free chemo-enzymatic epoxidation of oleic acid showed the relative conversion to oxirane above 60 % for epoxidation at 40 °C and H_2O_2 concentration of 30 % by [256]. Obtained results are also similar to oleic acid self-epoxidation reported by Yadav and Manjula Devi where the similar oxygen content of 4.0-5.0 % has been achieved. It must be mentioned that this epoxidation was carried out in toluene solution and reported oxirane oxygen contents were achieved for much higher H_2O_2 excess than reported here (1.6-3.7 H_2O_2 per 1.0 mole of oleic acid) [257]. Lastly, the presented results can be compared to the solvent-free epoxidation of linoleic acid reported by Orellana-Coca et al. where about 70 % of relative conversion to oxirane was achieved. When a much higher excess of H_2O_2 was used (3.5-8 mmol H_2O_2 per mmol of linoleic acid) conversion to oxirane was close to 90-100 % after 8 hours [258]. This indicates that our epoxidation method could be improved by using higher excess of H_2O_2 which will be carried out in future studies.

Table 3.20

Summary of the highest achieved relative conversion to oxirane and respective relative conversion of double bonds at respective synthesis time

	Synthesis time, h	OO _{ex} ,%	RCO,%	Iodine value, g I ₂ /100g	UBC, %	S, %
C=C/ H_2O_2 molar ratio	TOFA epoxidation Novozym®435 = 3.0 w%; H_2O_2 w% = 20%					
1.0/1.0	7	4.65	52.2	50.6	67.4	77.5
1.0/1.1	7	4.49	50.5	43.0	72.3	69.9
1.0/1.2	7	4.02	45.1	52.1	66.4	68.0
Novozym®435 wt.%	TOFA epoxidation C=C/ H_2O_2 = 1.0/1.1; H_2O_2 w% = 20%					
1.5 %	7	3.19	35.9	74.8	51.8	69.3
3.0 %	7	4.49	50.5	43.0	72.3	69.9
4.5 %	7	5.14	57.8	34.7	77.6	74.4
H_2O_2 wt.%	TOFA epoxidation C=C/ H_2O_2 = 1.0/1.1; Novozym®435 = 3.0 wt.%					
15 %	7	3.76	42.2	63.8	58.8	58.8
20 %	7	4.49	50.5	43.0	72.3	69.9
25 %	7	5.54	62.2	45.0	71.0	87.7
30 %	7	6.00	67.4	37.0	76.1	76.1
35 %	6	5.07	57.0	30.4	80.4	70.9

Conclusions of TOFA Epoxidation

- The epoxidation of free fatty acids of TOFA can be done in a similar way to RO epoxidation.
- A method of TOFA epoxidation that agrees with the principles of Green chemistry was developed.

- Developed process avoided the synthesis of intermediate products like TOFA methyl esters and no solvent was necessary for the TOFA epoxidation.
- Ion exchange Amberlite IR 120H resin catalyst delivered superior RCO than conventional H₂SO₄ catalyst (RCO of 45.5 and 19.7 % respectively).
- Amberlite IR 120H promoted undesired side reactions of oxirane ring opening at a much smaller degree than conventional H₂SO₄ catalyst.
- Eley-Rideal surface reaction mechanism model was successfully applied to the TOFA epoxidation process.
- The developed model showed that unfortunately, Amberlite IR 120H ion exchange resin promotes the undesired oxirane ring cleavage reactions almost to the same level as the epoxidation of the double bonds.
- Novel Lipase based heterogeneous phase catalyst was applied for TOFA epoxidation and the highest RCO = 67.4 % was achieved at relatively low catalyst content of 3.0 wt.%.
- Novozym®435 Lipase based catalyst was selected as the most promising catalyst as it allowed to develop simple, solvent-free, without use of intermediate products, high efficiency (RCO>67 %), low energy requirement (T_{stynt} = 40 °C), sustainable TOFA epoxidation process.

REFERENCES

- [1] M. Szycher, *Szycher's Handbook of Polyurethanes*, First Edit, CRC Press, 1999.
- [2] M. Ionescu, *Chemistry and technology of polyols for polyurethanes.*, 2007. doi:10.1002/pi.2159.
- [3] Grand View Research Inc. Report ID: 5741307, *Polyols Market Size, Share & Trends Analysis Report By Product, By Application And Segment Forecasts, 2018 - 2025*, 2018.
- [4] S. Fu, Y. Qin, L. Qiao, X. Wang, F. Wang, Propylene oxide end-capping route to primary hydroxyl group dominated CO₂-polyol, *Polymer (Guildf)*. 153 (2018) 167–172. doi:10.1016/j.polymer.2018.08.014.
- [5] S. Liu, X. Wang, Polymers from carbon dioxide: Polycarbonates, polyurethanes, *Curr. Opin. Green Sustain. Chem.* 3 (2017) 61–66. doi:10.1016/j.cogsc.2016.08.003.
- [6] R.R. Romero, A Study of the Reaction Kinetics of Polyisocyanurate Foam Formulations using Real-time FTIR, *J. Cell. Plast.* 41 (2005) 339–359. doi:10.1177/0021955X05055115.
- [7] M.F. Sonnenschein, *Polyurethanes: Science, Technology, Markets, and Trends*, 2015. doi:10.1002/9781118901274.
- [8] G. Vairo, L. Bertucelli, L. Pellacani, P. Golini, L. Luca, Enhanced Polyisocyanurate Foams for Metal Faced Panels, in: *Polyurethanes, Polyurethanes Tech. Conf. 2010*, Curran Associates, 2010: pp. 360–369. doi:978-1-617-82706-8.
- [9] U. Stirna, U. Cabulis, I. Beverte, Water-blown polyisocyanurate foams from vegetable oil polyols, *J. Cell. Plast.* 44 (2008) 139–160. doi:10.1177/0021955X07084705.
- [10] M. Kurańska, A. Prociak, U. Cabulis, M. Kirpluks, J. Ryszkowska, M. Auguścik, Innovative porous polyurethane-polyisocyanurate foams based on rapeseed oil and modified with expandable graphite, *Ind. Crops Prod.* 95 (2017) 316–323. doi:10.1016/j.indcrop.2016.10.039.
- [11] E. Delebecq, J. Pascault, B. Boutevin, F. Ganachaud, On the Versatility of Urethane / Urea Bonds: Reversibility , Blocked, *Chem. Rev.* 113 (2013) 80–118. doi:10.1021/cr300195n.
- [12] R.W.K. Jr., Isocyanates, in: *Encycl. Toxicol.* (Third Ed., 2014. doi:http://dx.doi.org/10.1016/B978-0-12-386454-3.00865-4.
- [13] R.A. Sheldon, Green and sustainable manufacture of chemicals from biomass: state of the art, *Green Chem.* 16 (2014) 950–963. doi:10.1039/C3GC41935E.
- [14] J. Philp, The bioeconomy, the challenge of the century for policy makers, *N. Biotechnol.* 40 (2018) 11–19. doi:10.1016/j.nbt.2017.04.004.
- [15] C. Zhang, T.F. Garrison, S.A. Madbouly, M.R. Kessler, Recent advances in vegetable oil-based polymers and their composites, *Prog. Polym. Sci.* 71 (2017) 91–143. doi:10.1016/j.progpolymsci.2016.12.009.
- [16] L. Montero De Espinosa, M.A.R.R. Meier, Plant oils: The perfect renewable resource for polymer science?!, *Eur. Polym. J.* 47 (2011) 837–852. doi:10.1016/j.eurpolymj.2010.11.020.
- [17] U. Biermann, U. Bornscheuer, M.A.R. Meier, J.O. Metzger, H.J. Schäfer, Oils and Fats as Renewable Raw Materials in Chemistry, *Angew. Chemie Int. Ed.* 50 (2011) 3854–3871. doi:10.1002/anie.201002767.
- [18] Z.S. Petrovic, Polyurethanes from Vegetable Oils, *Polym. Rev.* 48 (2008) 109–155. doi:10.1080/15583720701834224.
- [19] J.G. Drobny, *Handbook of Thermoplastic Elastomers*, 2014. doi:10.1016/B978-0-323-22136-8.00006-5.
- [20] A.S. Carlsson, Plant oils as feedstock alternatives to petroleum – A short survey of potential oil crop platforms, *Biochimie.* 91 (2009) 665–670.

- doi:10.1016/j.biochi.2009.03.021.
- [21] Foreign Agricultural Service, United States Department of Agriculture Report: Oilseeds: World Markets and Trade, 2019.
- [22] R. Krautgartner, L. Lefebvre, L. Rehder, M. Boshnakova, M. Dobrescu, B. Flach, J. Wilson, D. Faniadis, M. Guerrero, B. Williams, EU-28 Oilseeds and Products Annual 2016, 2016.
- [23] R. Krautgartner, G. Golya, L.E. Rehder, M. Boshnakova, M. Dobrescu, B. Flach, J. Wilson, D. Faniadis, M. Guerrero, S. Bolla, EU-28 Oilseeds and Products Annual 2019, 2019.
- [24] G. Lligadas, J.C. Ronda, M. Galià, V. Cádiz, Oleic and Undecylenic Acids as Renewable Feedstocks in the Synthesis of Polyols and Polyurethanes, *Polymers (Basel)*. 2 (2010) 440–453. doi:10.3390/polym2040440.
- [25] U. Stirna, A. Fridrihsone, M. Misane, D. Vilsone, L. State, W. Chemistry, Rapeseed Oil as Renewable Resource for Polyol Synthesis, *Environ. Clim. Technol.* 6 (2011) 85–90. doi:10.2478/v10145-011-0012-4.
- [26] M. Kirpluks, U. Cābulis, M. Kurańska, A. Prociak, Three Different Approaches for Polyol Synthesis from Rapeseed Oil, *Key Eng. Mater.* 559 (2013) 69–74. doi:10.4028/www.scientific.net/KEM.559.69.
- [27] M. Desroches, M. Escouvois, R. Auvergne, S. Caillol, B. Boutevin, From Vegetable Oils to Polyurethanes: Synthetic Routes to Polyols and Main Industrial Products, *Polym. Rev.* 52 (2012) 38–79. doi:10.1080/15583724.2011.640443.
- [28] S.G. Tan, W.S. Chow, Biobased epoxidized vegetable oils and its greener epoxy blends: A review, *Polym. - Plast. Technol. Eng.* 49 (2010) 1581–1590. doi:10.1080/03602559.2010.512338.
- [29] T. Saurabh, M. Patnaik, S.L. Bhagt, V.C. Renge, Epoxidation of vegetable oils:, A Rev. *Int. J. Adv. Eng. Technol.* 2 (2011) 491–501.
- [30] M.M. Patel, B.P. Patel, N.K. Patel, Utilization of soya-based polyol for High solid PU-coating application, *Int. J. Plast. Technol.* 16 (2012) 67–79. doi:10.1007/s12588-012-9030-8.
- [31] R. Mungroo, N.C. Pradhan, V. V. Goud, A.K. Dalai, Epoxidation of canola oil with hydrogen peroxide catalyzed by acidic ion exchange resin, *J. Am. Oil Chem. Soc.* 85 (2008) 887–896. doi:10.1007/s11746-008-1277-z.
- [32] T.S. Omonov, E. Kharraz, J.M. Curtis, The epoxidation of canola oil and its derivatives, *RSC Adv.* 6 (2016) 92874–92886. doi:10.1039/c6ra17732h.
- [33] M. Kirpluks, D. Kalnbunde, Z. Walterova, U. Cabulis, Rapeseed Oil as Feedstock for High Functionality Polyol Synthesis, (2017) 1–23.
- [34] S. Sinadinovic-Fiser, M. Jankovi, O. Borota, Epoxidation of castor oil with peracetic acid formed in situ in the presence of an ion exchange resin, *Chem. Eng. Process. Process Intensif.* 62 (2012) 106–113. doi:10.1016/j.cep.2012.08.005.
- [35] A.S.A. Hazmi, M.M. Aung, L.C. Abdullah, M.Z. Salleh, M.H. Mahmood, Producing Jatropha oil-based polyol via epoxidation and ring opening, *Ind. Crops Prod.* 50 (2013) 563–567. doi:10.1016/j.indcrop.2013.08.003.
- [36] V. V. Goud, A. V. Patwardhan, S. Dinda, N.C. Pradhan, Kinetics of epoxidation of jatropha oil with peroxyacetic and peroxyformic acid catalysed by acidic ion exchange resin, *Chem. Eng. Sci.* 62 (2007) 4065–4076. doi:http://dx.doi.org/10.1016/j.ces.2007.04.038.
- [37] P.D. Meshram, R.G. Puri, H. V Patil, Epoxidation of Wild Safflower (*Carthamus oxyacantha*) Oil with Peroxy acid in presence of strongly Acidic Cation Exchange Resin IR- 122 as Catalyst, *Int. J. ChemTech Res.* 3 (2011) 1152–1163.
- [38] V. V. Goud, A. V. Patwardhan, N.C. Pradhan, Studies on the epoxidation of mahua oil

- (*Madhumica indica*) by hydrogen peroxide, *Bioresour. Technol.* 97 (2006) 1365–1371. doi:10.1016/j.biortech.2005.07.004.
- [39] S. Dinda, A. V. Patwardhan, V. V. Goud, N.C. Pradhan, Epoxidation of cottonseed oil by aqueous hydrogen peroxide catalysed by liquid inorganic acids, *Bioresour. Technol.* 99 (2008) 3737–3744. doi:10.1016/j.biortech.2007.07.015.
- [40] V. V. Goud, A. V. Patwardhan, S. Dinda, N.C. Pradhan, Epoxidation of karanja (*Pongamia glabra*) oil catalysed by acidic ion exchange resin, *Eur. J. Lipid Sci. Technol.* 109 (2007) 575–584. doi:10.1002/ejlt.200600298.
- [41] J.C. de Haro, I. Izarra, J.F. Rodríguez, Á. Pérez, M. Carmona, J.F. Rodríguez, Ángel Pérez, M. Carmona, J.F. Rodríguez, Á. Pérez, M. Carmona, Modelling the epoxidation reaction of grape seed oil by peracetic acid, *J. Clean. Prod.* 138 (2016) 70–76. doi:https://doi.org/10.1016/j.jclepro.2016.05.015.
- [42] A.E. V Hagström, U. Törnvall, M. Nordblad, R. Hatti-Kaul, J.M. Woodley, Chemo-enzymatic epoxidation-process options for improving biocatalytic productivity, *Biotechnol. Prog.* 27 (2011) 67–76. doi:10.1002/btpr.504.
- [43] H. Rakotondramaro, J. Wärnå, L. Estel, T. Salmi, S. Leveneur, Cooling and stirring failure for semi-batch reactor: Application to exothermic reactions in multiphase reactor, *J. Loss Prev. Process Ind.* 43 (2016) 147–157. doi:10.1016/j.jlp.2016.05.011.
- [44] J. V. de Quadros, R. Giudici, Epoxidation of soybean oil at maximum heat removal and single addition of all reactants, *Chem. Eng. Process. Process Intensif.* 100 (2016) 87–93. doi:10.1016/j.cep.2015.11.007.
- [45] V. Casson Moreno, V. Russo, R. Tesser, M. Di Serio, E. Salzano, Thermal risk in semi-batch reactors: The epoxidation of soybean oil, *Process Saf. Environ. Prot.* 109 (2017) 529–537. doi:10.1016/j.psep.2017.05.001.
- [46] X. Wang, Q. Tang, G.M. Popowicz, B. Yang, Y. Wang, A mechanistic study into the epoxidation of carboxylic acid and alkene in a mono, di-acylglycerol lipase, *Biochem. Biophys. Res. Commun.* 460 (2015) 392–396. doi:10.1016/j.bbrc.2015.03.044.
- [47] F. Björkling, H. Frykman, S.E. Godtfredsen, O. Kirk, Lipase catalyzed synthesis of peroxy-carboxylic acids and lipase mediated oxidations., *Tetrahedron.* 48 (1992) 4587–4592. doi:10.1016/S0040-4020(01)81232-1.
- [48] M. Rüschen, S. Warwel, Complete and partial epoxidation of plant oils by lipase-catalyzed perhydrolysis, *Ind. Crops Prod.* 9 (1999) 125–132. doi:10.1016/S0926-6690(98)00023-5.
- [49] R. de C.S. Schneider, L.R.S. Lara, T.B. Bitencourt, M. da G. Nascimento, M.R. dos S. Nunes, Chemo-enzymatic epoxidation of sunflower oil methyl esters, *J. Braz. Chem. Soc.* 20 (2009) 1473–1477. doi:10.1590/S0103-50532009000800013.
- [50] S. Sun, X. Ke, L. Cui, G. Yang, Y. Bi, F. Song, X. Xu, Enzymatic epoxidation of *Sapindus mukorossi* seed oil by perstearic acid optimized using response surface methodology, *Ind. Crops Prod.* 33 (2011) 676–682. doi:10.1016/j.indcrop.2011.01.002.
- [51] S. Sun, G. Yang, Y. Bi, H. Liang, Enzymatic epoxidation of corn oil by perstearic acid, *J. Am. Oil Chem. Soc.* 88 (2011) 1567–1571. doi:10.1007/s11746-011-1820-1.
- [52] T. Vlček, Z.S. Petrović, Optimization of the chemoenzymatic epoxidation of soybean oil, *J. Am. Oil Chem. Soc.* 83 (2006) 247–252. doi:10.1007/s11746-006-1200-4.
- [53] J.M.R. Da Silva, T.B. Bitencourt, M.A. Moreira, M. Da Graça Nascimento, Enzymatic epoxidation of β -caryophyllene using free or immobilized lipases or mycelia from the Amazon region, *J. Mol. Catal. B Enzym.* 95 (2013) 48–54. doi:10.1016/j.molcatb.2013.05.021.
- [54] H. Lu, S. Sun, Y. Bi, G. Yang, R. Ma, H. Yang, Enzymatic epoxidation of soybean oil methyl esters in the presence of free fatty acids, *Eur. J. Lipid Sci. Technol.* 112 (2010) 1101–1105. doi:10.1002/ejlt.201000041.

- [55] J.M.R. Da Silva, M.D.G. Nascimento, Chemoenzymatic epoxidation of citronellol catalyzed by lipases, *Process Biochem.* 47 (2012) 517–522. doi:10.1016/j.procbio.2011.12.019.
- [56] W.S.D. Silva, A.A.M. Lapis, P.A.Z. Suarez, B.A.D. Neto, Enzyme-mediated epoxidation of methyl oleate supported by imidazolium-based ionic liquids, *J. Mol. Catal. B Enzym.* 68 (2011) 98–103. doi:10.1016/j.molcatb.2010.09.019.
- [57] X. Zhang, X. Wan, H. Cao, R. Dewil, L. Deng, F. Wang, T. Tan, K. Nie, Chemoenzymatic epoxidation of *Sapindus mukurossi* fatty acids catalyzed with *Candida* sp. 99–125 lipase in a solvent-free system, *Ind. Crops Prod.* 98 (2017) 10–18. doi:10.1016/j.indcrop.2017.01.013.
- [58] N.E. Marcovich, M. Kurańska, A. Prociak, E. Malewska, K. Kulpa, Open cell semi-rigid polyurethane foams synthesized using palm oil-based bio-polyol, *Ind. Crops Prod.* 102 (2017) 88–96. doi:10.1016/j.indcrop.2017.03.025.
- [59] P. Rojek, A. Prociak, Effect of different rapeseed-oil-based polyols on mechanical properties of flexible polyurethane foams, *J. Appl. Polym. Sci.* 125 (2012) 2936–2945. doi:10.1002/app.36500.
- [60] M. Kurańska, A. Prociak, The influence of rapeseed oil-based polyols on the foaming process of rigid polyurethane foams, *Ind. Crops Prod.* 89 (2016) 182–187. doi:10.1016/j.indcrop.2016.05.016.
- [61] M. Zieleniewska, M.K. Leszczyński, M. Kurańska, A. Prociak, L. Szczepkowski, M. Krzyżowska, J. Ryszkowska, M. Krzyżowska, J. Ryszkowska, M. Krzyżowska, J. Ryszkowska, M. Krzyżowska, Preparation and characterisation of rigid polyurethane foams using a rapeseed oil-based polyol, *Ind. Crops Prod.* 74 (2015) 887–897. doi:10.1016/j.indcrop.2015.05.081.
- [62] U. Stirna, A. Fridrihsone-Girone, V. Yakushin, D. Vilsons, Processing and properties of spray-applied, 100% solids polyurethane coatings from rapeseed oil polyols, *J. Coatings Technol. Res.* 11 (2014) 409–420. doi:10.1007/s11998-013-9545-8.
- [63] C. Tu, Yuan, P. Kiatsimkul, G. Suppes, F.-H. Hsieh, Physical properties of water-blown rigid polyurethane foams from vegetable oil-based polyols, *J. Appl. Polym. Sci.* 105 (2007) 453–459. doi:10.1002/app.26060.
- [64] E. Sastre, J. Pe, C. Ma, Solid catalysts for the synthesis of fatty esters of glycerol, polyglycerols and sorbitol from renewable resources, 27 (2004).
- [65] M. a. Mosiewicki, M.I. Aranguren, A. Mosiewicki, Mirna, I. Aranguren, Mirta, M. a. Mosiewicki, M.I. Aranguren, A short review on novel biocomposites based on plant oil precursors, *Eur. Polym. J.* 49 (2013) 1243–1256. doi:10.1016/j.eurpolymj.2013.02.034.
- [66] S. Dutta, N. Karak, Effect of the NCO / OH ratio on the properties of *Mesua Ferrea* L. seed oil-modified polyurethane resins, 56 (2006) 49–56. doi:10.1002/pi.1914.
- [67] R.R. Nayak, G. Ray, B. Guru, S. Lenka, Polymer-Plastics Technology and Engineering Comparative Studies of Interpenetrating Polymer Networks Derived from Soybean Oil – Based Polyurethane and Cardanol m-Aminophenol Dye Comparative Studies of Interpenetrating, (2007) 37–41. doi:10.1081/PPT-120027475.
- [68] R. Tanaka, S. Hirose, H. Hatakeyama, Preparation and characterization of polyurethane foams using a palm oil-based polyol, *Bioresour. Technol.* 99 (2008) 3810–3816. doi:10.1016/j.biortech.2007.07.007.
- [69] A. Hejna, M. Kirpluks, P. Kosmela, U. Cabulis, J. Haponiuk, Ł. Piszczyk, The influence of crude glycerol and castor oil-based polyol on the structure and performance of rigid polyurethane-polyisocyanurate foams, *Ind. Crops Prod.* 95 (2017) 113–125. doi:10.1016/j.indcrop.2016.10.023.
- [70] S. Chuayjuljit, A. Maungchareon, O. Saravari, Preparation and Properties of Palm Oil-Based Rigid Polyurethane Nanocomposite Foams, *J. Reinf. Plast. Compos.* 29 (2010)

- 218–225. doi:10.1177/0731684408096949.
- [71] M. Kurańska, A. Prociak, M. Kirpluks, U. Cabulis, Polyurethane–polyisocyanurate foams modified with hydroxyl derivatives of rapeseed oil, *Ind. Crops Prod.* 74 (2015) 849–857. doi:10.1016/j.indcrop.2015.06.006.
- [72] A. Prociak, U. Cabulis, M. Kuranska, M. Kirpluks, Cellular structure and physical-mechanical properties of rigid polyurethane-polyisocyanurate foams prepared from rapeseed oil-based polyols, *Przem. Chem.* 99 (2014) 2253–2258. doi:dx.medra.org/10.12916/przemchem.2014.2253.
- [73] M. Kurańska, P. Aleksander, K. Mikelis, C. Ugis, Porous polyurethane composites based on bio-components, *Compos. Sci. Technol.* 75 (2013) 70–76. doi:10.1016/j.compscitech.2012.11.014.
- [74] A. Fridrihsone, U. Stirna, B. Lazdina, M. Misane, D. Vilsone, Characterization of polyurethane networks based on rapeseed oil derived polyol, *Eur. Polym. J.* 49 (2013) 1204–1214. doi:10.14314/polimery.2014.333.
- [75] A.B. Chaudhari, A. Anand, S.D. Rajput, R.D. Kulkarni, V.V. Gite, Synthesis, characterization and application of *Azadirachta indica* juss (neem oil) fatty amides (AIJFA) based polyurethanes coatings: A renewable novel approach, *Prog. Org. Coatings.* 76 (2013) 1779–1785. doi:10.1016/j.porgcoat.2013.05.016.
- [76] T.H. Khoe, F. Otey, E.N. Frankel, J.C. Cowan, Polyurethane foams from hydroxymethylated fatty diethanolamides, *J. Am. Oil Chem. Soc.* 50 (1973) 331–333. doi:10.1007/BF02641367.
- [77] G. Lligadas, J.C. Ronda, M. Galià, V. Cádiz, Renewable polymeric materials from vegetable oils: a perspective, *Mater. Today.* 16 (2013) 337–343. doi:10.1016/j.mattod.2013.08.016.
- [78] F. Seniha Güner, Y. Yağcı, a. Tuncer Erciyes, Polymers from triglyceride oils, *Prog. Polym. Sci.* 31 (2006) 633–670. doi:10.1016/j.progpolymsci.2006.07.001.
- [79] M. Poletto, H.L. Ornaghi Júnior, A.J. Zattera, Native cellulose: Structure, characterization and thermal properties, *Materials (Basel).* 7 (2014) 6105–6119. doi:10.3390/ma7096105.
- [80] N. Mahmood, Z. Yuan, J. Schmidt, C. Xu, C. Charles, C. Xu, C. Charles, Depolymerization of lignins and their applications for the preparation of polyols and rigid polyurethane foams: A review, *Renew. Sustain. Energy Rev.* 60 (2016) 317–329. doi:10.1016/j.rser.2016.01.037.
- [81] C. Chio, M. Sain, W. Qin, Lignin utilization: A review of lignin depolymerization from various aspects, *Renew. Sustain. Energy Rev.* 107 (2019) 232–249. doi:10.1016/j.rser.2019.03.008.
- [82] P. Cinelli, I. Anguillesi, A. Lazzeri, Green synthesis of flexible polyurethane foams from liquefied lignin, *Eur. Polym. J.* 49 (2013) 1174–1184. doi:10.1016/j.eurpolymj.2013.04.005.
- [83] C.A. Cateto, M.F. Barreiro, A.E. Rodrigues, M.N. Belgacem, Optimization study of lignin oxypropylation in view of the preparation of polyurethane rigid foams, *Ind. Eng. Chem. Res.* 48 (2009) 2583–2589. doi:10.1021/ie801251r.
- [84] E. a. B.D.A.B. da B. Silva, M. Zabkova, J.D.D. Araújo, C. a. A. Cateto, M.F.F. Barreiro, M.N.N. Belgacem, a. E.E. Rodrigues, An integrated process to produce vanillin and lignin-based polyurethanes from Kraft lignin, *Chem. Eng. Res. Des.* 87 (2009) 1276–1292. doi:10.1016/j.cherd.2009.05.008.
- [85] C.A. Cateto, M.F. Barreiro, A.E. Rodrigues, M.N. Belgacem, Kinetic study of the formation of lignin-based polyurethanes in bulk, *React. Funct. Polym.* 71 (2011) 863–869. doi:10.1016/j.reactfunctpolym.2011.05.007.
- [86] S. Gómez-Fernández, L. Ugarte, T. Calvo-Correas, C. Peña-Rodríguez, M.A. Corcuera,

- A. Eceiza, Properties of flexible polyurethane foams containing isocyanate functionalized kraft lignin, *Ind. Crops Prod.* 100 (2017) 51–64. doi:10.1016/j.indcrop.2017.02.005.
- [87] X. Luo, Y. Xiao, Q. Wu, J. Zeng, Development of high-performance biodegradable rigid polyurethane foams using all bioresource-based polyols: Lignin and soy oil-derived polyols, *Int. J. Biol. Macromol.* 115 (2018) 786–791. doi:10.1016/j.ijbiomac.2018.04.126.
- [88] A.N. Hayati, D.A.C. Evans, B. Laycock, D.J. Martin, P.K. Annamalai, A simple methodology for improving the performance and sustainability of rigid polyurethane foam by incorporating industrial lignin, *Ind. Crops Prod.* 117 (2018) 149–158. doi:10.1016/j.indcrop.2018.03.006.
- [89] A. Arshanitsa, L. Krumina, G. Telysheva, T. Dizhbite, Exploring the application potential of incompletely soluble organosolv lignin as a macromonomer for polyurethane synthesis, *Ind. Crops Prod.* 92 (2016) 1–12. doi:10.1016/j.indcrop.2016.07.050.
- [90] C. Zhang, H. Wu, M.R.K. Kessler, High bio-content polyurethane composites with urethane modified lignin as filler, *Polymer (Guildf)*. 69 (2015) 52–57. doi:10.1016/j.polymer.2015.05.046.
- [91] X. Zhang, Y. Kim, T.L. Eberhardt, R. Shmulsky, Lab-scale structural insulated panels with lignin-incorporated rigid polyurethane foams as core, *Ind. Crops Prod.* 132 (2019) 292–300. doi:10.1016/j.indcrop.2019.02.035.
- [92] L. Upton, Project focus: Creating high purity lignin and affordable platform chemicals from wood-based sugars., *Bio-Based World Ltd T/A Bio Mark. Insights.* (2019).
- [93] D. Peters, V. Stojcheva, Crude tall oil low ILUC risk assessment; Comparing global supply and demand, 2017. <http://www.upmbiofuels.com/whats-new/other-publications/Documents/Publications/ecofys-crude-tall-oil-low-iluc-risk-assessment-report.pdf>.
- [94] T. Aro, P. Fatehi, Tall oil production from black liquor: Challenges and opportunities, *Sep. Purif. Technol.* 175 (2017) 469–480. doi:10.1016/j.seppur.2016.10.027.
- [95] A. Keskin, A. Yaşar, M. Gürü, D. Altiparmak, Usage of methyl ester of tall oil fatty acids and resinic acids as alternative diesel fuel, *Energy Convers. Manag.* 51 (2010) 2863–2868. doi:10.1016/j.enconman.2010.06.025.
- [96] S.A. Cashman, K.M. Moran, A.G. Gaglione, Greenhouse Gas and Energy Life Cycle Assessment of Pine Chemicals Derived from Crude Tall Oil and Their Substitutes, *J. Ind. Ecol.* 20 (2016) 1108–1121. doi:10.1111/jiec.12370.
- [97] V. Zeltins, V. Yakushin, U. Cabulis, M. Kirpluks, Crude tall oil as raw material for rigid polyurethane foams with low water absorption, 2017. doi:10.4028/www.scientific.net/SSP.267.17.
- [98] K. Mizera, M. Kirpluks, U. Cabulis, M. Leszczyńska, M. Półka, J. Ryszkowska, Characterisation of urethane elastomers containing tall oil based polyols, *Ind. Crops Prod.* 113 (2018) 98–110. doi:10.1016/j.indcrop.2018.01.019.
- [99] V. Yakushin, I. Sevastyanova, D. Vilsonė, M. Kirpluks, Effect of intumescent flame retardants on the properties of polyurethanes based on tall oil fatty acids esters, *Medziagotyra.* 21 (2015) 225–226. doi:10.5755/j01.ms.21.2.5784.
- [100] V. Yakushin, U. Stirna, I. Sevastyanova, D. Vilsonė, V. Zeltins, M. Kirpluks, Properties of polyurethanes based on tall oil fatty acids ester with different types of flame retardants, 2013. doi:10.4028/www.scientific.net/KEM.559.115.
- [101] K. Pietrzak, M. Kirpluks, U. Cabulis, J. Ryszkowska, Effect of the addition of tall oil-based polyols on the thermal and mechanical properties of urethane elastomers, *Polym. Degrad. Stab.* 108 (2014) 201–211. doi:10.1016/j.polymdegradstab.2014.03.038.
- [102] A. Kairyte, M. Kirpluks, A. Ivdre, U. Cabulis, S. Vaitkus, I. Pundienė, Cleaner

- production of polyurethane foam: Replacement of conventional raw materials, assessment of fire resistance and environmental impact, *J. Clean. Prod.* 183 (2018) 760–771. doi:10.1016/j.jclepro.2018.02.164.
- [103] U. Cabulis, M. Kirpluks, U. Stirna, M.J.J. Lopez, M.C.D.C.D.C. Vargas-Garcia, F. Suarez-Estrella, J. Moreno, M. Del Carmen Vargas-Garcia, F. Suárez-Estrella, J. Moreno, M.C.D.C.D.C. Vargas-Garcia, F. Suarez-Estrella, J. Moreno, M. Del Carmen Vargas-Garcia, F. Suárez-Estrella, J. Moreno, Rigid polyurethane foams obtained from tall oil and filled with natural fibers: Application as a support for immobilization of lignin-degrading microorganisms, *J. Cell. Plast.* 48 (2012) 500–515. doi:10.1177/0021955X12443142.
- [104] U. Törnvall, P. Börjesson, L.M. Tufvesson, R. Hatti-Kaul, ORIGINAL RESEARCH: Biocatalytic production of fatty epoxides from rapeseed & tall oil derivatives: Process & environmental evaluation, *Ind. Biotechnol.* 5 (2009) 184–192. doi:10.1089/ind.2009.3.184.
- [105] B. Hedman, P. Piispanen, E. Alami, T. Norin, Synthesis and Characterization of Surfactants via Epoxidation of Tall Oil Fatty Acid, *J. Surfactants Deterg.* 6 (2003) 47–53.
- [106] F. Balo, Feasibility Study of “Green” Insulation Materials Including Tall Oil: Environmental, Economical and Thermal Properties, *Energy Build.* 86 (2014) 161–175. doi:10.1016/j.enbuild.2014.09.027.
- [107] S. Tan, T. Abraham, D. Ference, C.W. Macosko, Rigid polyurethane foams from a soybean oil-based Polyol, *Polymer (Guildf).* 52 (2011) 2840–2846. doi:10.1016/j.polymer.2011.04.040.
- [108] L. Ugarte, A. Saralegi, R. Fernández, L. Martín, M.A. Corcuera, A. Eceiza, Flexible polyurethane foams based on 100% renewably sourced polyols, *Ind. Crops Prod.* 62 (2014) 545–551. doi:10.1016/j.indcrop.2014.09.028.
- [109] E. Ferri, D. Talentino, Bio-resins from cashew nutshell oil, *Reinf. Plast.* 55 (2011) 29–31. doi:10.1016/S0034-3617(11)70074-1.
- [110] M. Acar, S. Çoban, B. Hazer, Novel Water Soluble Soya Oil Polymer from Oxidized Soya Oil Polymer and Diethanol Amine, *J. Macromol. Sci. Part A.* 50 (2013) 287–296. doi:10.1080/10601325.2013.755443.
- [111] E. Rusen, A. Mocanu, F. Rizea, A. Diacon, I. Calinescu, L. Mititeanu, D. Dumitrescu, A.-M. Popa, Post-consumer PET Bottles Recycling, *Mater. Plast.* 50 (2013) 201–207.
- [112] I. Vitkauskienė, R. Makuška, Glycolysis of industrial poly(ethylene terephthalate) waste directed to bis(hydroxyethylene) terephthalate and aromatic polyester polyols, *Chemija.* 19 (2008) 29–34.
- [113] M.R. Patel, J. V. Patel, V.K. Sinha, Polymeric precursors from PET waste and their application in polyurethane coatings, *Polym. Degrad. Stab.* 90 (2005) 111–115. doi:10.1016/j.polymdegradstab.2005.02.017.
- [114] X. Luo, Y. Li, Synthesis and Characterization of Polyols and Polyurethane Foams from PET Waste and Crude Glycerol, *J. Polym. Environ.* 22 (2014) 318–328. doi:10.1007/s10924-014-0649-8.
- [115] P.M. Spasojevic, V. V. Panic, J. V. Dzunuzovic, A.D. Marinkovic, A.J.J. Woortman, K. Loos, I.G. Popovic, High performance alkyd resins synthesized from postconsumer PET bottles, *RSC Adv.* 5 (2015) 62273–62283. doi:10.1039/c5ra11777a.
- [116] M. Kathalewar, N. Dhopatkar, B. Pacharane, A. Sabnis, P. Raut, V. Bhave, Chemical recycling of PET using neopentyl glycol: Reaction kinetics and preparation of polyurethane coatings, *Prog. Org. Coatings.* 76 (2013) 147–156. doi:10.1016/j.porgcoat.2012.08.023.
- [117] H. Beneš, J. Slabá, Z. Walterová, D. Rais, Recycling of waste poly(ethylene

- terephthalate) with castor oil using microwave heating, *Polym. Degrad. Stab.* 98 (2013) 2232–2243. doi:10.1016/j.polymdegradstab.2013.08.019.
- [118] A. Paberza, A. Fridrihsone-Girone, A. Abolins, U. Cabulis, Polyols from recycled poly(ethylene terephthalate) flakes and rapeseed oil for polyurethane foams, *Polimery/Polymers.* 60 (2015) 572–578. doi:10.14314/polimery.2015.572.
- [119] S. Gaidukovs, G. Gaidukova, A. Ivdre, U. Cabulis, Viscoelastic and Thermal Properties of Polyurethane Foams Obtained from Renewable and Recyclable Components, *J. Renew. Mater.* (2018). doi:10.7569/jrm.2018.634112.
- [120] A. Ivdre, A. Fridrihsone-Girone, A. Abolins, U. Cabulis, Effect of different concentration of rapeseed oil and recycled poly (ethylene terephthalate) in polyols for rigid polyurethane foams, *J. Cell. Plast.* 54 (2018) 161–177. doi:10.1177/0021955X16670585.
- [121] A. Ivdre, G.D. Soto, U. Cabulis, Polyols Based on Poly(ethylene terephthalate) and Tall Oil: Perspectives for Synthesis and Production of Rigid Polyurethane Foams, *J. Renew. Mater.* 4 (2016) 285–293. doi:10.7569/jrm.2016.634122.
- [122] L. Zhang, M. Zhang, Y. Zhou, L. Hu, The study of mechanical behavior and flame retardancy of castor oil phosphate-based rigid polyurethane foam composites containing expanded graphite and triethyl phosphate, *Polym. Degrad. Stab.* 98 (2013) 2784–2794. doi:10.1016/j.polymdegradstab.2013.10.015.
- [123] P. Acuña, Z. Li, M. Santiago-Calvo, F. Villafañe, M. ángel Rodríguez-Perez, D.Y. Wang, Influence of the characteristics of expandable graphite on the morphology, thermal properties, fire behaviour and compression performance of a rigid polyurethane foam, *Polymers (Basel).* 11 (2019). doi:10.3390/polym11010168.
- [124] G. Wypych, *Handbook of Fillers 4th Edition*, ChemTec Publishing, 2016. doi:10.1108/prt.1999.12928bae.002.
- [125] M. Modesti, A. Lorenzetti, F. Simioni, M. Checchin, Influence of different flame retardants on fire behaviour of modified PIR/PUR polymers, *Polym. Degrad. Stab.* 74 (2001) 475–479. doi:10.1016/S0141-3910(01)00171-9.
- [126] X. Chen, J. Li, M. Gao, Thermal Degradation and Flame Retardant Mechanism of the Rigid Polyurethane Foam Including Functionalized Graphene Oxide, *Polymers (Basel).* 11 (2019) 78. doi:10.3390/polym11010078.
- [127] K. Ashida, *Polyurethane and Related Foams*, CRC Press, 2006.
- [128] B. Schartel, T.R. Hull, Development of fire-retarded materials — Interpretation of cone calorimeter data, (2007) 327–354. doi:10.1002/fam.
- [129] B. Xiang-Cheng, T. Jian-Hua, L. Zhong-Ming, L. Zhong-Yuan, L. Ai, Dependence of flame-retardant properties on density of expandable graphite filled rigid polyurethane foam, *J. Appl. Polym. Sci.* 104 (2007) 3347–3355. doi:10.1002/app.25933.
- [130] X.-M. Hu, D.-M. Wang, Enhanced fire behavior of rigid polyurethane foam by intumescent flame retardants, *J. Appl. Polym. Sci.* 129 (2013) 238–246. doi:10.1002/app.38722.
- [131] L. Gao, G. Zheng, Y. Zhou, L. Hu, G. Feng, Y. Xie, Synergistic effect of expandable graphite, melamine polyphosphate and layered double hydroxide on improving the fire behavior of rosin-based rigid polyurethane foam, *Ind. Crops Prod.* 50 (2013) 638–647. doi:10.1016/j.indcrop.2013.07.050.
- [132] X. Hu, D. Wang, S. Wang, Synergistic effects of expandable graphite and dimethyl methyl phosphonate on the mechanical properties, fire behavior, and thermal stability of a polyisocyanurate–polyurethane foam, *Int. J. Min. Sci. Technol.* 23 (2013) 13–20. doi:10.1016/J.IJMST.2013.01.003.
- [133] B. Xiang-Cheng, T. Jian-Hua, L. Zhong-Ming, Flame retardancy of hollow glass microsphere/rigid polyurethane foams in the presence of expandable graphite, *J. Appl.*

- Polym. Sci. 109 (2008) 1935–1943. doi:10.1002/app.27786.
- [134] D.K. Chattopadhyay, D.C. Webster, Thermal stability and flame retardancy of polyurethanes, *Prog. Polym. Sci.* 34 (2009) 1068–1133. doi:10.1016/j.progpolymsci.2009.06.002.
- [135] M. Kurańska, U. Cabulis, M. Auguścik, A. Prociak, J. Ryszkowska, M. Kirpluks, Bio-Based Polyurethane-Polyisocyanurate Composites with an Intumescent Flame Retardant, *Polym. Degrad. Stab.* 127 (2016) 11–19. doi:10.1016/j.polymdegradstab.2016.02.005.
- [136] M. Thirumal, D. Khastgir, G.B. Nando, Y.P. Naik, N.K. Singha, Halogen-free flame retardant PUF: Effect of melamine compounds on mechanical, thermal and flame retardant properties, *Polym. Degrad. Stab.* 95 (2010) 1138–1145. doi:10.1016/j.polymdegradstab.2010.01.035.
- [137] M. Thirumal, K. Dipak, N.K. Singha, S.B. Manjunath, Y.P. Naik, Effect of expandable graphite on the properties of intumescent flame-retardant polyurethane foam, *J. Appl. Polym. Sci.* 110 (n.d.) 2586–2594. doi:10.1002/app.28763.
- [138] Z. Xiao-Guang, G. Lan-Lan, Z. Wei-Qin, T. Jian-Hua, Y. Ling, L. Zhong-Ming, Expandable graphite-methyl methacrylate-acrylic acid copolymer composite particles as a flame retardant of rigid polyurethane foam, *J. Appl. Polym. Sci.* 122 (n.d.) 932–941. doi:10.1002/app.34198.
- [139] D. Sophie, B.M. Le, B. Serge, D. René, V. Hervé, C. Giovanni, E. Berend, L. Chris, R. Toon, Expandable graphite: A fire retardant additive for polyurethane coatings, *Fire Mater.* 27 (n.d.) 103–117. doi:10.1002/fam.812.
- [140] M. Modesti, a. Lorenzetti, F. Simioni, G. Camino, Expandable graphite as an intumescent flame retardant in polyisocyanurate-polyurethane foams, *Polym. Degrad. Stab.* 77 (2002) 195–202. doi:10.1016/S0141-3910(02)00034-4.
- [141] L. Shi, Z.M. Li, M.B. Yang, B. Yin, Q.M. Zhou, C.R. Tian, J.H. Wang, Expandable graphite for halogen-free flame-retardant of high-density rigid polyurethane foams, *Polym. - Plast. Technol. Eng.* 44 (2005) 1323–1337. doi:10.1080/03602550500208145.
- [142] M. Kirpluks, U. Cabulis, V. Zeltins, L. Stiebra, A. Avots, Rigid polyurethane foam thermal insulation protected with mineral intumescent mat, *Autex Res. J.* 14 (2014) 259–269. doi:10.2478/aut-2014-0026.
- [143] D. Price, Y. Liu, T.R. Hull, G.J. Milnes, B.K. Kandola, A.R. Horrocks, Burning behaviour of foam/cotton fabric combinations in the cone calorimeter, *Polym. Degrad. Stab.* 77 (2002) 213–220. doi:10.1016/S0141-3910(02)00036-8.
- [144] T.M. Kotresh, R. Indushekar, M.S. Subbulakshmi, S.N. Vijayalakshmi, A.S.K. Prasad, K. Gaurav, Evaluation of foam/single and multiple layer Nomex fabric combinations in the cone calorimeter, *Polym. Test.* 24 (2005) 607–612. doi:10.1016/j.polymertesting.2005.03.001.
- [145] H.-J. Duan, H.-Q. Kang, W.-Q. Zhang, X. Ji, Z.-M. Li, J.-H. Tang, Core-shell structure design of pulverized expandable graphite particles and their application in flame-retardant rigid polyurethane foams, *Polym. Int.* 63 (2014) 72–83. doi:10.1002/pi.4489.
- [146] Z. Zheng, J. Yan, H. Sun, Z. Cheng, W. Li, H. Wang, X. Cui, Preparation and characterization of microencapsulated ammonium polyphosphate and its synergistic flame-retarded polyurethane rigid foams with expandable graphite, *Polym. Int.* 63 (2014) 84–92. doi:10.1002/pi.4477.
- [147] L. Ye, X.-Y. Meng, X. Ji, Z.-M. Li, J.-H. Tang, Synthesis and characterization of expandable graphite-poly(methyl methacrylate) composite particles and their application to flame retardation of rigid polyurethane foams, *Polym. Degrad. Stab.* 94 (2009) 971–979. doi:10.1016/j.polymdegradstab.2009.03.016.
- [148] Y. Li, X. Luo, S. Hu, *Bio-based Polyols and Polyurethanes*, Springer, 2015.

- [149] H. Dai, L. Yang, B. Lin, C. Wang, G. Shi, Synthesis and Characterization of the Different Soy-Based Polyols by Ring Opening of Epoxidized Soybean Oil with Methanol, 1,2-Ethanediol and 1,2-Propanediol, *J. Am. Oil Chem. Soc.* 86 (2009) 261–267. doi:10.1007/s11746-008-1342-7.
- [150] C.-S.S.C.S. Wang, L.-T.T.L.T. Yang, B.-L.L. Ni, G. Shi, H. Dai, L.-T.T.L.T. Yang, B. Lin, C.-S.S.C.S. Wang, S. Guang, L.-T.T.L.T. Yang, B.-L.L. Ni, G. Shi, Polyurethane networks from different soy-based polyols by the ring opening of epoxidized soybean oil with methanol, glycol, and 1,2-propanediol, *J. Appl. Polym. Sci.* 114 (2009) 125–131. doi:10.1002/app.30493.
- [151] M. Farias, M. Martinelli, D.P. Bottega, Epoxidation of soybean oil using a homogeneous catalytic system based on a molybdenum (VI) complex, *Appl. Catal. A Gen.* 384 (2010) 213–219. doi:10.1016/j.apcata.2010.06.038.
- [152] Z. Xing, G. Wu, S. Huang, S. Chen, H. Zeng, Preparation of microcellular cross-linked polyethylene foams by a radiation and supercritical carbon dioxide approach, *J. Supercrit. Fluids.* 47 (2008) 281–289. doi:10.1016/j.supflu.2008.08.009.
- [153] T. Lvii, J. Ryszkowska, S. Urea-urethane, Supermolecular structure , morphology and physical properties of urea-urethane elastomers, 12 (2012).
- [154] M. Zieleniewska, M. Auguścik, A. Prociak, P. Rojek, J. Ryszkowska, Polyurethane-urea substrates from rapeseed oil-based polyol for bone tissue cultures intended for application in tissue engineering, *Polym. Degrad. Stab.* 108 (2014) 1–19. doi:10.1016/j.polymdegradstab.2014.03.010.
- [155] T. Pretsch, I. Jakob, W. Müller, Hydrolytic degradation and functional stability of a segmented shape memory poly(ester urethane), *Polym. Degrad. Stab.* 94 (2009) 61–73. doi:10.1016/j.polymdegradstab.2008.10.012.
- [156] Y.I. Tien, K.H. Wei, Hydrogen bonding and mechanical properties in segmented montmorillonite / polyurethane nanocomposites of different hard segment ratios, 42 (2001) 3213–3221.
- [157] M. Kirpluks, U. Cabulis, A. Ivdre, M. Kuranska, M. Zieleniewska, M. Auguscik, Mechanical and Thermal Properties of High-Density Rigid Polyurethane Foams from Renewable Resources, *J. Renew. Mater.* 4 (2016) 86–100. doi:10.7569/JRM.2015.634132.
- [158] S. Vijayakumar, P.R. Rajakumar, Infrared spectral analysis of waste pet samples, 4 (2012) 58–65.
- [159] E. Žagar, J. Grdadolnik, An infrared spectroscopic study of H-bond network in hyperbranched polyester polyol, *J. Mol. Struct.* 658 (2003) 143–152. doi:10.1016/S0022-2860(03)00286-2.
- [160] X. Liu, K. Xu, H. Liu, H. Cai, J. Su, Z. Fu, Y. Guo, M. Chen, Preparation and properties of waterborne polyurethanes with natural dimer fatty acids based polyester polyol as soft segment, *Prog. Org. Coatings.* 72 (2011) 612–620. doi:10.1016/j.porgcoat.2011.07.002.
- [161] S.G. Prasad, A. De, U. De, Structural and Optical Investigations of Radiation Damage in Transparent PET Polymer Films, *Int. J. Spectrosc.* 2011 (2011) 1–7. doi:10.1155/2011/810936.
- [162] P.K. Roy, R. Mathur, D. Kumar, C. Rajagopal, Tertiary recycling of poly(ethylene terephthalate) wastes for production of polyurethane-polyisocyanurate foams, *J. Environ. Chem. Eng.* 1 (2013) 1062–1069. doi:10.1016/j.jece.2013.08.019.
- [163] S. Emmerich, NIST Technical Note 1921 Characterization of Emissions from Spray Polyurethane Foam NIST Technical Note 1921 Characterization of Emissions from Spray Polyurethane Foam, (1921).
- [164] R. Rao, L. Mondy, D. Noble, V. Brunini, K. Long, C. Roberts, N. Wyatt, M. Celina, K. Thompson, J. Tinsley, Density predictions using a finite element/level set model of

- polyurethane foam expansion and polymerization, *Comput. Fluids*. 175 (2018) 20–35. doi:10.1016/j.compfluid.2018.08.010.
- [165] M. Kirpluks, L. Stiebra, A. Trubaca-Boginska, U. Cabulis, J. Andersons, A. Trubaca-Boginska, U. Cabulis, J. Andersons, Rigid closed-cell PUR foams containing polyols derived from renewable resources: The effect of polymer composition, foam density, and organoclay filler on their mechanical properties, in: K. Thakur, Vijay, M.K. Thakur, M.R. Kessler (Eds.), *Handb. Compos. from Renew. Mater.*, Scrivener Publishing LLC, 2017: pp. 313–339. doi:10.1002/9781119441632.ch31.
- [166] L. Jiao, H. Xiao, Q. Wang, J. Sun, Thermal degradation characteristics of rigid polyurethane foam and the volatile products analysis with TG-FTIR-MS, *Polym. Degrad. Stab.* 98 (2013) 2687–2696. doi:10.1016/j.polymdegradstab.2013.09.032.
- [167] K.P. Menard, *Dynamic Mechanical Analysis A Practical Introduction*, 1999. doi:10.1201/9781420049183.ch2.
- [168] S. Sinha Ray, M. Okamoto, Polymer/layered silicate nanocomposites: A review from preparation to processing, *Prog. Polym. Sci.* 28 (2003) 1539–1641. doi:10.1016/j.progpolymsci.2003.08.002.
- [169] Y.I. Tien, K.H. Wei, The effect of nano-sized silicate layers from montmorillonite on glass transition, dynamic mechanical, and thermal degradation properties of segmented polyurethane, *J. Appl. Polym. Sci.* 86 (2002) 1741–1748. doi:10.1002/app.11086.
- [170] A. Nohales, V. Costa, P. Félix, C.M. Gómez, C. Europe, Influence of Polycarbonatediol content on Properties of Polyurethanes Elastomers, (n.d.) 2–4.
- [171] L. Wu, J. Van Gemert, R.E. Camargo, Rheology Study in Polyurethane Rigid Foams, Huntsman Corp. Tech. Pap. (2009) 12.
- [172] L.W. Hill, Calculation of crosslink density in short chain networks, *Prog. Org. Coatings*. 31 (1997) 235–243. doi:10.1016/S0300-9440(97)00081-7.
- [173] R.R. Romero, R.A. Grigsby, E.L. Rister, J.K. Pratt, D. Ridgway, A Study of the Reaction Kinetics of Polyisocyanurate Foam Formulations using Real-time FTIR, *J. Cell. Plast.* 41 (2005) 339–359. doi:10.1177/0021955X05055115.
- [174] J. Xu, T. Wu, C. Peng, S. Adegbite, Influence of acid and alkali pre-treatments on thermal degradation behaviour of polyisocyanurate foam and its carbon morphology, *Polym. Degrad. Stab.* 141 (2017) 104–118. doi:10.1016/j.polymdegradstab.2017.05.018.
- [175] B. Raffel, High Throughput Screening of Rigid Polyisocyanurate Foam Formulations: Quantitative Characterization of Isocyanurate Yield via the Adiabatic Temperature Method, *J. Cell. Plast.* 42 (2006) 17–47. doi:10.1177/0021955X06060943.
- [176] B.-H. Kim, K. Yoon, D.C. Moon, D. Cheul, D.C. Moon, D. Cheul, D.C. Moon, D. Cheul, Thermal degradation behavior of rigid and soft polyurethanes based on methylene diphenyl diisocyanate using evolved gas analysis- (gas chromatography)– mass spectrometry, *J. Anal. Appl. Pyrolysis*. 98 (2012) 236–241. doi:10.1016/j.jaap.2012.09.010.
- [177] M.M. Coleman, D.J. Skrovanek, J. Hu, P.C. Painter, Hydrogen Bonding in Polymer Blends. 1. FTIR Studies of Urethane-Ether Blends, *Macromolecules*. 21 (1988) 59–65. doi:10.1021/ma00179a014.
- [178] I. Javni, W. Zhang, Z.S. Petrović, Soybean-oil-based polyisocyanurate rigid foams, *J. Polym. Environ.* 12 (2004) 123–129. doi:10.1023/B:JOOE.0000038543.77820.be.
- [179] F. V Billotto, M.M. Mirdamadi, B.A. Pearson, Design, Application Development, and Launch of Polyurethane Foam Systems in Vehicle Structures, *SAE Tech. Pap.* (2003). doi:10.4271/2003-01-0333.
- [180] M. Kirpluks, U. Cabulis, J. Andersons, G. Japins, K. Kalnins, Modeling the Effect of Foam Density and Strain Rate on the Compressive Response of Polyurethane Foams, *SAE Int. J. Mater. Manuf.* 11 (2018). doi:10.4271/05-11-02-0014.

- [181] M.C. Hawkins, B. O'Toole, D. Jackovich, Cell Morphology and Mechanical Properties of Rigid Polyurethane Foam, *J. Cell. Plast.* 41 (2005) 267–285. doi:10.1177/0021955X05053525.
- [182] S.H. Goods, C.L. Neuschwanger, C.C. Henderson, D.M. Skala, Mechanical properties of CRETE, a polyurethane foam, *J. Appl. Polym. Sci.* 68 (1998) 1045–1055. doi:10.1002/(SICI)1097-4628(19980516)68:7<1045::AID-APP2>3.0.CO;2-F.
- [183] L. Marsavina, D.M. Constantinescu, E. Linul, D.A. Apostol, T. Voiconi, T. Sadowski, Refinements on fracture toughness of PUR foams, *Eng. Fract. Mech.* 129 (2014) 54–66. doi:10.1016/j.engfracmech.2013.12.006.
- [184] M.E. Kabir, M.C. Saha, S. Jeelani, Tensile and fracture behavior of polymer foams, *Mater. Sci. Eng. A.* 429 (2006) 225–235. doi:10.1016/j.msea.2006.05.133.
- [185] Y. Benveniste, A new approach to the application of Mori-Tanaka's theory in composite materials, *Mech. Mater.* 6 (1987) 147–157. doi:10.1016/0167-6636(87)90005-6.
- [186] R. Hashemi, R. Avazmohammadi, H.M. Shodja, G.J. Weng, Composites with superspherical inhomogeneities, *Philos. Mag. Lett.* 89 (2009) 439–451. doi:10.1080/09500830903019020.
- [187] I. Sevostianov, A. Giraud, ON the compliance contribution tensor for a concave superspherical pore, *Int. J. Fract.* 177 (2012) 199–206. doi:10.1007/s10704-012-9754-7.
- [188] J. Andersons, M. Kirpluks, L. Stiebra, U. Cabulis, Anisotropy of the stiffness and strength of rigid low-density closed-cell polyisocyanurate foams, *Mater. Des.* 92 (2016) 836–845. doi:10.1016/j.matdes.2015.12.122.
- [189] J. Andersons, U. Cābulis, L. Stiebra, M. Kirpluks, E. Spārniņš, U. Cābulis, L. Stiebra, M. Kirpluks, E. Spārniņš, U. Cabulis, L. Stiebra, M. Kirpluks, E. Spārniņš, Modeling the mode I fracture toughness of anisotropic low-density rigid PUR and PIR foams, *Int. J. Fract.* 205 (2017) 111–118. doi:10.1007/s10704-017-0194-2.
- [190] L. Gong, S. Kyriakides, W.Y. Jang, Compressive response of open-cell foams. Part I: Morphology and elastic properties, *Int. J. Solids Struct.* 42 (2005) 1355–1379. doi:10.1016/j.ijsolstr.2004.07.023.
- [191] H. Kolsky, An Investigation of the Mechanical Properties of Materials at very High Rates of Loading, *Proc. Phys. Soc. Sect. B.* 62 (1949) 676. <http://stacks.iop.org/0370-1301/62/i=11/a=302>.
- [192] S. Rao, V.P.W. Shim, S.E. Quah, Dynamic mechanical properties of polyurethane elastomers using a nonmetallic Hopkinson bar, *J. Appl. Polym. Sci.* 66 (1997) 619–631. doi:10.1002/(SICI)1097-4628(19971024)66:4<619::AID-APP2>3.0.CO;2-V.
- [193] B. Song, W. Chen, Z. Liu, S.Z. Erhan, Compressive properties of soybean oil-based polymers at quasi-static and dynamic strain rates, *J. Appl. Polym. Sci.* 99 (2006) 2759–2770. doi:10.1002/app.22627.
- [194] W.W. Chen, a. M. Rajendran, B. Song, X. Nie, Dynamic fracture of ceramics in armor applications, *J. Am. Ceram. Soc.* 90 (2007) 1005–1018. doi:10.1111/j.1551-2916.2007.01515.x.
- [195] H. Kuhn, Medlin Dana, ASM Handbook, Volume 8, Mechanical Testing and Evaluation, ASM International, Ohio 44073-0002, 2000.
- [196] M. Avalle, G. Belingardi, A. Ibba, Mechanical models of cellular solids: Parameters identification from experimental tests, *Int. J. Impact Eng.* 34 (2007) 3–27. doi:10.1016/j.ijimpeng.2006.06.012.
- [197] Q. Liu, G. Subhash, X.-L. Gao, A Parametric Study on Crushability of Open-Cell Structural Polymeric, *J. Porous Mater.* 12 (2005) 233–248. doi:10.1007/s10934-005-1652-1.
- [198] A. Nagy, W.L. ko, U.S. Lindholm, Mechanical Behavior of Foamed Materials Under

- Dynamic Compression, *J. Cell. Plast.* 10 (1974) 127–134. doi:10.1177/0021955X7401000306.
- [199] D.A. Apostol, D.M. Constantinescu, Temperature and speed of testing influence on the densification and recovery of polyurethane foams, *Mech. Time-Dependent Mater.* 17 (2013) 111–136. doi:10.1007/s11043-012-9179-8.
- [200] U. Cabulis, I. Sevastyanova, J. Andersons, I. Beverte, Rapeseed oil-based rigid polyisocyanurate foams modified with nanoparticles of various type, *Polimery/Polymers.* 59 (2014) 207–212. doi:10.14314/polimery.2014.207.
- [201] L. Mkrtychyan, M. Maier, U. Huber, Structural polyurethane foam: Testing and modelling for automotive applications, *Int. J. Crashworthiness.* 13 (2008) 523–532. doi:10.1080/13588260802221310.
- [202] M. Schulz, D. Kourkoulas, Regulation (EU) No 333/2014, *Off. J. Eur. Union.* (2014) 15–21. <http://eur-lex.europa.eu/legal-content/EN/TXT/PDF/?uri=CELEX:32014R0333&from=EN>.
- [203] R.K. Helling, D. a. Russell, Use of life cycle assessment to characterize the environmental impacts of polyol production options, *Green Chem.* 11 (2009) 380. doi:10.1039/b815833a.
- [204] R.K. Helling, D. a. Russell, Investigation of the Trade-off Between Lightweight and Battery Cost for an Aluminium-intensive, *Green Chem.* 11 (2009) 380. doi:10.1039/b815833a.
- [205] E. Cischino, F. Di Paolo, E. Mangino, D. Pullini, C. Elizetxea, C.C.C.C. Maestro, E. Alcalde, J.D. Christiansen, An Advanced Technological Lightweighted Solution for a Body in White, *Transp. Res. Procedia.* 14 (2016) 1021–1030. doi:10.1016/j.trpro.2016.05.082.
- [206] E. Cischino, Z. Vuluga, C.E. Ezeiza, I.L. Benito, E. Mangino, J. De Claville Christiansen, C.-G. Sanporean, F. Di Paolo, M. Kirpluks, P. Cabulis, A Concrete and Viable Example of Multimaterial Body: The Evolution Project Main Outcomes, in: *Procedia CIRP*, 2017: pp. 300–305. doi:10.1016/j.procir.2017.03.292.
- [207] C.G. Sanporean, Z. Vuluga, C. Radovici, D.M. Panaitescu, M. Iorga, J.D. Christiansen, A. Mosca, Polypropylene/organoclay/SEBS nanocomposites with toughness-stiffness properties, *RSC Adv.* 4 (2014) 6573–6579. doi:10.1039/c3ra45325a.
- [208] S. Pardo-Alonso, E. Solórzano, L. Brabant, P. Vanderniepen, M. Dierick, L. Van Hoorebeke, M.A. Rodríguez-Pérez, 3D Analysis of the progressive modification of the cellular architecture in polyurethane nanocomposite foams via X-ray microtomography, *Eur. Polym. J.* 49 (2013) 999–1006. doi:10.1016/j.eurpolymj.2013.01.005.
- [209] P. Mondal, D.V. Khakhar, Rigid Polyurethane–Clay Nanocomposite Foams: Preparation and Properties, *J. Appl. Polym. Sci.* 103 (2007) 2802–2809. doi:10.1002/app.
- [210] T. Widya, C. Macosko, Nanoclay-Modified Rigid Polyurethane Foam, *J. Macromol. Sci. Part B Phys.* 44 (2005) 897–908. doi:10.1080/00222340500364809.
- [211] S. Estravis, J. Tirado-Mediavilla, M. Santiago-Calvo, J.L. Ruiz-Herrero, F. Villafañe, M.Á. Rodríguez-Pérez, Rigid polyurethane foams with infused nanoclays: Relationship between cellular structure and thermal conductivity, *Eur. Polym. J.* 80 (2016) 1–15. doi:10.1016/j.eurpolymj.2016.04.026.
- [212] J.M. Herrera-Alonso, E. Marand, J.C. Little, S.S. Cox, Transport properties in polyurethane/clay nanocomposites as barrier materials: Effect of processing conditions, *J. Memb. Sci.* 337 (2009) 208–214. doi:10.1016/j.memsci.2009.03.045.
- [213] S. Pardo-Alonso, E. Solórzano, S. Estravis, M. a. Rodríguez-Perez, J. a. de Saja, In situ evidence of the nanoparticle nucleating effect in polyurethane–nanoclay foamed systems, *Soft Matter.* 8 (2012) 11262. doi:10.1039/c2sm25983d.
- [214] J.H. Park, S.C. Jana, Mechanism of Exfoliation of Nanoclay Particles in Epoxy-Clay

- Nanocomposites, *Macromolecules*. 36 (2003) 2758–2768. doi:10.1021/ma021509c.
- [215] M. Joshi, B. Adak, B.S. Butola, Polyurethane nanocomposite based gas barrier films, membranes and coatings: A review on synthesis, characterization and potential applications, *Prog. Mater. Sci.* 97 (2018) 230–282. doi:10.1016/j.pmatsci.2018.05.001.
- [216] M. Thirumal, D. Khastgir, N.K. Singha, B.S. Manjunath, Y.P. Naik, Effect of a nanoclay on the mechanical, thermal and flame retardant properties of rigid polyurethane foam, *J. Macromol. Sci. Part A Pure Appl. Chem.* 46 (2009) 704–712. doi:10.1080/10601320902939101.
- [217] P. Mondal, D.V. Khakhar, Regulation of Cell Structure in Water Blown Rigid Polyurethane Foam, *Macromol. Symp.* 216 (2004) 241–254. doi:10.1002/masy.200451223.
- [218] S. Gaidukovs, R.D. Maksimov, U. Cabulis, E. Plume, A. Stunda-Zujeva, Mechanical Properties of a Rigid Polyurethane/Montmorillonite Composite Prepared by Using a Biopolyol, *Mech. Compos. Mater.* 49 (2013) 333–344.
- [219] A. Krishnan, L.R. Xu, A simple effective flaw model on analyzing the nanofiller agglomeration effect of nanocomposite materials, *J. Nanomater.* 2012 (2012). doi:10.1155/2012/483093.
- [220] M. Danowska, Ł. Piszczyk, M. Strankowski, M. Gazda, J.T. Haponiuk, Rigid polyurethane foams modified with selected layered silicate nanofillers, *J. Appl. Polym. Sci.* 130 (2013) 2272–2281. doi:10.1002/app.39432.
- [221] M. Berta, C. Lindsay, G. Pans, G. Camino, Effect of chemical structure on combustion and thermal behaviour of polyurethane elastomer layered silicate nanocomposites, *Polym. Degrad. Stab.* 91 (2006) 1179–1191. doi:10.1016/j.polymdegradstab.2005.05.027.
- [222] Z. Xu, X. Tang, J. Zheng, Thermal stability and flame retardancy of rigid polyurethane foams/organoclay nanocomposites, *Polym. Plast. Technol. Eng.* 47 (2008) 1136–1141. doi:10.1080/03602550802391607.
- [223] A. Prociak, G. Rokicki, J. Ryszkowska, *Materialy poliuretanowe*, 1st ed., Wydawnictwo Naukowe PWN, Warsaw, 2014.
- [224] L. Gao, G. Zheng, Y. Zhou, L. Hu, G. Feng, M. Zhang, Synergistic effect of expandable graphite, diethyl ethylphosphonate and organically-modified layered double hydroxide on flame retardancy and fire behavior of polyisocyanurate-polyurethane foam nanocomposite, *Polym. Degrad. Stab.* 101 (2014) 92–101. doi:10.1016/j.polymdegradstab.2013.12.025.
- [225] C.N. Hoang, C.T. Pham, T.M. Dang, D. Hoang, P. Lee, S. Kang, J. Kim, Novel Oligo-Ester-Ether-Diol Prepared by Waste Poly (ethylene terephthalate) Glycolysis and Its Use in Preparing Thermally Stable and Flame Retardant Polyurethane Foam, *Polymers (Basel)*. 11 (2019) 1–17. doi:10.3390/polym11020236.
- [226] J.G. Quintiere, *Fundamentals of Fire Phenomena*, John Wiley & Sons Ltd, The Atrium, Southern Gate, Chichester, 2006.
- [227] A.S. Hansen, Prediction of heat release in the single burning item test, *Fire Mater.* 26 (2002) 87–97. doi:10.1002/fam.789.
- [228] Noteikumi par Latvijas būvnormatīvu LBN 201-15 " Būvju ugunsdrošība ", in: Minist. Kabineta Noteikumi Nr.333, 2015: pp. 1–39.
- [229] L. Stefan, European fire classification of construction products, new test method “SBI”, and introduction of the European classification system into German building regulations, *Otto-Graf-Journal* Vol. 16 (2005) 151–166.
- [230] M. Kirpluks, *Dabas izcelsmes pildvielu ietekme uz talleļlas poliolu putupoliuretānu īpašībām*, Riga Technical University, 2012.
- [231] A. Prociak, M. Kurańska, U. Cabulis, M. Kirpluks, Rapeseed oil as main component in

- synthesis of bio-polyurethane-polyisocyanurate porous materials modified with carbon fibers, *Polym. Test.* 59 (2017) 478–486. doi:10.1016/j.polymertesting.2017.03.006.
- [232] A. Fridrihsone-Girone, U. Stirna, M. Misane, B. Lazdiņa, L. Deme, Spray-applied 100% volatile organic compounds free two component polyurethane coatings based on rapeseed oil polyols, *Prog. Org. Coatings.* 94 (2016) 90–97. doi:10.1016/j.porgcoat.2015.11.022.
- [233] P.K. Gamage, M. O’brien, L. Karunanayake, Epoxidation of some vegetable oils and their hydrolysed products with peroxyformic acid - Optimised to industrial scale, *J. Natl. Sci. Found. Sri Lanka.* 37 (2009) 229–240. doi:10.4038/jnsfsr.v37i4.1469.
- [234] E. Milchert, A. Smagowicz, The Influence of Reaction Parameters on the Epoxidation of Rapeseed Oil with Peracetic Acid, *J. Am. Oil Chem. Soc.* 86 (2009) 1227–1233. doi:10.1007/s11746-009-1455-7.
- [235] P. Adducts, Fast Fourier Transform IR Characterization of Epoxy GY Systems Crosslinked with Aliphatic and Cycloaliphatic EH Polyamine Adducts, (2010) 684–696. doi:10.3390/s100100684.
- [236] N. Ostah, G. Lawson, S. Zafar, G. Harrington, J. Hicks, Investigation of amine and polyol functionality in extracts of polyurethane wound management dressings using MALDI-MS, *Analyst.* 125 (2000) 111–114. doi:10.1039/a906601b.
- [237] K. Aou, A.K. Schrock, V. V. Ginzburg, P.C. Price, Characterization of polyurethane hard segment length distribution using soft hydrolysis/MALDI and Monte Carlo simulation, *Polymer (Guildf).* 54 (2013) 5005–5015. doi:10.1016/j.polymer.2013.07.014.
- [238] J.G. Speight, Gasification for Synthetic Fuel Production, 2014. doi:10.1016/B978-0-85709-802-3.00010-2.
- [239] K. White, N. Lorenz, T. Potts, W. Roy Penney, R. Babcock, A. Hardison, E.A. Canuel, J.A. Hestekin, Production of biodiesel fuel from tall oil fatty acids via high temperature methanol reaction, *Fuel.* 90 (2011) 3193–3199. doi:10.1016/j.fuel.2011.06.017.
- [240] S.P. Pyl, T. Dijkmans, J.M. Antonykuty, M.-F. Reyniers, A. Harlin, K.M. Van Geem, G.B. Marin, Wood-derived olefins by steam cracking of hydrodeoxygenated tall oils, *Bioresour. Technol.* 126 (2012) 48–55. doi:10.1016/j.biortech.2012.09.037.
- [241] J. V. Satur, B.P. Calabria, M. Hoshino, S. Morita, Y. Seo, Y. Kon, T. Takagi, Y. Watanabe, L. Mutele, S. Foya, Flotation of rare earth minerals from silicate-hematite ore using tall oil fatty acid collector, *Miner. Eng.* 89 (2016) 52–62. doi:10.1016/j.mineng.2016.01.004.
- [242] N.C. Goud, V. V., Patwardhan, A. V. and Pradha, Kinetics of in-situ epoxidation of natural triglycerides catalyzed by acidic ion exchange resin, *Ind. Eng. Chem. Res.* 46 (2007) 3078–3085.
- [243] N. Sad, K. Polymer, Kinetics of in situ Epoxidation of Soybean Oil in Bulk Catalyzed by Ion Exchange Resin, 78 (2001).
- [244] R.L. Musante, R.J. Grau, M.A. Baltanás, Kinetic of liquid-phase reactions catalyzed by acidic resins: The formation of peracetic acid for vegetable oil epoxidation, *Appl. Catal. A Gen.* 197 (2000) 165–173. doi:10.1016/S0926-860X(99)00547-5.
- [245] Z.S. Petrović, A. Zlatanić, C.C. Lava, S. Sinadinović-Fišer, Epoxidation of soybean oil in toluene with peroxyacetic and peroxyformic acids - Kinetics and side reactions, *Eur. J. Lipid Sci. Technol.* 104 (2002) 293–299. doi:10.1002/1438-9312(200205)104:5<293::AID-EJLT293>3.0.CO;2-W.
- [246] L.H. Gan, S.H. Goh, K.S. Ooi, Kinetic studies of epoxidation and oxirane cleavage of palm olein methyl esters, *J. Am. Oil Chem. Soc.* 69 (1992) 347–351. doi:10.1007/BF02636065.
- [247] M. Yan, E.M. Frank, E.W. Cochran, Effects of Vegetable Oil Composition on

- Epoxidation Kinetics and Physical Properties, *JAOCS, J. Am. Oil Chem. Soc.* 95 (2018) 209–216. doi:10.1002/aocs.12014.
- [248] X. Sun, X. Zhao, W. Du, D. Liu, Kinetics of formic acid-autocatalyzed preparation of performic acid in aqueous phase, *Chinese J. Chem. Eng.* 19 (2011) 964–971. doi:10.1016/S1004-9541(11)60078-5.
- [249] R. Liang, A. Hu, M. Hatat-Fraile, Z. N., Fundamentals on Adsorption, Membrane Filtration, and Advanced Oxidation Processes for Water Treatment. In: Hu A., Apblett A. (eds) *Nanotechnology for Water Treatment and Purification.*, Springer, Cham, 2014. doi:10.1007/978-3-319-06578-6.
- [250] T. Cooney, F. Cardona, T. Tran-Cong, Kinetics of in situ epoxidation of hemp oil under heterogeneous reaction conditions: an overview with preliminary results, *Proc. 1st Int. Postgrad. Conf. Eng. Des. Dev. Built Environ. Sustain. Wellbeing.* (2011) 106–111. <http://eprints.usq.edu.au/19247>.
- [251] S. Sinadinović-Fišer, M. Janković, Z.S. Petrović, Kinetics of in situ epoxidation of soybean oil in bulk catalyzed by ion exchange resin, *J. Am. Oil Chem. Soc.* 78 (2001) 725–731. doi:10.1007/s11746-001-0333-9.
- [252] A. Demirbas, Methylation of wood fatty and resin acids for production of biodiesel, *Fuel* 90 (2011) 2273–2279. doi:10.1016/j.fuel.2011.02.037.
- [253] P.P. Polizelli, F.D.A. Facchini, G.O. Bonilla-Rodriguez, Stability of a lipase extracted from seeds of *pachira aquatica* in commercial detergents and application tests in poultry wastewater pretreatment and fat particle hydrolysis, *Enzyme Res.* 2013 (2013) 1–6. doi:10.1155/2013/324061.
- [254] J.A.P. da Silva, N.S.M. Cardozo, C.L. Petzhold, Enzymatic synthesis of andiroba oil based polyol for the production of flexible polyurethane foams, *Ind. Crops Prod.* 113 (2018) 55–63. doi:10.1016/j.indcrop.2018.01.020.
- [255] M. Kirpluks, E. Vanags, A. Abolins, A. Fridrihsone, U. Cabulis, Chemo-enzymatic oxidation of tall oil fatty acids as a precursor for further polyol production, *J. Clean. Prod.* 215 (2019) 390–398. doi:10.1016/j.jclepro.2018.12.323.
- [256] C. Orellana-Coca, U. Törnvall, D. Adlercreutz, B. Mattiasson, R. Hatti-Kaul, Chemo-enzymatic epoxidation of oleic acid and methyl oleate in solvent-free medium, *Biocatal. Biotransformation.* 23 (2005) 431–437. doi:10.1080/10242420500389488.
- [257] G.D. Yadav, K. Manjula Devi, A kinetic model for the enzyme-catalyzed self-epoxidation of oleic acid, *J. Am. Oil Chem. Soc.* 78 (2001) 347–351. doi:10.1007/s11746-001-0267-2.
- [258] C. Orellana-Coca, S. Camocho, D. Adlercreutz, B. Mattiasson, R. Hatti-Kaul, Chemo-enzymatic epoxidation of linoleic acid: Parameters influencing the reaction, *Eur. J. Lipid Sci. Technol.* 107 (2005) 864–870. doi:10.1002/ejlt.200500253.